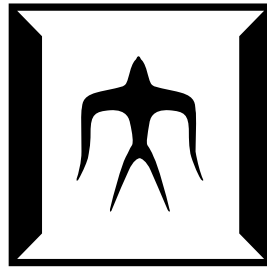


論文 / 著書情報  
Article / Book Information

題目(和文)	
Title(English)	Antigen presenting cells-targeted liposome by Levilactobacillus brevis surface layer protein coating
著者(和文)	陳政霖
Author(English)	Zheng Lin Tan
出典(和文)	学位:博士(学術), 学位授与機関:東京工業大学, 報告番号:甲第12261号, 授与年月日:2022年9月22日, 学位の種別:課程博士, 審査員:山本 直之,八木 透,林 宣宏,折原 芳波,小倉 俊一郎
Citation(English)	Degree:Doctor (Academic), Conferring organization: Tokyo Institute of Technology, Report number:甲第12261号, Conferred date:2022/9/22, Degree Type:Course doctor, Examiner:,,,,,
学位種別(和文)	博士論文
Type(English)	Doctoral Thesis

**Antigen presenting cells-targeted liposome  
by *Levilactobacillus brevis*  
surface layer protein coating**



**Tan, Zheng Lin**

**Dissertation**

presented to School of Life Science and Technology of  
Tokyo Institute of Technology  
in partial fulfilment of the requirement for the Degree of

**Doctor of Philosophy**

**Tokyo Institute of Technology**

**July 2022**

---

## Declaration

I hereby declare that the works in this dissertation, "Antigen Presenting Cells-Targeted Liposome by *Levilactobacillus brevis* Surface Layer Protein Coating", have been carried out in School of Life Science and Technology of Tokyo Institute of Technology. Sequencing of SlpB, oral administration of liposomes, euthanasia and dissection for intestine isolation were carried out with the help of Professor Dr. Naoyuki Yamamoto, transmission electron micrographs were taken by Professor Dr. Yoshitaka Kitamoto, and other works are conducted by me.

The information derived from literature has been duly acknowledged in the text and reference. No part of this dissertation was previously submitted and presented for any diploma or degree at any institute.

All works in this dissertation are complied with ethics guidelines, regional and international laws.

No funding is declared for this work, and I declare that patent for both SlpA- and SlpB-functionalised liposomes and their uses was applied.

---

Zheng Lin Tan

---

## Abstract

Drug delivery to intestinal antigen presenting cells (APCs) is a challenging task due to the harsh and diverse environment in mammalian gastrointestinal (GI) tract, short retention time in intestines, mucosal and endothelial barriers which prevent the drugs from accessing Peyer's patches where APCs resides. To deliver drugs to intestinal APCs, the drugs should be encapsulated in carriers which are stable against environment in GI tract and possess APCs-targeting capability. In this study, a targeted ligand drug delivery system to target intestinal APCs was developed through coating of carriers with SlpB from *Levilactobacillus brevis*.

SlpB from *Lv. brevis* was extracted with 5 M lithium chloride solution and coated on drug carriers. The adsorption capacity of SlpB on all drug carriers evaluated in this study was 400 mg g<sup>-1</sup> [SlpB LP<sup>-1</sup>]. The adsorption curve was compared to the concentration of SlpB required to achieve maximum stability of SlpB-coated liposome (SlpB-LP), and the liposome coated with SlpB at maximum coating capacity showed maximum stability. Formation of 12.9 nm-thick layer of SlpB on liposome was observed with microscopy, and analysis with electrophoretic mobility showed that SlpB reduces  $\zeta$  potential of anionic liposomes. Improvement of colloid stability of liposome via SlpB-coating due to increase in absolute  $\zeta$  potential was confirmed with narrower size distribution of SlpB-LP.

SlpB-coating enhance stability of liposome against pH ranging from pH 2 – 9. Robustness of SlpB-adsorption on the surface of liposome under various pH was confirmed, and the result suggests that SlpB-adsorption was stable. Furthermore, stability against 0.5 – 3.0% gall solution which can emulsify liposome, and stability against simulated gastric fluid and simulated intestinal fluid which contains pepsin and pancreatin were also improved by SlpB-coating. The result suggests that SlpB has improved stability of liposomes under all gut-mimicking environments.

Furthermore, endocytosis of SlpB-coated carriers was evaluated with dendritic cell (DC) and macrophage (M $\Phi$ ). I have found that SlpB-coating has significantly enhanced endocytosis of carriers into DC and M $\Phi$ . The effect of size of liposome on endocytosis was negligible. Investigation of receptors which binds to SlpB suggests that SlpB binds to DC-SIGN and Mincle

---

which are both C-type lectins, through glycan chain.

*In vivo* study suggests that SlpB could improve stability of liposome in GI tract by 5.4- and 6.1-fold at 1 h and 3 h after oral administration. SlpB has facilitated enrichment of LP in Peyer's patches and blood, while no unspecific absorption into intestine and low retention in liver was detected. Enrichment of liposome in Peyer's patches is correlated to bioavailability, and SlpB has improved bioavailability by 427.6-fold. Unlike SlpA, no unspecific absorption of SlpB-LP to intestine and mucosal layer was detected. The route of SlpB-LP delivery to intestinal APCs was through transcytosis by M cells and specific endocytosis by CD23<sup>+</sup> APCs, which consist of follicular DC and MΦ. Improved antigen presentation at interfollicular region and germinal centre were also confirmed.

Moreover, SlpB also exhibit adjuvant effect which might improve therapeutic effect of drug. Production of IL-6, IL-10, IL-12 and IL-17 increased significantly when DC was co-stimulated with ovalbumin and SlpB or lipopolysaccharide and SlpB. Evaluation with  $\alpha$ -galactosylceramide-loaded liposome ( $\alpha^{\text{GC}}\text{LP}$ ) showed increase in expression of anti-tumour cytokines both *in vitro* and *in vivo*. For instance, SlpB- $\alpha^{\text{GC}}\text{LP}$  has increased production of IL-12 and decreased production of IL-10, while upregulated expression of IL-6, IL-10, TNF- $\alpha$  in DC. On the other hand, *in situ* expression of IL-4 and IL-5 were downregulated, while expression of IL-12, IFN- $\gamma$  and TNF- $\alpha$  were upregulated in Peyer's patches of mice administered with SlpB- $\alpha^{\text{GC}}\text{LP}$  compared to  $\alpha^{\text{GC}}\text{LP}$ . The results have suggested that oral delivery of SlpB-LP could enhance therapeutic effect through improved stability of liposome, specific uptake of drug carriers by APCs, and induction of adjuvant effect, which has stimulated injection-like effect.

To investigate the mechanism of SlpB-binding to APCs, presence of glycan chain in SlpB was investigated. N-glycan structure was revealed in SlpB by treatment with N-glycosidase. The function of sugar chain in DC-interaction was confirmed with competitive assay with D-glucose, D-galactose and D-mannose. Fragments of trypsinised SlpB which are responsible for DC-binding were identified, and the result suggests that 4 fragments with highest hydrophilicity were responsible in DC-binding.

In conclusion, coating of SlpB from *Lv. brevis* has improved stability of liposome, functionalised to enhance transcytosis through M cells, enhanced endocytosis by APCs via specific binding with the receptors and potentiated the therapeutic of drugs.

**Keywords:** *Levilactobacillus brevis*; surface layer protein; targeted-ligand drug delivery system; adjuvant effect; C-type lectins; oral administration of drugs

---

## Acknowledgement

First of all, I would like to thank Professor Dr. Naoyuki Yamamoto for guidance and helps throughout the journey to complete this dissertation. Professor Dr. Naoyuki Yamamoto has also contributed to *in vivo* studies in this work, particularly in administration of liposome, euthanasia of mice, and isolation of tissues. This work would not be so successful without the contributions of Professor Dr. Naoyuki Yamamoto.

I would also like to express my gratitude to Associate Professor Dr. Kazuhiko Miyana (Jichi Medical University) for fruitful discussion which led to the formation of theories in this dissertation.

I am grateful to Professor Dr. Yoshitaka Kitamoto for provision of carbon-electrode cuvette for  $\zeta$  potential analysis and the access of nanoparticle analyser. Professor Dr. Yoshitaka Kitamoto has also contributed in TEM analysis of liposomes, particularly in negative staining and obtaining micrographs.

I would like to extend my appreciation to open facility center of Tokyo Institute of Technology, Mrs. Ayako Takada and Mrs. Atsumi Sakaguchi, Mr. Masato Koizumi for the access of laser scanning microscope, cryostat and matrix assisted laser desorption ionization-time of flight mass spectrometer; Dr. Yasuyuki Ishii for provision of liposomal  $\alpha$ -galactosylceramide.

To LOTTE foundation, for non-research-based scholarship which has covered my living expenses and the supports from the officers throughout my doctoral degree.

Without prior works and discoveries, this work could never have begun. I would like to thank all the predecessors who have laid foundations which have led to the design of this study: Professor Emeritus Dr. Uwe B. Sleytr for discovery of Slps and the capability of Slps to self-assemble on liposome; Professor Emerita Dr. Airi Palva for discovery and characterisation of Slps from *Lv. brevis*; Professor Dr. Edgardo Anibal Disalvo for the study on the mechanism of improvement of stability of cationic liposome by Slp-coating; Professor Dr. Bernd Lepenies for discovery of adjuvant effect of Slp on macrophage, and many others.

I would like to give a big gratitude to my family, particularly my parents who have been very supportive throughout my doctoral degree.

Lastly, to the courageous I had, for me to dive into this whole new field; to the frontline staffs who have kept the world moving despite of the coronavirus pandemic throughout my doctoral degree. Without any of these factors, I would not have completed this dissertation within 1 year and 9 months. Thank you.

# List of Abbreviation

Abbreviation	Term
Ab	Antibody
APC	Antigen presenting cell
BSA	Bovine serum albumin
CD	Cluster of differentiation
cDNA	complementary deoxyribonucleic acid
CF	Carboxyfluorescein
CFDA	Carboxyfluorescein diacetate
DC	Dendritic cell
DC-SIGN	Dendritic cell-specific intercellular adhesion molecule-3-grabbing non-integrin
DDS	Drug delivery system
DMSO	Dimethyl sulphoxide
DPPC	L, $\alpha$ -dipalmitoyl-phosphatidylcholine
DPPG	L, $\alpha$ -dipalmitoylphosphatidylglycerol
EDTA	Ethylenediaminetetraacetic acid
ELISA	Enzyme-linked immunosorbent assay
FDA	Food and Drug Administration
FITC	Fluorescein isothiocyanate
GAPDH	Glyceraldehyde-3-phosphate dehydrogenase
GC	Germinal centre
GI	Gastrointestinal
GP2	Glycoprotein 2
HPLC	High performance liquid chromatography
IFN	Interferon
IFR	Interfollicular region
IL	Interleukin
LiCl	Lithium chloride
LP	Liposome
LPS	Lipopolysaccharide
M cell	Microfold cell
mDC	Mature dendritic cell
MFI	Mean fluorescence intensity
Mincle	Macrophage inducible C-type lectin
mRNA	Messenger ribonucleic acid
MRS	Man, Rogosa & Sharpe
M $\Phi$	Macrophage
OVA	Ovalbumin
PBS	Phosphate-buffered saline
PI	Propidium iodide
pLP	Polydisperse liposome
PVDF	Polyvinylidene fluoride
RFI	Ratio of fluorescence intensity
RPMI	Roswell Park Memorial Institute

---

Abbreviation	Term
RT-qPCR	Reverse transcription-quantitative polymerase chain reaction
SDS-PAGE	Sodium dodecyl sulphate-polyacrylamide gel electrophoresis
SED	Subepithelial dome
SGF	Simulated gastric fluid
SIF	Simulated intestinal fluid
Slp	Surface layer protein
spLP	Sonicated polydisperse liposome
sRPMI	Roswell Park Memorial Institute 1640 medium with 9.1% fetal bovine serum
TCR	T cell receptor
TEM	Transmission electron microscope
T <sub>H</sub>	T helper
TLDDS	Targeted-ligand drug delivery system
TLR	Toll-like receptor
TNF	Tumour necrosis factor
UEA-1	Ulex europaeus agglutinin 1
Umod	Uromodulin
αGC	α-galactosylceramide

---



# Contents

<b>1</b>	<b>Introduction</b>	<b>1</b>
1.1	Strategies Proposed for Oral Delivery of Drugs . . . . .	2
1.2	Surface Layer Proteins . . . . .	5
1.2.1	Slp-Coating on Liposome . . . . .	8
1.3	Objective . . . . .	11
1.4	Research Strategy . . . . .	11
1.5	Structure of Dissertation . . . . .	12
<b>2</b>	<b>Preparation and Characterisation of Surface Layer Protein-Coated Liposomes</b>	<b>13</b>
2.1	Methods . . . . .	14
2.1.1	Preparation of Surface Layer Protein B . . . . .	14
2.1.2	Fluorescent Labelling of SlpB . . . . .	15
2.1.3	$\zeta$ Potential and Particle Size of SlpB-Coated Liposome . . . . .	15
2.1.4	Fluorescent Imaging of SlpB-LP . . . . .	16
2.1.5	Transmission Electron Microscopy of SlpB-LP . . . . .	17
2.1.6	Coating of SlpB on Various Drug Carriers . . . . .	17
2.1.7	Optimal Concentration of SlpB for Maximum Stability . . . . .	18
2.1.8	Stability of SlpB-Coated Liposomes in Gut Mimicking Environment . . . . .	18
2.2	Results . . . . .	19
2.2.1	Preparation of Surface Layer Protein B . . . . .	19
2.2.2	$\zeta$ Potential and Particle Size of SlpB-Coated Liposome . . . . .	19
2.2.3	Fluorescent Imaging of SlpB-LP . . . . .	21
2.2.4	Transmission Electron Microscopy of SlpB-LP . . . . .	21
2.2.5	Coating of SlpB on Various Drug Carriers . . . . .	24
2.2.6	Optimal Concentration of SlpB for Maximum Stability . . . . .	26
2.2.7	Stability of SlpB-Coated Liposomes in Various pH . . . . .	26

2.2.8	Robustness of SlpB Adsorption on Liposomes . . . . .	28
2.2.9	SlpB Enhances Stability of Liposomes in Gall Solution . . . . .	28
2.2.10	SlpB Enhances Stability of Liposomes in Simulated Gut Fluids . . . . .	30
2.3	Discussion . . . . .	32
2.3.1	Coating of SlpB on Liposomes . . . . .	32
2.3.2	SlpB Enhanced Stability of Liposomes . . . . .	33
2.3.3	Advantages of SlpB-Coating Compared to other Slps . . . . .	34
2.4	Summary . . . . .	34
<b>3</b>	<b>SlpB Enhances Endocytosis and Induces Adjuvant Effect for Antigen Presenting Cells</b>	<b>36</b>
3.1	Methods . . . . .	37
3.1.1	Maintenance and Differentiation of THP-1 Cells . . . . .	37
3.1.2	Interaction of SlpB with APCs . . . . .	37
3.1.3	Endocytic Kinetic of Liposome by APCs . . . . .	38
3.1.4	Imaging of Endocytosis of Liposome . . . . .	38
3.1.5	Effect of Particle Size on Endocytosis . . . . .	39
3.1.6	Microbeads Endocytosis by Antigen Presenting Cells . . . . .	39
3.1.7	Bacteria Endocytosis by Antigen Presenting Cells . . . . .	39
3.1.8	Effect of SlpB-LP on Endocytosis of LP . . . . .	40
3.1.9	Effect of SlpB-Stimulation on Particles Endocytosis . . . . .	40
3.1.10	Effect of SlpB-Stimulation on Production of DC-SIGN . . . . .	40
3.1.11	Comparison with Other Types of Ligands . . . . .	40
3.1.12	Endocytosis under Inhibition of Actin Condensation . . . . .	41
3.1.13	Adjuvant Effect of SlpA and SlpB . . . . .	41
3.1.14	Cytokine Production of Antigen Presenting Cells Treated with $\alpha^{GC}LP$ . . . . .	41
3.1.15	mRNA Expression of DC Treated with $\alpha^{GC}LP$ . . . . .	42
3.2	Results . . . . .	42
3.2.1	Maintenance and Differentiation of THP-1 Cells . . . . .	42
3.2.2	Interaction of SlpB with DC . . . . .	45
3.2.3	SlpB-Coating Enhances Endocytosis by Antigen Presenting Cells . . . . .	49
3.2.4	Potential Mechanism of SlpB-Induced Endocytosis . . . . .	60
3.2.5	Comparison with Other Types of Slps as Ligands . . . . .	65

3.2.6	Comparison Across Carriers . . . . .	65
3.2.7	Adjuvant Effect of SlpB . . . . .	68
3.2.8	Cytokine Production in $\alpha^{GC}$ LP-Treated APC . . . . .	70
3.3	Discussion . . . . .	73
3.3.1	SlpB Enhances Endocytosis of Particles . . . . .	73
3.3.2	Advantages of SlpB against Other Slps . . . . .	75
3.3.3	SlpB Induces Adjuvant Effect and Improves Therapeutic Effect . . . . .	75
3.4	Summary . . . . .	76
<b>4</b>	<b><i>In vivo</i> Uptake of Liposomes in Peyer's Patches</b>	<b>78</b>
4.1	Methods . . . . .	79
4.1.1	Conservation of Content Encapsulated in Liposomes . . . . .	79
4.1.2	<i>In vivo</i> Stability of SlpB-Coated Liposome . . . . .	79
4.1.3	Absorption of Liposomes into Intestine and Uptake into Peyer's Patches . . . . .	80
4.1.4	Availability of Dye in Liver . . . . .	80
4.1.5	Transcytosis of Liposome through M cells . . . . .	80
4.1.6	Endocytosis of Liposome into Antigen-Presenting Cells . . . . .	81
4.1.7	Therapeutic Effect of SlpB-coated Drug Loaded Liposome . . . . .	81
4.2	Result . . . . .	82
4.2.1	Conservation of Content Encapsulated in Liposomes . . . . .	82
4.2.2	Stability of SlpB-LP <i>in vivo</i> . . . . .	82
4.2.3	Distribution of SlpB-LP in Gut . . . . .	84
4.2.4	Transcytosis of Liposome through M cells . . . . .	86
4.2.5	Endocytosis of Liposome into Antigen-Presenting Cells . . . . .	89
4.2.6	Therapeutic Effect of SlpB-coated Drug Loaded Liposome . . . . .	91
4.3	Discussion . . . . .	91
4.3.1	Stability, Biodistribution and Endocytosis of SlpB-LP by Intestinal APCs . . . . .	91
4.3.2	SlpB-Coating Improved Therapeutics Effect of Drugs . . . . .	94
4.4	Summary . . . . .	96
<b>5</b>	<b>Mechanism of SlpB-DC Binding</b>	<b>97</b>
5.1	Methods . . . . .	97
5.1.1	Identification of Sugar in SlpB . . . . .	97

5.1.2	Competitive Binding Assay for SlpB with Sugars . . . . .	99
5.1.3	<i>In silico</i> Analysis of Sugar-SlpB Interaction . . . . .	99
5.1.4	Trypsinisation of SlpB . . . . .	99
5.1.5	Binding of SlpB Fragments to DC . . . . .	99
5.2	Results . . . . .	100
5.2.1	Glycosylation of SlpB and Its Function in DC Interaction . . . . .	100
5.2.2	Prediction of DC-Binding Fragments in SlpB . . . . .	104
5.3	Discussion . . . . .	107
5.4	Summary . . . . .	109
<b>6</b>	<b>Conclusion and Future Prospect</b>	<b>110</b>
6.1	Summary and Discussion . . . . .	110
6.2	Future Prospects and Applications . . . . .	112

<b>Appendix A Materials and Apparatus</b>	<b>117</b>
A.1 Materials . . . . .	117
A.2 Apparatus . . . . .	120
A.3 Primers for RT-qPCR . . . . .	121
<b>Appendix B Gradient Extraction from <i>Lv. brevis</i> JCM 1059</b>	<b>122</b>
<b>Appendix C Standard Curve for Protein Quantification</b>	<b>123</b>
C.1 Bradford Method . . . . .	123
C.2 UV Method . . . . .	124
<b>Appendix D Fluorescent Labelling of SlpB</b>	<b>125</b>
<b>Appendix E Zeta Potential of Important Materials Used</b>	<b>126</b>
<b>Appendix F Optimisation of Protocols for Differentiation and Polarisation of     THP-1 Monocyte</b>	<b>127</b>
F.1 Optimisation of Concentration of PMA . . . . .	129
F.2 Optimal Concentration of LPS for DC Maturation . . . . .	133
<b>Appendix G Supplementary Figures</b>	<b>135</b>
G.1 Micrographs used in statistical analysis in Figure 4.5 (n) . . . . .	135
G.2 Micrographs used in statistical analysis in Figure 4.7 (h) . . . . .	136
<b>Appendix H Growth Curves of <i>Lv. brevis</i> and THP-1 Cells</b>	<b>137</b>
H.1 Growth of <i>Lv. brevis</i> JCM1059 . . . . .	137
H.2 Growth of THP-1 Monocytes . . . . .	137

## List of Figures

1.1	Graphical representation of challenges in gut . . . . .	4
1.2	Scanning electron micrographs of Peyer's patches . . . . .	4
1.3	Slps facilitate immune sampling of bacteria by APCs . . . . .	7
1.4	Evolutionary analysis of Slp based on amino acids sequence . . . . .	10
1.5	Graphical representation of research strategy. . . . .	12
2.1	SDS-PAGE of products extracted from the surface of <i>Lv. brevis</i> JCM 1059 . . . . .	20
2.2	$\zeta$ potential of liposome measured with liposome adsorbed with various concentration of SlpB . . . . .	22
2.3	Volume probability of liposomes measured with dynamic light scattering . . . . .	22
2.4	Fluorescence micrographs of SlpB-LP and SlpB-pLP . . . . .	23
2.5	Fluorescent micrograph of single $\text{Cy5SlpB-FITC-OVA}_{\text{LP}}$ . . . . .	23
2.6	Morphology of SlpB-LP . . . . .	23
2.7	Adsorption of SlpB on various types of carriers . . . . .	25
2.8	Fluorescent imaging of SlpB-coated solid microparticles . . . . .	25
2.9	Stability of liposome coated with various concentration of SlpB in deionised water . . . . .	27
2.10	Stability of liposomes under various pH conditions . . . . .	27
2.11	Robustness of SlpB-coating on pLP . . . . .	29
2.12	Stability of liposomes in various concentration of gall solution . . . . .	31
2.13	Stability of liposomes in simulated gastric fluid and simulated intestinal fluid . . . . .	31
3.1	Micrographs of various phenotypes of THP-1 derived cells . . . . .	43
3.2	Micrographs of expression of Mincle on M $\Phi$ and DC-SIGN on DC . . . . .	43
3.3	Expression of DC-SIGN and Mincle on various phenotypes of THP-1 derived cells . . . . .	44
3.4	SlpB binds to DC . . . . .	46
3.5	SlpB binds to Mincle and DC-SIGN . . . . .	46
3.6	SlpB blocks the binding of Ab against DC-SIGN to DC . . . . .	47

---

3.7	Sequence alignment of SlpB . . . . .	48
3.8	Flow cytometric analysis of DC co-incubated with 10 $\mu$ M PI for 70 min . . . . .	50
3.9	Endocytosis of liposomes by APCs . . . . .	51
3.10	Pinocytosis of $\text{Cy}^3\text{-OVA}_{\text{LP}}$ and $\text{SlpB-Cy}^3\text{-OVA}_{\text{LP}}$ by DC for 30 min and 70 min . . . . .	53
3.11	Particle size distribution of pLP and spLP . . . . .	55
3.12	Effect of particle size on endocytosis of liposome . . . . .	55
3.13	Phagocytosis of microbeads by $\text{M}\Phi$ and DC . . . . .	57
3.14	Phagocytosis of <i>Lp. plantarum</i> with and without SlpB by $\text{M}\Phi$ and DC . . . . .	59
3.15	Endocytosis of <i>E. coli</i> DH5 $\alpha$ by APCs . . . . .	61
3.16	Effect of uptake of SlpB-LP on endocytic activity of DC . . . . .	61
3.17	Endocytosis of liposome by DC after SlpB-treatment for various length of time . . . . .	63
3.18	Endocytosis of <i>Lp. plantarum</i> by DC after SlpB-treatment for various length of time . . . . .	63
3.19	Upregulation of expression of DC-SIGN after SlpB stimulation . . . . .	64
3.20	SlpA extracted from <i>L. acidophilus</i> JCM 1132 . . . . .	66
3.21	Effect of various Slps on endocytosis by APCs . . . . .	66
3.22	Type of endocytosis involved in internalisation of liposome and solid microparticles with <i>Lp. plantarum</i> as example . . . . .	67
3.23	Cytokines production of SlpB-stimulated DC . . . . .	69
3.24	Cytokines production of SlpB-stimulated $\text{M}\Phi$ . . . . .	69
3.25	Cytokines production of $\alpha^{\text{GC}}\text{LP}$ -stimulated APCs . . . . .	71
3.26	Cytokines production mDC stimulated with $\alpha^{\text{GC}}\text{LP}$ . . . . .	71
3.27	Mean mRNA expression of various cytokines in DC at 8, 16 and 24 h after stimulation with $\alpha^{\text{GC}}\text{LP}$ or $\text{SlpB-}\alpha^{\text{GC}}\text{LP}$ . . . . .	72
3.28	Chemical structure of $\alpha^{\text{GC}}$ . . . . .	76
4.1	Conservation of fluorescence intensity from fluorophore in whole sample . . . . .	83
4.2	SlpB-coating enhanced the stability of liposome <i>in vivo</i> . . . . .	83
4.3	Distribution of SlpB-LP in various tissues related to oral delivery . . . . .	85
4.4	Relationship of concentration of fluorophores in Peyer's patches and blood plasma . . . . .	85
4.5	SlpB enhanced transcytosis of liposome through M cells on Peyer's patches . . . . .	87
4.6	Signal intensity of GP2 and DC-SIGN from Peyer's patches after administered with LP or SlpB-LP . . . . .	88

---

4.7	Uptake of liposome into mice Peyer's patches. . . . .	90
4.8	mRNA expression of various cytokines in mice Peyer's patches 8 h after administration with $\alpha^{\text{GC}}\text{LP}$ or $\text{SlpB-}\alpha^{\text{GC}}\text{LP}$ . . . . .	92
5.1	Sugar binding domain on SlpB receptors. (a) Interaction of tetramannose to carbohydrate recognition domain (CRD) of DC-SIGN (PDB: 1SL4). (b) Interaction of trehalose to Mincle (PDB: 4KZV). . . . .	98
5.2	Identification of sugars in SlpB . . . . .	101
5.3	Monosaccharides inhibit binding of SlpB to DC . . . . .	101
5.4	Predicted structure of N-terminal of SlpB and its sugar binding sites . . . . .	103
5.5	Chromatograms which indicate fragments of SlpB binds to DC . . . . .	105
5.6	Binding assay of fragments of SlpB to DC . . . . .	106
5.7	Predicted model of SlpB/DC-SIGN interaction . . . . .	108
6.1	Function of charge in SlpB-lipid interaction and SlpB-DC interaction, and mechanism of endocytosis . . . . .	113
B.1	SDS-PAGE of product extracted with 1 M to 5 M LiCl solution . . . . .	122
C.1	Standard curve of Bradford method measured by BSA . . . . .	124
D.1	SDS-PAGE of Cy5-labelled SlpB . . . . .	125
E.1	$\zeta$ potential of materials used in this study . . . . .	126
F.1	Microscopic inspection of well plate after cell detachment . . . . .	128
F.2	Expression of DC-SIGN induced by 50 nM PMA stimulation followed by 20 ng $\text{ml}^{-1}$ rhIL-4, each for 48 h incubation in 37°C, 5.0% $\text{CO}_2$ humidified incubator . . . . .	128
F.3	Morphology of THP-1 monocytes after stimulation with various concentration of PMA for various length of time. . . . .	130
F.4	Colour of culture medium after 48 h recovery . . . . .	131
F.5	Flow cytometry analysis of DC-SIGN expression of DC stimulated with various concentration of PMA . . . . .	131
F.6	Relative density of DC-SIGN expressed in DC stimulated with various concentration of PMA . . . . .	132
F.7	Difference in cell morphology based on scattering signal . . . . .	134



F.8	Relationship between IL-6 production and cell viability against concentration of LPS . . . . .	134
G.1	Micrographs used in statistical analysis in Figure 4.5 (n) . . . . .	135
G.2	Micrographs used in statistical analysis in Figure 4.7 (h) . . . . .	136
H.1	Growth curve of <i>Lv. brevis</i> JCM1059 when incubated statically at 30°C . . . . .	138
H.2	Example of growth curve of THP-1 monocytes when cultured in tissue culture flasks and incubated statically in 37°C, 5.0% CO <sub>2</sub> humidified incubator . . . . .	138

# Chapter 1

## Introduction

The function of drugs depend on its dosage<sup>[1]</sup>. Overdose or delivery of drugs to undesired site result in adverse effect, which will cause mortality of patients in some case. Therefore, drugs have to be administered at correct dose, at targeted location. Conventionally, to ensure enough concentration of drugs are delivered to their target site, drugs were usually administered overdose, which results in various adverse effect and suffering of patients.

Drug delivery systems (DDSs) were developed to address the above-mentioned problem in drug delivery. First generation DDSs which have been developed since 1950s have exploited 4 major drug release mechanisms, i.e., diffusion, dissolution, osmosis, and ion-exchange to achieve control release of drugs. To date, most orally administered drugs still depend on diffusion and dissolution of drugs in gut.

However, first generation DDS did not answer the needs of drug targeting. When drugs are administered orally, portion of drug molecules are absorbed by gastrointestinal (GI) tract into portal vein and delivered to target site by blood vessels. This system possess 3 great limitations: (1) first pass elimination by liver<sup>[2]</sup> which results in low bioavailability; (2) clearance by macrophage<sup>[3]</sup> which reduces retention time in blood; (3) delivery of drugs to undesired site which results in adverse effect.

Second generation DDS was developed to ensure delivery of drugs to target site in biological system. This system, which is also known as targeted-ligand DDS (TLDDS) or smart DDS, is an attractive approach in DDS. TLDDS achieve high targeting precision by incorporating ligand recognised by specific cells into drugs vehicle (or cargo). Then, ligand-receptor interaction will facilitate drugs accumulation at target site and achieve controlled release of drugs.

There are two ways to administer TLDDS-encapsulated drugs, i.e., (1) through injection or dripping and (2) oral delivery. Generally, injection or dripping of drugs (1) is invasive, (2) carriers of drugs are subject to clearance by immunocytes in blood stream, (3) results in strong adverse effect, e.g., anaphylaxis due to coating of carriers with synthetic polymers<sup>[4]</sup>, (4) inconvenient

and time-consuming as patients are required to visit medical facility, and for dripping of drugs, patients have to be immobilised throughout the process, (5) cost inefficient as professional medical staffs are required for drugs administration, (6) which all of the stated disadvantages have resulted in low patients preference and higher degree of suffering.

On the other hand, oral administration of drugs can address all the drawbacks of drug administration through injection and dripping, allow access of drugs into the largest mammalian immune organ, i.e., Peyer's patches, and into both blood stream and lymph depending on the hydrophilicity of drugs<sup>[5]</sup>. Access to Peyer's patches and lymph is particularly attracting features of oral delivery of drugs, particularly for immunomodulating drugs. Delivery through lymph not only bypass first pass elimination of drugs by liver<sup>[6,7]</sup>, but also prevent drugs from enzymatic degradation in GI tract wall. However, environment in GI tract is harsh and diverse (Figure 1.1). Oral delivery is subject to the challenges of various salts, pH and enzymatic reaction throughout GI tract. Furthermore, mechanical stress induced by agitation and changes in pH will results in instability of drugs. In stomach (pH 1 - 3), various enzymatic activities which could degrade proteins and drugs take place, and the resident time in stomach is 0.5 - 4 h, depends on the fasting condition of patients. When drugs arrive in small intestine, they will come into environment which induce poor aqueous solubility, encounter intestinal mucosal barrier which block the access of drugs, and the resident time range from 1 - 2 h, which is short for drugs absorption<sup>[8]</sup>. Furthermore, bile can emulsify lipid, and lipase in pancreatic juice could digest lipids, e.g., liposome. Sugar and polymers coating of carriers will also be digested by various enzymes. Wide pH ranges and mechanical stress in GI tract is also a challenge to the choice of ligand, as most ligands can only be stable in either acidic, neutral or alkaline environment, but not across the range of pH 1 - 9.

## 1.1 Strategies Proposed for Oral Delivery of Drugs

Various approaches have been proposed for oral delivery of drugs, either by enhancing stability of carriers or facilitating targeted delivery of carriers by surface functionalisation.

Peyer's patches are immune organs located in mammals' gut<sup>[9]\*</sup> (Figure 1.2 (a-b)). Epithelial surface of Peyer's patches forms a nature barrier against intestinal content in lumen, separating luminal and subepithelial environments. Microfold (M) cells are developed among enterocytes in the epithelial surface of Peyer's patches. M cells are specialised transcytic cells responsible

---

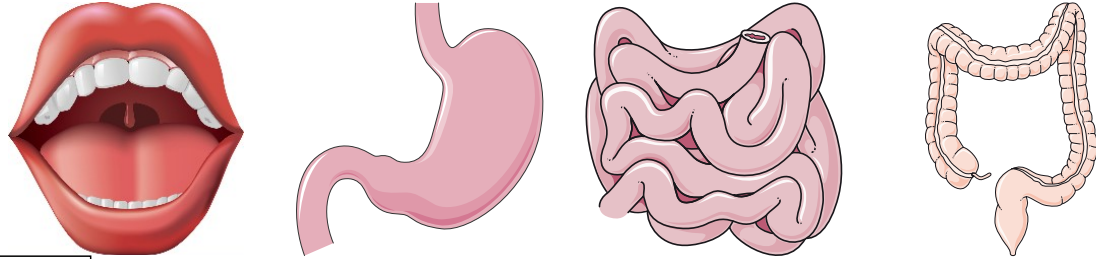
\* p. 7, 15, 22, 24

to transcytose bacteria and nanoparticles into Peyer's patches<sup>[10,11]</sup> (Figure 1.2 (c - d)). The transcytic property of M cells can be exploited for drug delivery to antigen presenting cells (APCs) in Peyer's patches. As M cells is capable to transcytose solid particles, various strategy has been proposed to enhance stability of drugs carriers by encapsulating drugs compound in solid nanoparticles or bacteria.

For instances, previous study has demonstrated intestinal DC-targeting by functionalising M cells targeting-arginylglycylaspartic acid on DC-targeting RGD-modified chitosan nanoparticles. The formulation has also protected heat shock proteins 65-6×P277 (H6P) encapsulated in nanoparticles against intestinal environment. The result showed enhanced transportation of chitosan nanoparticles into Peyer's patches, targeted endocytosis by DC, and anti-diabetic effect induced by H6P. However, the carriers were administered by loop ligated method, and the stability of nanoparticles against diverse environment in GI tract remained uncertain<sup>[12]</sup>. Particularly, stability of nanoparticle might be compromised in acidic environment of stomach.

Recently, a nanocomposite which target M cells by functionalising 3-aminopropyl-functionalised magnesium phyllosilicate (aminoclay)-insulin complex with ulex europaeus agglutinin 1 (UEA-1) has been developed<sup>[13]</sup>. The drug-clay complex was coated with Eudragit® L-100, which is a pH responsive polymer capable to dissolve at  $\text{pH} > 6.0$ . Eudragit® L-100 protects the nanocomposite from degradation in stomach; when the nanocomposites reach intestine, which has  $\text{pH} > 6.0$ , Eudragit® L-100 dissolve, and UEA-1 binds specifically to villi and M cells to enhance absorption of drugs. However, coating with pH responsive polymer has limited practical application. In real-life settings, nanoparticles have to pass through mouth and oesophagus where the pH is  $> 6.0$  before it has been delivered to stomach. Thus, the nanocomposites are susceptible to degradation by gastric juice.

Furthermore, the uptake of solid microparticles (both nanoparticles and bacteria) are less efficient than liposome due to difference in endocytic pathway. Despite of the higher tendency of liposomes to be endocytosed by cells, they are relatively unstable in gut environment. To date, 27 formulations of liposomal drugs have been approved by the U.S. Food and Drug Administration (FDA)<sup>[14]</sup>, with an addition of 2 vaccines for COVID-19 which sum up to 29 formulations. However, none of these formulations is administered orally, suggesting the technical complexity of oral delivery of liposomes in spite of the importance of this technology, particularly leakage of drugs compound from liposomes, emulsification of liposome by bile acid, enzymatic hydrolysis by lipase, degradation by mechanical stress, and instability due to pH changes.



Properties	Mouth	Stomach	Intestine	Colon
	pH 5 - 7 5 - 60 s	pH 1 - 3 0.5 - 4 h	pH 6 - 7.5 1 - 2 h	pH 5 - 9 12 - 24 h
	<ul style="list-style-type: none"> <li>• Salts</li> <li>• Enzymes</li> </ul>	<ul style="list-style-type: none"> <li>• Salts</li> <li>• Enzymes</li> <li>• Agitation</li> </ul>	<ul style="list-style-type: none"> <li>• Salts, bile</li> <li>• Enzymes</li> <li>• Agitation</li> </ul>	<ul style="list-style-type: none"> <li>• Bacteria</li> <li>• Enzymes</li> <li>• Agitation</li> </ul>
Challenges	<ul style="list-style-type: none"> <li>• Taste</li> </ul>	<ul style="list-style-type: none"> <li>• Gastric degradation</li> </ul>	<ul style="list-style-type: none"> <li>• Poor aqueous solubility</li> <li>• Lipid emulsification</li> <li>• Mucosal barrier</li> <li>• Short residence time</li> </ul>	<ul style="list-style-type: none"> <li>• Poor aqueous solubility</li> <li>• Mucosal barrier</li> <li>• Bacteria</li> </ul>

Figure 1.1 Graphical representation of challenges in gut.

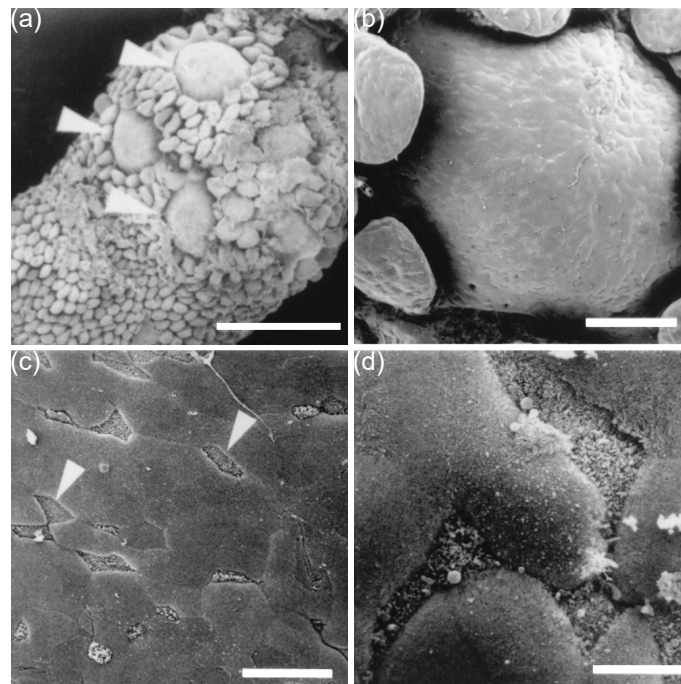


**Figure 1.2** Scanning electron micrographs of Peyer's patches. (a) Peyer's patches are villusless surface located in small intestine (indicated with white arrows). The scale bar is 700  $\mu\text{m}$ . (b) Epithelial surface of Peyer's patch. The scale bar is 100  $\mu\text{m}$ . (c) Distribution of M cells on the surface of Peyer's patches. M cells can be recognised from SEM with their dark, short brush border (indicated with white arrows). The scale bar is 20  $\mu\text{m}$ . (d) Close-up micrograph of M cells. The scale bar is 6  $\mu\text{m}$ . Adapted with permission from Ref 15.

*To achieve oral delivery of drugs to target intestinal APCs, it is important to develop a TLDDS which could enhance stability of carriers against gut environment, and to target intestinal APCs via ligand-receptors interaction.*

## 1.2 Surface Layer Proteins

Intense studies on gut microbiota have discovered that their surface layer proteins (Slps) are the component which involves in interaction with host cells (Figure 1.3), particularly through binding to intestinal cells and extracellular matrices (ECMs) in gastrointestinal tract (Table 1.1), and involves in immunomodulation<sup>[16–22]</sup>. For instances, SlpA from *Lactobacillus acidophilus* (*L. acidophilus*) could facilitate transcytosis of bacteria by M cells via SlpA-uromodulin interaction<sup>[23]</sup>, and enhanced phagocytosis by dendritic cells via SlpA-dendritic cell-specific intercellular adhesion molecule-3-grabbing non-integrin (DC-SIGN) interaction<sup>[24]</sup>. Other lactobacilli, e.g., *Levilactobacillus brevis* (*Lv. brevis*), *Ligilactobacillus salivarius* (*Lg. salivarius*), *Lentilactobacillus kefir* (*Lt. kefir*) also possess Slps which interact with intestinal cells and APCs. These properties of Slps indicate that Slps are actively interacting with receptors of cells in human immune system, and these proteins are promising candidate ligands for drug delivery system of immunomodulators.

However, some Slps are unapplicable in drug delivery system, e.g., extraction of Slp from *C. difficile*<sup>[25]</sup> might lead to co-extraction of other pathogenic surface layer components. On the other hand, most species in genera of lactobacilli are generally non-pathogenic<sup>[26]</sup>, which the surface layer components can be safely used in food and drugs with least concern on pathogenicity. Comparing the characteristics of Slps from lactobacilli and Slps from other genus (Table 1.2) shows that Slps from lactobacilli generally exhibit high isoelectric point, which is resulted from higher ratio of positive to negative charged amino acid residues. As Slps binds to negatively-charged bacterial surface via non-covalent bonding, thus, Slps with higher isoelectric point generally possess higher binding affinity compared to Slps with lower isoelectric points. This property of Slps from lactobacilli is more advantageous than Slps from other genera, as these Slps from lactobacilli can maintain their binding to the surface of carriers in environment with higher pH, e.g., in small intestine and colon.

**Table 1.1** Relationship between Slp and receptor

Strains	Slp	Receptor	Targeted location	Ref
Lactobacilli				
<i>L. acidophilus</i> NCFM	SlpA	DC-SIGN	Dendritic cell	24
<i>L. acidophilus</i> L-92	SlpA	Uromodulin	M cell	23
<i>L. acidophilus</i> 33199	SlpA	Fibronectin	Human intestinal epithelial cell line	27
<i>L. acidophilus</i> CIC 6074	Slp	-	Caco-2 cell	28
<i>L. acidophilus</i> ATCC 4356	Slp	DC-SIGN	Human dendritic cell	29
		Collagen (I, IV)	ECM	30,31
<i>L. crispatus</i> JCM 5810	CbsA	Laminin	ECM	22
		Teichoic acid	Bacteria	22
<i>L. helveticus</i> MIMLh5	SlpA	TLR2	Human macrophage cell U937	32
<i>L. helveticus</i> ATCC 12046	Slp	DC-SIGN	Human dendritic cell	29
<i>Lv. brevis</i> ATCC 8287	SlpA	Fibronectin	Human intestinal epithelial cell line	21
		DC-SIGN	Human dendritic cell	29
<i>Lv. brevis</i> ATCC 14869	Slp	Mincle	Antigen presenting cell	33
		Fibronectin	Human intestinal epithelial cell line	27
<i>Lg. agilis</i> 43564	SlpA	Fibronectin	Human intestinal epithelial cell line	27
<i>Lg. salivarius</i> REN	CbpA	Enolase	Human colorectal adenocarcinoma cell	34
<i>Lt. kefir</i> CIDCA8315	Slp	-	Red blood cell	35
			<i>Saccharomyces lipolytica</i>	36
<i>Lt. kefir</i> JCM 5818	Slp	DC-SIGN	Human dendritic cell	29
<i>Lt. parakefir</i> CICDA8328	Slp	-	Red blood cell	35
Clostridium				
<i>C. difficile</i> 630	Cwp2	-	Caco-2 cell	37
<i>C. difficile</i>	Slp	TLR4	Bone marrow-derived dendritic cell	38
Aeromonas				
<i>A. salmonicida</i> A449	VapA	Fibronectin	ECM	39
		Laminin		39
Bacillus				
<i>B. anthracis</i> AP422	BslA	Laminin	ECM	40
Tannerella				
<i>T. forsythia</i> ATCC 43047	G-Slp	Mincle	Macrophage	19
Sulfolobus				
<i>Sulfolobus</i>	Slp	FlaF	-	41

<sup>a</sup> Abbreviation: *L. acidophilus*: *Lactobacillus acidophilus*; *L. crispatus*: *Lactobacillus crispatus*; *L. helveticus*: *Lactobacillus helveticus*; *Lv. brevis*: *Levilactobacillus brevis*; *Lg. agilis*: *Ligilactobacillus agilis*; *Lg. salivarius*: *Ligilactobacillus salivarius*; *Lt. kefir*: *Lentilactobacillus kefir*; *Lt. parakefir*: *Lentilactobacillus parakefir*; *C. difficile*: *Clostridium difficile*; *A. salmonicida*: *Aeromonas salmonicida*; *B. anthracis*: *Bacillus anthracis*; *T. forsythia*: *Tannerella forsythia*; ECM: Extracellular matrix; TLR: Toll-like receptor

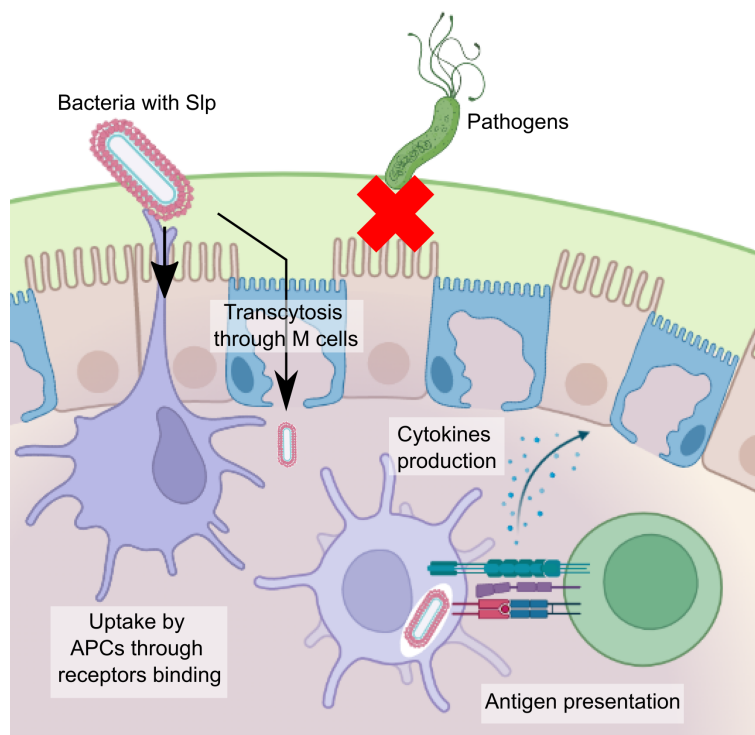


**Figure 1.3** Slps facilitate immune sampling of bacteria by APCs. Slps enhance transcytosis of bacteria into Peyer’s patches by M cells, and phagocytosis by APCs. Then, the bacteria are lysed in endosome or phagosome. The antigen contains in bacteria are presented to T cells, and immunomodulation occurs, e.g., via cytokines production. Without Slps, access of pathogens to Peyer’s patches are limited.

**Table 1.2** Comparison of lactobacilli Slps with Slps from bacteria of other genera.

	Slp from lactobacilli	Slp from other genus
General characteristics	<ul style="list-style-type: none"> <li>• Represent 10 – 15% of all proteins expressed (abundant in expressing strain)</li> <li>• Crystalline arrays are 2.5 – 35 nm thick</li> <li>• 70% porosity</li> <li>• 31.9 – 38.7% hydrophobic amino acid</li> <li>• Non-covalently bind to bacterial surface</li> <li>• Single band in SDS-PAGE</li> <li>• 40 - 60% [mol] hydrophobic amino acids</li> </ul>	
Isoelectric point	High	Low
Toxicity	Non-pathogenic	Might be poisonous
Size, kDa	25 - 71	40 - 200
Hydroxylated amino acid	23 - 33%	15%
Lysine content	10% (basic)	< 10% (acidic)
Positive/negative charged residue	High	Low



Sequencing analysis has revealed that there are only approximately 5% lactobacilli possess Slps. Phylogenetic analysis based on amino acid sequence (Figure 1.4) categorise these Slps from lactobacilli into 2 categories, which I define them as Group A Slps, which consists of Slps from *L. acidophilus* group, and Group B Slps which consists of Slps from *Lv. brevis* group. Hereinafter, I define Group A Slps as SlpAs and Group B Slps as SlpBs, unless otherwise mentioned for some exceptions, e.g., SlpA from *Lv. brevis* or SlpB from *L. acidophilus*, etc. SlpAs and SlpBs differed from their position of functional domains. Generally, Slps exhibit mostly 2 separated morphological regions, (1) cell wall binding domain and (2) self-assembly domain. Cell wall binding domain is conserved across species, and this domain exhibit high isoelectric point and is hydrophilic; in contrast, non-conserved self-assembly domain is hydrophobic, and exhibit low isoelectric point. The self-assembly domain with low isoelectric point is located in N-terminal for SlpAs, while it is located in C-terminal of SlpBs. Interestingly, although it has been demonstrated that C-terminal of SlpAs bind to cell wall, while N-terminal binds to extracellular matrices, e.g., fibronectin and collagen<sup>[42]</sup>; N-terminal of Group B Slps bind to both cell wall and host proteins, i.e., receptors and extracellular matrices<sup>[21,43]</sup>. Furthermore, unlike SlpAs which bind to lipoteichoic acid as anchor<sup>[42]</sup>, SlpBs bind to cell surface via hydrogen bonding<sup>[44]</sup>. These fascinating properties of SlpBs render them an attractive ligand for drug delivery, particularly to be coated on various surface without peptidoglycan or lipoteichoic acid as anchor.

Moreover, Slps are self-assembling crystalline array proteinaceous subunits which form the outermost layer of bacteria and archaea<sup>[45]</sup>. These proteinaceous subunits of Slps generally self-assemble into 2-dimensional crystalline arrays, which form oblique (p1, p2), square (p4) or hexagonal (p3, p6) space group symmetry<sup>[46]</sup>. Crystalline array formed on the surface of bacteria are generally tightly packed, and has pore size ranging from 10 - 100 Å, which could limit and even prevent penetration of large molecule. Furthermore, Slps could resist enzymatic hydrolysis at their crystalline domain<sup>[43,47]</sup>. Study has also demonstrated that Slps could protect bacteria from changes in temperature and ion concentration<sup>[48]</sup>. By exploiting these protective properties of Slps, we could protect liposome from enzymatic hydrolysis, and constant changes in pH and salinity in GI tract.

### 1.2.1 Slp-Coating on Liposome

Slps can reassembled spontaneously on air-water and oil-water interfaces, on solid surfaces, in suspension, and driven by entropy<sup>[46]</sup>, which make the process of functionalisation simple. By

co-incubating liposome with Slps, Slps can be self-adsorbed on the surface of liposome through charge interaction, condensed and self-catalysed to form crystalline array<sup>[49]</sup>.

Various groups have studied the recrystallisation and application of Slps to improve stability of drugs carriers, particularly liposome<sup>[50–57]</sup>. Mader et al. have demonstrated stabilisation of liposomes coated with Slp from *Geobacillus stearothermophilus* against shear forces, ultrasonication and temperature shift from 25°C to 55°C<sup>[51]</sup>. For liposomes coated with Slp from *Lv. brevis* and treated with glutaraldehyde, 74.5% carboxyfluorescein (CF) remained enclosed in liposome after 60 min, while 65.9% CF remained enclosed after 120 min in pH 2.5, compared to 44.6% and 28.7% respectively from liposome without Slp-coating. Furthermore, more than 90% CF remained enclosed in liposome coated with *Lv. brevis* after 60 min; more than 80% remained enclosed after 120 min at 37°C at pH 7, with or without glutaraldehyde treatment<sup>[55]</sup>. Increase in pH and thermal stability were also observed for liposome coated with Slp from *Lt. kefirii*<sup>[55]</sup>. Study has also shown that SlpA from *L. acidophilus* could enhance thermal stability, storage stability and serum stability of liposome<sup>[57]</sup>. Regardless glycosylation, coating of Slps of lactobacilli could improve stability of liposomes against both physical and chemical stress.

However, problems remained with Slp-coated liposomes. Slp-coating could decrease surface charge of liposome to negatively-charged<sup>[55,57,58]</sup>. Alteration of surface charge of liposome by Slp might interfere endocytosis of liposomes by cells<sup>[59,60]</sup>. Furthermore, some Slps could interact with extracellular matrix, which results in drug released at epithelial or mucosal layer before encountering intestinal APCs, e.g., drug delivery with liposomes coated either with SlpAs from *L. acidophilus*<sup>[61]</sup> or *L. helveticus*<sup>[58,62]</sup> have suggested that liposomes were delivered to epithelial cells or mucosal layer of gut. While this approach is useful for delivery of peptides and vaccine which do not required cell-targeting, it might result in unexpected adverse effect on other types of immunomodulators.

The bursting of liposome before reaching intestinal APCs might be due to the interaction of self-assemble domain of SlpAs with extracellular matrices<sup>[31,63]</sup>, as shown in Table 1.1 and discussed in this section. Binding of Slps to extracellular matrices, e.g., mucosal layer or gut epithelial cells resulted in uptake of liposomes into these cells, thus retention of liposome and drug release before reaching intestinal APCs.

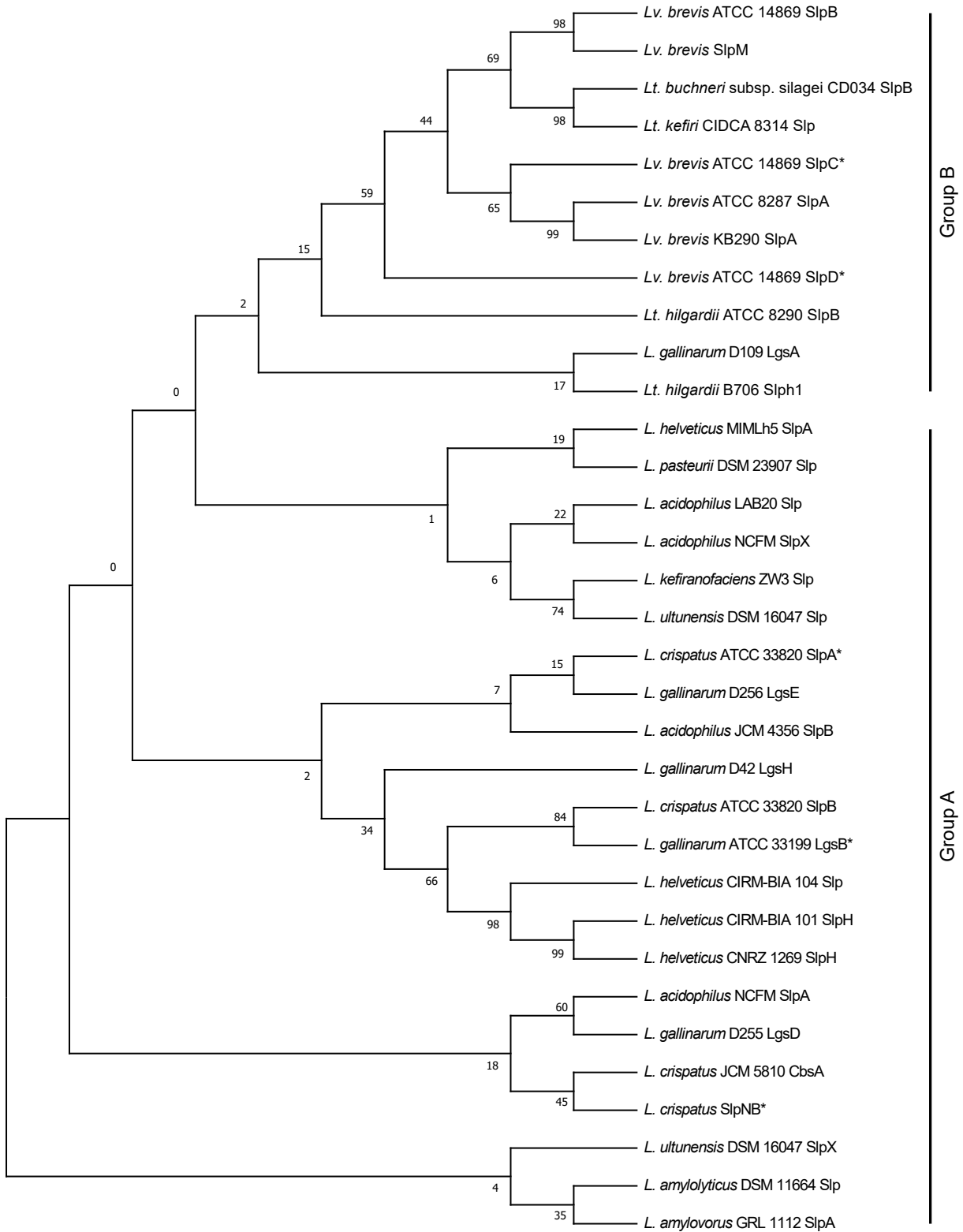


**Figure 1.4** Evolutionary analysis of Slp based on amino acids sequence by maximum likelihood method. The evolutionary history was inferred by using the Maximum Likelihood method and JTT matrix-based model<sup>[64]</sup>. The bootstrap consensus tree inferred from 500 replicates is taken. The percentage of replicate trees in which the associated taxa clustered together in the bootstrap test 500 replicates are shown next to the branches.

### 1.3 Objective

The objective of this study is to investigate the potential of Slp-coated carriers as TLDDS to target intestinal APCs.

The objective of this study can be further divided into 3 goals:

1. Improvement of the stability of liposome in GI tract
2. Induction of intestinal APCs-targeting effect
3. Improvement of therapeutic effect of immunomodulating drugs

Both stability of liposome and cell targeting capability are important aspects in intestinal APCs-targeting, while adjuvant effect is important to improve therapeutic effect of drugs. SlpB from *Lv. brevis* JCM 1059 has been shown to exhibit these properties, and it is potential ligand to improve stability of liposome, induce APCs targeting effect in gut, and to enhance therapeutic effect of immunomodulatory drugs at the same time. In this study, I aim to improve the stability of liposome in gut mimicking environment by exploiting the property of SlpB to self-assemble into protective crystalline array on various interfaces, particularly, water-oil interface. Then, I will investigate the potential of SlpB as ligand for receptors on intestinal APCs and M cells in Peyer's patches. Adjuvant effect induced by SlpB will be evaluated, and the improvement of therapeutic effect through SlpB-coating will be investigated with drug-loaded liposome.

### 1.4 Research Strategy

To overcome challenges remained in prior studies, I have selected SlpB from *Lv. brevis* JCM 1059 as ligand. Sequence alignment and analysis (which will be shown in Chapter 3) suggests that its binding domain is in the opposite terminal to self-assemble domain, thus could prevent unspecific binding to extracellular matrices and to epithelial cells. Reduction of unspecific binding raises the opportunity of delivery of carrier into Peyer's patches where intestinal APCs reside. Furthermore, prior studies have already shown that SlpB binds to Mincle of macrophage ( $M\Phi$ ), and potentially binds to DC-SIGN on DC, which makes it a good ligand to target APCs. My research strategy is summarised in Figure 1.5.

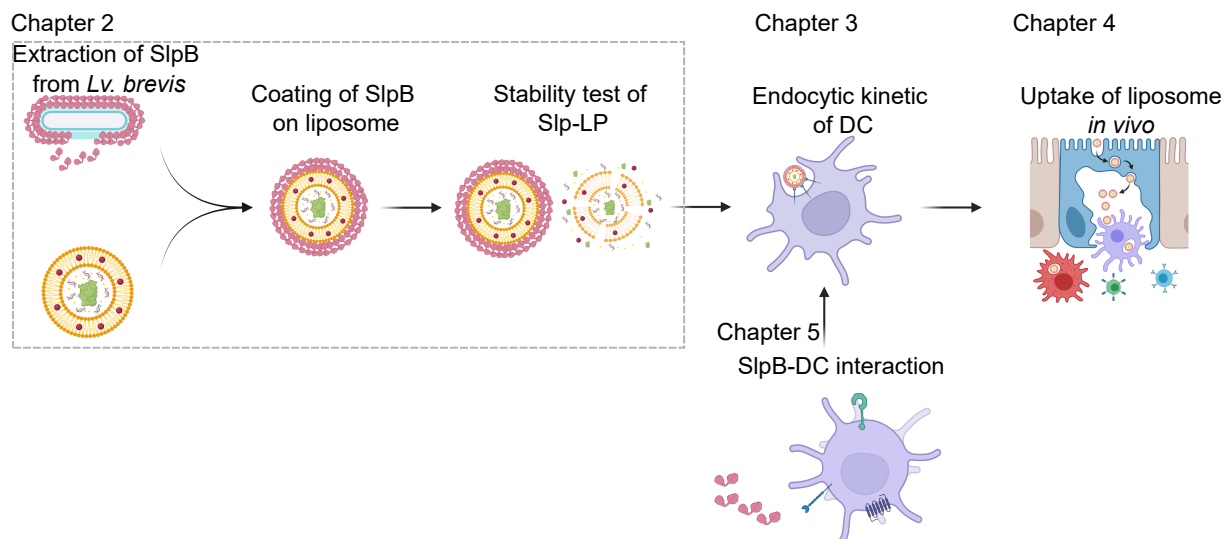


**Figure 1.5** Graphical representation of research strategy.

## 1.5 Structure of Dissertation

This dissertation is structured as follows:

Chapter 2 discusses the method to prepare SlpB-coated carriers with focus on liposomes, and the characterisation of SlpB-coated carriers. Furthermore, I will also discuss stability of SlpB-coated liposome in various gut mimicking environment *in vitro*.

Chapter 3 discusses the interaction of SlpB with DC-SIGN and investigates whether SlpB-coating will improve endocytosis of carriers by APCs. Moreover, the possibility of improvement therapeutic effect of drugs due to enhanced endocytosis will also be explored.

Chapter 4 investigates oral delivery of SlpB-coated liposome to intestinal APCs, and therapeutic effect of drug-loaded liposomes improved by the advantages provided by SlpB-coating.

Chapter 5 explores the mechanism of interaction of SlpB with DC.

List of materials, apparatus and primers used in this study, supplementary figures of micrographs used in statistical analysis, physical properties of materials, e.g.,  $\zeta$  potential, supplementary curves, and data related to phenotypes of cells, growth of bacteria, protocols for proteins extraction are listed in Appendices.

## Chapter 2

# Preparation and Characterisation of Surface Layer Protein-Coated Liposomes

While bacterial surfaces are generally negatively-charged, prior studies have focused on Slp-coating on cationic liposomes which have opposite surface charge compared to bacterial surfaces. These studies have investigated the physiochemical properties of SlpBs-coated cationic liposomes, and demonstrated that Slp-coating could enhanced stability of cationic liposomes<sup>[55,65]</sup>. However, coating of Slp on the surface of anionic liposomes were not reported. It is possible that coating of Slp on anionic liposomes can preserve their native orientation and probably the space group symmetry of crystalline array due to charge similarity to bacterial surface. Furthermore, higher concentration of Slp might be able to be coated on anionic liposome as Slp from lactobacilli are generally positively charged due to their high isoelectric point. Anionic surface of liposome provides higher density of charge to attract Slp, and for Slp to coat on the surface.

Stability is the most critical shortcoming of liposome as drug delivery system, particularly as drug carrier for oral administration, due to the complex and harsh environment in gut. Therefore, it is important to enhance stability of liposome against various pH, bile acid, enzymatic degradation, salinity and mechanical stress to enable proper function of liposome as drug carriers for oral delivery.

Various studies have reported that Slp-coating enhances stability of liposome in various pH, bile acid, pancreatic juice, serum, and against physical and mechanical stress<sup>[51,55,57]</sup>. These benefits of Slp-coating improve stability of carriers, particularly liposome in gut environment and in sera, thus increase the chance of drugs delivery to their target site, while preventing unspecific delivery and degradation of drugs due to degradation of carriers. Higher density of SlpB-coating and correctly formed crystalline array might increase the stability of liposome, particularly against enzymatic degradation.

In addition, cationic liposomes are poisonous to cells, with the highest toxicity to phagocytic

cells<sup>[66,67]</sup>. Therefore, anionic liposome might be a more suitable drug carrier for drug delivery to APCs.

In this chapter, I will investigate the possibility to coat SlpB on anionic surface and characterise SlpB-coated carriers. SlpB will be extracted from *Lv. brevis* JCM 1059 and coated on drug carriers. Coating of SlpB will be confirmed with microscopy and adsorption curve measured by  $\zeta$  potential and fluorescence intensity. Then, I will investigate the potential of SlpB in improving stability of anionic liposomes in simulated GI environment *in vitro*.

## 2.1 Methods

### 2.1.1 Preparation of Surface Layer Protein B

To prepare seed culture of *Lv. brevis*, 1  $\mu$ l cyro-preserved *Lv. brevis* JCM 1059 was inoculated in 10 ml Man, Rogosa & Sharpe (MRS) broth in a sterile screw-capped test tube. The test tube was tightly capped, sealed with Parafilm<sup>®</sup>, and incubated statically at 30.0°C for 48 h.

Then, the culture was inoculated in fresh MRS broth in medium bottle at 1000<sup>-1</sup> dilution factor, tightly capped, sealed with Parafilm<sup>®</sup>, and incubated statically in 30.0°C incubator for another 48 h. For each lot of *Lv. brevis* JCM 1059, 4 ml of culture was collected, and equally distributed into 4 microcentrifuge tubes. A tube of culture was used to determine turbidity by measuring optical density at 600 nm, while 3 tubes of culture were used to determine the dry cell mass of *Lv. brevis* JCM 1059 contained in 1 ml culture.

*Lv. brevis* JCM 1059 was pelleted at 5,600  $\times g$ , 4°C for 15 min. The pellet was washed with phosphate-buffered saline (PBS; -). Then, the pellet was suspended with 1 M lithium chloride (LiCl) solution at 10<sup>-1</sup> volume of original culture and agitate with mini-rotator at 2 rad s<sup>-1</sup> for 30 min, twice, to remove surface layer associated protein. SlpB was extracted with 5 M LiCl solution at 10<sup>-1</sup> volume of original culture and agitated with mini-rotator at 2 rad s<sup>-1</sup> for 30 min. The concentration of LiCl solution used in this dissertation is justified in Appendix B.

Protein extracted from *Lv. brevis* JCM 1059 was filtered through 0.22  $\mu$ m polyvinylidene fluoride (PVDF) membrane and dialysed against 300-volume of deionised water for 20 h at 4°C. Then, 20  $\mu$ l of each fraction was analysed with sodium dodecyl sulphate-polyacrylamide gel electrophoresis (SDS-PAGE; 10%) and stained with silver. The concentration of SlpB was measured with both absorbance at 280 nm and Bradford assay with bovine serum albumin (BSA) as standard. The method for protein quantification was compared and justified in Appendix C.

### 2.1.2 Fluorescent Labelling of SlpB

For fluorescence imaging of SlpB on carriers, SlpB was labelled with tetramethylrhodamine (Cy3), 6-[[2-[5-[1-[6-(succinimidyl-oxo)-6-oxohexyl]-3,3-dimethyl-5-sulphonato-1H-indole-2(3H)-ylidene]-1,3-pentadienyl]-3,3-dimethyl-5-sulphonato-3H-indole-1-ium]-1-yl] hexanoic acid succinimidyl (Cy5) or fluorescein isothiocyanate (FITC).

SlpB in 0.1 M carbonate-bicarbonate buffer (pH 9.2) was supplemented to Cy3, Cy5 or FITC dissolved in dimethyl sulphoxide (DMSO). The mixture was agitated in dark for 120 min, followed by dialysis against 300-volume of deionised water for 20 h at 4°C to remove free-dye molecule, DMSO and salts.

Concentration of labelled SlpB was quantified with NanoDrop spectrophotometer, and adjusted either by concentration with 10 K centrifugal filter unit or dilution with deionised water. SlpB labelled with FITC, Cy3 and Cy5 are known as <sup>FITC</sup>SlpB, <sup>Cy3</sup>SlpB and <sup>Cy5</sup>SlpB respectively.

### 2.1.3 $\zeta$ Potential and Particle Size of SlpB-Coated Liposome

To detect the adsorption of SlpB on liposomes and to identify the maximum adsorption capacity of liposome, adsorption curve of SlpB on liposome was prepared. Monodisperse lyophilised anionic liposome (LP; Coatsome EL-01-A; ratio of L, $\alpha$ -dipalmitoyl-phosphatidylcholine (DPPC): cholesterol: L, $\alpha$ -dipalmitoylphosphatidylglycerol (DPPG) = 3: 4: 3; polydispersity index by dynamic light scattering = 0.09) was rehydrated with deionised water at 50 mg ml<sup>-1</sup>, and diluted to 1 mg ml<sup>-1</sup>; polydisperse anionic liposome (pLP; Presome PPG-1; ratio of DPPC: cholesterol: DPPG = 1: 1: 0.2; polydispersity index by dynamic light scattering = 1.23) was rehydrated with deionised water at concentration of 1 mg ml<sup>-1</sup> and heat at 60°C for 30 min to dissolve the liposome. pLP was used to evaluate the effect of size and polydispersity of liposome on SlpB-coating, stability of liposome and endocytosis of liposome. Then, 10  $\mu$ g liposome at 20°C was supplemented to various concentration of SlpB, agitated for 120 min at 20°C, and centrifuged at 16,000  $\times g$  to remove excess SlpB.

To measure the electrophoretic mobility of liposome, 150  $\mu$ l suspension was injected into carbon electrode cuvette, and electrophoretic mobility of liposomes were measured with nano particle analyser by electric field of 4 V at 25°C.

Changes in  $\zeta$  potential of liposomes can be detected by electrophoretic mobility of liposomes when an electric field is charged across the suspension. The relationship between electric mobility



of liposomes and  $\zeta$  potential is defined as:

$$\zeta = \frac{U\eta}{\varepsilon f(\kappa r)} \quad (2.1)$$

where  $\zeta$  is  $\zeta$  potential,  $U$  is electrophoretic mobility,  $\eta$  is the viscosity of solvent,  $\varepsilon$  is dielectric constant of solvent,  $f(\kappa r)$  is Henry's function.

Here, electrophoretic mobility is defined as

$$U = \frac{\lambda\nu_d}{2En\sin(\frac{\theta}{2})} \quad (2.2)$$

where  $\lambda$  is the wavelength of laser,  $\nu_d$  is the frequency of scattered light,  $E$  is electric field,  $n$  is refractive index of solvent, and  $\theta$  is the angle of frequency shift of scattered light. Smoluchowski equation was used as Henry's function in Equation 2.1, and an adsorption curve of SlpB on each type of liposome was plotted.

#### 2.1.4 Fluorescent Imaging of SlpB-LP

Adsorption of SlpB on the surface of liposome is confirmed with fluorescent imaging of SlpB-LP. LP was rehydrated in FITC solution at final concentration of 100  $\mu\text{M mg}^{-1}$  [FITC LP<sup>-1</sup>]. The mixture was agitated at 20°C for 60 min to facilitate encapsulation of FITC; for pLP, lyophilised pLP was rehydrated in FITC solution at final concentration of 100  $\mu\text{M mg}^{-1}$  [FITC pLP<sup>-1</sup>] and agitated at 60°C, which is above phase transition temperature for lipid, for 60 min to facilitate encapsulation of FITC. Excess FITC was removed either by centrifugation at 16,000  $\times g$  for 30 min, or by ultrafiltration with 10 K centrifugal filter unit.

Then, liposomal FITC (FITC<sub>LP</sub>) and polydisperse liposomal FITC (FITC<sub>pLP</sub>) was co-incubated with Cy<sup>3</sup>SlpB at concentration of 400  $\text{mg g}^{-1}$  [SlpB LP<sup>-1</sup>] and agitated at 20°C for 120 min. Excess Cy<sup>3</sup>SlpB was removed by centrifugation at 16,000  $\times g$  for 30 min. Cy<sup>3</sup>SlpB-FITC<sub>LP</sub> and Cy<sup>3</sup>SlpB-FITC<sub>pLP</sub> prepared was observed with laser scanning microscope.

To confirm spatial relationship of LP and SlpB, giant Cy<sup>5</sup>SlpB-coated liposomal FITC-conjugated ovalbumin (Cy<sup>5</sup>SlpB-FITC-OVA<sub>LP</sub>) was prepared and observed. Cy<sup>5</sup> was used instead of Cy<sup>3</sup> to reduce the noise from buffer and crosstalk from FITC; while FITC-OVA was used instead of FITC to confirm the potential of macromolecule encapsulation in liposome. FITC-OVA<sub>LP</sub> was prepared by encapsulating 20  $\mu\text{g mg}^{-1}$  [FITC-OVA LP<sup>-1</sup>] with methods previously described. Then, Cy<sup>5</sup>SlpB was coated on the surface of liposome, and observed with fluorescence microscope.

### 2.1.5 Transmission Electron Microscopy of SlpB-LP

The morphology of LP and SlpB-LP were also observed with a transmission electron microscope (TEM) operated at 200 kV. Samples were diluted with deionised water and 10  $\mu$ l of diluted samples were deposited on electron microscopy grid. Excess sample was blotted with a piece of filter paper and the sample was stained with 1% phosphotungstic acid negative stain.

### 2.1.6 Coating of SlpB on Various Drug Carriers

To investigate the potential to evaluate SlpB-adsorption on carriers and to confirm the result obtained from  $\zeta$  potential measurement, various concentration of  $\text{Cy}^5\text{SlpB}$  was co-incubated with 10  $\mu$ g LP to prepare  $\text{Cy}^5\text{SlpB-LP}$  as described in Section 2.1.3. Then, the fluorescent intensity was measured, and an adsorption curve was plotted.

To study adsorption property of SlpB on the surface of both microbeads and *Lactiplantibacillus plantarum* (*Lp. plantarum*), various concentration of  $\text{Cy}^3\text{SlpB}$  was co-incubated with 10  $\mu$ g dry mass of acrylate hydrophilic microbeads or 5 M LiCl solution-treated *Lp. plantarum* JCM 1149 for 120 min with agitation at 20°C and washed twice with PBS (-) with centrifugation at  $5,600 \times g$  to remove excess SlpB. The fluorescent intensity was measured, and an adsorption curve for each sample was plotted.

To confirm coating of SlpB on the surface of microbeads and *Lp. plantarum*, fluorophores were conjugated on both carriers and SlpB. Microbead used in this study was amino groups-conjugated, therefore, it can be labelled with Cy3 dye as described in Section 2.1.2. Briefly, microbeads suspended in 0.1 M carbonate-bicarbonate buffer (pH 9.2) was supplemented to Cy3. The mixture was agitated in dark for 120 min, followed by centrifugation at  $5,600 \times g$  for 10 min and washed with PBS(-) thrice.

*Lp. plantarum* JCM 1149 was cultured to stationary phase, collected by centrifugation at  $5,600 \times g$  for 15 min, and resuspended in PBS (-; pH 8.3). Then, 2  $\mu$ M carboxyfluorescein diacetate (CFDA) was supplemented to the suspension and incubated in 30°C for 120 min. Excess CFDA was removed by centrifugation and washing the pellet of *Lp. plantarum* with PBS (-) thrice. Carboxyfluorescein-stained *Lp. plantarum* ( $\text{CF}Lp. plantarum$ ) was washed with 1 M LiCl solution twice, and 5 M LiCl solution twice to remove Slp-like proteins bound on the surface.

Then,  $\text{FITC}^{\text{SlpB}}$  was coated on microbeads;  $\text{Cy}^3\text{SlpB}$  was coated on *Lp. plantarum* at final concentration of  $400 \text{ mg g}^{-1}$  [SlpB carriers $^{-1}$  (dry mass)] as described previously. After washing

with PBS (-), the products were observed with fluorescent microscope.

### 2.1.7 Optimal Concentration of SlpB for Maximum Stability

SlpB-FITC<sub>LP</sub> coated with various concentration of SlpB was prepared and the liposomes were incubated in deionised water for 60 min at 37°C. After incubation, the liposomes were centrifuged at 16,000 × *g* for 30 min to remove leaked FITC and the pellet was resuspended in deionised water. Control was prepared by centrifuging SlpB-FITC<sub>LP</sub> before incubation at 16,000 × *g* for 30 min, and resuspended the pellet in deionised water to reduce the influence of leakage due to centrifugation.

Fluorescence intensity was measured, and the relative stability of liposome,  $S_{relative}$  was defined as the fraction of FITC remain encapsulated in liposome (Equation 2.3).

$$S_{relative} = \frac{I}{I_0} \times 100 \quad (2.3)$$

where  $I_0$  is fluorescence intensity after washing of liposome and before incubation, and  $I$  is fluorescence intensity of sample after incubation and washing.

The relative stability of SlpB-LP was plotted against concentration of SlpB to identify the optimal concentration of SlpB required to achieve maximum stability.

### 2.1.8 Stability of SlpB-Coated Liposomes in Gut Mimicking Environment

The stability of SlpB-LP under various pH correspond to gut environment was evaluated. Hydrochloric acid (pH 2) which correspond to the acidity of stomach was prepared by titration; deionised water was used to mimic the pH of intestine; phthalate buffer (pH 4) was used as buffer correspond to the pH at the lower end of stomach; tetraborate buffer solution (pH 9) was used to mimic pH in colon.

FITC<sub>LP</sub>, FITC<sub>pLP</sub>, SlpB-FITC<sub>LP</sub>, SlpB-FITC<sub>pLP</sub> were prepared and the stability of liposomes in each type of buffers was evaluated as described in Section 2.1.7. After incubation at 37°C for 60 min, the liposomes were centrifuged at 16,000 × *g* for 30 min, the pellets were suspended in fresh buffers and 0.1 M sodium hydroxide solution was supplemented to each suspension to prevent protonation of FITC in acidic environment. Then, the fluorescence intensity was measured and the relative stability of liposome was evaluated.

The robustness of SlpB-coating on the surface of liposome was evaluated by SDS-PAGE. SlpB-pLP was prepared and incubated in buffers of various pH for 60 min at 37°C. Then, the

SlpB-pLP was centrifuged at  $16,000 \times g$  for 30 min, the supernatants were collected, and the pellets were suspended in equal volume of deionised water. pLP and SlpB-pLP incubated in deionised water for 2 min was used as reference. Both supernatants and pellets were analysed with SDS-PAGE stained with silver.

The stability of liposome in gut-mimicking environment was further evaluated with stability of liposome in gall solution, simulated gastric fluid (SGF) and simulated intestinal fluid (SIF). Various concentration of gall solution (pH 6) was prepared by dissolving gall powder in deionised water; SGF and SIF was prepared as the formulation of U.S. Pharmacopoeia. Then, the stability of LP and SlpB-LP 60 min after incubation in these gut mimicking environments were evaluated.

## 2.2 Results

### 2.2.1 Preparation of Surface Layer Protein B

After removing impurities, which are surface layer associated proteins located on the surface of *Lv. brevis* JCM 1059 (Figure 2.1 (a - b)), a single band with apparent molecular mass of 52 kDa was obtained from fraction extracted with 5 M LiCl solution (Figure 2.1 (c - d)). This purified protein was identified as SlpB, which is the only Slp expressed on *Lv. brevis* JCM 1059 cultured under anaerobic condition<sup>[68]</sup>. The identity of the band was further confirmed with proteome analysis based on matrix-assisted laser desorption/ionisation time of flight mass spectrometry/mass spectrometry as SlpB from *Lv. brevis* JCM 1059.

Based on data obtained, the yield of SlpB was calculated. The yield of SlpB was  $6.74 \text{ mg g}^{-1}$  dry cell mass (0.67%).

The result of fluorescent labelling of SlpB was shown in Appendix D.

### 2.2.2 $\zeta$ Potential and Particle Size of SlpB-Coated Liposome

Adsorption of compounds on liposome can be detected and quantified by the changes in  $\zeta$  potential of liposomes<sup>[69]</sup>, due to the changes in electrical potential in slipping plane of particles induced by the changes in surface potential.

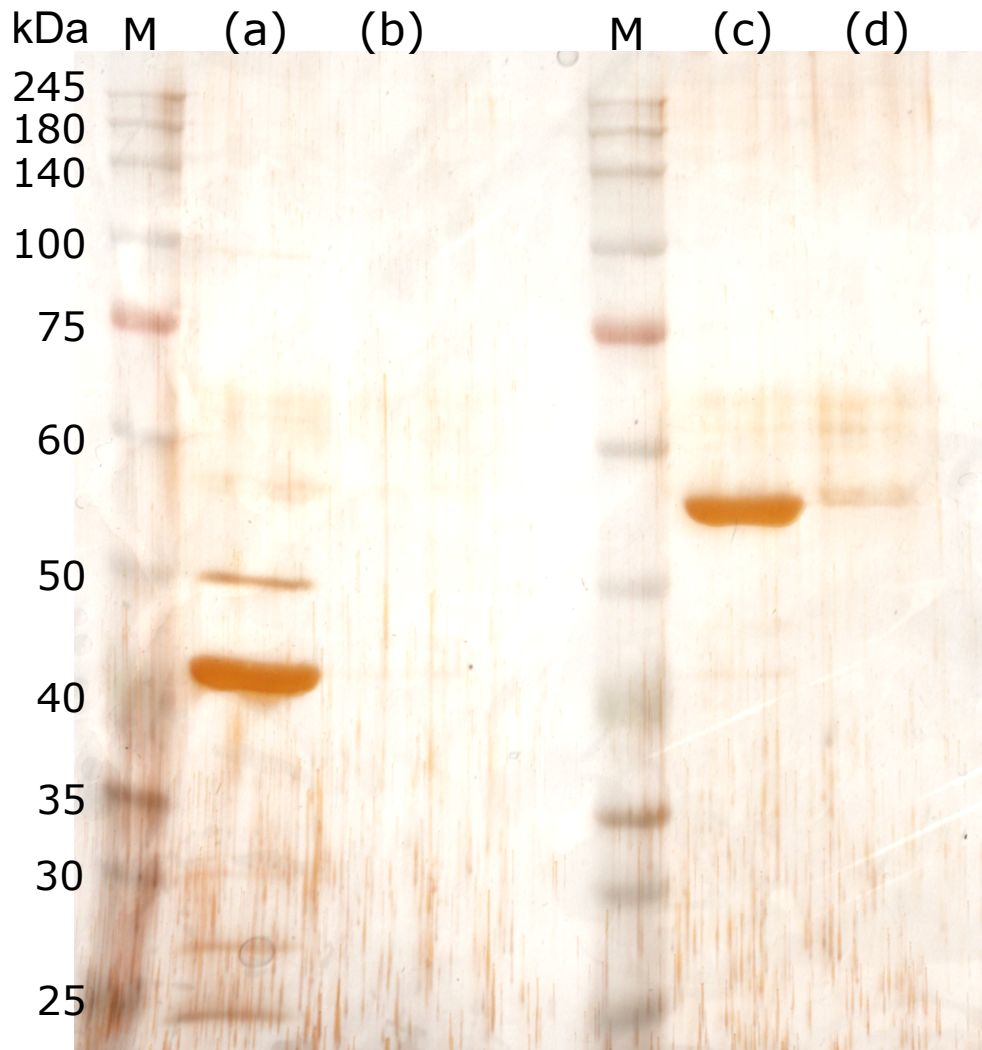


**Figure 2.1** SDS-PAGE of extracts from the surface of *Lv. brevis* JCM 1059 with 1 M and 5 M LiCl solution, stained with silver. (a) first fraction of extraction with 1 M LiCl solution, (b) second fraction of extraction with 1 M LiCl solution, (c) first fraction of extraction with 5 M LiCl solution, (d) second fraction of extraction with 5 M LiCl solution. M indicates protein molecular weight marker.

Adsorption of SlpB on liposome surface was confirmed with reduction in  $\zeta$  potential of liposome (Figure 2.2).  $\zeta$  potential of bare LP was -45.0 mV, which approximates measurement reported in prior study<sup>[70]</sup>. This suggests that the materials parameters were correctly defined. Minimum  $\zeta$  potential at -77.6 mV was achieved when LP was co-incubated with 400 mg SlpB g<sup>-1</sup> LP, which indicates the maximum adsorption capacity of SlpB on liposome was 400 mg g<sup>-1</sup> [SlpB LP<sup>-1</sup>] (Figure 2.2 (a)). On the other hand, the  $\zeta$  potential of bare pLP was -19.4mV, and decreased to a minimum of -108.3 mV when coated with 400 mg g<sup>-1</sup> [SlpB LP<sup>-1</sup>] (Figure 2.2 (b)).

Furthermore, the size of LP and SlpB-LP were confirmed with dynamic light scattering method using nano particle analyser (Figure 2.3). Increase in mean particle size by 30.5 nm was observed when LP was coated with 400 mg g<sup>-1</sup> [SlpB LP<sup>-1</sup>], suggesting that a single layer of SlpB crystalline array has been formed on the surface of LP\*.

### 2.2.3 Fluorescent Imaging of SlpB-LP

For both LP and pLP, co-localisation of signal from FITC and Cy<sup>3</sup>SlpB was observed (Figure 2.4). Furthermore, rim of SlpB was discovered around LP in merge channel of fluorescence micrographs, which suggested that SlpB was adsorbed on the surface of liposome. However, it was uncertain if SlpB was encapsulated in both LP and pLP.

To answer the question whether SlpB was encapsulated in LP, giant liposome of SlpB-LP was observed. Micrographs of Cy<sup>5</sup>SlpB-FITC-OVA LP show that the signal from FITC OVA was enclosed in Cy<sup>5</sup>SlpB-LP (Figure 2.5), suggesting that SlpB was adsorbed on the surface of LP rather than being encapsulated.

### 2.2.4 Transmission Electron Microscopy of SlpB-LP

To verify the formation of SlpB layer on surface of liposome and investigate whether morphological changes have occurred when SlpB was coated on liposome, LP and SlpB-LP were observed with TEM. No morphological change of liposome was observed from electron micrographs (Figure 2.6).

---

\* Particle size is defined as diameter of nanoparticle. Therefore, 30.5 nm increase in particle size indicates 15.25 nm increase in thickness.

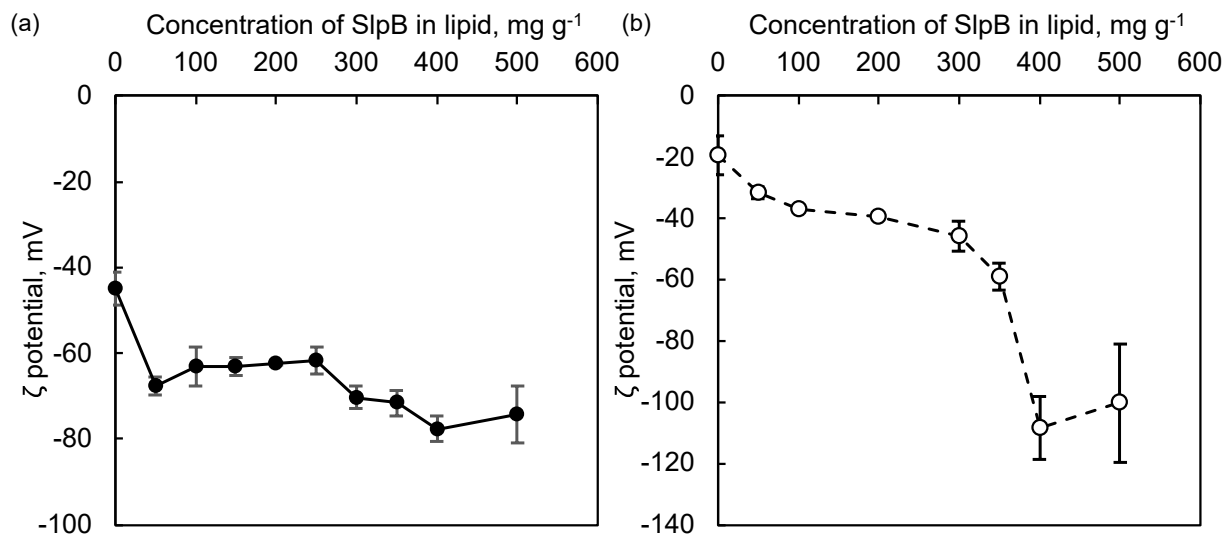


**Figure 2.2**  $\zeta$  potential of liposome measured with liposome adsorbed with various concentration of SlpB. (a) LP, (b) pLP. The plots represent data obtained from triplicate sample in independent test and the error bars represent standard deviation of mean.

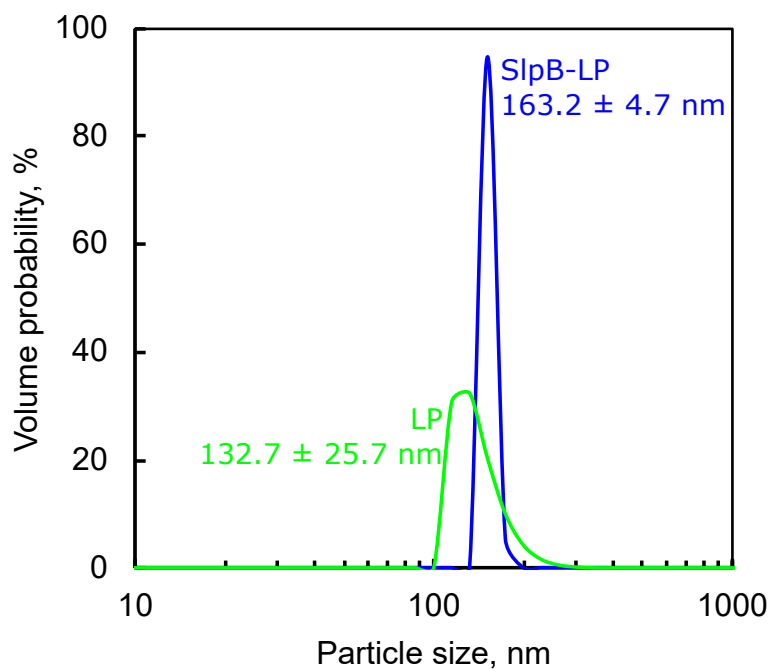


**Figure 2.3** Volume probability of liposomes measured with dynamic light scattering. The numbers indicate mean and standard deviation of particle size.

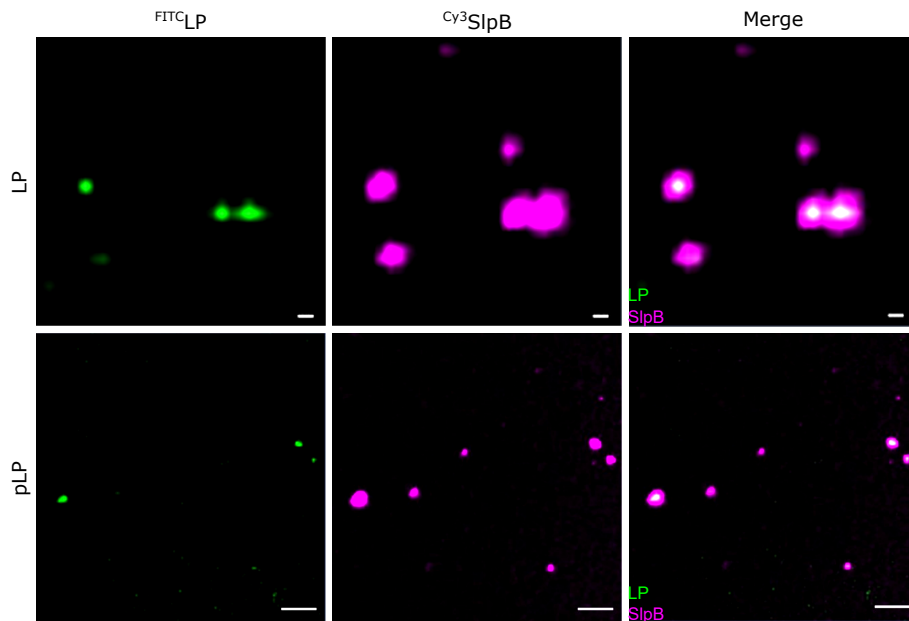


**Figure 2.4** Fluorescence micrographs of  $\text{Cy}_3\text{SlpB-FITC-LP}$  for both LP and pLP. The scale bars for LP were 100 nm; the scale bars for pLP were 5  $\mu\text{m}$ .

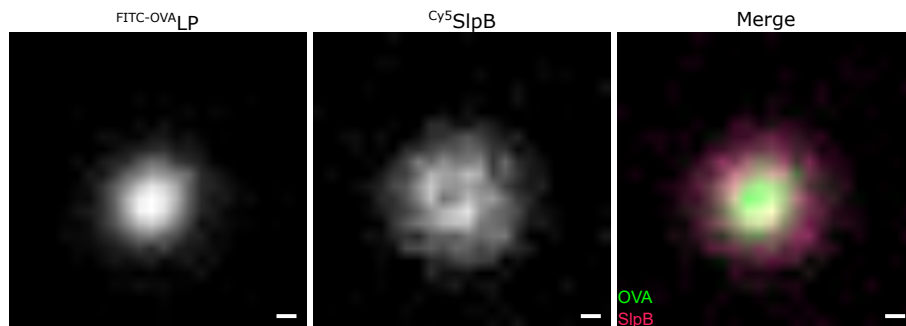


**Figure 2.5** Fluorescent micrograph of single  $\text{Cy}_5\text{SlpB-FITC-OVA-LP}$  at (a) FITC channel, (b) Cy5 channel, (c) merge channel. The scale bars are 1  $\mu\text{m}$ .

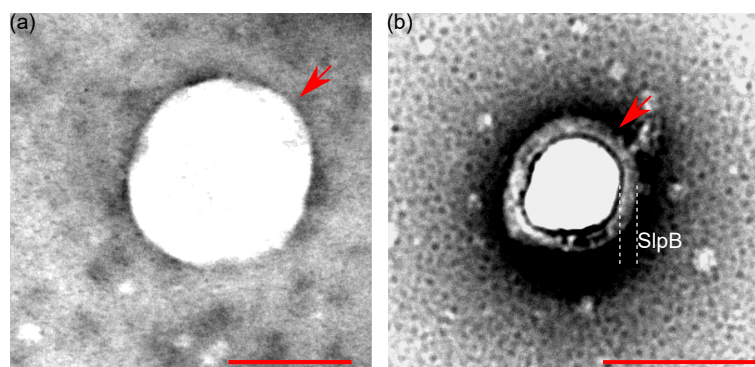


**Figure 2.6** Morphology of SlpB-coated liposome. Transmission electron micrographs of (a) LP and (b) SlpB-LP. Red arrows show the location of liposomes. The scale bars represent 100 nm.



On the other hand, a 12.9 nm-thick layer was observed on the outer surface of SlpB-LP (Figure 2.6 (b)). The thickness is in agree with the thickness of SlpB single layer formed on the surface of *Lv. brevis* JCM 1059<sup>[68]</sup>, suggested that a single layer of SlpB crystalline array has been formed on the surface of liposome. SlpB single layer has contributed to 21.8% diameter of SlpB-LP. Both the thickness of SlpB and the ratio of SlpB to SlpB-LP approximate the measurement obtained from dynamic scattering method (Figure 2.3). Both results from TEM and dynamic light scattering suggest that SlpB forms a single layer on the surface of liposome.

## 2.2.5 Coating of SlpB on Various Drug Carriers

Besides liposomes, various carriers, e.g., polymeric drugs carriers<sup>[71]</sup> and bacteria<sup>[72-74]</sup> have been used in drug delivery. In this section, I investigate the potential of SlpB-coating on various carriers.

Although Equation 2.1 does not possess limitation for the size of particles, large particles, e.g., microbeads and bacteria are subject to the effect gravity and inertia, rendering  $\zeta$  potential less significant due to inertia<sup>[75]</sup> and sedimentation. Meanwhile, as SlpB forms single layer crystalline array on the surface of carriers, it is possible to obtain an adsorption curve by measuring the amount of fluorescent SlpB adsorbed on the surface of carriers. To verify this assumption, I have measured adsorption of SlpB on the surface of LP by fluorescence intensity (Figure 2.7 (a)), and compared the adsorption curve to  $\zeta$  potential measurement. The trend of SlpB-adsorption curve is similar for both curves measured by  $\zeta$  potential (Figure 2.2 (a)) and fluorescent intensity suggests that fluorescent SlpB can be used to evaluate adsorption of SlpB on the surface of carriers.

After co-incubating various concentration of <sup>Cy3</sup>SlpB to microbeads and *Lp. plantarum*, the fluorescence intensities were measured, and an adsorption curve was plotted for each carrier. Both curves suggest that SlpB can be coated on microbeads and *Lp. plantarum* (Figure 2.7 (b - c)), and the maximum adsorption capacity of SlpB on both carriers were 400 mg g<sup>-1</sup> [SlpB carrier<sup>-1</sup>].

To confirm whether SlpB were coated on the surface of microbeads and *Lp. plantarum*, carriers coated with 400 mg g<sup>-1</sup> [SlpB carrier<sup>-1</sup>] were observed with fluorescent microscope. A thin layer of SlpB was observed at the edge of microbead (Figure 2.8 (a)) and *Lp. plantarum* (Figure 2.8 (b)) indicate that SlpB has been coated on the surface of both microbeads and *Lp. plantarum*.

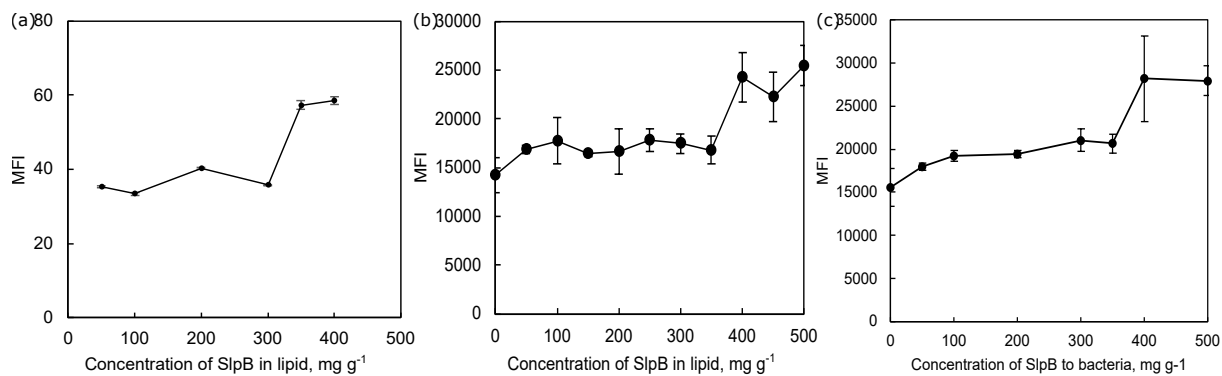


**Figure 2.7** Adsorption of SlpB on various types of carriers. Adsorption of SlpB on (a) LP, (b) microbeads and (c) *Lp. plantarum* JCM 1149. The plots represent data obtained from triplicate sample in independent test and the error bars represent standard deviation of mean.

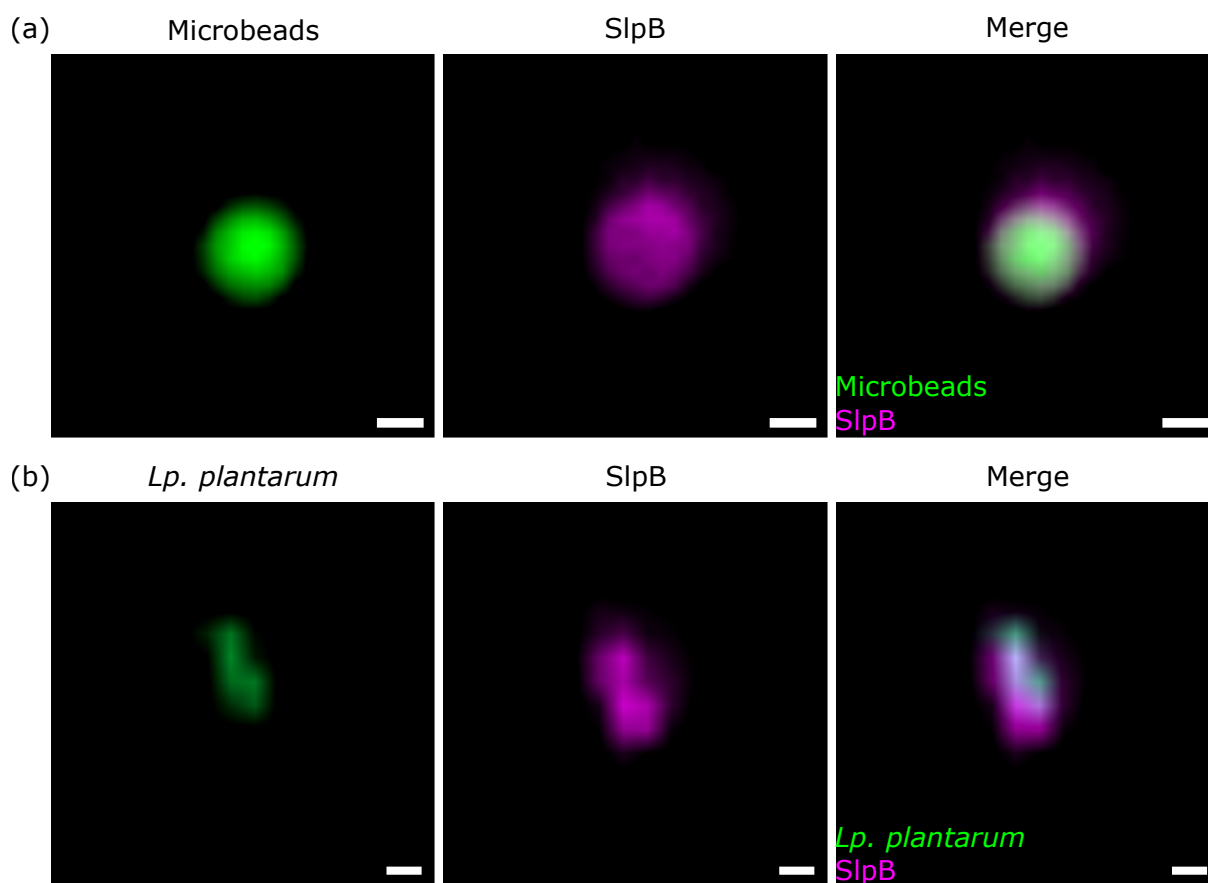


**Figure 2.8** Fluorescent imaging of SlpB-coated solid microparticles. Fluorescent micrographs of (a) SlpB-microbeads and (b) SlpB-*Lp. plantarum*. The scale bars are 1  $\mu\text{m}$ .

### 2.2.6 Optimal Concentration of SlpB for Maximum Stability

Although I have shown that the maximum adsorption capacity of SlpB on liposome was  $400 \text{ mg g}^{-1} [\text{SlpB LP}^{-1}]$  (Figure 2.2, 2.7 (a)), it remained unclear that whether the adsorption curve is related to stability. In this section, I investigate the optimal concentration of SlpB required to be coated on liposome to achieve maximum stability.

As shown in Figure 2.9, retention of FITC increased from 72.1% to 98.9% when LP was coated with  $400 \text{ mg g}^{-1} \text{ SlpB}$ , which indicates that maximum stability of liposome achieved by SlpB-coating is defined by maximum adsorption capacity of SlpB on liposome. Hereafter, SlpB-LP in this dissertation is defined as liposome coated with  $400 \text{ mg g}^{-1} [\text{SlpB LP}^{-1}]$ .

### 2.2.7 Stability of SlpB-Coated Liposomes in Various pH

Then, the stability of SlpB-LP in various pH was evaluated. Buffers with gut environment mimicking pH, i.e., pH 2 for stomach, pH 4 for the interface between stomach and duodenum, pH 7 for small intestine and pH 9 for colon, were prepared, and both LP and SlpB-LP were incubated in these buffers for 60 min at  $37^\circ\text{C}$ .

Regardless of the polydispersity of liposomes, SlpB-coating could enhance the stability of liposome across broad range of pH (Figure 2.10). At pH 7, SlpB has improved the stability of LP by 1.4-fold, from 72.1% FITC retention to 98.9% FITC retention, while the stability of pLP was improved by 1.2-fold, from 78.2% to 96.9%. The enhancement of stability was particularly distinctive at pH 9, where the stability of LP was improved by 1.9-fold, from 32.4% to 61.5%; while improving the stability of pLP by 6.8-fold from 3.0% to 22.3%.

As pLP used in this study contains higher concentration of cholesterol in its formulation<sup>†</sup>, higher stability has been achieved by pLP at neutral to acidic pH compared to LP due to the enhanced membrane rigidity. Thus, the increase in stability enhanced by SlpB for pLP was smaller compared to LP. Statistical significance of improvement of stability by Slp-coating was detected in all samples.

However, it remained unclear whether SlpB-coating remains robust on the surface of liposome under various pH, given that some Slp-like protein, e.g., glyceraldehyde-3-phosphate dehydrogenase (GAPDH)<sup>[76]</sup> will detach from the surface of lactobacilli at high pH. Thus, further investigation of the robustness of SlpB adsorption is required.

---

<sup>†</sup> 45.5% compared to 40.0% in LP

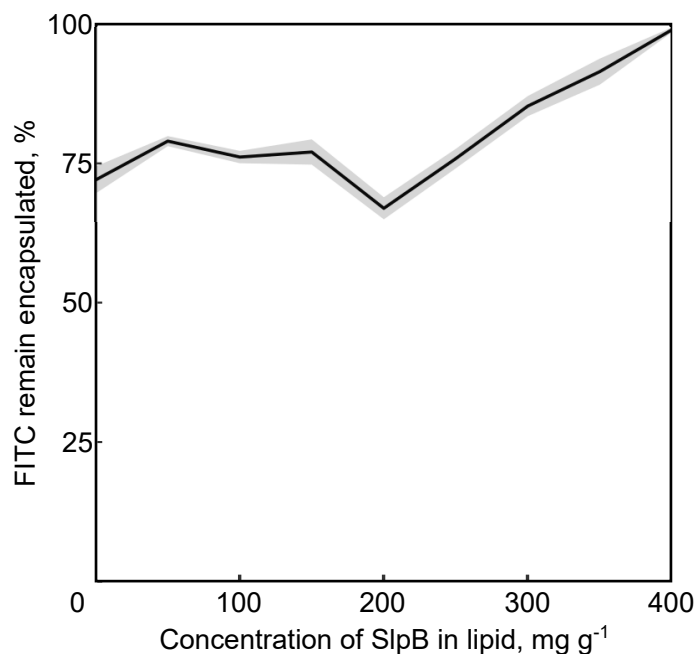


**Figure 2.9** Stability of liposome coated with various concentration of SlpB in deionised water (pH 7) after 60 min incubation at 37°C. Stability of liposome was evaluated by percentage of FITC remain encapsulated after incubation. The plots represent data obtained from triplicate sample in independent test and the shaded region represent standard deviation of mean.

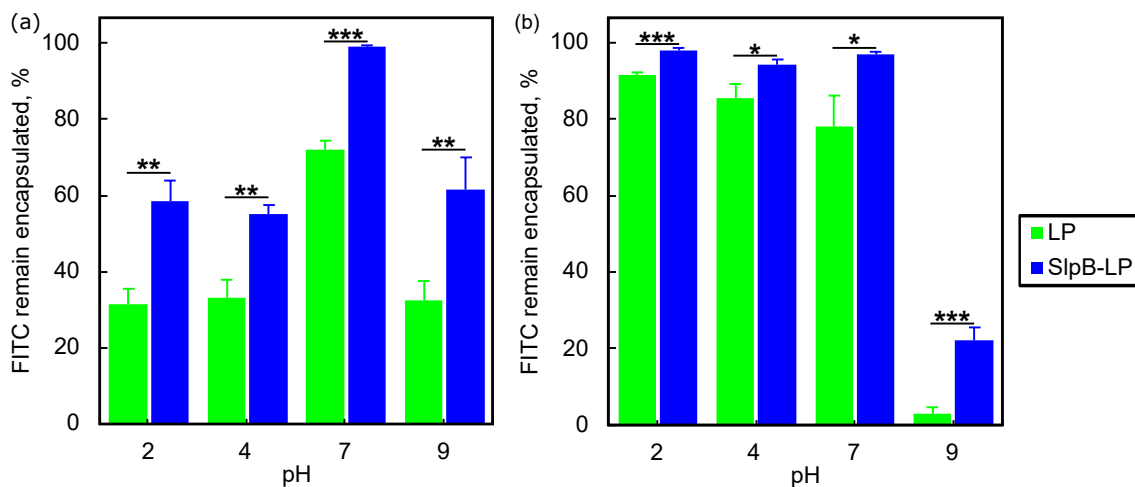


**Figure 2.10** Stability of liposomes under various pH conditions. (a) LP, (b) pLP. The plots represent data obtained from triplicate sample in independent test and the error bars represent standard deviation of mean. Statistical significance was evaluated with Student's t-test. \*  $p < 0.05$ , \*\*  $p < 0.01$ , \*\*\*  $p < 0.001$ .

### 2.2.8 Robustness of SlpB Adsorption on Liposomes

The robustness of SlpB adsorption on liposome was evaluated by SDS-PAGE analysis and stained with silver after incubation in buffers with various pH for 60 min. If SlpB was detached from liposomes, then, SlpB can be detected in supernatant; if SlpB was degraded, more than 1 band can be detected in either supernatant or pellet, else SlpB can only be detected in pellet as single band. As shown in Figure 2.11, a single band of SlpB was observed in pellet for all samples of SlpB-pLP, and no band was observed in supernatant, suggesting that SlpB remain attached on the surface of pLP after incubation.

### 2.2.9 SlpB Enhances Stability of Liposomes in Gall Solution

Besides the diversity of pH in GI tract, another physicochemical barrier which liposomes encounter in gut is gall solution. Gall solution in gut contains bile acid and lecithin which could emulsify and dissolve cholesterol in liposome, compromising their stability. Therefore, it is important to evaluate the stability of liposomes in gall solution. As the concentration of bile salts in small intestines range from 0.2 - 2% [w/v]<sup>[77]</sup>, stability of liposomes in 0.5 - 3% [w/v] gall solution was evaluated, and the relationships between concentration of gall solution and relative stability of liposomes were plotted (Figure 2.12). As shown in Figure 2.12, SlpB-coating has improved stability of liposome against various concentration of bile acid. In 3% gall solution, SlpB has improved the stability of LP by 1.2-fold, which increase the retention of FITC in LP from 54.9% to 66.2%, while the stability of pLP was enhanced by 35.4-fold from 2.0% to 68.9% FITC retention by SlpB-coating.

Coating of liposomes with SlpB has increased the rigidity of liposome, which has enhanced their stability. Crystalline array formed on the surface of liposomes has improved stability of liposome against emulsifying effect of bile acid and lecithin.

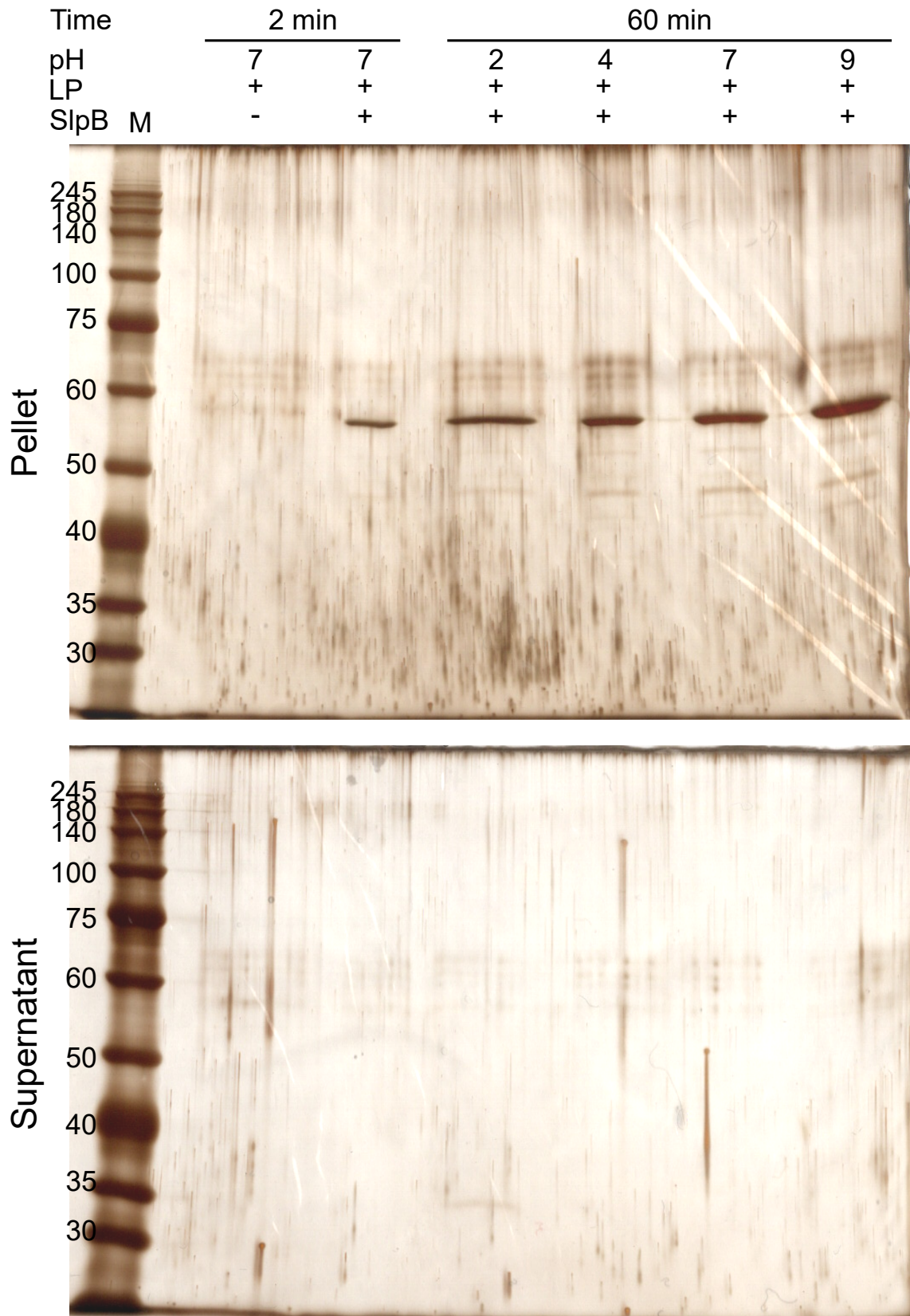


**Figure 2.11** Robustness of SlpB-coating on pLP after incubating in buffers with various pH for 60 min.

### 2.2.10 SlpB Enhances Stability of Liposomes in Simulated Gut Fluids

To further investigate the potential of SlpB in enhancing the stability of liposomes in GI tract, stability of liposomes in SGF and SIF were investigated. SGF contains pepsin in pH 1 hydrochloric acid, while SIF contains pancreatin<sup>‡</sup> in pH 7, which could hydrolyse and oxidise liposomes. Figure 2.13 shows that SlpB enhanced stability of liposomes in both SGF and SIF. In SGF, SlpB has improved stability of LP by 1.6-fold from 41.5% to 68.0% FITC retention, while no significant improvement of stability of pLP was observed. On the other hand, in pancreatin containing SIF, SlpB-coating has improved the stability of LP by 5.0-fold from 2.8% to 14.1% FITC retention, while it improved the stability of pLP by 6.5-fold from 1.9% to 12.5%.

---

<sup>‡</sup> Pancreatin contains lipase, pepsin, trypsin, protease and other pancreatic enzymes

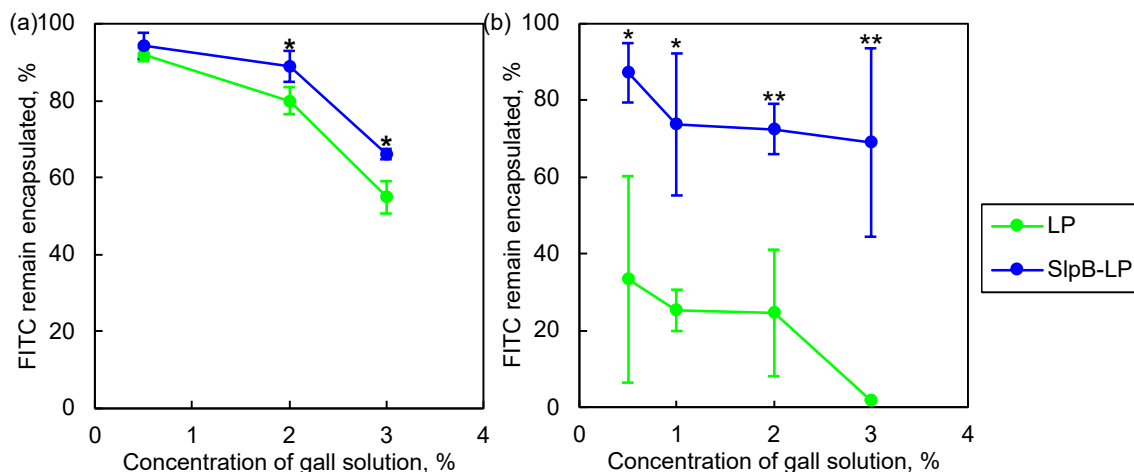


**Figure 2.12** Stability of liposomes in various concentration of gall solution. (a) LP, (b) pLP. The plots represent data obtained from triplicate sample in independent test and the error bars represent standard deviation of mean. Statistical significance was evaluated with Student's t-test. \*  $p < 0.05$ , \*\*  $p < 0.01$ .

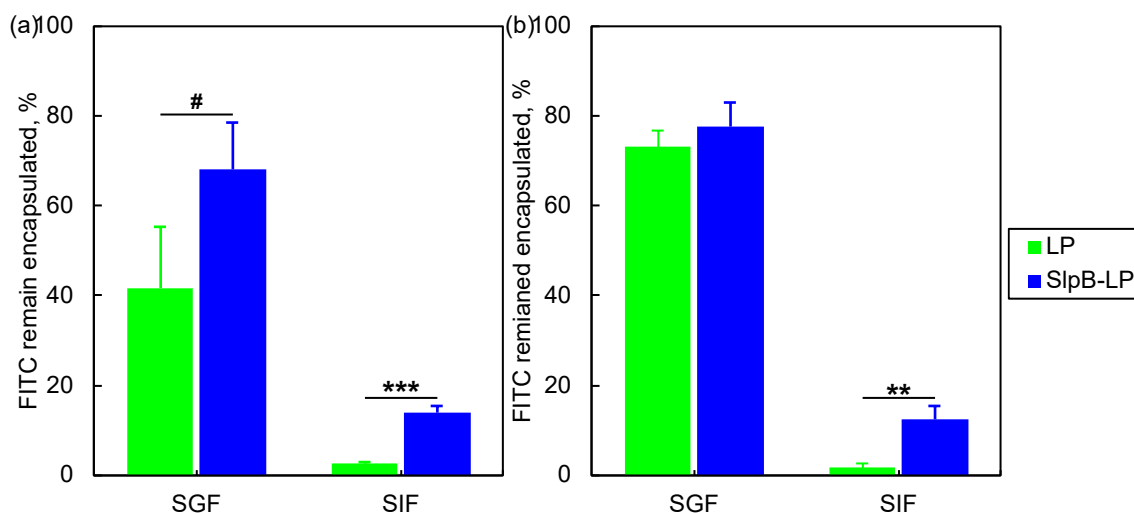


**Figure 2.13** Stability of liposomes in simulated gastric fluid (SGF) and simulated intestinal fluid (SIF). (a) LP, (b) pLP. Both SGF and SIF were prepared as the formulation of U.S. Pharmacopoeia. SGF contains pepsin at pH 1, and SIF contains pancreatin at pH 7. The plots represent data obtained from triplicate sample in independent test and the error bars represent standard deviation of mean. Statistical significance was evaluated with Student's t-test. #  $p < 0.1$ , \*\*  $p < 0.01$ , \*\*\*  $p < 0.001$ .



## 2.3 Discussion

### 2.3.1 Coating of SlpB on Liposomes

In this chapter, I have demonstrated coating of SlpB on the surface of anionic liposome. Interestingly, for bare LP which the  $\zeta$  potential was similar to 5 M LiCl-treated *Lv. brevis*, the  $\zeta$  potential after coating with 400 mg g<sup>-1</sup> [SlpB LP<sup>-1</sup>] was similar to native *Lv. brevis* with SlpB (Appendix E). This result suggested that crystalline array formed on the surface of anionic liposome was similar to *Lv. brevis*. If the structure of SlpB crystalline array formed on the surface of LP differed from the structure of SlpB formed on the surface of *Lv. brevis*, the charge would be different due to difference in area exposed to slipping plane. Therefore, it can be deduced that the structure of crystalline array of SlpB formed on liposome is similar to that of *Lv. brevis*.

Although different composition of liposome might result in difference in final  $\zeta$  potential achieved when liposomes were coated with SlpB at maximum adsorption capacity (Figure 2.2), the maximum adsorption capacity was equal, which suggest that SlpB coating does not depend on the composition of liposomes. Moreover, in contrast to maximum adsorption capacity of SlpB at 200 mg g<sup>-1</sup> [SlpB LP<sup>-1</sup>] on cationic liposome as reported by previous study<sup>[55]</sup>, 400 mg g<sup>-1</sup> [SlpB LP<sup>-1</sup>] can be adsorbed on the surface of anionic liposome, which suggests that maximum capacity of SlpB adsorption depends on surface charge, but not magnitude of charge of liposome.

Computation of the isoelectric point of each terminal of SlpB suggests that N-terminal of SlpB which binds to bacteria surface was 9.87, whereas the isoelectric point of self-assembling C-terminal is 5.42. In neutral pH, surface binding N-terminal is positively-charged, thus, N-terminal preferentially attract to negatively-charged surface and induce formation of crystalline array on C-terminal. Formation of crystalline array, which expose the negatively charge domain of SlpB which is more negatively-charged compared to surface of liposome at outer surface, result in reduction of surface charge.

Regardless of  $\zeta$  potential of bare liposomes, the adsorption curve of SlpB of both liposomes followed a similar trend. This observation resembles the trend of adsorption of Slp from *Lv. brevis* on cationic liposomes as reported in Ref 55. A plateau on each curve can be observed, which suggests incomplete shielding of liposome surface by SlpB when liposomes were co-incubated with 50 - 350 mg g<sup>-1</sup> [SlpB LP<sup>-1</sup>]; a sudden decrease in  $\zeta$  potential can be observed when 400 mg g<sup>-1</sup> [SlpB LP<sup>-1</sup>] was coated on the surface of liposome, indicates formation of crystalline array of SlpB which completely cover the surface of liposome.

### 2.3.2 SlpB Enhanced Stability of Liposomes

Coating of SlpB on the surface of liposomes has increased both the colloid stability of liposomes and their stability against various gut mimicking environment, which might prolong the storage of liposomal drugs and allow oral delivery. As shown in Figure 2.2, SlpB decreases the  $\zeta$  potential of anionic liposomes, thus, enhancing the colloid stability of liposomes. Improvement of colloid stability led to narrower size distribution of SlpB-LP compared to LP (Figure 2.3). Positive skewness was observed for the size distribution of LP, suggesting that LP was aggregated during measurement, while SlpB-LP remained stable throughout the process of measurement.

Improvement of liposomes stability by SlpB-coating is resulted from attachment of SlpB on the surface of LP, which not only increased the rigidity of lipid membrane, but also act as diffusion barrier to non-electrolytes<sup>[65]</sup>, thus, reduce the leakage of FITC, damage of lipid membrane induced by pH changes and emulsification by gall solution.

Furthermore, the crystalline array formed by SlpB can act as molecular filter which has limited the access of macromolecule. Crystalline array formed by SlpB on *Lv. brevis* has lattice constant  $\alpha = 8.4$  nm,  $\beta = 5.0$  nm,  $\gamma = 80^\circ$ . On the other hand, hydrodynamic diameter of enzymes contained in pancreatin, e.g., lipase is 230 Å<sup>[78]</sup>, which is larger than the lattice constant of SlpB on bacterial surface. The crystalline array of SlpB formed on the surface of liposome might be similar to bacterial surface, and the array might have limited the access of enzyme to lipid membrane, thus reducing hydrolysis and oxidisation, and protecting the integrity of lipid membrane<sup>§</sup>.

As Slps can be extracted via chaotropic agents, they bind through non-covalent bonds, e.g., hydrogen bonding. In this case, charges of binding domains play an important role in adsorption. Consider the surface of lactobacilli are negatively charged in neutral environment due to the present of teichoic acid, the isoelectric point of binding domain of Slp(-like) proteins have to be high enough to bind to bacterial surface via electrostatic force. High isoelectric point of SlpB allow it to maintain its charge at high pH, which is below its isoelectric point, therefore provide stable electrostatic force for binding through charge interaction. This property of SlpB has enabled robust attachment of SlpB on the surface of liposome in high pH environments (Figure 2.11), which correspond to intestine and colon.

<sup>§</sup> Hydrodynamic diameter is defined by considering protein as a perfect sphere. It is not equivalent to the size of proteins. For instance, for the case of lipase (RSCB PDB: 1OIL), the distance between Gly<sup>200</sup> and Leu<sup>317</sup> is 24.42 Å; the distance between Pro<sup>131</sup> and Leu<sup>234</sup> is 40.50 Å, which is small enough to pass through the crystalline array formed by SlpB. This suggest that enzyme can pass through the SlpB lattice at certain orientation. Therefore, crystalline array serves to limit but not prevent the access of enzyme.

Furthermore, SlpB-coating has also enhanced stability of liposome in SIF and SGF. Proteome analysis of trypsin-hydrolysed SlpBs has shown that the signal intensity of C-terminal was low<sup>[43]</sup>, suggested that C-terminal could resist enzymatic degradation. The hydrolytic-resistant C-terminal of SlpB could self-assemble into tight crystalline array which protect liposomes against enzymatic degradation. This resistance against enzymatic degradation has contributed to high stability of SlpB-LP in SGF and SIF.

### 2.3.3 Advantages of SlpB-Coating Compared to other Slps

In contrast to other Slps-expressing microorganisms, lactobacilli are generally regarded as safe. Thus, Slps from lactobacilli are more favourable ligand to target APCs in gut, compared Slps from other genera.

Generally, Slps from lactobacilli exhibit high isoelectric point at binding domains compared to Slps from other species and other surface components from lactobacilli. Computation of isoelectric point of binding domain of various types of Slp(-like) proteins, i.e., SlpA from *L. acidophilus*, SlpB from *Lv. brevis*, elongation factor Tu from *Limosilactobacillus reuteri* and GAPDH from *Lp. plantarum* shows that the isoelectric point for binding domain of SlpA was 9.92, SlpB was 9.87, EF-Tu was 5.09 and GAPDH was 6.82. As electrostatic force is responsible for coating of Slps and other components on the surface of lactobacilli, high isoelectric point offers robust adsorption of protein to surface. Detachment of other surface components from lactobacilli at neutral pH, which is the pH in intestine are discussed in prior studies<sup>[79]</sup>.

Besides liposomes, SlpB can also be coated on the surface of other carriers, e.g., microbeads and bacteria, which could expand the repertoire of drug carriers which can be used in oral delivery of immunomodulatory drugs.

## 2.4 Summary

In this chapter, I have shown that SlpB can be coated on various carriers with focus on anionic liposomes. SlpB was extracted from *Lv. brevis* JCM 1059, and a single band of protein with molecular mass of 52 kDa was confirmed with SDS-PAGE. Then, SlpB was coated on LP and pLP, and the  $\zeta$  potential was measured. SlpB-coating decreases the  $\zeta$  potential of liposomes, which has in turn improved the colloid stability of liposomes. Particle size analysis by dynamic light scattering, fluorescent imaging and electron microscopic analysis of SlpB-LP suggest that SlpB form a single layer of crystalline array on the surface of liposome.

Moreover, I have shown that SlpB has enhanced stability of liposomes against gut mimicking environments. SlpB-coating on the surface of liposomes was robust against broad pH range from pH 2 to pH 9. Robust attachment of SlpB on the surface of liposomes has ensured that SlpB could improve the stability of liposomes in environment with broad range of pH. Furthermore, SlpB-coating has also improved stability of liposomes in gall solution of various concentration, and in SGF and SIF. Improvement in the stability of liposomes by SlpB has make SlpB-LP an attractive carrier for oral delivery of drugs.

## Chapter 3

# SlpB Enhances Endocytosis and Induces Adjuvant Effect for Antigen Presenting Cells

In the previous chapter, I have shown that SlpB-LP is stable against broad pH range, gall solution, SGF and SIF. However, the targeting effect of SlpB-LP to APCs was undetermined.

An important aspect which determines the potential of a compound as targeting ligand is its capability to bind to specific receptors. Receptor-mediated endocytosis is induced through specific ligand-receptors interaction, thus improving endocytosis of carriers by specific cells. In this chapter, I evaluate the targeting effect of SlpB to APCs, and investigate whether SlpB-coating enhances endocytosis by APCs. There are 3 major types of antigen presenting cells in mammals, i.e., MΦs, DCs and B cells. As B cells are weak endocytic cells, MΦs and DCs are the main APCs involve in endocytosis. Thus, MΦs and DCs are the major target to be studied.

In addition, another benefit of SlpB in improving therapeutics effect of drugs has remained undiscussed. Generally, Slps could induced immunomodulatory effect in host cells<sup>[16-22]</sup>, suggesting that Slps might induce adjuvant effect which could improved therapeutic effect of drugs. Wu et al. have demonstrated improved cancer immunotherapy by immunising mice with Slp-functionalised doxorubicin-loaded polymeric nanoparticles via intravenous injection<sup>[80]</sup>. All mice immunised with Slp-functionalised doxorubicin-loaded polymeric nanoparticles has survived for at least 21 days without obvious body weight loss compared to 40% for mice injected with Slp and 80% for mice injected with doxorubicin-loaded polymeric nanoparticles.

On the other hand, Acosta et al. have shown that Slp from *Lv. brevis* could modulate the function of APCs via Mincle-Syk-Card9 axis, which results in immunomodulation and production of IL-10 and transforming growth factor (TGF)- $\beta$ <sup>[33]</sup>. The adjuvant effect offered by Slps can be leveraged to improved therapeutic effect of drugs, besides elevated stability and uptake.

In this chapter, I will investigate whether SlpB-coating could enhance endocytosis by APCs, induce adjuvant effect, and improve therapeutic effect of drugs based on the benefits it provided.

## 3.1 Methods

### 3.1.1 Maintenance and Differentiation of THP-1 Cells

THP-1 monocyte (JRCB0112) used in this dissertation was maintained at  $2 - 9 \times 10^5$  cells  $\text{ml}^{-1}$  in Roswell Park Memorial Institute (RPMI) 1640 medium<sup>[81]</sup> supplemented with 9.1% heat inactivated fetal bovine serum. Incubation was conducted in  $37.0^\circ\text{C}$ , 5.0%  $\text{CO}_2$  humidified incubator. Throughout this dissertation, the medium used to maintain THP-1 monocyte is known as supplemented RPMI 1640 (sRPMI) medium.

Experiments were conducted in 24- and 96-well tissue culture plate. THP-1 monocyte suspended in sRPMI medium supplemented with 20 nM phorbol 12-myristate 13-acetate (PMA) was seeded into each well at density of  $2.0 \times 10^3$  cells  $\text{mm}^{-2}$ , and incubated in  $37.0^\circ\text{C}$ , 5.0%  $\text{CO}_2$  humidified incubator for 48 h to differentiate into immature  $\text{M}\Phi$  (im $\text{M}\Phi$ ; M0 phenotype). im $\text{M}\Phi$  was allowed to rest in sRPMI medium for 72 h. To polarise im $\text{M}\Phi$  to pro-inflammatory  $\text{M}\Phi$  ( $\text{M}\Phi$ ; M1 phenotype), culture was replaced with fresh sRPMI medium supplemented with  $10 \text{ ng ml}^{-1}$  recombinant human interferon  $\gamma$  (rhIFN- $\gamma$ ) and  $100 \text{ ng ml}^{-1}$  lipopolysaccharide (LPS) from *Escherichia coli* (*E. coli*) O26; for dendritic cell (DC; M2a phenotype) polarisation, culture was replaced with fresh sRPMI medium supplemented with  $20 \text{ ng ml}^{-1}$  recombinant human interleukin 4 (rhIL-4), and incubated for 48 h. Depending on application, DC can further be matured into mature DC (mDC) by incubating DC in sRPMI supplemented with  $100 \text{ ng ml}^{-1}$  LPS for another 24 h.

To confirm induction of cells with expression of signature receptors, the cells were detached and collected, fixed with 3.7% formaldehyde and 0.8% methanol, blocked with 3% BSA, followed by incubation with either mouse Ab against hDC-SIGN or mouse Ab against human Mincle (hMincle), and FITC-conjugated goat Ab against mouse IgG. For each sample, 5,000 cells were analysed with flow cytometer.

Protocol for induction was justified in Appendix F.

### 3.1.2 Interaction of SlpB with APCs

DC was detached from well plates and co-incubated with 3% BSA in PBS (-) for 60 min. After that, the cells were washed thrice in PBS (-) and co-incubated with  $10 \text{ }\mu\text{g ml}^{-1}$  FITC-SlpB in fresh sRPMI at  $37^\circ\text{C}$ . Then, the cells were collected by centrifugation at  $194 \times g$  for 5 min, washed thrice, and fixed with 3.7% formaldehyde and 0.8% methanol in PBS (-). Fixed cells

were washed thrice and analysed with flow cytometer.

To investigate binding of SlpB to receptors on M $\Phi$  and DC, i.e., Mincle and DC-SIGN, both M $\Phi$  and DC were fixed with 5% formalin solution and washed thrice. Then, M $\Phi$  was co-incubated with Ab against Mincle; DC was co-incubated with Ab against DC-SIGN for 60 min at 37°C to block the access of SlpB to hMincle and hDC-SIGN. The cells were washed thrice to remove excess Abs, and co-incubated with 10  $\mu\text{g ml}^{-1}$   $^{\text{Cy5}}$ SlpB for 60 min at 37°C. After incubation, the cells were washed thrice and the fluorescence intensity was analysed with microplate reader.

To eliminate the effect of potential unspecific binding of SlpB to Abs, the capability of SlpB to block the binding of Ab to DC-SIGN was evaluated. DC-SlpB complex was fixed and blocked with BSA. Then, the cells were incubated with 200  $\text{ng ml}^{-1}$  mouse Ab against hDC-SIGN followed by FITC-conjugated goat Ab against mouse IgG to stain DC-SIGN\*. The cells were washed thrice, suspended in 100  $\mu\text{l}$  PBS (-) and analysed with microplate reader; number of cells was counted with Bürker-Türk haemocytometer. The fluorescence intensity was normalised with number of cells.

### 3.1.3 Endocytic Kinetic of Liposome by APCs

Liposomal propidium iodide ( $^{\text{PI}}$ LP) was prepared by rehydrating desired amount of anionic liposome in PI solution at 100  $\mu\text{M mg}^{-1}$  [ $^{\text{PI}}$ LP $^{-1}$ ]. SlpB- $^{\text{PI}}$ LP was prepared as described in Section 2.1.8.

Prior supplementation of LPs, culture supernatant of both M $\Phi$  and DC was replaced with fresh sRPMI medium to remove debris and dead cell, which are PI $^{+}$  and will result in false positivity. Then, both M $\Phi$  and DC was co-incubated with LPs for various length of time in 37.0°C, 5.0% CO $_2$  humidified incubator. Cells were washed with D-PBS (-) twice to remove excessive liposome, detached, and resuspended in D-PBS (-). Cell suspension was filtered through 40  $\mu\text{m}$  mesh filter and analysed with flow cytometer.

To obtain endocytic kinetic curves, mean fluorescence intensity (MFI) of negative control (cells without co-incubation with any LP) was subtracted from MFI of each sample. Then, the mean and standard deviation was calculated, and kinetic curves were plotted.

### 3.1.4 Imaging of Endocytosis of Liposome

Liposomal  $^{\text{Cy3}}$ OVA ( $^{\text{Cy3-OVA}}$ LP) was prepared by rehydrating LP in 20  $\mu\text{g mg}^{-1}$  [ $^{\text{Cy3}}$ OVA LP $^{-1}$ ] and agitated in dark for 60 min. Then, SlpB was coated as described in Section 2.1.8.

---

\* Staining of hDC-SIGN on fixed DC was confirmed in Appendix F

DC was co-incubated with either  $\text{Cy}^3\text{-OVA}_{\text{LP}}$  or  $\text{SlpB-Cy}^3\text{-OVA}_{\text{LP}}$  for 30 min and 70 min. Then, the DCs were washed twice with D-PBS (-), and immediately fixed with 3.7% formaldehyde and 0.8% methanol. DC-SIGN was stained as described in Section 3.1.2 to determine the region enclosed by cell membrane, while nucleus was stained with 1  $\mu\text{M}$  DAPI solution as counterstain. The stained DCs were immersed in PBS and observed with laser scanning microscope.

### 3.1.5 Effect of Particle Size on Endocytosis

To prepare liposome with different size, polydisperse LP (pLP) suspension was sonicated with 60 s sonication and 10 s rest cycle for 10 cycles. Then, the size and polydispersity index of pLP and sonicated pLP (spLP) were measured with dynamic light scattering method.

Polydisperse liposomal propidium iodide ( $\text{PI}_{\text{pLP}}$ ), sonicated polydisperse liposomal propidium iodide ( $\text{PI}_{\text{spLP}}$ ),  $\text{SlpB-PI}_{\text{pLP}}$  and  $\text{SlpB-PI}_{\text{spLP}}$  were prepared as described in Section 2.1.4 by replacing FITC with PI. Then, liposomes were supplemented to APCs and co-incubated for 70 min. Endocytosis of liposome was analysed as described in Section 3.1.3.

### 3.1.6 Microbeads Endocytosis by Antigen Presenting Cells

$\text{Cy}^3\text{Beads}$  and  $\text{SlpB-Cy}^3\text{beads}$  were prepared with methods described in Section 2.1.6. Either  $\text{Cy}^3\text{beads}$  or  $\text{SlpB-Cy}^3\text{beads}$  was co-incubated with  $\text{M}\Phi$  or DC for various length of time, and the multiplicity of infection (MOI) was 100. Then, the cells were analysed, and endocytic curves of microbeads were prepared as described in Section 3.1.3.

### 3.1.7 Bacteria Endocytosis by Antigen Presenting Cells

To investigate whether SlpB enhances endocytosis of lactobacilli,  $\text{CF}_{\text{Lp. plantarum}}$  and  $\text{SlpB-CF}_{\text{Lp. plantarum}}$  was prepared as described as Section 2.1.6 and co-incubated with APCs for various length of time at MOI of 100. The experiments were conducted as in Section 3.1.3.

To investigate whether SlpB enhanced phagocytosis of *E. coli*, *E. coli* DH5 $\alpha$  was cultured to stationary phase in 37°C, 100 rpm incubator shaker. Then, *E. coli* was stained with CFDA and co-incubated with 400  $\text{mg g}^{-1}$  [ $\text{SlpB bacteria}^{-1}$ ] as the method used to prepared  $\text{SlpB-CF}_{\text{Lp. plantarum}}$  as described in Section 2.1.6. Then, either  $\text{CF}_{\text{E. coli}}$  or  $\text{SlpB-CF}_{\text{E. coli}}$  was co-incubated with  $\text{M}\Phi$  or DC for 4 h at MOI of 100, and endocytosis was analysed with flow cytometry as described in Section 3.1.3. The fluorescence intensity obtained from decuplicate independent samples were analysed statistically.



### 3.1.8 Effect of SlpB-LP on Endocytosis of LP

A set of DC was incubated with <sup>FITC</sup>LP for 30 min. Then, excess <sup>FITC</sup>LP was removed by washing with PBS (-) for 3 times, followed by incubation with either SlpB-<sup>PI</sup>LP or <sup>PI</sup>LP for 30 min. Another set of DC was incubated with SlpB-<sup>PI</sup>LP for 30 min, washed and incubated with <sup>FITC</sup>LP for 30 min. Cells without incubating with LP and cells incubated with both <sup>FITC</sup>LP and SlpB-<sup>PI</sup>LP simultaneously for 60 min were used as control. The result was analysed as described in Section 3.1.3, and dot plot of each set of samples was plotted

### 3.1.9 Effect of SlpB-Stimulation on Particles Endocytosis

Prior co-incubation with LP, DC was stimulated with 10 µg ml<sup>-1</sup> SlpB for 0, 30 and 60 min. Then, DC was washed with PBS (-) thrice to remove SlpB attached on cells. SlpB-stimulated DC were co-incubated with <sup>PI</sup>LP at 37°C, 5% CO<sub>2</sub> humidified incubator for 60 min. Excessive <sup>PI</sup>LP was removed by washing the cells with PBS (-) thrice. The cells were detached and analysed with flow cytometer.

To investigate the effect of SlpB-stimulation on endocytosis of solid particles, *Lp. plantarum* was used as model. <sup>CF</sup>*Lp. plantarum* was treated with 5 M LiCl solution and washed with PBS (-) thrice to remove surface components. Then, DC was stimulated with SlpB for 1 h prior co-incubation with <sup>CF</sup>*Lp. plantarum*. Phagocytosis was analysed at 0.5 and 2.0 h after co-incubation with <sup>CF</sup>*Lp. plantarum*.

### 3.1.10 Effect of SlpB-Stimulation on Production of DC-SIGN

After stimulation with SlpB for 60 min, DC was treated with 2.5 g l<sup>-1</sup> trypsin in 1 mM ethylenediaminetetraacetic acid (EDTA) for 5 min to detach the cells and to remove SlpB attached on receptors. Then, the cells were fixed with 3.7% formaldehyde and 0.8% methanol. Permeation of cells was avoided to prevent detection of intracellular DC-SIGN. Then, DC-SIGN was stained with Abs and the concentration of DC-SIGN on cell surface was analysed with flow cytometer as described in Section 3.1.2.

### 3.1.11 Comparison with Other Types of Ligands

SlpA was extracted from *L. acidophilus* JCM 1132 as described in Chapter 2 and analysed with SDS-PAGE. Then, either 400 mg g<sup>-1</sup> SlpA or SlpB was coated on <sup>PI</sup>LP or 5 M LiCl solution treated <sup>CF</sup>*Lp. plantarum*. Liposomes were supplemented to APCs and co-incubated for 60 min,

while <sup>CF</sup>*Lp. plantarum* were co-incubated with APCs for 4 h at MOI of 100 and analysed as described in Section 3.1.3.

### 3.1.12 Endocytosis under Inhibition of Actin Condensation

A set of DC was treated with 10  $\mu$ M cytochalasin D<sup>[82]</sup> for 60 min prior incubation with carriers. Then, DC were co-incubated <sup>PI</sup>LP or SlpB-<sup>PI</sup>LP for 60 min, and with SlpB-<sup>CF</sup>*Lp. plantarum* for 120 min. Endocytosis was analysed as described in Section 3.1.3, and the changes in endocytosis by DC with and without cytochalasin D treatment were compared.

### 3.1.13 Adjuvant Effect of SlpA and SlpB

To evaluate adjuvant effect of SlpB on DC, DCs were incubated with 100 ng ml<sup>-1</sup> LPS with 10  $\mu$ g ml<sup>-1</sup> filtered sterile SlpB or 300  $\mu$ g ml<sup>-1</sup> OVA with 10  $\mu$ g ml<sup>-1</sup> SlpB. All reagents used are filtered sterile. SlpB was tested with limulus amebocyte lysate assay to confirm that endotoxin was below detection limit.

The adjuvant effect of SlpB on M $\Phi$  was also evaluated with 300  $\mu$ g ml<sup>-1</sup> OVA and 5  $\mu$ g ml<sup>-1</sup> SlpB as described in Ref 33.

### 3.1.14 Cytokine Production of Antigen Presenting Cells Treated with $\alpha^{GC}$ LP

To prepare SlpB- $\alpha^{GC}$ LP,  $\alpha^{GC}$ LP (contains 5 mg ml<sup>-1</sup>  $\alpha^{GC}$  in 50 mg ml<sup>-1</sup> LP<sup>†</sup>) was coated with 20 mg SlpB ml<sup>-1</sup>  $\alpha^{GC}$ LP. Endotoxin of sample was tested with limulus amebocyte lysate assay, and the endotoxin of SlpB and  $\alpha^{GC}$ LP were below detection limit.

$\alpha^{GC}$ LP or SlpB- $\alpha^{GC}$ LP was supplemented to M $\Phi$ , DC or mDC at 10  $\mu$ l  $\alpha^{GC}$ LP ml<sup>-1</sup> cell culture. After co-incubation for 60 min in 37.0°C, 5.0% CO<sub>2</sub> humidified incubator, cells were washed with D-PBS (-) thrice, and the medium was replaced with fresh sRPMI medium. Production of free cytokines in culture medium was measured with enzyme-linked immunosorbent assay (ELISA) kit after 48 h incubation in 37.0°C, 5.0% CO<sub>2</sub> humidified incubator.

IL-12/IL-23 (p40), IL-10, IL-17A and IL-6 which are representative cytokines for T helper (T<sub>H</sub>)1, T<sub>H</sub>2, T<sub>H</sub>17 responses were measured. ELISAs were conducted as manufacturer's instructions with 1 M sulphuric acid was used as stop solution. For each set of assays conducted, a calibration curve was plotted. Cytokines production was calculated based on calibration curves and analysed statistically.

---

<sup>†</sup> The composition of LP is unknown. The  $\zeta$  potential of  $\alpha^{GC}$ LP is in Appendix E.

### 3.1.15 mRNA Expression of DC Treated with $\alpha^{GC}LP$

DC was supplemented with either  $\alpha^{GC}LP$  or SlpB- $\alpha^{GC}LP$  at final concentration of  $10 \mu\text{l}$   $\alpha^{GC}LP \text{ ml}^{-1}$  cell culture and incubated in  $37.0^{\circ}\text{C}$ , 5.0%  $\text{CO}_2$  humidified incubator for 60 min. Then, the cells were washed with D-PBS (-) thrice, the culture medium was replaced with equal volume of fresh sRPMI medium, and incubated in  $37.0^{\circ}\text{C}$ , 5.0%  $\text{CO}_2$  humidified incubator. Cells were collected and total RNA was extracted at 8 h, 16 h and 24 h after treatment. Total RNA was extracted according to manufacturer's protocol of Qiagen RNeasy mini kit with materials listed in Appendix A. Quantity and quality of RNA was evaluated with NanoDrop spectrophotometer, and equal amount of RNA samples were mixed, and reverse transcribed into complementary DNA (cDNA) with qPCR RT master mix. The resulting cDNA was diluted 5-fold with nuclease-free water and mixed with primers listed in Appendix A. The mixtures were incubated in a StepOne Real Time PCR system according to the manufacturer's instructions. The data obtained were normalised with messenger RNA (mRNA) expression level of  $\beta$ -actin as housekeeping gene.

## 3.2 Results

### 3.2.1 Maintenance and Differentiation of THP-1 Cells

In *in vitro* study, THP-1 monocyte<sup>[83]</sup> was used as model cell as it can be induced into both M $\Phi$  and DC. Figure 3.1 shows the micrographs of various phenotypes of THP-1-derived cells which have been used in this study.

The expression of signature receptors on M $\Phi$  and DC were confirmed on specific phenotype by microscopic analysis (Figure 3.2) and flow cytometry (Figure 3.3).  $> 90\%$  cells express DC-SIGN for DC and Mincle for M $\Phi$ . The result shows that DC-SIGN was specifically expressed on DC, while Mincle was specifically expressed on M $\Phi$ , which suggest the specificity of expression on these receptors on specific phenotype of cell, i.e., Mincle on M $\Phi$  and DC-SIGN on DC. The result also suggested that THP-1 monocytes can be properly induced into each desired phenotype.

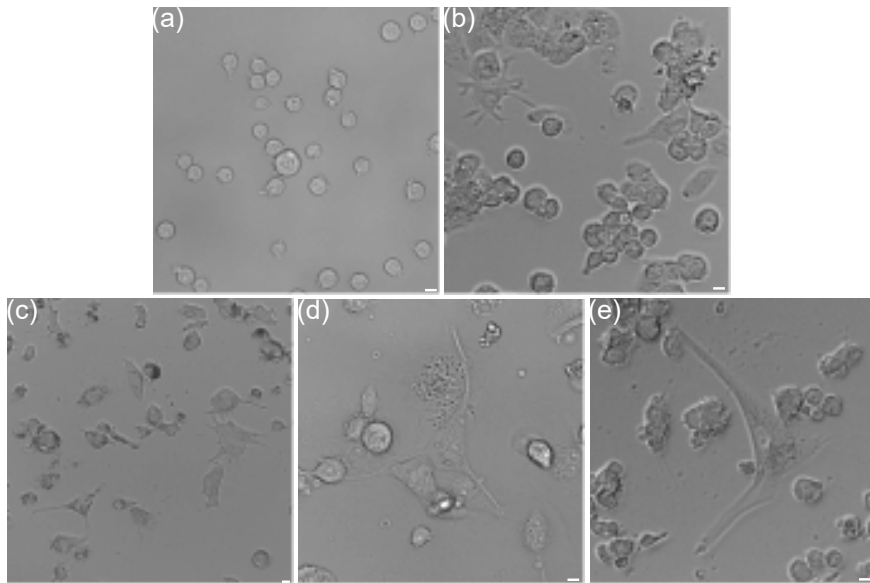


**Figure 3.1** Micrographs of various phenotypes of THP-1-derived cells. (a) THP-1 monocytes, (b) imMΦ, (c) MΦ, (d) DC, (e) mDC. The scale bars are 10  $\mu\text{m}$ .

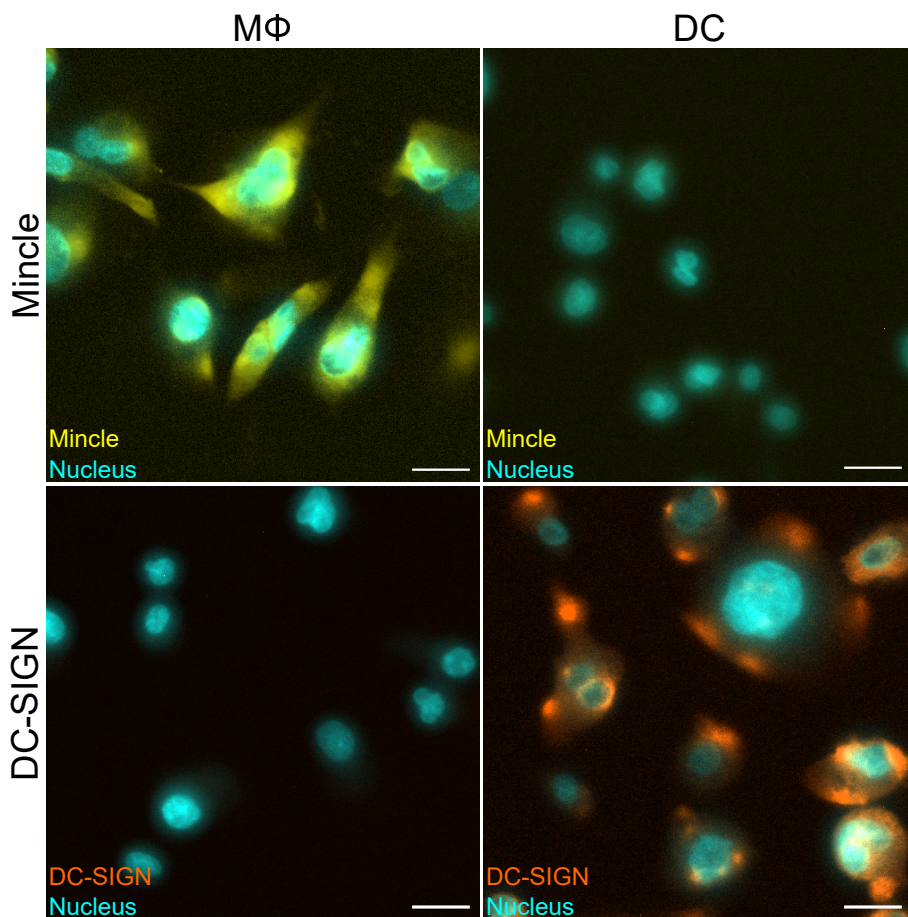


**Figure 3.2** Micrographs of expression of Mincle on MΦ and DC-SIGN on DC. The scale bars are 25  $\mu\text{m}$ .

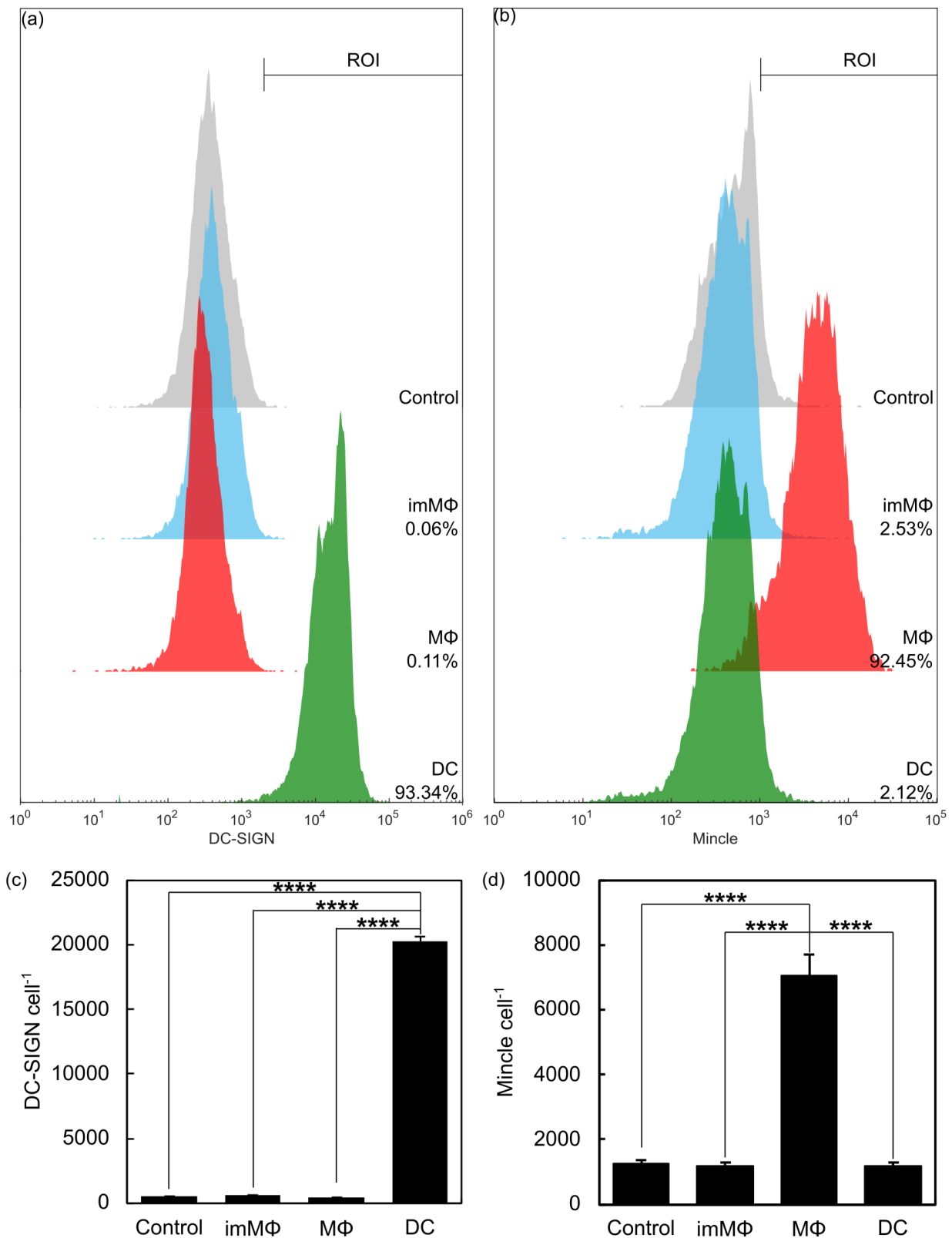


**Figure 3.3** Expression of DC-SIGN and Mincle on various phenotypes of THP-1-derived cells. Representative histogram obtained from flow cytometric analysis for (a) DC-SIGN and (b) Mincle. 5,000 cells were analysed for each sample. Grey areas indicate control. The numbers indicate percentage of cells in gated region. Statistical analysis of (c) DC-SIGN and (d) Mincle on each phenotypes. The plots represent data obtained from triplicate sample in independent test and the error bars represent standard deviation of mean. Statistical significance was evaluated by one-way analysis of variance (ANOVA) test followed by post-hoc testing using Tukey multi comparisons test. \*\*\*\*  $p < 0.0001$ .

### 3.2.2 Interaction of SlpB with DC

Prior study has shown that Slp from *Lv. brevis* binds to Mincle on M $\Phi$ <sup>[33]</sup>. Although study has also shown that Slp from *Lv. brevis* binds to DC-SIGN<sup>[29]</sup>, the result has raised concerns as Slp from *Lv. brevis* did not prevent Slp from *L. acidophilus*, a ligand of DC-SIGN, from binding DC-SIGN. Therefore, it is important to investigate whether SlpB from *Lv. brevis* binds to receptor on DC.

After co-incubating with FITC-SlpB, distinct increase in fluorescence intensity originated from SlpB was observed (Figure 3.4). Approximately 87.1% DC binds to SlpB. Considered the ratio of DC-SIGN<sup>+</sup> DC in this study, almost all DC-SIGN<sup>+</sup> DC binds to SlpB, which suggests that SlpB binds to DC.

Slp from *Lv. brevis* has been shown to bind to Mincle<sup>[33]</sup>, which is a C-type lectin on M $\Phi$ . Therefore, it potentially binds to other C-type lectin on DC, probably DC-SIGN, which SlpA from *L. acidophilus* binds to<sup>[24]</sup>. As Ab against SlpB is not commercially available, I have investigated the binding of SlpB to Mincle and DC-SIGN with Ab against Mincle and DC-SIGN.

Figure 3.5 shows that SlpB could bind to both Mincle and DC-SIGN. After 60 min pre-incubation of M $\Phi$  and DC with Ab against hMincle or Ab against hDC-SIGN, binding of SlpB to M $\Phi$  and DC were reduced by 1.5- and 1.7-fold respectively, which suggests that SlpB binds to DC-SIGN and Mincle.

To further eliminate the effect of potential unspecific binding of SlpB to Abs, binding of SlpB to DC-SIGN was assessed by blocking the access Abs to DC-SIGN with SlpB (Figure 3.6). Pre-blocking of DC with SlpB reduced the signal intensity originated from Ab against hDC-SIGN by 1.2-fold, which suggested that the result obtained in Figure 3.5 was robust against unspecific binding of SlpB to Abs.

As both Mincle and DC-SIGN are C-type lectins which interact with sugar, I have aligned the amino acid sequence of SlpB with carbohydrates binding domains as described in *C. difficile* toxins (ToxA) and *Streptococcus mutans* glucosyltransferases (GBP)<sup>[84]</sup> which are responsible for glycoconjugation, to confirm the location of SlpB responsible for DC-SIGN and Mincle binding (Figure 3.7). All the sugar binding sites are located in N-terminal of SlpB.

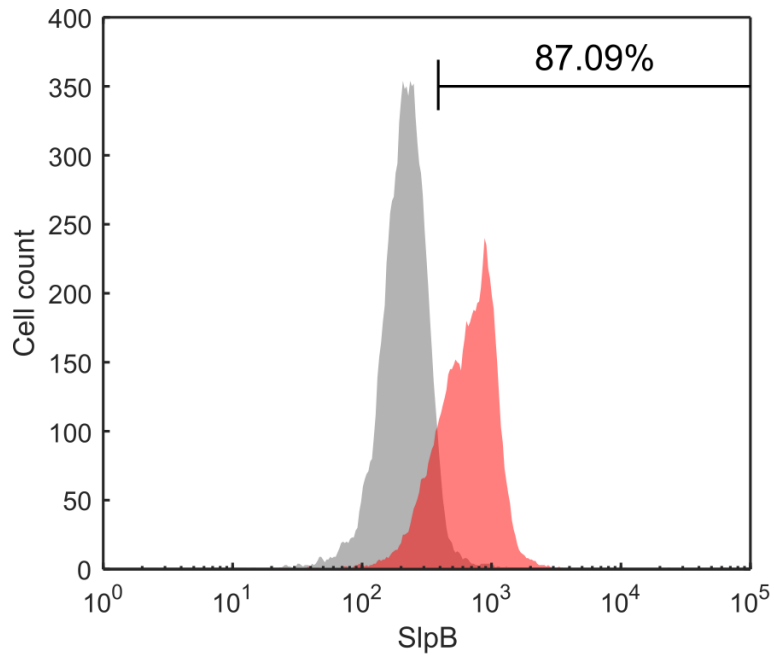


**Figure 3.4** SlpB binds to DC. Flow cytometric analysis of SlpB binding to DC. 10,000 cells were analysed for each sample. Grey area indicates control. The number indicates percentage of cells in gated region.

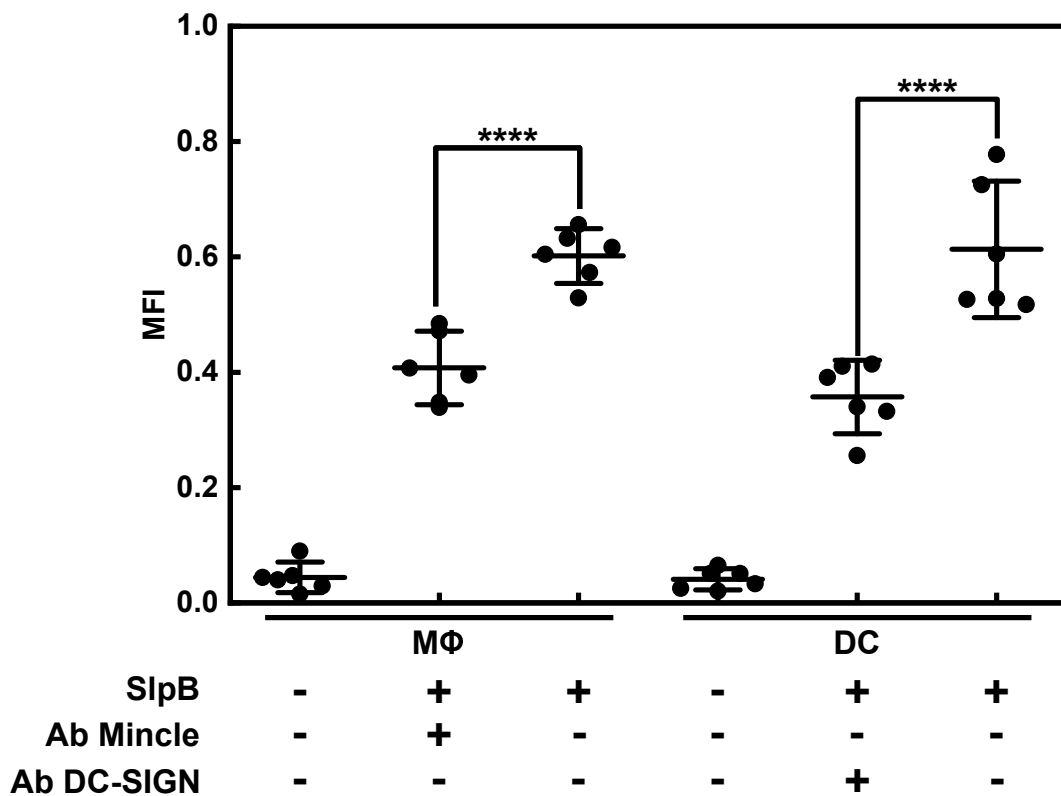


**Figure 3.5** SlpB binds to Mincle and DC-SIGN. The plots represent data obtained from sextuplicate sample in independent test and the error bars represent 95% confidence interval of mean. Statistical significance was evaluated by one-way ANOVA test followed by post-hoc testing using Tukey multi comparisons test. \*\*\*\*  $p < 0.0001$ .

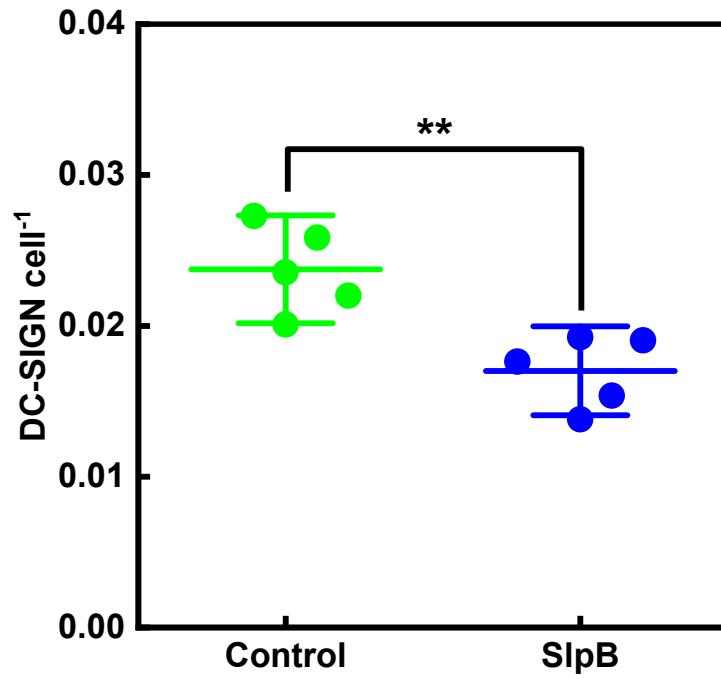


**Figure 3.6** SlpB blocks the binding of Ab against DC-SIGN to DC. The plot represents data obtained from quintuplicate sample in independent test and the error bars represent 95% confidence interval of mean. Statistical significance was evaluated with Student's t-test. \*\*  $p < 0.01$ .



SlpB	<b>K</b> <u><b>SAAKVT</b></u> SDKVL <b>T</b> <u><b>DDATKRN</b></u> VNLTGTNAIYSKPGTVKGAKVVATTTAKNLNKSTTSREN	60
von Eichel-Streiber	-----TIDGKKYYFN-----	
FnB	-----	
Cof	-DTAPVR-----	
ActA	-----	
SlpB	FRAYRVAK <u><b>TNRGSIYYK</b></u> VVSYN <u><b>KAYRGWVYG</b></u> GKSDTAFAGGLTSYD <u><b>TFKEGT</b></u> LTADQKSG	120
von Eichel-Streiber	-----TIDGKKYYF-----KAVTGWQTI-----	
FnB	-----SFEEDT-----	
Cof	-----	
ActA	-----	
SlpB	NYKLANPGKTEAGLTYK <u><b>QPAWTQYKIGK</b></u> TIADTTAYKDATFSV <u><b>DKVGT</b></u> <u><b>RTREGDTWVHV</b></u> V	180
von Eichel-Streiber	-----DGkwYYFDxNG-----GWQTI DGkwYYFDX	
FnB	-----	
Cof	-----	
ActA	-----PKVFKKIKDAGKWVRDK	
SlpB	<u><b>NQ</b></u> NTADTKAD <u><b>GW</b></u> ILLSNLQTNAFNEASQVKVINNLKGETLKSFNYNVGTATNTNAAD	240
von Eichel-Streiber	NG---KAVTGWQTI DGkwYYFDXNG-----	
FnB	-----	
Cof	-----S	
ActA	ID-----	
SlpB	<u><b>NTVYDSTA</b></u> TPTKFADGFA <u><b>ATVKNALAG</b></u> TGYTVDGTNALNRVANLKS GSTLTIIYATEGTQK	300
von Eichel-Streiber	-----	
FnB	-----	
Cof	KM VYASSK-----DALRRALNG-----	
ActA	-----	
SlpB	PSTVSVFAQYPDTPSINQVKVATADQTKDGVADAATAQNLINQPAATTLFTGVEGKSFTA	360
von Eichel-Streiber	-----	
FnB	-----	
Cof	-----	
ActA	-----	
SlpB	TEALAYLNGNASMKKLTSPSWTETS <u><b>GSTSVTYQ</b></u> WVLTSPQAFAGQYGS PFSAIYTAKKTV	420
von Eichel-Streiber	-----	
FnB	-----EEDKPKYE-----	
Cof	-----	
ActA	-----	
SlpB	VPATGSNDNNTDNPIANGVVSSTPTANPTDTTK	453
von Eichel-Streiber	-----	
FnB	-----	
Cof	-----	
ActA	-----	

**Figure 3.7** Sequence alignment of SlpB to carbohydrates binding domains as described in *C. difficile* toxins (ToxA) and *Streptococcus mutans* glucosyltransferases (GBP)<sup>[84]</sup> which is responsible for glycoconjugation. Other binding motifs, e.g., binding domain from fibronectin binding protein B (FnB) from *Staphylococcus aureus*<sup>[85]</sup>, actin binding protein from *Listeria monocytogenes* (ActA) and SipA from *Salmonella typhimurium*<sup>[86,87]</sup>, and actin binding domain from cofilin<sup>[88]</sup> were identified mainly in N-terminal of SlpB. Upper case letters indicate highly conserved residues or residues with an identity of 50% or higher. X, variable residue.

Interestingly, alignment with other binding motifs, e.g., binding domain from fibronectin binding protein B (FnB) from *Staphylococcus aureus*<sup>[85]</sup>, actin binding protein from *Listeria monocytogenes* (ActA) and SipA from *Salmonella typhimurium*<sup>[86,87]</sup>, and actin binding domain from cofilin<sup>[88]</sup> suggests that all the common binding domains of SlpB can be found in its N-terminal, which potentially reduce unspecific binding to extracellular matrices (Figure 3.7)), in contrast to SlpA from *L. acidophilus*, *L. helveticus*, etc.

### 3.2.3 SlpB-Coating Enhances Endocytosis by Antigen Presenting Cells

In previous subsection, I have shown that SlpB is a ligand of DC-SIGN; while prior study has shown that SlpB is a ligand of Mincle<sup>[33]</sup>, which suggests that SlpB is a potential ligand to both M $\Phi$  and DC. As M $\Phi$  and DC are usually co-localised in immune organ, it is difficult to overlook the effect of either type of APCs. Therefore, the effect of SlpB on the endocytosis of both types of cells are investigated.

#### SlpB Enhances Endocytosis of Liposome

To study endocytosis of liposome, PI dissolved in deionised water was used as indicator. PI is live cell impermeable dye, which could reduce the noise generated by leakage of dye from liposome during incubation, rendering it a more robust tool to evaluate endocytosis of liposome compared to other dyes. Flow cytometric analysis of DC after co-incubating with 10  $\mu$ M PI for 70 min (Figure 3.8) shows no distinct shift in distribution of fluorescent intensity, which suggests that PI did not permeate the membrane of live cells.

To determine the optimal time of co-incubation required to facilitate active endocytosis of LPs by APCs, time-lapse flow cytometric analysis was performed (Figure 3.9). For both M $\Phi$  and DC, MFI increased significantly 60 min after co-incubation with SlpB-<sup>PI</sup>LP compared to <sup>PI</sup>LP. The fluorescence intensity increased by 3.4-fold at 60 min and 1.5-fold at 70 min for M $\Phi$ ; 2.4-fold at 60 min and 2.3-fold at 70 min for DC. The result suggested that 60 min is required for SlpB to induce active endocytosis of liposome (Figure 3.9 (a - b)).

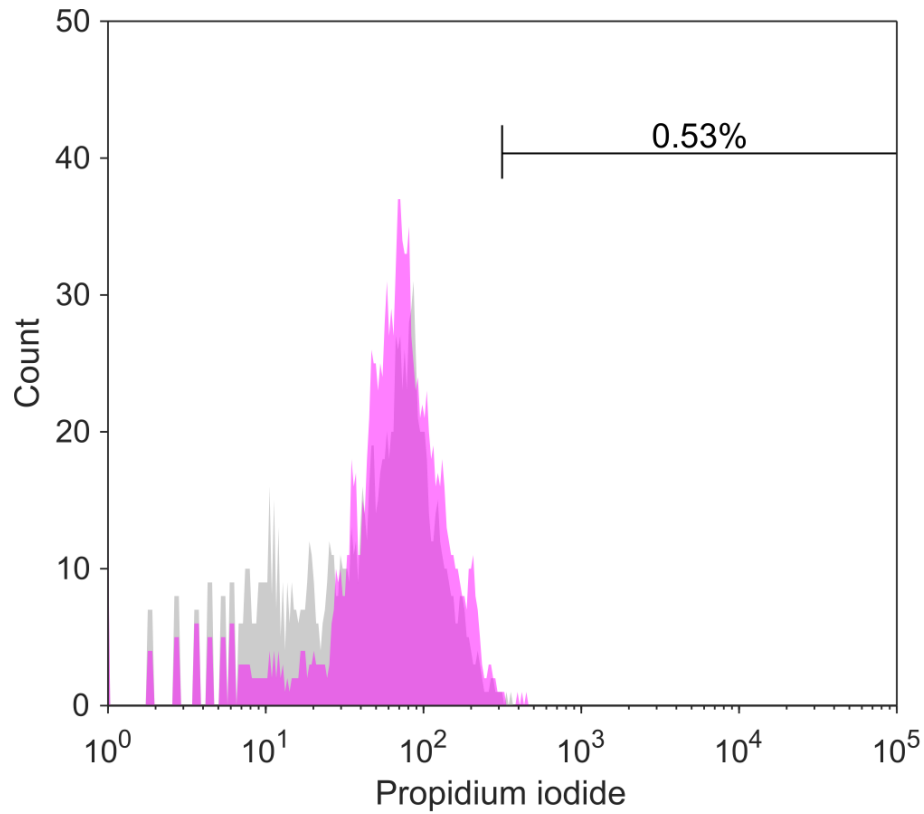


**Figure 3.8** Flow cytometry analysis of DC co-incubated with 10  $\mu$ M PI for 70 min. 1,500 cells were analysed for each sample. Grey area indicates control. The number indicates percentage of cells in gated region.

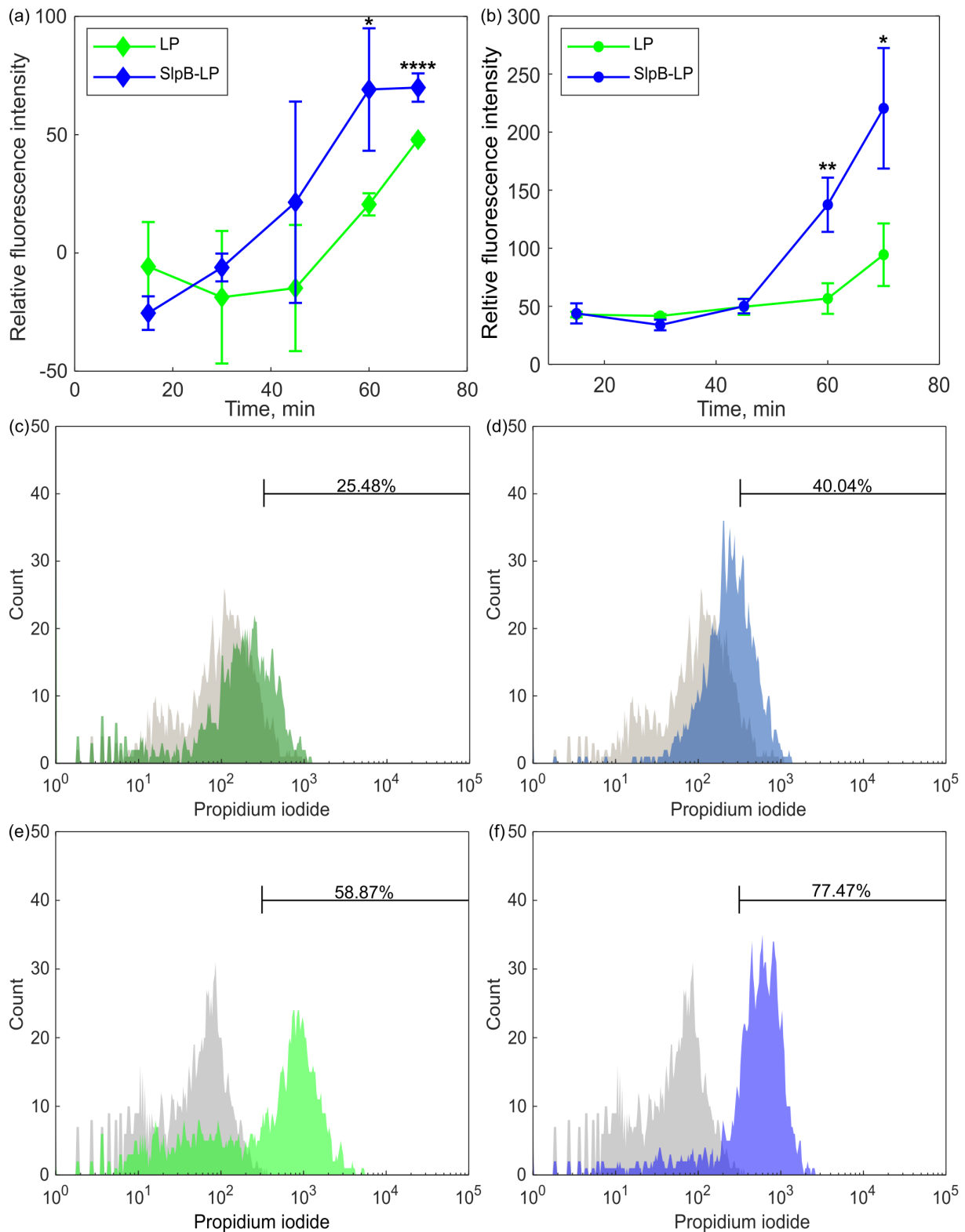


**Figure 3.9** Endocytosis of liposomes by APCs. Kinetics of liposome endocytosis by (a) MΦ and (b) DC. The plots represent data obtained from triplicate sample in independent test and the error bars represent standard deviation of mean. Statistical significance was evaluated with Student's t-test. \*  $p < 0.05$ , \*\*  $p < 0.01$ , \*\*\*\*  $p < 0.0001$ . Representative histograms of MΦ co-incubated with (c)  $^{PI}LP$  and (d) SlpB- $^{PI}LP$  for 70 min; DC co-incubated with (e)  $^{PI}LP$  and (f) SlpB- $^{PI}LP$  for 70 min. 1,500 cells were analysed for each sample. Grey areas indicate control. The numbers indicate percentage of cells in gated region.

The property of membrane impermeability of PI originates from its hydrophilicity. With LP as carrier, PI was able to be delivered to 25.5% M $\Phi$  and 58.9% DC at 70 min co-incubation. Delivery of PI was further enhanced by SlpB-coating, which resulted in 40.0% and 77.5% PI<sup>+</sup> M $\Phi$  and DC respectively (Figure 3.9 (c - f)), compared to 0.5% for PI in deionised water.

The histogram obtained from cells 70 min after co-incubation with PI<sup>I</sup>LP and SlpB-PI<sup>I</sup>LP (Figure 3.9 (c - f)) revealed that besides enhanced endocytosis of LP through ligand-receptor interaction, SlpB has also facilitated even distribution of LP among cells. A narrower peak width and higher frequency was observed on both histograms of cells co-incubated with SlpB-PI<sup>I</sup>LP. Furthermore, increases in percentage of PI<sup>+</sup> cells and MFI for cells co-incubated with SlpB-PI<sup>I</sup>LP was also observed.

To further confirm the condition of LPs endocytosis in cells, i.e., whether the LPs were attached to the surface of cells or endocytosed into cells, imaging of DCs after 30 min and 70 min co-incubated with LPs were conducted. As PI is potentially dissolved in methanol, which is used as stabiliser in formaldehyde solution, and diffuse through cell membrane upon fixation, Cy3-conjugated ovalbumin (Cy<sup>3</sup>OVA) was encapsulated in LP instead of PI, and DC was chosen as model for its higher endocytic capacity (Figure 3.9 (a - b)).

The micrographs show that liposomes were endocytosed into DCs for all samples (Figure 3.10). MFI of Cy<sup>3</sup>OVA within region enclosed by the signal of DC-SIGN was quantified and compared among samples. Higher intensity of LP per pixel<sup>2</sup> was found in DC co-incubated with SlpB-Cy<sup>3</sup>-OVA<sup>I</sup>LP, confirmed that SlpB-coating has enhanced endocytosis of LP by DC via ligand-mediated endocytosis.

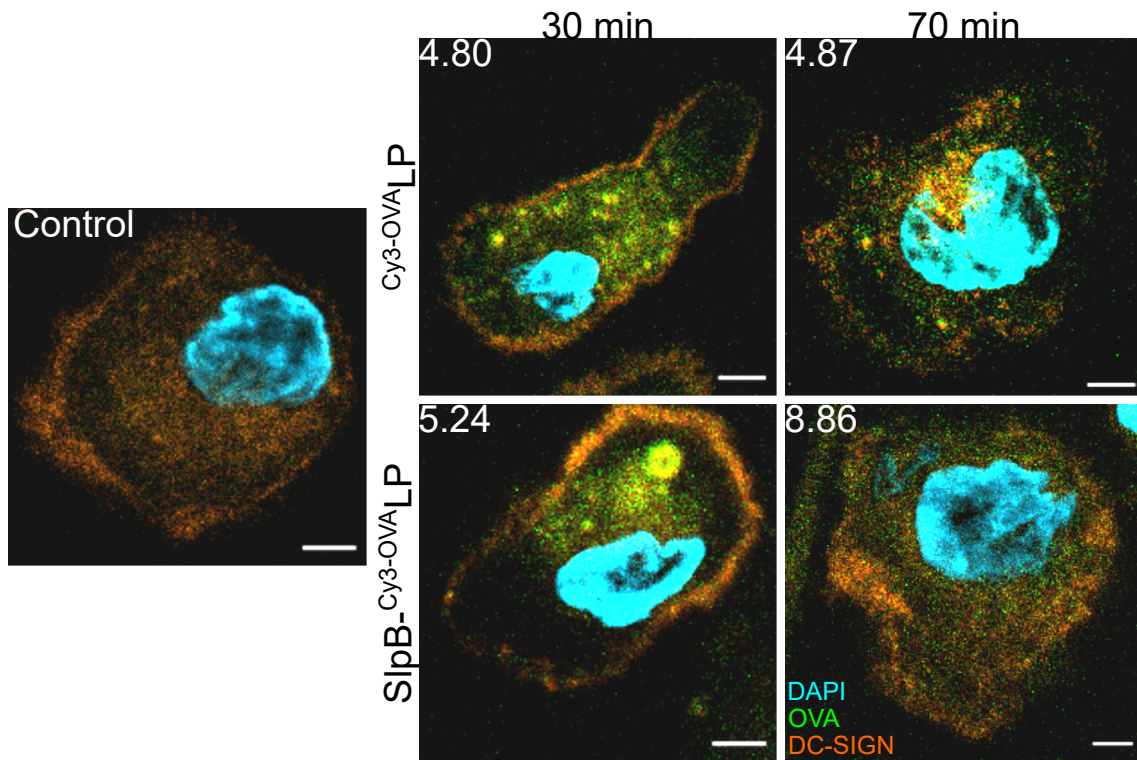


**Figure 3.10** Pinocytosis of  $Cy^3$ -OVA<sub>1</sub>LP and SlpB- $Cy^3$ -OVA<sub>1</sub>LP by DC at 30 min and 70 min co-incubation. The number in each diagram indicates MFI of  $Cy^3$ OVA of area enclosed by DC-SIGN. The scale bars are 5  $\mu$ m.

### **Effect of Particle Size on Endocytosis**

Although prior study<sup>[89]</sup> has suggested that particle size of liposome will affect endocytosis of liposome, the effect of particle size of liposome on endocytosis by professional phagocytes was not investigated. In this section, I investigated the relationship between particle size and endocytosis by professional phagocytes.

After sonication, both mean and standard deviation of particle size of spLP were reduced by 20-fold compared to pLP, and the polydispersity index was reduced from 1.23 to 0.80 (Figure 3.11).

pLP and spLP with or without SlpB were co-incubated with M $\Phi$  and DC, and the effect of the size of liposomes on endocytosis were compared. Regardless particle size and polydispersity of liposomes, SlpB has enhanced endocytosis by both M $\Phi$  and DC. With SlpB-coating, endocytosis of pLP increased by 3.2-fold for M $\Phi$  and 1.9-fold for DC, while endocytosis of spLP increased by 4.4-fold for M $\Phi$  and 1.8-fold for DC (Figure 3.12).

On the other hand, reduced particle size of liposome has decreased endocytosis of liposomes by both M $\Phi$  and DC (Figure 3.12). Although no statistical significance between pLP and spLP was detected in M $\Phi$ , the data pair was statistical different; while statistical significance was observed for DC. Endocytosis of spLP decreased by 2.2-fold, and SlpB-spLP decreased by 2.4-fold after sonication. Liposome with larger particle size sediment during incubation, thus increase the probability of contact between liposome and cells, which in turn increase the endocytosis of liposomes by APCs.

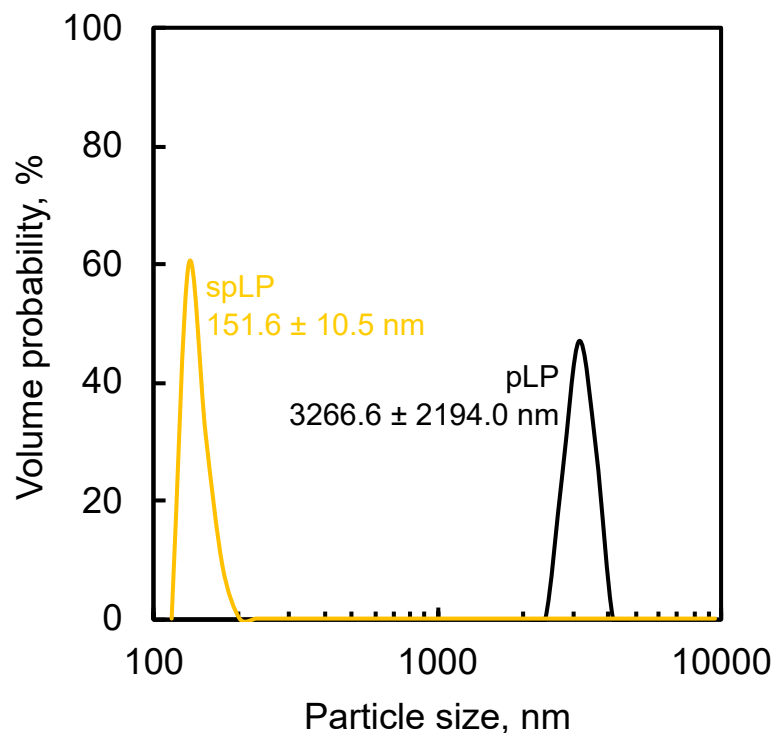


**Figure 3.11** Particle size distribution of pLP and spLP measured by dynamic light scattering method.

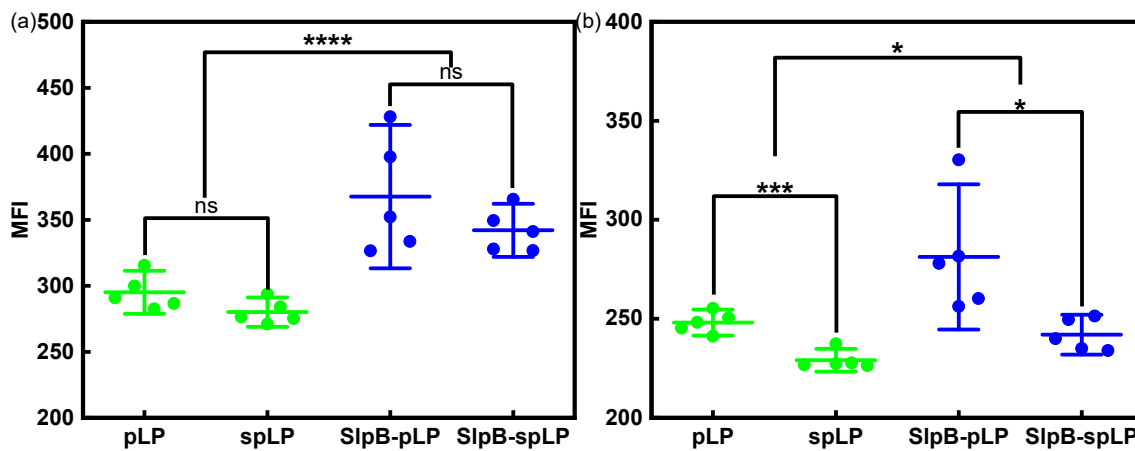


**Figure 3.12** Effect of particle size on endocytosis of liposome. Endocytosis by (a) MΦ and (b) DC. The plots represent data obtained from quintuplicate sample in independent test and error bars represent 95% confidence interval of mean. Statistical significance was evaluated with Student's t-test. \*  $p < 0.05$ , \*\*\*  $p < 0.001$ , \*\*\*\*  $p < 0.0001$ . ns indicates non-significant,



### Microbeads Endocytosis by Antigen Presenting Cells

Besides liposomes, various carriers are also used as drug vehicles for various purposes, i.e., solid microcapsules are used as vehicle to achieve slow-release of drugs<sup>[90,91]</sup> while recombinant bacteria<sup>[92-94]</sup> are used to deliver recombinant proteins. In Section 2.2.5, I have demonstrated that SlpB can be coated on microbeads and bacteria besides liposomes. In this section, I investigate whether SlpB-coating will also increase endocytosis of these carriers.

From the kinetic curve of phagocytosis (Figure 3.13), MFI increased by 2.1-, 2.0-, and 2.7-fold for M $\Phi$  co-incubated with microbeads for 1, 2, and 4 h respectively; 5.1-fold for DC co-incubated with microbeads for 4 h. As M $\Phi$  has higher phagocytic activity than DC, significant increase in endocytosis of microbeads was observed within 1 h co-incubation (Figure 3.13(a)), while 4 h was required for DC to significantly increase endocytosis of microbeads (Figure 3.13 (b)).

However, as fluorophore was conjugated on the surface of microbeads, SlpB-coating might have quenched some fluorophore, which resulted in reduced fluorescence intensity. Analysing the fraction of cells which have endocytosed microbeads (Figure 3.13 (c - d)) revealed that SlpB-coating has increased phagocytosis of microbeads by M $\Phi$  in 1 h as in phagocytic curve described by fluorescence intensity, while it required 2 h for DC to elevate phagocytosis of microbeads by 1.3-fold instead of 4 h.

Moreover, analysing representative histogram of M $\Phi$  and DC at 4 h after co-incubation with microbeads (Figure 3.13 (e - h)) suggests that SlpB has increased phagocytic activity of both M $\Phi$  and DC. Comparing the distribution of cells in gated region in Figure 3.13 (e - h), higher frequency of cells are detected in the region where fluorescence intensity  $> 10^4$ , which suggests that SlpB has increased both the fraction of cells which have phagocytosed microbeads and the phagocytic capacity of cells.

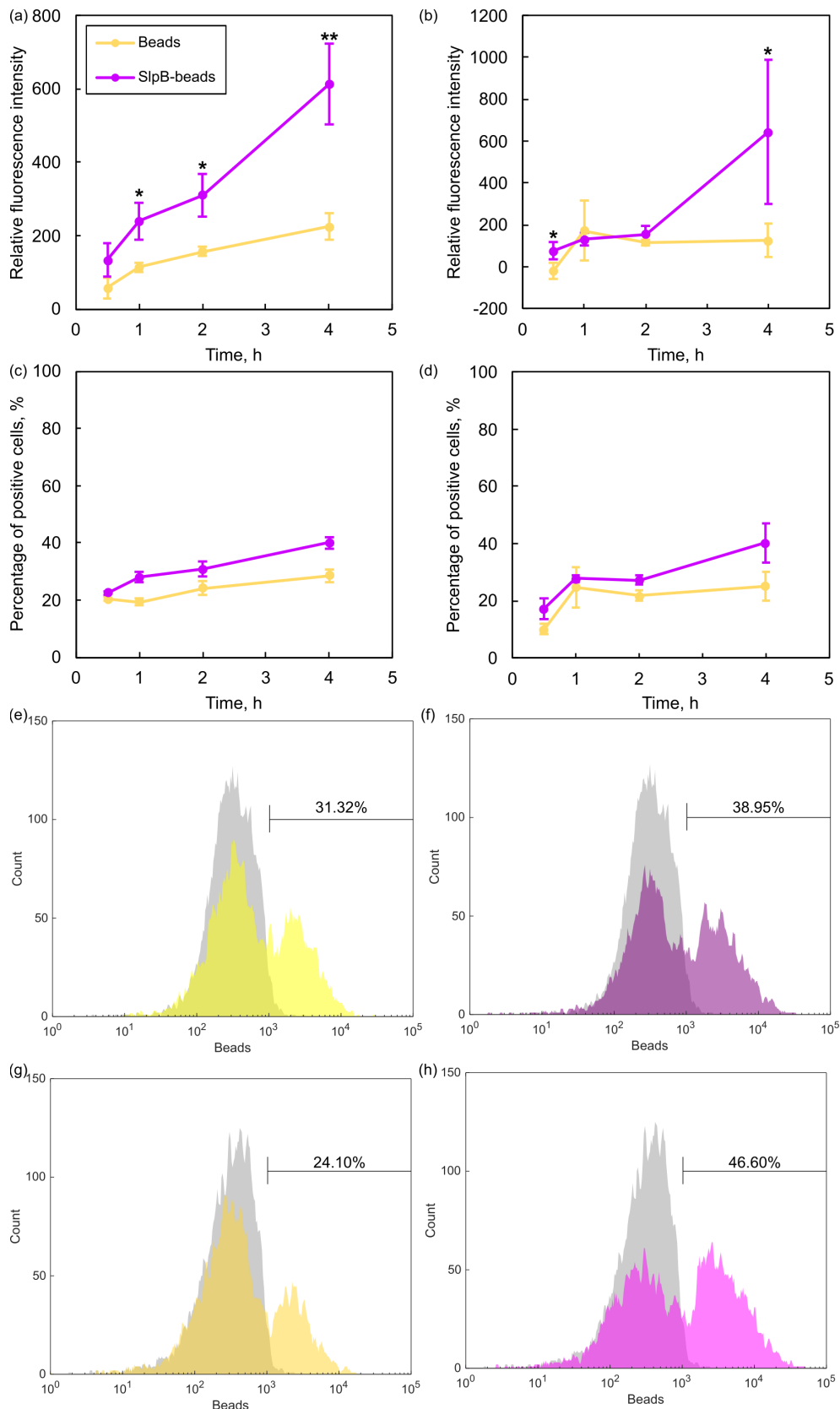


**Figure 3.13** Phagocytosis of microbeads by MΦ and DC. Phagocytic kinetic of (a) MΦ and (b) DC. MOI = 100. The plots represent data obtained from triplicate sample in independent test and the error bars represent standard deviation of mean. Statistical significance was evaluated with Student's t-test. \*  $p < 0.05$ , \*\*  $p < 0.01$ . Phagocytic kinetic evaluated by percentage of positive cells in gated region for (c) MΦ and (d) DC. Representative histogram of MΦ co-incubated with (e)  $Cy3$  beads and (f) SlpB- $Cy3$  beads, and DC co-incubated with (g)  $Cy3$  beads and (h) SlpB- $Cy3$  beads for 4 h. 5,000 cells were analysed for each sample. Grey areas indicate control and the numbers indicate percentage of cells in gated region.

### Bacteria Endocytosis by Antigen Presenting Cells

To investigate whether SlpB enhances endocytosis of Gram-positive bacteria, <sup>CF</sup>*Lp. plantarum* and SlpB-<sup>CF</sup>*Lp. plantarum* was prepared as described as Section 2.2.5 and co-incubated with APCs for various length of time.

Relative fluorescence intensity increased by 2.4-, 2.1-, 1.8-, 1.9-fold for M $\Phi$  co-incubated with SlpB-*Lp. plantarum* for 0.5, 1, 2, 4 h respectively; 1.2- and 1.8-fold for DC co-incubated with SlpB-*Lp. plantarum* for 2 and 4 h respectively based on the phagocytic curves obtained (Figure 3.14 (a)). For M $\Phi$ , 30 min was required to significantly increases phagocytosis of SlpB-*Lp. plantarum* compared to *Lp. plantarum* (Figure 3.14 (a)), while 2h was required for DC to elevate phagocytosis of SlpB-*Lp. plantarum* significantly (Figure 3.14 (b)).

Analysing histogram of flow cytometric analysis of M $\Phi$  and DC 4 h after co-incubation with *Lp. plantarum* and SlpB-*Lp. plantarum* shows that a more distinct peak shift in fluorescence intensity and higher fluorescence intensity was achieved by DC in gated region despite of longer time required to significantly increase phagocytosis (Figure 3.14 (c - f)), which suggests that DC has higher phagocytic capacity, while M $\Phi$  has a higher phagocytic activity.

To expand the application of SlpB-coated bacteria in drug delivery, the potential of SlpB in enhancing phagocytosis of Gram-negative bacteria was investigated. Figure 3.15 shows phagocytosis of *E. coli* by M $\Phi$  and DC at 4 h after co-incubation. The interaction of M $\Phi$ -*E. coli* and DC-*E. coli* have been confirmed by phagocytosis of bare *E. coli*. After subtracting control, SlpB has increased phagocytosis of *E. coli* by M $\Phi$  by 1.5-fold, while it increased phagocytosis by DC by 1.4-fold.

These results suggest that SlpB-coating on both Gram-positive and Gram-negative bacteria could significantly improve phagocytosis by APCs.

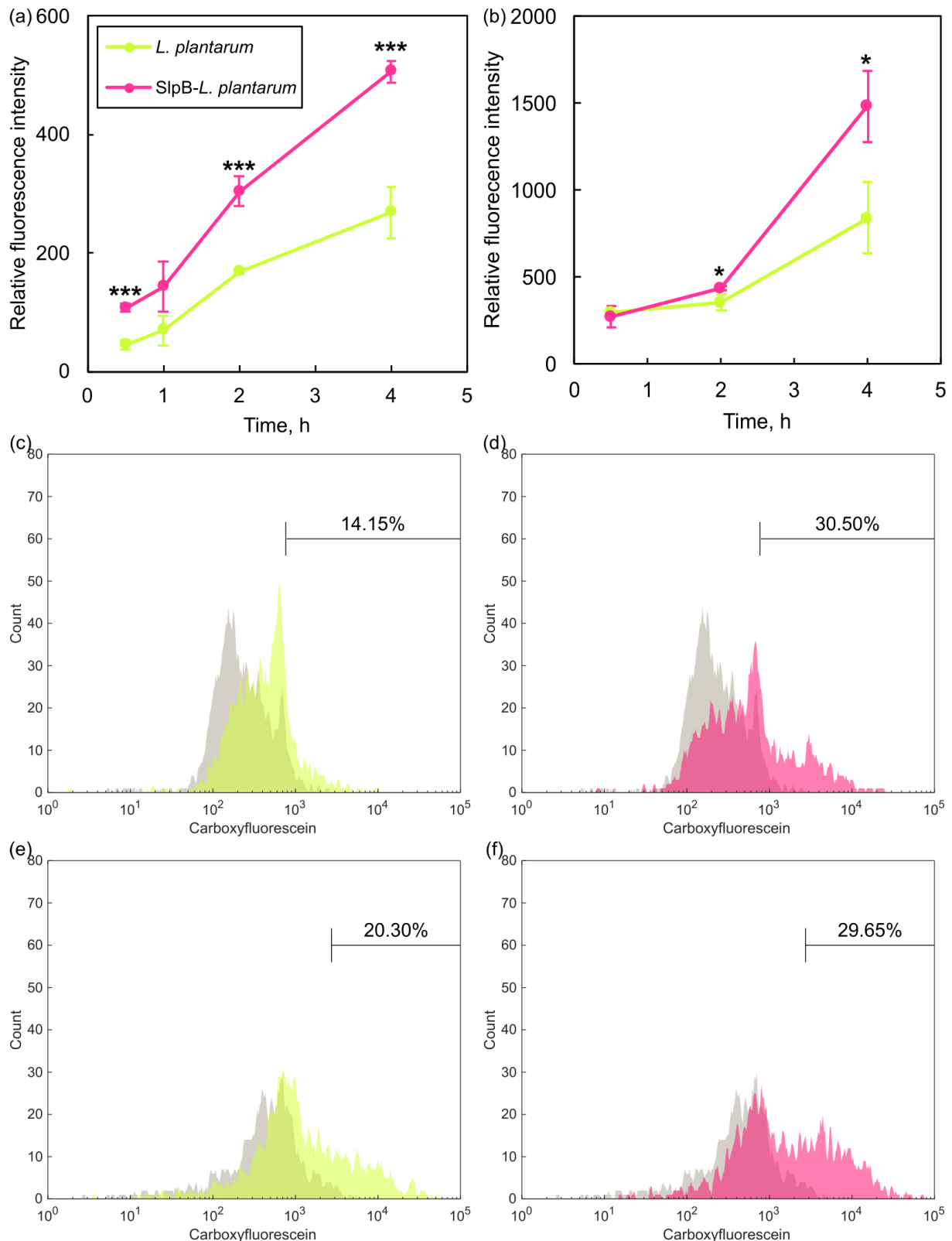


**Figure 3.14** Phagocytosis of *Lp. plantarum* with and without SlpB by MΦ and DC. Phagocytic kinetic of (a) MΦ and (b) DC. MOI = 100. The plots represent data obtained from triplicate sample in independent test and the error bars represent standard deviation of mean. Statistical significance was evaluated with Student's t-test. \*  $p < 0.05$ , \*\*\*  $p < 0.001$ . Representative histograms of MΦ co-incubated with (c) <sup>CF</sup>*Lp. plantarum* and (d) SlpB-<sup>CF</sup>*Lp. plantarum*, and DC co-incubated with (e) <sup>CF</sup>*Lp. plantarum* and (f) SlpB-<sup>CF</sup>*Lp. plantarum* for 4 h. 2,000 cells were analysed for each sample. Grey areas indicate control and the numbers indicate percentage of cells in gated region.

### 3.2.4 Potential Mechanism of SlpB-Induced Endocytosis

I have demonstrated that SlpB could enhance endocytosis of liposome by both M $\Phi$  and DC with focus on DC. In this section, I discuss the potential mechanism of SlpB-induced enhancement of endocytosis.

Through ligand-receptors interaction, SlpB might induced ligand-mediated endocytosis, which is specific to APCs, thus enhanced endocytosis of liposome.

To investigate the effect of endocytosis of SlpB-LP on endocytic activity of LP, I have evaluated whether stimulation with SlpB-LP could enhance endocytosis of LP (Figure 3.16). When DC was incubated first with LP (Figure 3.16 (b - c)), increase in intensity related to either LP was small, which suggest that LP alone does not affect the endocytosis by DC. As discussed in Section 3.2.3, 60 min was required for SlpB to elevate endocytosis of SlpB-LP. Therefore, incubating with SlpB-LP for 30 min after incubation with LP for 30 min does not result in difference in endocytosis of liposomes.

On the other hand, when DC was incubated either first with SlpB-LP or with both SlpB-LP and LP simultaneously, endocytic activity was enhances, and almost all DC was stained with either type of LP (Figure 3.16 (d - e)). This observation suggests that SlpB-LP could activate pathway related to enhanced endocytosis in DC.

To confirmed if this activation originated from SlpB alone or both SlpB and LP are required to enhance the endocytosis, influence of SlpB on endocytosis of liposome by DC was investigated by co-incubation of SlpB and LP with DC sequentially.

In crease in both fluorescence intensity and percentage of LP<sup>+</sup> cells suggested that SlpB could stimulate DC and enhanced endocytosis of LP by DC (Figure 3.17). As shown in Section 3.2.2, SlpB binds to DC-SIGN on DC. Binding to DC-SIGN results in rapid internalisation of particles with a speed of 1  $\mu\text{m s}^{-1}$  [95]. Activation of DC by SlpB-DC-SIGN interaction might increase the endocytic activity of DC.

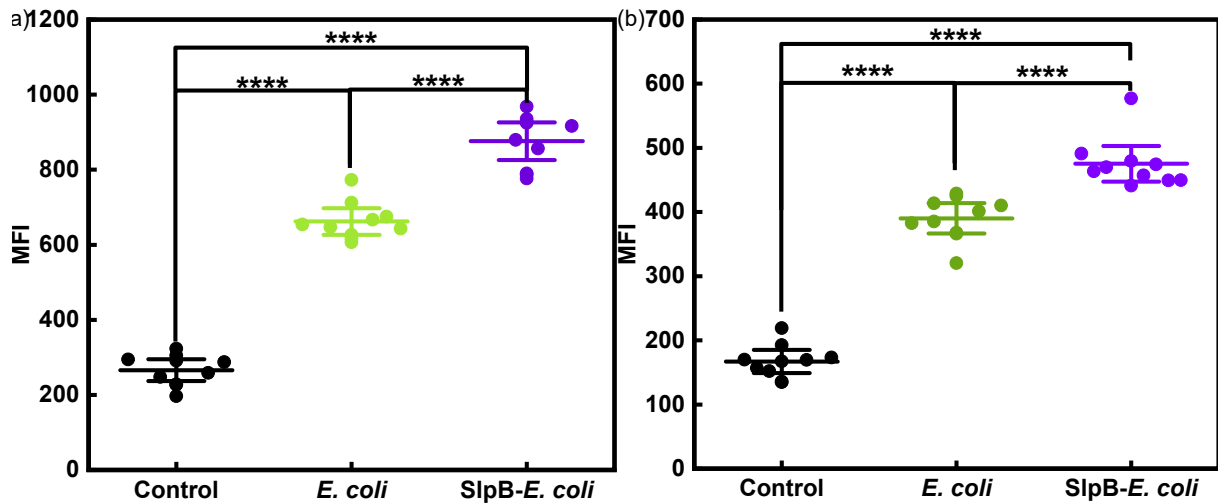


**Figure 3.15** Endocytosis of *E. coli* DH5 $\alpha$  by APCs. MOI = 100. The plots represent data obtained from decuplicate samples in independent test and the error bars represent 95% confidence interval of mean. 5,000 cells were analysed for each sample. Statistical significance was evaluated by one-way ANOVA test followed by post-hoc testing using Tukey multi comparisons test. \*\*\*\*  $p < 0.0001$ .

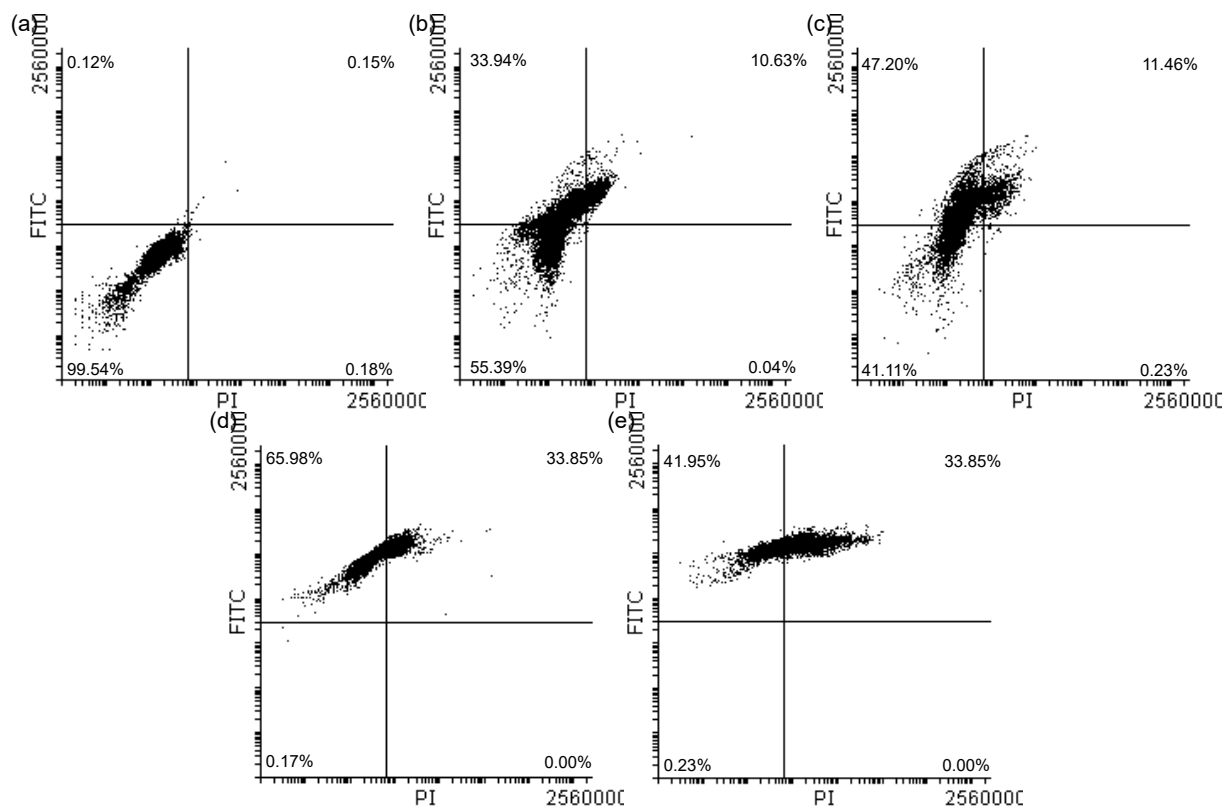


**Figure 3.16** Effect of uptake of SlpB-LP on endocytic activity of DC. (a) Control DC, (b) DC co-incubated with FITC-LP for 30 min followed by SlpB-PI-LP for 30 min, (c) DC co-incubated with FITC-LP for 30 min followed by PI-LP for 30 min, (d) DC co-incubated with SlpB-PI-LP for 30 min followed by FITC-LP for 30 min, (e) DC co-incubated with FITC-LP and SlpB-PI-LP for 60 min. 2,000 cells were analysed for each sample.

Besides liposome, I have also evaluated the effect of SlpB stimulation on phagocytosis of *Lp. plantarum*. Enhanced endocytosis by DC via SlpB-stimulation does not only limit to liposome. Phagocytosis of *Lp. plantarum* has also been increased after DC was stimulated with SlpB for 1 h (Figure 3.18), which support the model that activation of DC via SlpB-DC-SIGN interaction could increase endocytic activity of DC.

Rapid movement of DC-SIGN in DC might increase receptors recycling, which potentially create a feed-forward loop to increase the density of DC-SIGN on cell surface. To verify this hypothesis, I have measured the concentration of DC-SIGN on cell surface 60 min after stimulation with SlpB. Distinct peak shift can be observed from histogram when cells were stimulated with SlpB, while no increase in DC-SIGN on cell surface was observed when other protein, e.g., BSA was co-incubated with DC (Figure 3.19), which suggests that SlpB could increase the availability of DC-SIGN on cell surface, potentially through activation of DC by SlpB-DC-SIGN binding.

Stimulation of rapid movement of DC-SIGN in DC by SlpB might explain higher endocytic capacity of DC compared to M $\Phi$ , even though M $\Phi$  exhibit higher endocytic activity.

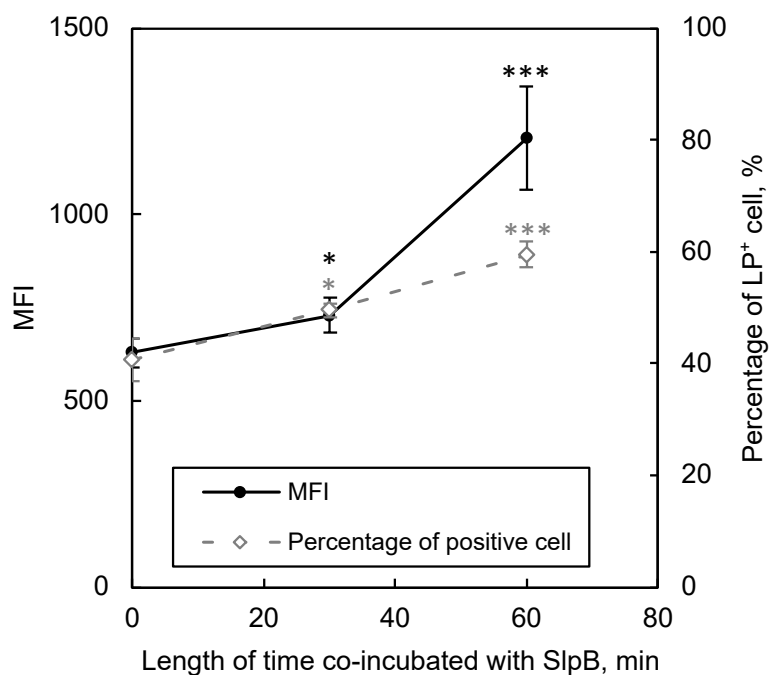


**Figure 3.17** Endocytosis of liposome by DC after SlpB-treatment for various length of time prior co-incubation with  $^{PI}LP$ . The plots represent data obtained from triplicate sample in independent test and the error bars represent standard deviation of mean. Statistical significance of each plot against control was evaluated with Student's t-test. \*  $p < 0.05$ , \*\*\*  $p < 0.001$ .

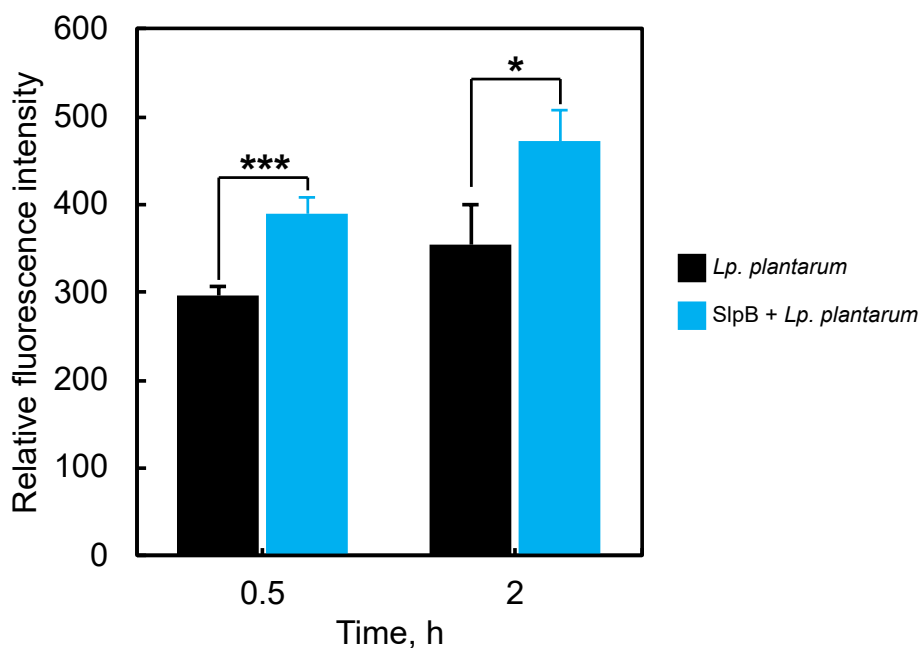


**Figure 3.18** Endocytosis of *Lp. plantarum* by DC after SlpB-treatment for various length of time prior co-incubation with *Lp. plantarum*. The plots represent data obtained from triplicate sample in independent test and the error bars represent standard deviation of mean. Statistical significance of each plot against control was evaluated with Student's t-test. \*  $p < 0.05$ , \*\*\*  $p < 0.001$ .



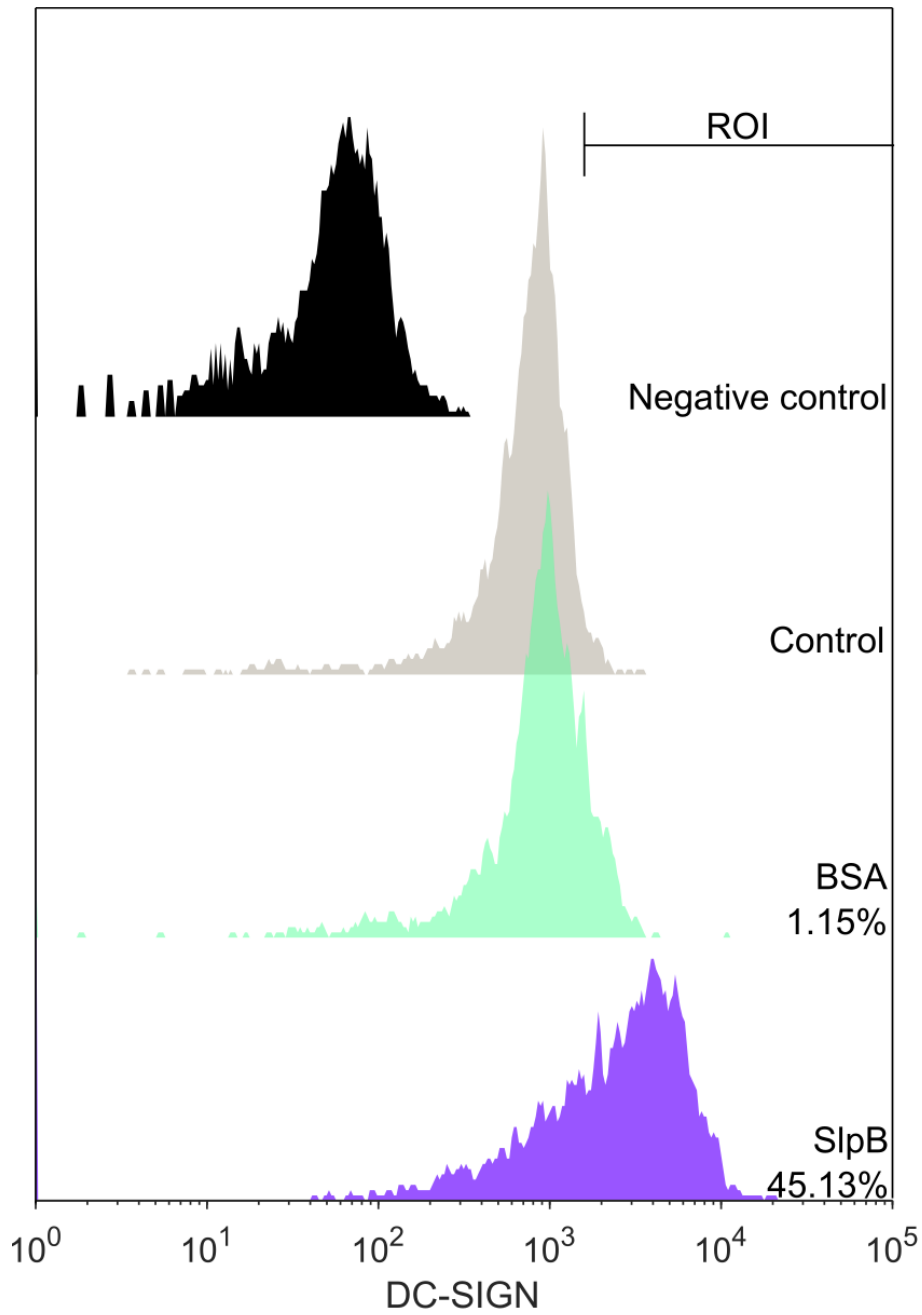


**Figure 3.19** Upregulation of expression of DC-SIGN after SlpB stimulation. 5,000 cells were analysed for each sample. The numbers indicate percentage of cells in region of interest (ROI).

### 3.2.5 Comparison with Other Types of Slps as Ligands

Although previous studies have shown that SlpA from *L. helveticus* binds to mucus layer<sup>[58]</sup> and Slp-like proteins detached from bacteria surface at higher pH in intestine, which makes these Slps unfavourable for intestinal APCs targeting, it remains a question whether the capability of SlpB to improve endocytosis is more superior, or at least equal to other Slps. In this section, I compare the capability of various Slps to induce endocytosis of carriers by APCs.

SlpA was extracted from *L. acidophilus* JCM 1132 as described in Chapter 2 and analysed with SDS-PAGE (Figure 3.20). A single band at approximately 50 kDa was observed, which corresponds to SlpA from *L. acidophilus*. Then, endocytosis of SlpA-LP and SlpB-LP were compared 60 min after co-incubation with MΦ or DC. Regardless of the type of Slps, endocytosis of liposome by both MΦ or DC increased significantly (Figure 3.21 (a)).

The effect of SlpA, SlpB and Slp-like proteins on native surface of *Lp. plantarum* on phagocytosis of *Lp. plantarum* were compared. All type of Slps(-like proteins) have enhanced phagocytosis of *Lp. plantarum* (Figure 3.21 (b)). No difference was observed among the enhancement of endocytosis by SlpA, SlpB or Slp-like protein.

However, it is important to note that although these Slp(-like) proteins have also improved endocytosis by APCs, they are not as stable nor specific in targeting. For instance, SlpAs binds to mucosal layer of gut<sup>[58]</sup>, thus carriers coated with SlpA might not be able to cross mucosal barriers and deliver to intestinal APCs; on the other hand, Slp-like proteins usually have low isoelectric point, which results in detachment in intestine. Thus, SlpB is more advantageous compared to other types of Slps, given similar endocytosis enhancing effect exhibited by all Slps.

### 3.2.6 Comparison Across Carriers

Actin dependent phagocytosis is generally less effective compared to other types of endocytosis as it requires profound reorganisation of cytoskeleton, which is limited by various biophysical constraints. Therefore, it is preferentially to utilise delivery through other pathways.

Treatment with cytochalasin D decreased endocytosis of SlpB-*Lp. plantarum*, suggesting that endocytosis of *Lp. plantarum* was actin-dependent phagocytosis (Figure 3.22 (c, f)); inhibition of actin-condensation did not affect endocytosis of both <sup>PI</sup>LP and SlpB-<sup>PI</sup>LP (Figure 3.22 (a - b, d - e)), suggesting that endocytosis of liposome is actin-independent, which explain why higher fluorescence intensity and fraction of endocytosis<sup>+</sup> cells were achieved by cells co-incubated with liposome in a shorter time (Figure 3.9) compared to other carriers (Figure 3.13, 3.14).

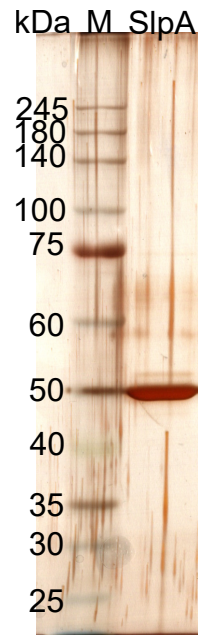


**Figure 3.20** SlpA extracted from *L. acidophilus* JCM 1132.

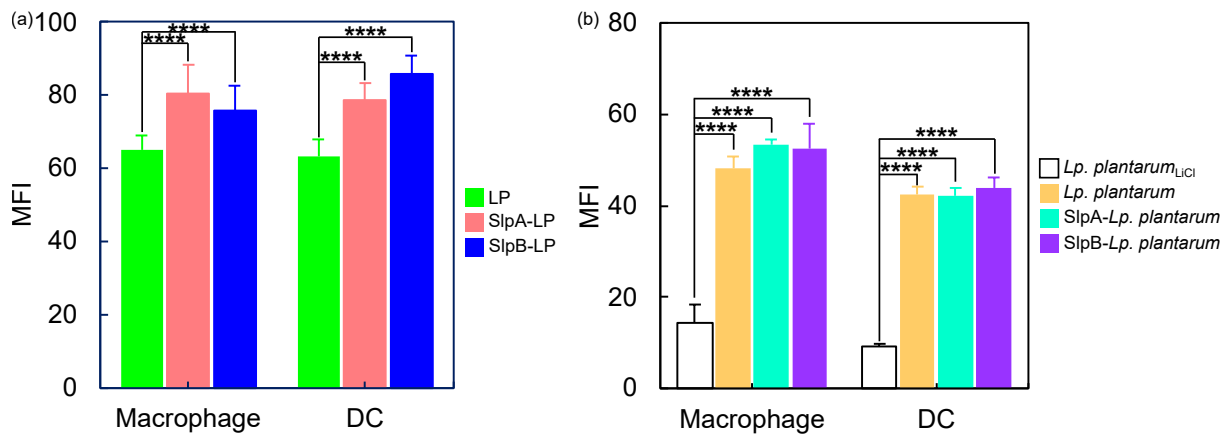


**Figure 3.21** Effect of various Slps on endocytosis by APCs. (a) Endocytosis of liposome coated with various Slps. (b) Phagocytosis of *Lp. plantarum* coated with various Slp(-like) proteins. The plots represent data obtained from triplicate sample in independent test and the error bars represent standard deviation of mean. Statistical significance was evaluated by one-way ANOVA test followed by post-hoc testing using Tukey multi comparisons test. \*\*\*\*  $p < 0.0001$ .

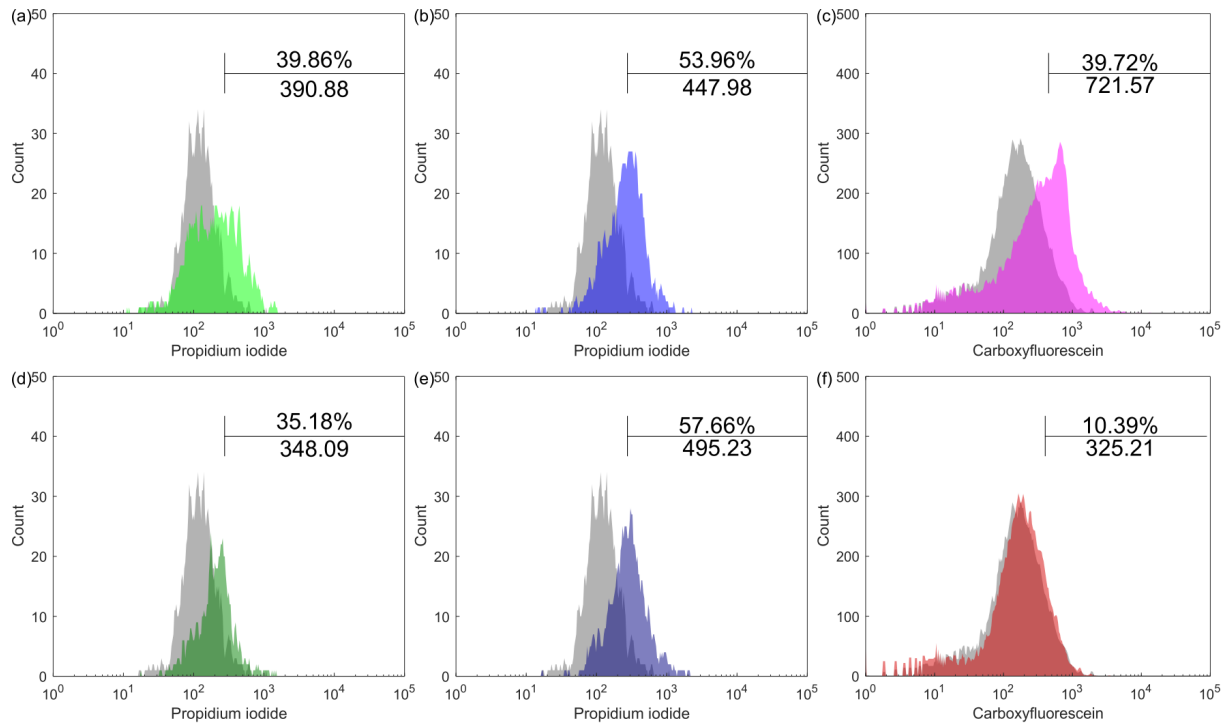


**Figure 3.22** Type of endocytosis involved in internalisation of liposome and solid microparticles with *Lp. plantarum* as example. Histogram of DC endocytosis of (a) LP, (b) SlpB-LP and (c) SlpB-*Lp. plantarum* without actin depolymeriser, and histogram of DC endocytosis of (d) LP, (e) SlpB-LP and (f) SlpB-*Lp. plantarum* with actin depolymeriser. 1,500 cells were analysed for each sample in (a) - (b), (d) - (e) and 10,000 cells were analysed for each sample in (c) and (f). The numbers above indicate percentage of cells in gated region, and the numbers below indicate fluorescence intensity.

### 3.2.7 Adjuvant Effect of SlpB

To investigate if SlpB exhibits adjuvant effect in DC, I have investigated extracellular cytokines production by DC after SlpB stimulation (Figure 3.23). When SlpB was supplemented with LPS, production of IL-6, IL-12/IL-23 (p40), IL-10 and IL-17A were enhanced; when SlpB was supplemented with OVA, which is a standard antigen, production of IL-6, IL-10 and IL-17A were improved.

Furthermore, the results obtained from prior study<sup>[33]</sup> was verified (Figure 3.24). Production of IL-17A by M $\Phi$  was significantly increased when SlpB was supplemented with OVA. These results suggested that SlpB is an adjuvant for APCs.

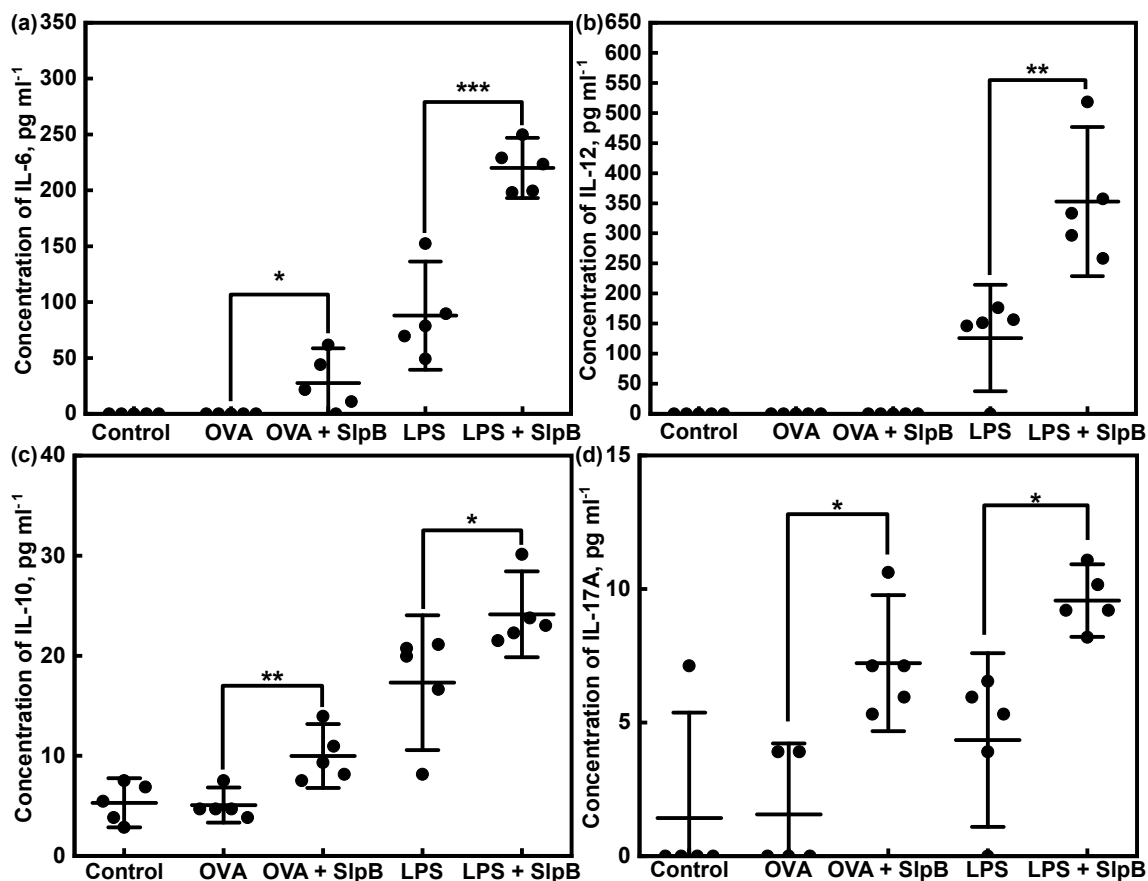


**Figure 3.23** Cytokines production of SlpB-stimulated DC. (a) IL-6, (b) IL-12/IL-23 (p40), (c) IL-10, (d) IL-17A production of DC after stimulation. The plots represent data obtained from quintuplicate sample in independent test and the error bars represent 95% confidence interval of mean. Statistical significance was evaluated by one-way ANOVA test followed by post-hoc testing using Tukey multi comparisons test. \*  $p < 0.05$ , \*\*  $p < 0.01$ , \*\*\*  $p < 0.001$ .

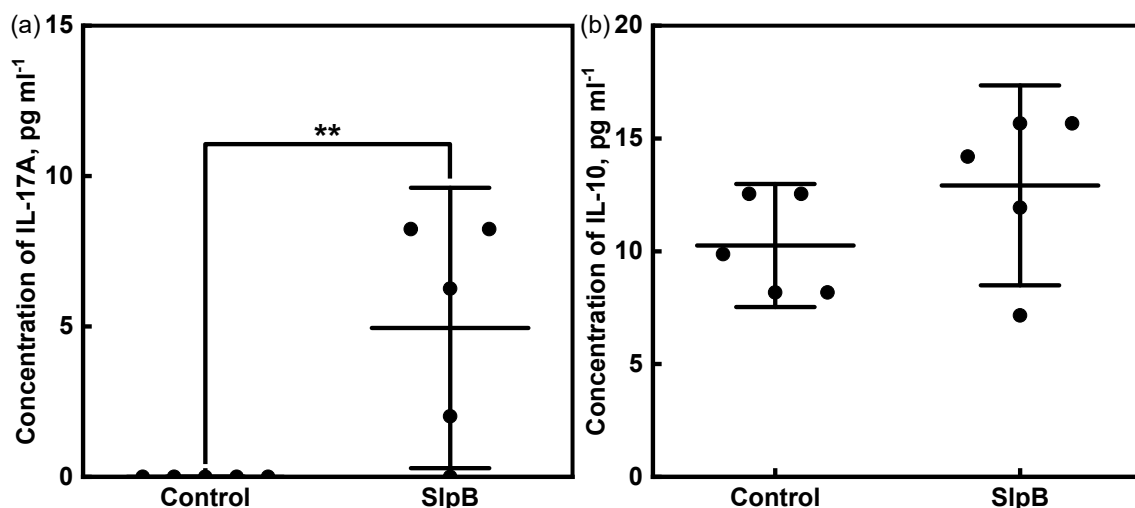


**Figure 3.24** Cytokines production of SlpB-stimulated MΦ. (a) IL-17A and (b) IL-10 production of MΦ after stimulation with SlpB. The plots represent data obtained from quintuplicate sample in independent test and the error bars represent 95% confidence interval of mean. Statistical significance was evaluated by Student's t-test. \*\*  $p < 0.01$ .

### 3.2.8 Cytokine Production in $\alpha^{\text{GC}}$ LP-Treated APC

As a proof of concept, (2*S*, 3*S*, 4*R*)-1-*O*-( $\alpha$ -D-galactopyranosyl)-16-methyl-2- [N- ((*R*) - 2 - hydroxytetracosanoyl) - amino] -1,3,4- heptadecanetriol ( $\alpha$ -galactosylceramide ( $\alpha^{\text{GC}}$ ); trade name: KRN7000), an immunomodulator was delivered to both M $\Phi$  and DC.

As T<sub>H</sub>1 polariser,  $\alpha^{\text{GC}}$  has induced T<sub>H</sub>1 responses in both M $\Phi$  and DC (Figure 3.25). Production of extracellular IL-10 was suppressed, which result in significant increase in the production of extracellular IL-12 from non-detectable in both control group and  $\alpha^{\text{GC}}$ LP-treatment group to 86.2 and 84.8 pg ml<sup>-1</sup> for M $\Phi$  and DC in SlpB- $\alpha^{\text{GC}}$ LP-treatment group respectively. Increases in production of IL-17A in SlpB- $\alpha^{\text{GC}}$ LP-treatment group in M $\Phi$  was also observed, suggesting that T<sub>H</sub>17 response was also induced. IL-6 was below detection limit for all samples.

T<sub>H</sub>2 responses-inducing effect of  $\alpha^{\text{GC}}$  was evaluated with mDC. Production of extracellular IL-6 and IL-12 were significantly decreased in SlpB- $\alpha^{\text{GC}}$ LP-treatment group, while production of extracellular IL-10 and IL-17A were below detection limits for all samples (Figure 3.26). This result suggests that enhanced endocytosis of SlpB- $\alpha^{\text{GC}}$ LP has significantly improved T<sub>H</sub>2 responses in mDC.

Both results shown in Figures 3.25 and 3.26 suggests that functionalisation of drugs-loaded liposomes with SlpB could improve therapeutic effect of drugs.

The effect of  $\alpha^{\text{GC}}$ LP and SlpB- $\alpha^{\text{GC}}$ LP on DC were further evaluated with mRNA expression of cytokines by DC, which is more sensitive compared to ELISA.

$\alpha^{\text{GC}}$  was first discovered for its anti-tumour effect<sup>[96]</sup>. Therefore,  $\alpha^{\text{GC}}$  could induce production of T<sub>H</sub>1 cytokines related to anti-tumour effect, e.g., tumour necrosis factor (TNF)- $\alpha$  (Figure 3.27). Furthermore,  $\alpha^{\text{GC}}$ LP has also upregulated expression of T<sub>H</sub>17 cytokines, e.g., IL-6 and IL-17. SlpB-coating has significantly upregulated expression of IL-6 in relative to  $\alpha^{\text{GC}}$ LP and TNF- $\alpha$  in relative to control. IL-2 was below detection limit for all samples.

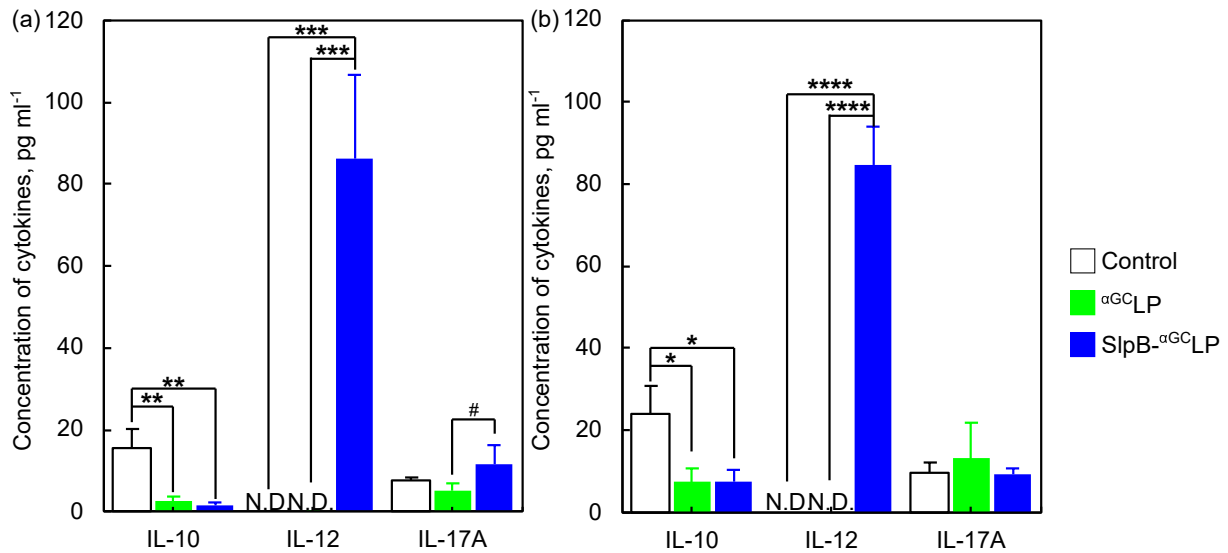


**Figure 3.25** Cytokines production of  $\alpha^{GC}LP$ -stimulated APCs. Production of extracellular cytokines detected in culture supernatant of (a) MΦ and (b) DC by ELISA. The plots represent data obtained from triplicate sample in independent test and the error bars represent standard deviation of mean. Statistical significance was evaluated by one-way ANOVA test followed by post-hoc testing using Tukey multi comparisons test. #  $p < 0.1$ , \*  $p < 0.05$ , \*\*  $p < 0.01$ , \*\*\*  $p < 0.001$ , \*\*\*\*  $p < 0.0001$ . N.D. indicates non-detectable.

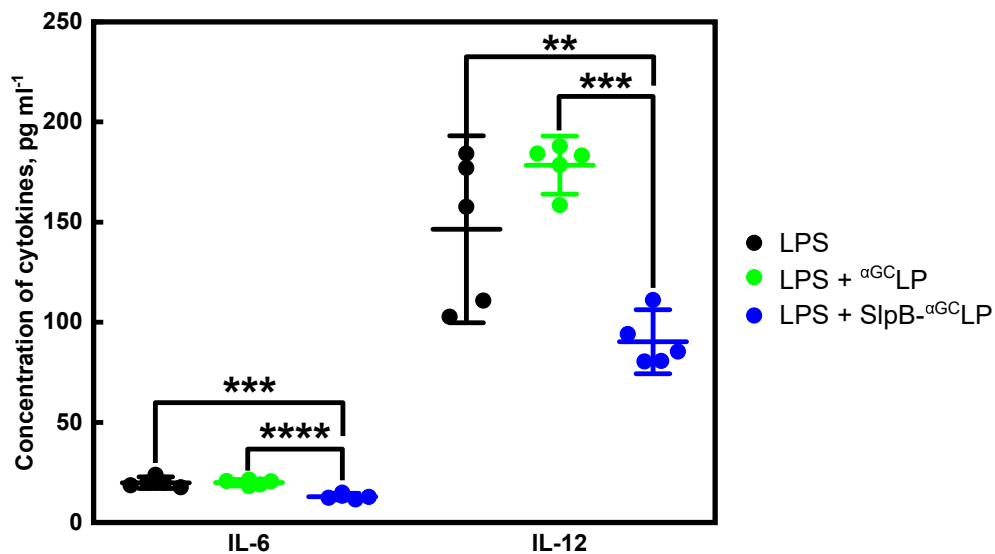


**Figure 3.26** Cytokines production mDC stimulated with  $\alpha^{GC}LP$ . The plots represent data obtained from quintuplicate sample in independent test and the error bars represent 95% confidence interval of mean. Statistical significance was evaluated by one-way ANOVA test followed by post-hoc testing using Tukey multi comparisons test. \*\*  $p < 0.01$ , \*\*\*  $p < 0.001$ , \*\*\*\*  $p < 0.0001$ .



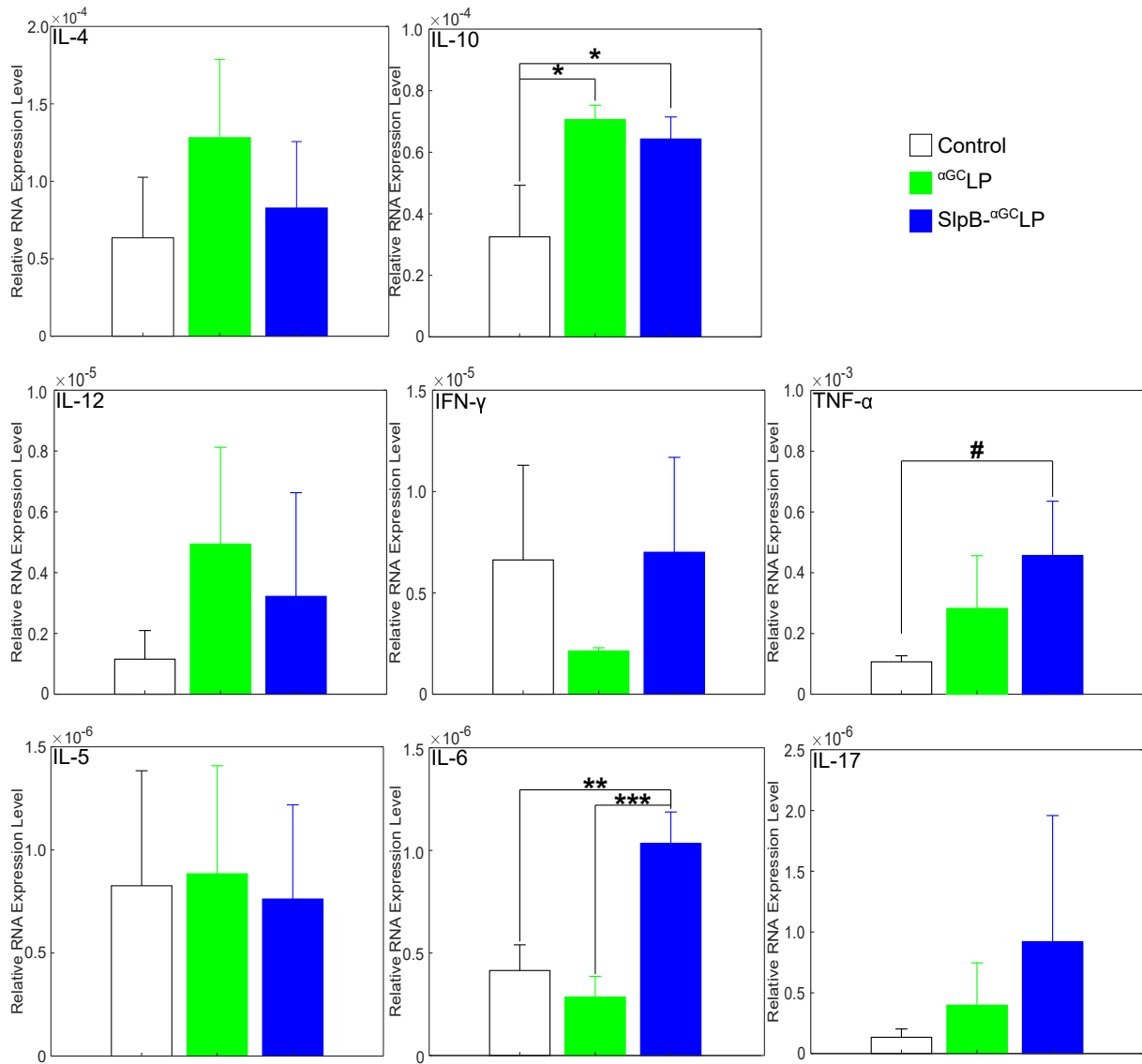


**Figure 3.27** Mean mRNA expression of various cytokines in DC at 8, 16 and 24 h after stimulation with  $\alpha$ GC LP or SlpB- $\alpha$ GC LP. The plots represent data obtained from triplicate sample in independent test and the error bars represent standard deviation of mean. Statistical significance was evaluated by one-way ANOVA test followed by post-hoc testing using Tukey multi comparisons test. #  $p < 0.1$ , \*  $p < 0.05$ , \*\*  $p < 0.01$ , \*\*\*  $p < 0.001$ .

## 3.3 Discussion

### 3.3.1 SlpB Enhances Endocytosis of Particles

In this chapter, I have shown that SlpB from *Lv. brevis* JCM 1059 is a ligand to Mincle and DC-SIGN. In previous study, the incapability of Slp from *Lv. brevis* to displace Slp from *L. acidophilus* might be due to lower affinity of Slp from *Lv. brevis* to DC-SIGN compared to SlpA from *L. acidophilus*. Although the receptors of SlpB can be found on both M $\Phi$  and DC, i.e., Mincle on M $\Phi$ <sup>[33]</sup> and DC-SIGN on DC, the endocytic activity of DC enhanced by SlpB was higher, probably due to the higher endocytic capacity of DC compared to M $\Phi$ <sup>[97]</sup>.

In addition, binding domains of SlpB to extracellular matrices and sugar were found in N-terminal through amino acid sequence alignment (Figure 3.7). This observation is in align with results obtained in prior studies that N-terminal of SlpBs could bind to both cell wall<sup>[43]</sup> and fibronectin<sup>[21]</sup>. The result suggest that SlpB might be more advantageous than SlpAs from *L. acidophilus* and *L. helveticus* (Group A Slps as shown in Figure 1.4) as ligand to target intestinal APCs. The extracellular matrices binding domains of SlpA are located in N-terminal of SlpA, while the cell wall binding domain is located in C-terminal, which resulted in unspecific delivery of liposome to mucosal layer<sup>[58,62]</sup>. With all the binding domain located in N-terminal which is covered by crystalline array formed by self-assemble C-terminal, unspecific binding can be reduced.

For the case of SlpB-LP, 60 min was required for SlpB to enhanced uptake of liposomes into M $\Phi$  and DC. Two reasons might contributed to this phenomenon. Firstly, the density of LP was small, thus time is required for LP to sediment to come into contact with both M $\Phi$  and DC which attach to the bottom of cell culture plate. Secondly, 45 min might be required for SlpB to activate certain pathway in DC to enhance endocytosis of liposome. Although the detail mechanism was not investigated, I have shown that pre-incubation of SlpB with DC for 30 min and 60 min followed by LP for 60 min could significantly increase endocytosis of liposome compared to DC without pre-incubation (Figure 3.17), which suggests that certain length of time is required to activate DC by SlpB for enhanced endocytosis.

There are various pathway for a cell to endocytose particles which do not contain any cell-targeting ligand. These pathways are mainly categorised by dynamin dependency. Dynamin dependent pathway are usually more effective compared to dynamin independent pathway which most of them depend on actin polymerisation, e.g., macropinocytosis and phagocytosis<sup>[98]</sup>. Even

for dynamin dependent pathway, endocytosis through some pathways, i.e., clathrin pathway has lower efficiency compared to other pathways, particularly in non-phagocytic cells. Besides these pathways, another pathway, i.e., caveolin-dependent pathway in which the substances are transported into intercellular space via caveolae<sup>[98,99]</sup>, was not classified by dynamin-dependency also involves in endocytosis. Studies conducted on various non-phagocytic cells showed that particle size affects endocytosis of particles, e.g., caco-2 cells were found to endocytose liposome up to 162.1 nm effectively, but not liposomes beyond this size<sup>[89]</sup>. Investigation with antagonist suggest that endocytosis of 97.8 nm and 162.1 nm liposomes are clathrin dependent; 72.3 nm liposome depends on dynamin, clathrin, macropinocytosis and caveolar-mediated endocytosis; while 40.6 nm liposome is dynamin dependent<sup>[89]</sup>.

Although the mechanism was not investigated, I have shown that particle size of liposome does not effect endocytosis of liposome by APCs. As shown in Figure 3.12, higher endocytic activity was observed for LP with larger size, probably due to the sedimentation of liposomes in medium, which have increased the probability of LP contacted to APCs membrane. On the other hand, when the size are large enough for sedimentation, shorter time is required to significantly increase phagocytosis of particles with smaller size. This phenomenon was observed in higher endocytosis capacity of *Lp. plantarum* compared to microbeads.

Another useful carrier for delivery of proteins, small molecule and gene is *E. coli*<sup>[100]</sup>. *E. coli* is a robust chassis for molecular engineering, which can be used as a carrier for gene amplification and overexpression of proteins. Furthermore, *E. coli* express LPS which can act as vaccine adjuvant<sup>[101]</sup>, thus enhancing the effect of immunomodulation. Although *E. coli* can induce phagocytosis by binding to scavenger receptor on M $\Phi$ <sup>[102]</sup> and DC-SIGN on DC<sup>[103]</sup>, if we could enhanced phagocytosis of *E. coli* through SlpB-coating, and increase phagocytosis of *E. coli*, we might be able to increase the therapeutic effect of drugs. For the case of DC, prior study has shown that pre-treatment of DC-SIGN expressing cells with Slp from lactobacilli could reduce *E. coli* infection<sup>[29]</sup>, which has suggested that the affinity of Slp-DC-SIGN binding is stronger than LPS-DC-SIGN binding. Stronger binding affinity of SlpB to DC-SIGN has resulted in increased endocytosis of SlpB-*E. coli* by APCs.

However, longer time was required to enhance endocytosis of microbeads and *Lp. plantarum* by DC compared to liposome. Endocytosis of both microbeads and *Lp. plantarum* depends on phagocytosis and macropinocytosis, while the endocytosis of liposome allow APCs to utilise all endocytic pathways (Figure 3.22), which results in higher endocytic efficiency of LP compared

to other carriers. As SlpB could improved the stability of liposome under various gut mimicking environments, LP becomes more advantageous compared to other carriers for shorter time is required to endocytose LP compared to other carriers due to the short resident time of carriers in intestine (10 - 20 min  $m^{-1}$  intestine).

### 3.3.2 Advantages of SlpB against Other Slps

In this chapter, I have shown that SlpB from *Lv. brevis* JCM 1059 is more advantageous compared to other Slps for the following reasons:

1. As *Lv. brevis* is non-pathogenic, SlpB is safe to be used in pharmaceuticals.
2. SlpB improved stability of LP in various gut mimicking environment.
3. SlpB attaches robustly on the surface of LP in gut environment.
4. SlpB binds to Mincle of M $\Phi$  and DC-SIGN of DC.
5. SlpB enhances endocytosis by M $\Phi$  and DC

These properties make SlpB an attractive ligand for intestinal APCs-targeting compared to other proteins.

### 3.3.3 SlpB Induces Adjuvant Effect and Improves Therapeutic Effect

Various factors have contributed to the improvement of therapeutic effect of drugs to APCs. Beside improved stability and targeted delivery of carriers, adjuvant effect of SlpB might have improved the therapeutic effect of drugs delivered by SlpB-LP.

$\alpha$ GC is a sphingolipid discovered in marine sponges in Okinawa, Japan, *Agelas mauritanicus*<sup>[104]</sup>, in a screen for anti-tumour natural compounds<sup>[96]</sup>. It consists of an acyl chain and a sphingosine chain connected via  $\alpha$ -linkage to galactose head group (Figure 3.28).  $\alpha$ GC binds to major histocompatibility complex class I-related protein, cluster of differentiation (CD)1d of antigen presenting cells. Particularly, hydrophobic acyl chain and sphingosine chain bind to A'- and C'-pocket in CD1d antigen binding groove respectively. Then, galactose head is presented to T cell receptor (TCR) on invariant natural killer T (iNKT) cells, forming a CD1d- $\alpha$ GC-TCR complex. iNKT cells are activated through antigen presentation by binding of galactose head group to TCR, and various immune responses, which includes T<sub>H</sub>1, T<sub>H</sub>2, T<sub>H</sub>17, T<sub>reg</sub> responses are induced. Copious amount of both regulatory, pro-inflammatory and anti-inflammatory cytokines were released followed by transactivation of natural killer cells, T cells and other APCs.

Thence, inducing various therapeutics effects, e.g., cancer treatment<sup>[105–108]</sup>, anergy<sup>[109]</sup>, treatment of autoimmune disease and virus infection<sup>[110]</sup>, and as adjuvant to vaccine for coronavirus disease 19<sup>[111]</sup>.



**Figure 3.28** Chemical structure of  $\alpha$ GC.

As acyl and sphingosine chain of  $\alpha$ GC are hydrophobic, they are incorporated in lipid membrane of LP.  $\alpha$ GC are incapable to bind to CD1d of APCs without lysing the liposomes through endocytosis. Therefore,  $\alpha$ GC LP does not act as ligand for drug delivery.

As  $T_H1$  polariser,  $\alpha$ GC LP has induced  $T_H1$  responses, and production of pro-inflammatory cytokines. The changes were detected in both ELISA and reverse transcription-quantitative polymerase chain reaction (RT-qPCR). With SlpB-coating, production and expression of pro-inflammatory cytokines, e.g., IL-12, TNF- $\alpha$ , and IL-6 were further enhanced either detected by ELISA or RT-qPCR, which has suggested that SlpB could improve therapeutic effect of immunomodulatory drugs through enhanced endocytosis and induction of adjuvant effect.

### 3.4 Summary

In this chapter, I have shown that SlpB-coating could enhance endocytosis of various types of carriers, which include liposomes, solid microparticles, Gram-positive and Gram-negative bacteria. Improved endocytosis originated from ligand-mediated endocytosis through specific interaction between SlpB and C-type lectins, i.e., Mincle and DC-SIGN. The result of sequence analysis suggested that SlpB possess sugar binding domain, which potentially interact with C-type lectins via sugar moiety. SlpB could also up-regulate production of DC-SIGN, and potentially increase membrane fluidity, which create a positive feedback loop to further increase endocytic activity. Furthermore, SlpB exhibit similar endocytosis-enhancing capability when compared to other Slps while demonstrating higher robustness and specificity. These properties make SlpB a better ligand compared to other Slps.

Furthermore, I have shown that SlpB could induce adjuvant effect in APCs. Synergy effect of

both improved endocytosis and adjuvant effect have resulted in improved therapeutic effect. As a proof of concept,  $\alpha^{\text{GC}}\text{LP}$  with and without SlpB-coating were used to stimulate APCs, and I have demonstrated that SlpB-coating could enhance cytokines production by APCs by inducing  $T_{\text{H}1}$  responses in  $M\Phi$  and DC, while inducing  $T_{\text{H}2}$  responses in mDC.

As SlpB could improve the stability of liposomes, which have diminished the disadvantages of liposomes in relative to other carriers, it is preferential to use liposomes as carriers for oral delivery, especially for immune targeting purpose, for (1) it can co-deliver hydrophilic and hydrophobic drugs which is more preferential for delivery of immunomodulators, particularly, co-delivery of drugs with adjuvant is possible, (2) shorter time is required for endocytosis of liposomes compared to other carriers is advantageous for drug delivery to intestinal APCs as the resident time of carriers in intestine is short, (3) higher amount of liposomes can be endocytosed by APCs, particularly in DC compared to other carriers and finally (4) low immunogenicity of bare liposomes results in milder adverse effect compared to other carriers. Particularly, when anionic liposomes are used, low carrier toxicity can be achieved. Hereafter, my study will focus on drug delivery based on SlpB-coated liposomes.

## Chapter 4

### ***In vivo* Uptake of Liposomes in Peyer's Patches**

Liposome is capable to deliver both hydrophobic and hydrophilic molecule, and exhibit low toxicity and antigenicity, which render it an effective carrier for drug delivery, particularly for the delivery of immunomodulating drugs.

In previous chapters, I have demonstrated that coating of liposomes with SlpB could improve stability of liposomes against gut mimicking environment and enhance endocytosis by APCs. Furthermore, higher endocytic capacity of liposomes compared to other types of carriers were also demonstrated, which make liposomes an attractive drug carriers.

However, targeting of APCs in Peyer's patches with liposomes have not been reported to date, as liposomes are unstable against environment in GI tract.

Although I have shown that SlpB-coating enhanced stability and endocytosis of liposomes by APCs *in vitro*, it is uncertain that whether these benefits can be transferred to *in vivo* system, given that biological system is more complex than *in vitro* system. Several factors, such as pinocytosis of liposome by other cells, as well as degradation and clearance of liposome are unpredictable by *in vitro* system. Furthermore, it remained unknown whether LPs can cross mucosal and epithelial barriers in intestine. Therefore, it is important to conduct *in vivo* study to understand the effectiveness of SlpB-LP in targeting APCs in Peyer's patches.

In this chapter, I will discuss delivery of SlpB-coated liposomes *in vivo*. The stability of liposomes *in vivo* will be evaluated. Then, the distribution of liposomes in tissues related to oral administration and route of uptake of liposome into APCs in Peyer's patches will be investigated. Finally, therapeutic effect induced by drug-loaded liposome will be assessed by measuring *in situ* mRNA expression of cytokines in Peyer's patches.

## 4.1 Methods

### 4.1.1 Conservation of Content Encapsulated in Liposomes

Theoretically, total fluorescence intensity of fluorophore encapsulated in liposome is conserved if the fluorophore is stable against its environment. To verify the conservation of fluorescence intensity, so to exploit this property in investigating the distribution of liposome, I have compared the sum of fluorescence intensity originated from leaked fluorophore and fluorophore remained encapsulated in liposomes after incubation in deionised water at 37°C for 60 min, to the fluorescence intensity from fluorophore encapsulated in liposome before incubation.

### 4.1.2 *In vivo* Stability of SlpB-Coated Liposome

Female BALB/c mice (12 weeks, 20 – 25 g, 20 mice, Charles River Strain obtained from Jackson Laboratory Japan) fasted for 3 h were randomly grouped into 5 groups ( $n = 4$  per group). A group of mice was used as control, 2 groups were administered with 200  $\mu\text{l}$  Cy5-pLP and 2 groups were administered with SlpB-Cy5-pLP (each contains 82.5  $\mu\text{g}$  pLP, and 0.5% Cy5 from content in vial dissolved in tris buffered saline) via oral gavage. At 1 h and 3 h after administration, the mice were euthanised. Blood, jejunum, ileum, and liver were immediately isolated.

Cold PBS (-) were injected into both jejunum and ileum, and the luminal content in both jejunum and ileum were collected. The flow through from jejunum and ileum were filled up to equal volume with PBS (-), and the suspensions were allowed to sit on ice for 10 min to allow sedimentation of solid particulate. Then, 1 ml supernatant was sampled and centrifuged at  $16,000 \times g$  for 30 min within 20 min after sample collection. The supernatants were collected into another tube, and the pellets were resuspended in 1 ml PBS (-). Fluorescence intensities for both supernatant and suspension of pellet were measured, and the fraction of fluorescence intensity of supernatant to pellet was calculated to evaluate leakage of Cy5 dye from liposome (Equation 4.1).

$$\text{Relative Leakage} = \frac{F_{\text{supernatant}}}{F_{\text{pellet}}} \quad (4.1)$$

where  $F_{\text{supernatant}}$  is the fluorescence intensity of supernatant obtained from supernatant of intestinal content in PBS (-) after centrifugation, and  $F_{\text{pellet}}$  is the fluorescence intensity of pellet obtained from supernatant of intestinal content in PBS (-).



The bloods collected were allowed to sit at room temperature for at least 30 min for clotting. Then, the blood samples were centrifuged at  $9,200 \times g$  to pellet the blood clot. 10  $\mu$ l plasma was diluted with 90  $\mu$ l PBS (-), and the fluorescence intensity was measured.

### 4.1.3 Absorption of Liposomes into Intestine and Uptake into Peyer's Patches

To investigate absorption of liposomes into intestine and uptake into Peyer's patches, 2 fragments of 5 mm intestines from jejunum and ileum without Peyer's patches, 2 jejunal Peyer's patches and 2 ileal Peyer's patches were isolated within 5 min of euthanasia. The samples were lysed with 1% polyethylene glycol mono-*p*-isooctylphenyl ether solution with vortex and vigorous shaking, followed by centrifugation at  $5,000 \times g$  for 5 min. 0.2-volume of supernatants were collected, and the fluorescence intensities were measured.

### 4.1.4 Availability of Dye in Liver

Livers were collected within 10 min of euthanasia of mice. Then, livers were lysed with 1% polyethylene glycol mono-*p*-isooctylphenyl ether solution with vortex and vigorous shaking, followed by centrifugation at  $5,000 \times g$  for 5 min. 0.2-volume of supernatants were collected. The fluorescence intensities, and absorbance at 280 nm were measured. Absorbance at 280 nm from 1% polyethylene glycol mono-*p*-isooctylphenyl ether solution was subtracted from absorbance of each sample, and the fluorescence intensity was normalised with absorbance.

### 4.1.5 Transcytosis of Liposome through M cells

BALB/c mice (female, 12 weeks, 20 – 25 g, 7 mice, Charles River Strain obtained from Jackson Laboratory Japan) fasted for 3 h were randomly grouped into 2 groups ( $n = 3$  per group). A group of mice were administered with 200  $\mu$ l FITC-OVALP and another group of mice were administered with SlpB-FITC-OVALP (each contains 2 mg LP and 40  $\mu$ g FITCOVA) via oral gavage. The remaining mouse was used as staining control. In this study, FITCOVA was used instead of fluorescent dye to prevent false positive due to leakage and diffusion of dye into tissue during fixing. Then, the mice were euthanised by cervical dislocation 60 min after administration of liposomes. Intestines were isolated, washed with ice-cold PBS (-) to remove luminal content, and fixed with ice-cold 3.7% formaldehyde and 0.8% methanol. Peyer's patches were manually identified and collected with a pair of curved scissors.

To prepare whole mount Peyer's patches, mesenteric side of intestines were cut, and permeabilised with 0.1% polyethylene glycol mono-*p*-isooctylphenyl ether solution. Then, the Peyer's

patches were washed for 3 times with PBS (-) followed by blocking with 3% BSA in PBS (-) for at least 2 h. To identify mature M cells in Peyer's patches, blocked Peyer's patches were incubated with rabbit Ab against mouse glycoprotein 2 (GP2) followed by DyLight™405-conjugated goat Ab against rabbit IgG. The stained Peyer's patches were mounted on glass and observed with laser scanning microscope

#### 4.1.6 Endocytosis of Liposome into Antigen-Presenting Cells

BALB/c mice (as in previous section) were administered with 200  $\mu$ l  $Cy3-OVA$ LP or SlpB- $Cy3-OVA$ LP (each contains 400  $\mu$ g anionic liposome and 8  $\mu$ g  $Cy3$ OVA) via oral gavage. Then, the mice were euthanised by cervical dislocation 60 min after administration of liposome. The intestines were isolated, washed with ice-cold PBS (-) to remove luminal content, and fixed with ice-cold 3.7% formaldehyde and 0.8% methanol. To prepare cryosection, 2 Peyer's patches were collected from each intestine and perfused intensely in 30% sucrose solution before embedding in optimal cutting temperature compound. Peyer's patches were cut transversely through the dome into 5  $\mu$ m thick section and mounted on glass slides.

To distinguish APCs in Peyer's patches, sections of Peyer's patches were blocked, stained with rabbit Ab against mouse CD23/Fc $\epsilon$ R2, followed by DyLight™405-conjugated goat Ab against rabbit IgG as described. CD23 is a receptor expressed mainly on APCs, i.e., naïve B cells, M $\Phi$ , and follicular DC. Thus, staining CD23 could identify APCs in Peyer's patches. The stained sections of Peyer's patches were observed with fluorescence microscope.

#### 4.1.7 Therapeutic Effect of SlpB-coated Drug Loaded Liposome

BALB/c mice (female, 9 weeks, 18 – 23 g, 9 mice, Charles River Strain obtained from Jackson Laboratory Japan) fasted for 3 h were randomly grouped into 3 groups ( $n = 3$  per group). Each group of mice were administered with either 200  $\mu$ l deionised water,  $\alpha^{GC}$ LP or SlpB- $\alpha^{GC}$ LP (contains 8  $\mu$ l  $\alpha^{GC}$ LP) by oral gavage, respectively. Mice were euthanised by cervical dislocation 8 h after oral administration. The Peyer's patches were isolated and snap frozen immediately. Total RNA was extracted according to manufacturer's protocol of Qiagen RNeasy mini kit with materials listed in Appendix A. Quantity and quality of RNA was evaluated with NanoDrop spectrophotometer. RNAs were reverse transcribed into cDNA with qPCR RT master mix. The resulting cDNA was diluted 5-fold with nuclease-free water and mixed with primers listed in Appendix A. The mixtures were incubated in a StepOne Real Time PCR system according to the manufacturer's instructions. The data obtained were normalised with mRNA expression

level of GAPDH as housekeeping gene.

## 4.2 Result

### 4.2.1 Conservation of Content Encapsulated in Liposomes

By comparing the fluorescence intensity, I have observed that the fluorescence intensity of fluorophore encapsulated in liposome before incubation is equal to the sum of fluorescence intensity from fluorophore remained encapsulated in liposome (pellet) and leaked fluorophore (supernatant) (Figure 4.1).

### 4.2.2 Stability of SlpB-LP *in vivo*

Both drugs and liposomes are subjected to degradation by various enzymatic degradation, mechanical stress, high salinity, and diverse pH environment in gut. Although I have shown that SlpB could enhance stability of LP *in vitro* (Chapter 2), it remained unclear whether SlpB could improve stability of LP in gut.

As shown in Figure 4.2, SlpB-coating has significantly reduced the leakage of fluorophore from liposome regardless the length of time after administration. The leakage of fluorophore from SlpB-LP was relatively constant at 1 h and 3 h, where the mean of ratio of fluorescence intensity (RFI) detected were 3.7 and 4.0 respectively compared to 1.6 from control. On the other hand, the leakage of fluorophore from LP was 5.4- and 6.1-fold higher than SlpB-LP at 1 h and 3 h respectively.

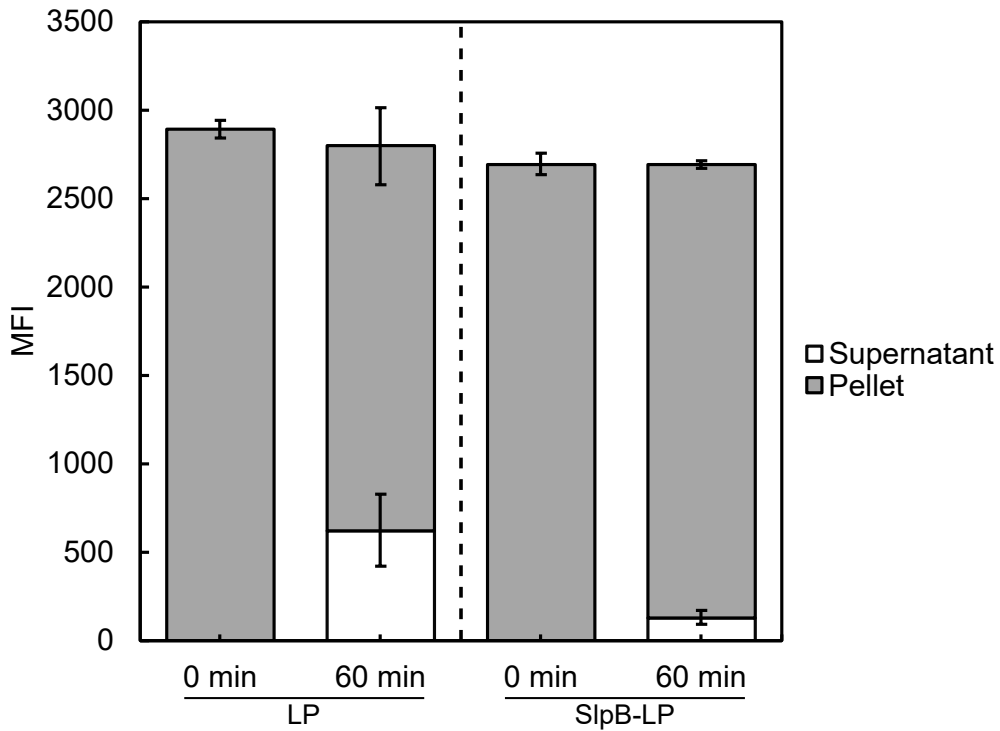


**Figure 4.1** Conservation of fluorescence intensity from fluorophore in whole sample. The sum of fluorescence intensity of supernatant and pellet after incubation (60 min) is equal to the fluorescence intensity of sample before incubation (0 min). The plots represent data obtained from triplicate samples in independent test and the error bars represent standard deviation of mean.

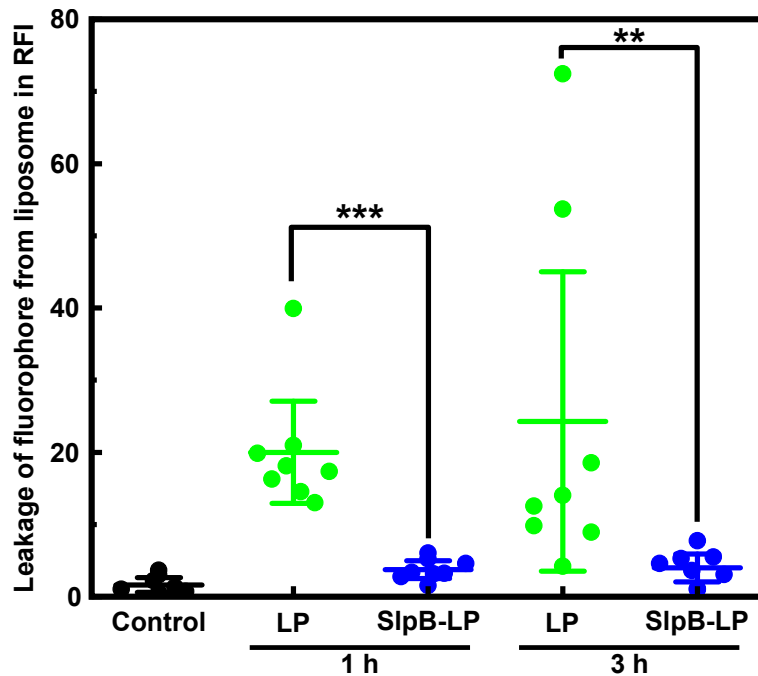


**Figure 4.2** SlpB-coating enhanced the stability of liposome *in vivo*. RFI obtained from fluorophore leaked into environment to fluorophore remained encapsulated in liposome 1 h and 3 h after oral administration of LP or SlpB-LP to mice. The plots represent data obtained from 4 biological replicates and 2 technical replicates. The error bars represents 95% confidence intervals of mean. Statistical significance was analysed with Mann–Whitney U test. \*\*  $p < 0.01$ , \*\*\*  $p < 0.001$

### 4.2.3 Distribution of SlpB-LP in Gut

By collecting both intestines (sans Peyer's patches) and Peyer's patches separately, we were able to evaluate the distribution of LP and SlpB-LP in intestines and Peyer's patches from supernatant of tissue lysate. As shown in Figure 4.3 (a – b), SlpB-LP has been specifically uptaken into Peyer's patches, but not into intestine through villi, while most of the LP were absorbed through villi. SlpB-coating has increased uptake of LP into Peyer's patches by 3.6-fold at 1 h, and 2.5-fold at 3 h; while reduced absorption into villi by 9.0-fold at 1 h, and 3.0-fold at 3 h.

Then, the availability of SlpB-LP in blood plasma and liver were traced. Orally administered drugs must be transported into lymph or blood vessel to trigger systemic response. To understand whether SlpB-coating could facilitate transportation of LP into systemic circulation, fluorescence intensity from fluorophore contained in blood plasma was measured. SlpB-coating has increased fluorescence intensity from fluorophore contained in blood by 1.7-fold at 1 h, 1.3-fold at 3 h (Figure 4.3 (c)).

Furthermore, I have measured the fluorescence intensity in supernatant of lysate of liver where drug metabolism takes place (Figure 4.3 (d)). Fluorescence intensity has been reduced by 2.5-fold at 1 h and 3 h when SlpB was coated on LP.

Interestingly, the absorption of fluorophores into Peyer's patches is correlate to the availability of fluorophores in blood plasma (Figure 4.4). The coefficient of correlation between the 2 parameters was 0.7. This result indicates that absorption of SlpB-LP could increases bioavailability of drugs.

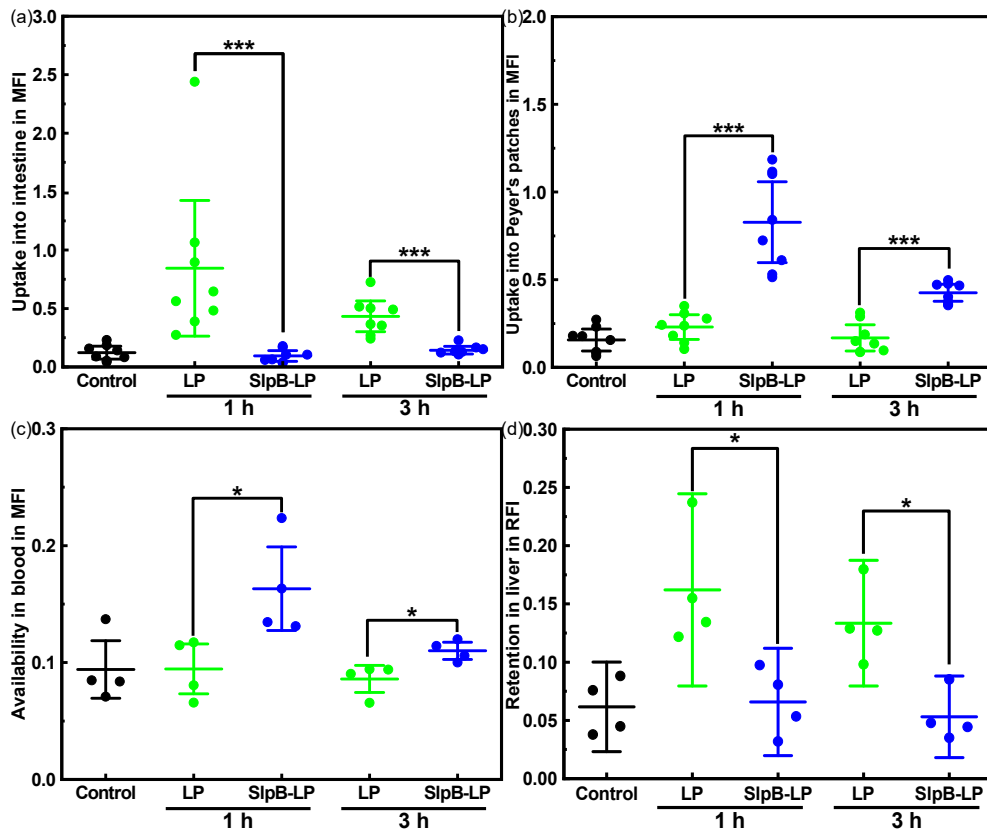


**Figure 4.3** Distribution of SlpB-LP in various tissues related to oral delivery. Availability of LP and SlpB-LP in (a) intestines, (b) Peyer's patches, (c) blood plasma and (d) liver of mice 1 h and 3 h after oral administration. Each category contains 4 biological replicates. For intestines and Peyer's patches, 2 technical replicates were prepared. The error bars represent 95% confidence interval of mean. Statistical significance was evaluated by Mann-Whitney U-test. \*  $p < 0.05$ , \*\*\*  $p < 0.001$ .

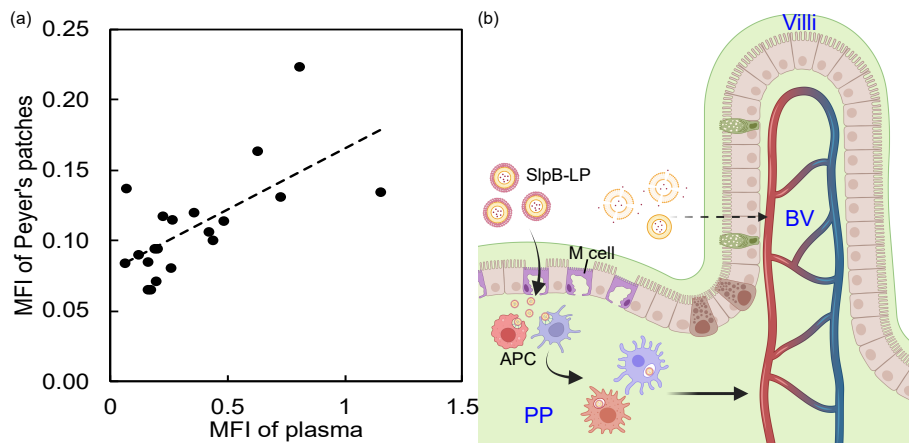


**Figure 4.4** Relationship of concentration of fluorophores in Peyer's patches and blood plasma. (a) Scatter plot of fluorescence intensity of fluorophore in Peyer's patches against fluorescence intensity of fluorophore in blood plasma. Linear regression was performed, and a linear curve was plotted. The coefficient of correlation is 0.7. (b) Illustration of transportation of SlpB-LP in gut. SlpB-LP was transported by APCs in Peyer's patches into blood vessels. Important components in illustration are labelled in black, APC: antigen presenting cell; regions in illustration are labelled in blue, PP: Peyer's patch, BV: blood vessel.

#### 4.2.4 Transcytosis of Liposome through M cells

*In vivo* study was conducted to investigate the process of transcytosis of SlpB-LP through follicle-associated epithelium (FAE) of Peyer's patches, which resulted in high concentration of fluorophore in Peyer's patches.

Observation of whole-mount Peyer's patches of mice administered with LP and SlpB-LP shows that LPs were enclosed in GP2<sup>+</sup> mature M cells (Figure 4.5). This observation indicates that liposomes were localised in mature M cells located at the higher region of Peyer's patches.

To investigate the relative location of liposomes to M cells, i.e., whether liposomes were attached on the surface of M cells or uptaken into M cells, 6 regions were randomly selected from each micrograph in Figure 4.5 (a) and orthogonal views of z-stack micrographs were prepared (Figure 4.5 (b - m)). The orthogonal views of micrographs show that all liposomes are located in or below M cells, but not attached on the surface. This observation suggests that all liposomes were either endocytosed or transcytosed by M cells. In fact, LP were removed from the surface of tissue during fixing as methanol contained in fixing solution will dissolve lipid. Therefore, LPs should not remain attached on the surface of Peyer's patches.

Then, the RFI of liposome to GP2 was analysed to evaluate whether SlpB-coating could enhance transcytosis of liposomes. Peyer's patches were manually identified from micrographs and gated (Appendix G.1). The MFI per pixel<sup>2</sup> of liposome and GP2 were analysed, and the ratio was calculated. Then, RFI of liposome to GP2 were analysed statistically (Figure 4.5 (n)). SlpB-coating has significantly increased uptake of liposome into M cells, which is potentially facilitated by ligand-mediated endocytosis.

To support the result of statistical analysis, intensity of GP2 from both set of samples were analysed (Figure 4.6 (a)). The intensity of GP2 from both set of samples are similar, which suggests that SlpB did not bind to GP2, and signal intensity of GP2 can be used to normalise signal intensity of LP. As comparison, DC-SIGN in Peyer's patches were stained with rabbit Ab against hDC-SIGN and Cy3-conjugated goat Ab against rabbit IgG as described, observed under microscope and the intensity of DC-SIGN was analysed. Signal intensity of DC-SIGN reduced significantly (Figure 4.6(b)) due to SlpB-blocking, which is in align with result obtained in *in vitro* study (Figure 3.6), suggesting that DC-SIGN is not a suitable indicator to normalise signal of LP and to label APCs in Peyer's patches in this study.

Although I have shown that SlpB-coating could increase uptake of LP into M cells, it remained unclear whether the LPs were transcytosed through M cells or endocytosed by M cells.

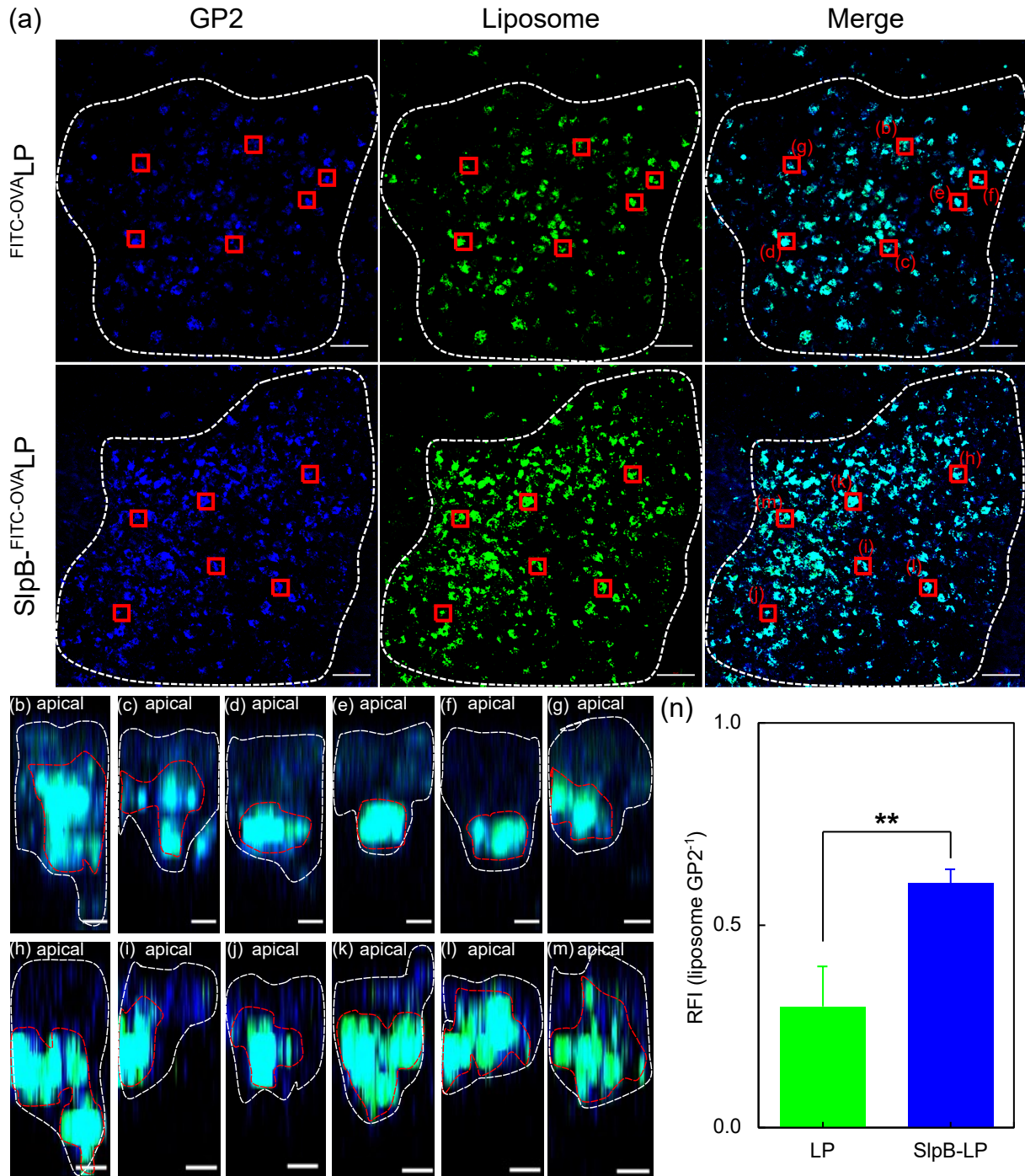


**Figure 4.5** SlpB enhanced transcytosis of liposome through M cells on Peyer's patches. (a) Representative micrographs of whole mount Peyer's patches. The scale bars are 50  $\mu\text{m}$ . (b - m) Orthogonal view of z-stack micrographs of randomly-selected region in (a). Liposomes are gated with red line, and the region of M cells are gated with white line. The scale bars are 5  $\mu\text{m}$ . (n) Statistical analysis of the ratio of fluorescence intensity of liposomes to GP2 in region gated with white line in (a) and Appendix G.1. The plots represent data obtained from 3 biological replicates and the error bars represent standard deviation of mean. Statistical significance was evaluated with Student's t-test. \*\*  $p < 0.01$ .



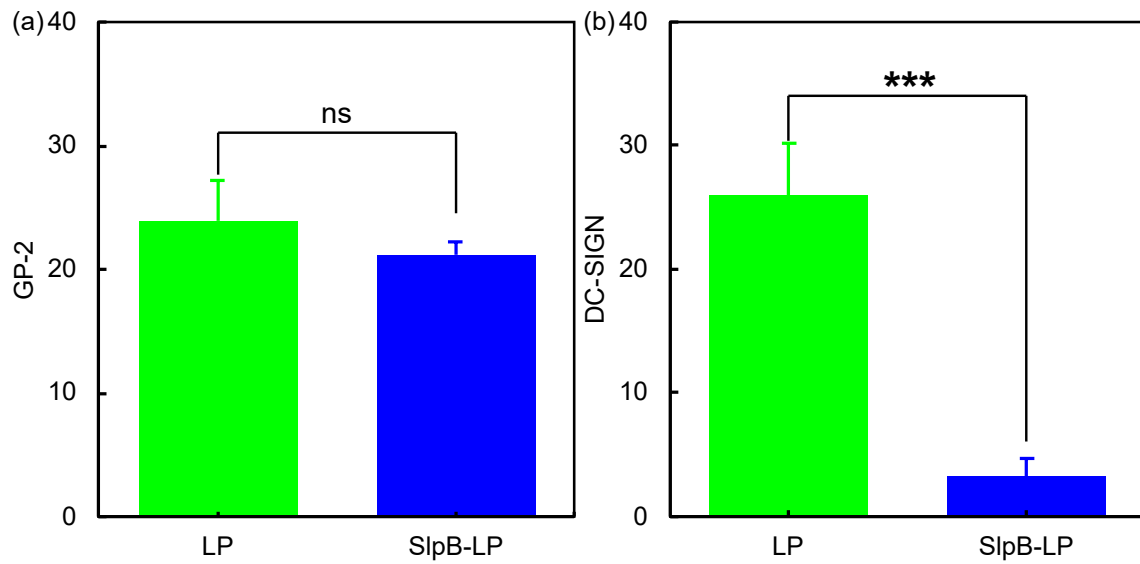


**Figure 4.6** Signal intensity of GP2 and DC-SIGN from Peyer's patches after administered with LP or SlpB-LP. Signal intensity per pixel<sup>2</sup> of (a) GP2 and (b) DC-SIGN. The plots represent data obtained from 3 biological replicates and the error bars represent standard deviation of mean. Statistical significance was evaluated with Student's t-test. \*\*\*  $p < 0.001$ . ns indicates non-significant.

### 4.2.5 Endocytosis of Liposome into Antigen-Presenting Cells

To answer whether liposomes were transcytosed through M cells or endocytosed by M cells, and whether liposomes were delivered specifically to APCs, cryosection of Peyer's patches were prepared.

To reduce crosstalk and to match the dose of drugs to be administered in later section, 200  $\mu$ l  $\text{Cy}^3\text{-OVA}_{\text{LP}}$  or  $\text{SlpB-Cy}^3\text{-OVA}_{\text{LP}}$  (each contains 400  $\mu$ g anionic liposome and 8  $\mu$ g  $\text{Cy}^3\text{OVA}$ ) were used in this section. Fluorescence micrographs have shown that SlpB has facilitated transcytosis of liposome into Peyer's patches (Figure 4.7).

Delivery of liposome to region beneath FAE suggests that liposomes were transcytosed through M cells, rather than endocytosed by M cells. Subepithelial dome (SED), interfollicular region (IFR) and germinal centre (GC) were identified and enlarged (Figure 4.7 (b - g)) to investigate the translocation and antigen presentation by APCs in Peyer's patches. Comparing signal intensity of liposome in each region, I found that SlpB could enhance transcytosis of LP into SED, and translocation of APCs with SlpB-LP to IFR and GC for antigen presentation. Furthermore, unspecific endocytosis of liposome was also observed in Peyer's patch of mice administered with LP, while all liposomes were endocytosed specifically by  $\text{CD}23^+$  cells for SlpB-LP (Figure 4.7 (a)), suggests that SlpB could target intestinal APCs.

Transcytosis of liposomes through M cells and into APCs in Peyer's patches were further analysed statistically. Peyer's patches were manually identified and gated. Then, the signal intensities of liposome and CD23 per pixel<sup>2</sup> in gated region (Appendix G.2) were analysed (Figure 4.7 (h - i)). Higher intensity of liposome in Peyer's patches of mice administered with SlpB-LP compared to those administered with LP, suggests that SlpB has facilitated active transcytosis of liposomes through M cells and into APCs. Moreover, similar intensity of CD23 in both Peyer's patches of mice administered with LP and SlpB-LP suggest that SlpB does not bind to CD23, thus did not generate bias in staining, and the distribution of APCs in Peyer's patches can be correctly identified by CD23.

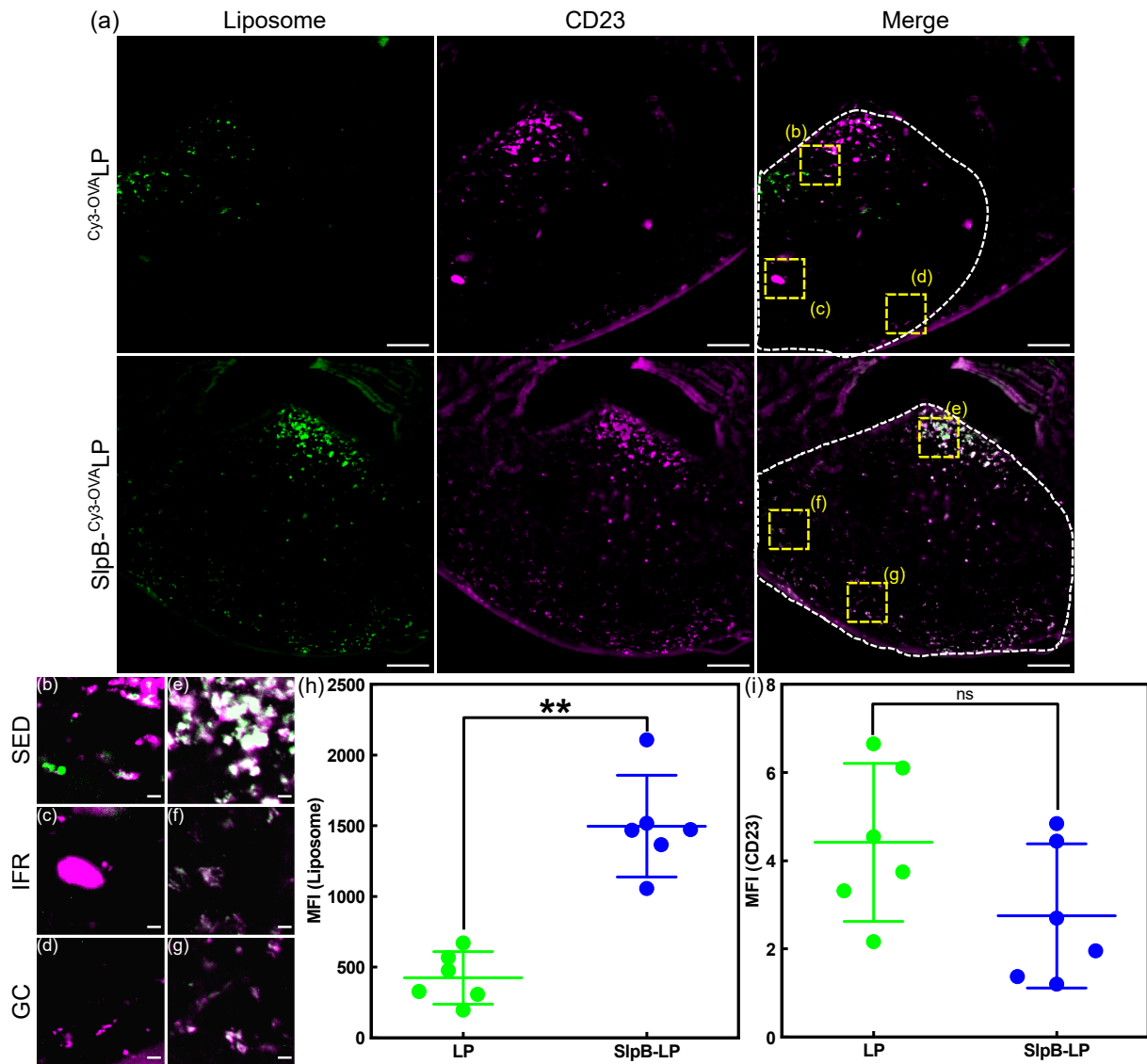


**Figure 4.7** Uptake of liposome into mice Peyer's patches. (a) Representative micrographs of cryosections of Peyer's patches. The scale bars are 100  $\mu\text{m}$ . (b - g) Regions correspond to SED, IFR and GC were marked in (a) and enlarged. The scale bars are 10  $\mu\text{m}$ . (h) Statistical analysis of the intensity of liposome in mice Peyer's patches in Appendix G.2; (i) statistical analysis of the intensity of CD23 in mice Peyer's patches. Each category contains 3 biological replicates and 2 technical replicates. The error bars represent 95% confidence interval of mean. Statistical significance was evaluated with Mann-Whitney U-test. \*\*:  $p < 0.01$ . ns indicates non-significant.

## 4.2.6 Therapeutic Effect of SlpB-coated Drug Loaded Liposome

So far, I have shown that SlpB has enhanced transcytosis of liposomes through M cells, stimulated active delivery of liposomes into APCs in Peyer's patches, and improved therapeutic effect of  $\alpha$ GC in *in vivo* study. In this section, I investigate whether enhanced transcytosis of LP through M cells, endocytosis by APCs and antigen presentation will improved therapeutic effect of drugs. All data pairs, except all data pairs in IL-10, control and SlpB- $\alpha$ GC LP for IFN- $\gamma$ , and control and  $\alpha$ GC LP for IL-17 are statistically different (Figure 4.8).

Compared to control group,  $\alpha$ GC LP upregulated expression of IL-4 and IL-6; downregulated expression of IL-5, IL-12 and IFN- $\gamma$ ; while the expression of IL-10, IL-17 and TNF- $\alpha$  remained constant. For mice administered with SlpB- $\alpha$ GC LP, the expression of IL-6, IL-12, IFN- $\gamma$  and TNF- $\alpha$  were upregulated; IL-4, IL-5 and IL-17 were downregulated, while IL-10 remained constant. Compared to  $\alpha$ GC LP, expression of pro-inflammatory cytokines, i.e., IL-12, IFN- $\gamma$  and TNF- $\alpha$  were significantly increased, while no statistical significance was observed for anti-inflammatory cytokines for mice administered with SlpB- $\alpha$ GC LP. This observation suggested that SlpB could improved therapeutic of drugs *in vivo*

## 4.3 Discussion

### 4.3.1 Stability, Biodistribution and Endocytosis of SlpB-LP by Intestinal APCs

In this chapter, I have shown that SlpB could enhance the stability of liposome in gut, and target APCs in Peyer's patches. In gut, mechanical stress, enzymatic degradation, e.g., pepsin hydrolysis, protease hydrolysis, lipase hydrolysis, constant changes in pH, and emulsification could result in degradation of liposome. SlpB has formed a protective layer on the surface of liposome, while rigidifying lipid membrane, which have increased the stability of LP in gut at 1 h and 3 h after oral administration.

Notably, evaluating the bioavailability of fluorophore in mice administered with LP showed that only a trace amount of dye was absorbed into blood. By scaling up the fluorescence intensity from in blood plasma to 0.5 ml (volume of plasma which can be obtained from 20 g mouse), and calculating the RFI of fluorophore in blood plasma to fluorophore in liposome prepared, I discovered that availability of fluorophore in blood plasma were 0.02% for mice administered with LP at 1 h, 7.3% and 1.7% for mice administered with SlpB-LP at 1 h and 3 h respectively. The fluorophore in blood of mice administered with LP for 3 h was below computation limit.

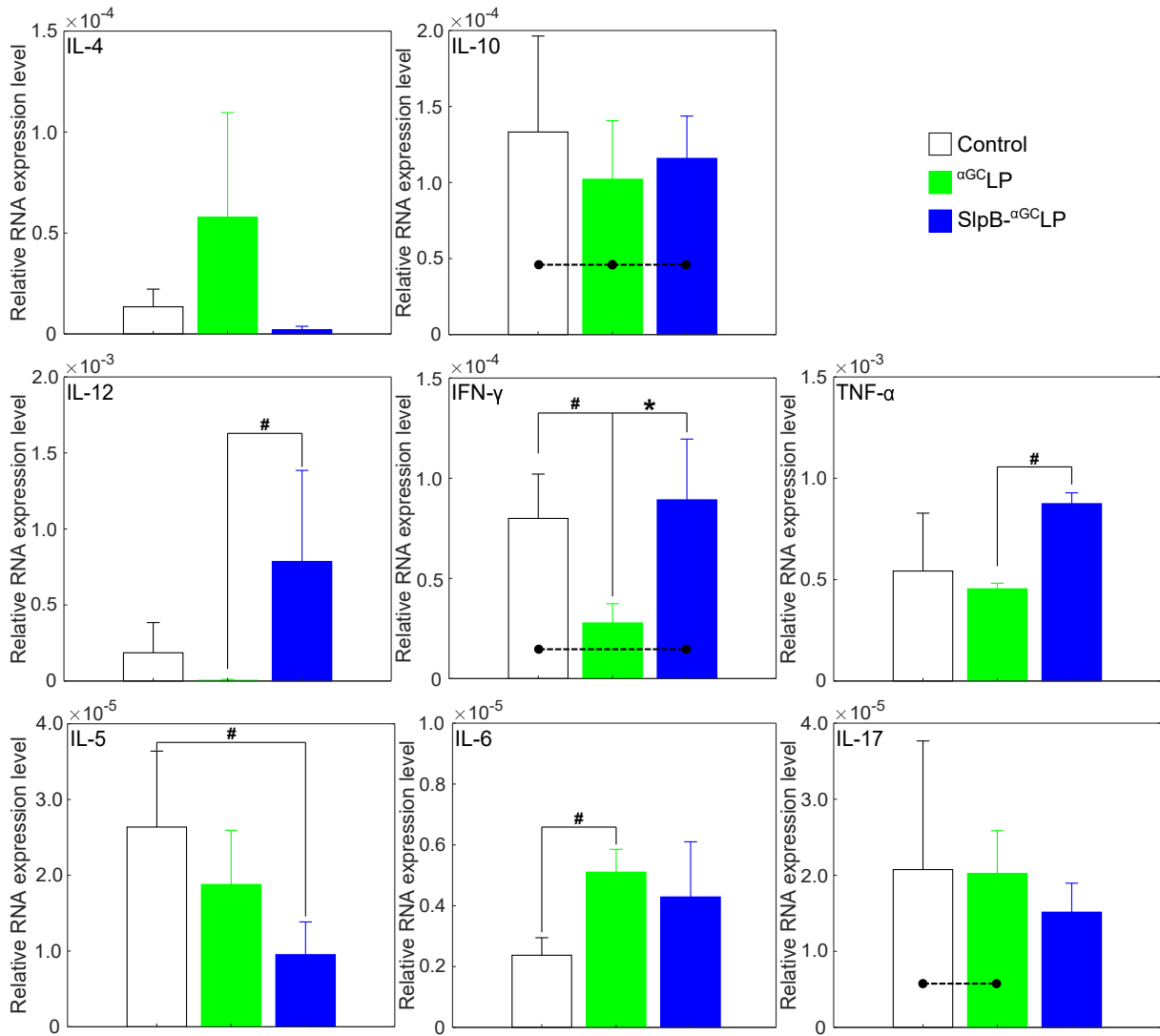


**Figure 4.8** mRNA expression of various cytokines in mice Peyer's patches 8 h after administration with  $\alpha^{GC}LP$  or SlpB- $\alpha^{GC}LP$ . The plots represent data obtained from 3 biological replicates and the error bars represent standard deviation of mean. Statistical significance was evaluated with one-way ANOVA test followed by post-hoc testing using Tukey multi comparisons test. #  $p < 0.1$ , \*  $p < 0.05$ . Dashed line indicates the data pair has no statistical difference.

Previous study suggested that Slp from *L. helveticus* binds to, and release the content of liposome to mucosal layer of GI tract<sup>[58,62]</sup>. Although this approach is fascinating in vaccine delivery, it does not enhance drug delivery to APCs in Peyer's patches, and weak in inducing systemic immune response. In this study, I discovered that the fluorescence intensity in intestines for mice administered with SlpB-LP did not increase in comparison with control, which suggested that SlpB-LP did not release its content in mucosal layer. This result might be due to the existence of both extracellular matrix binding site<sup>[112]</sup>, sugar-binding site and cell wall binding domain at N-terminal for SlpBs (Figure 3.7). As the binding sites are covered with crystalline array forming C-terminal, access of these binding sites to mucosal layer might be blocked, thus reducing the interaction to mucosal layer. This result further confirmed that the orientation of SlpB on LP is similar to those on bacterial surface. On the other hand, the mucin binding site of Group A Slps was found to be localised at crystalline array forming N-terminal, which is in opposite direction to cell wall binding domain at C-terminal<sup>[42]</sup>. This property results in unspecific binding of Slp to extracellular matrices, e.g., mucosal layer, which result in release of drugs in mucosal layer.

For mice administered with LP, 2 reasons contributed to the increases in fluorescence intensity in intestine. Without SlpB-coating, (1) unspecific uptake of LP occurred and (2) higher fraction of LP degradation resulted in higher fraction of leaked fluorophore (Figure 4.2). As villi has a larger surface layer to volume ratio, higher concentration of LP and leaked fluorophore were absorbed into intestines through intestinal villi compared to Peyer's patches (Figure 4.3(b)).

Interestingly, delivery through Peyer's patches has increased the concentration of fluorophore in blood plasma (Figure 4.3(c)). Concentration of fluorophore in Peyer's patches is correlated to concentration in blood plasma (Figure 4.4(a)), which suggest that delivery through Peyer's patches might be an important route for drugs delivery to systemic circulation (Figure 4.4(b)). The increase in bioavailability of compound might be resulted from the capability to bypass first pass elimination in liver (Figure 4.3(d)) via Peyer's patches targeting. Comparing the bioavailability of fluorophore for mice administered with LP to mice administered with SlpB-LP at 1 h after administration shows that bioavailability of SlpB-LP was 427.6-fold higher than LP.

Peyer's patches are the main and the most important lymphoid tissue in gut, which can usually be found at the anti-mesenteric side of small intestine subepithelial<sup>[9]</sup>. They are the largest lymphoid organs, which house more than 70% immunocytes in the body<sup>[113,114]</sup>. Peyer's patches are generally surrounded FAE, which separate the luminal microenvironment and gut

associated lymphoid tissue.

In Peyer's patches, microfold (M) cells are specialised cells distributed on higher region of FAE<sup>[115]</sup>, which transport luminal antigens or bacteria to the underlying immunocytes for immunomodulation<sup>[10,116,117]</sup>. For instance, prior study has shown that M cells are important to transport bacteria and beads into Peyer's patches with M cells deficient mice<sup>[10]</sup>. Furthermore, it was also found that orally administered liposome are transcytosed into Peyer's patches through M cells<sup>[11]</sup>.

Meanwhile, some commensal bacteria were found to be transcytosed through M cells by ligand-receptors interaction: FimH<sup>+</sup> bacteria, e.g., *E. coli* and *Salmonella enterica* serovar Typhimurium bind to glycoprotein 2 (GP2)<sup>[118]</sup>; *Brucella abortus* binds to cellular prion protein (PrP<sup>C</sup>)<sup>[119]</sup>; *L. acidophilus* binds to uromodulin (Umod)<sup>[123]</sup>;  $\beta_1$ -integrin activated with Allograft inflammation factor 1 (Aif1) binds to *Yersinia* spp.<sup>[120,121]</sup>. As a human-origin gut microbial cell, *Lv. brevis* JCM 1059 is subject to antigen sampling by APCs in gut. Thus, there must exist a receptor which facilitate transcytosis of *Lv. brevis* through M cells. And this mechanism could enhance transcytosis of SlpB-coated carriers through M cells, which results in increased uptake of SlpB-LP into Peyer's patches.

Various reasons have contributed to improved targeted delivery of SlpB-LP to APCs in Peyer's patches. Firstly, SlpB has improved stability of liposomes in gut environment (Figure 4.2), thus more SlpB-LP are available in intestine compared to LP. Then, SlpB has enhanced transcytosis of LP through M cells (Figure 4.5, 4.7). Although the mechanisms remain unknown, transcytosis is potentially improved by ligand-receptor interaction. Specific endocytosis of LP by APCs has also contributed to higher availability of LP in APCs in Peyer's patches. Furthermore, adjuvant effect of SlpB might have also contributed to enhanced translocation of APCs to, and antigen-presentation of APCs in antigen presenting sites.

### 4.3.2 SlpB-Coating Improved Therapeutics Effect of Drugs

In this study, I have shown that SlpB-LP could improve therapeutic effect of  $\alpha$ GC in relative to  $\alpha$ <sup>GC</sup>LP. RT-qPCR of extracted mouse Peyer's patches was conducted because of difficult detections of low level of cytokines in normal BALB/c mouse by ELISA methods. In previous studies, systemic delivery of 5  $\mu$ g  $\alpha$ GC per mouse was able to induce detectable cytokine production within 6–12 h<sup>[122]</sup>. In C57BL/6 mice, increased cytokine production in serum and RNA expression in Peyer's patches and the spleen were detected within 6 h after administration with

$\alpha$ GC-LP<sup>[123]</sup>. In the present study, induction of the production of various cytokines in Peyer's patches after oral administration of SlpB- $\alpha$ GC-LP and  $\alpha$ GC-LP were evaluated by RT-qPCR.

Prior studies have reported that intravenous injection of  $\alpha$ GC into both mice<sup>[124]</sup> and human<sup>[108]</sup> could increase the level of serum IL-12, IFN- $\gamma$  and TNF- $\alpha$ . Particularly, it was observed that presentation of  $\alpha$ GC to NKT cells rapidly activated NK cells after intravenous injection of  $\alpha$ GC<sup>[124]</sup>. Activation of NK cells thus induce tumour-killing activity of NK cells. Furthermore, it was also found that NKT cells could produce IL-13 upon stimulation with  $\alpha$ GC<sup>[125]</sup>.

In our study, expression of cytokines in Peyer's patches of mice administered with SlpB- $\alpha$ GC-LP resembles serum cytokines level of subjects (both mice and human) with intravenous administration of  $\alpha$ GC, which suggests that targeting effect of SlpB has facilitate antigen presentation of  $\alpha$ GC to T cells, thus inducing similar response to intravenous administration of  $\alpha$ GC. T<sub>H</sub>1 responses induced by  $\alpha$ GC thus reduce the production of T<sub>H</sub>2 cytokines, i.e., IL-4, IL-5 and IL-10. On the other hand, increases in concentration of IFN- $\gamma$  as a result of upregulation, negatively regulate production of IL-17<sup>[126]</sup>, thus downregulation of IL-17A.

Meanwhile, without SlpB-coating, LP was not delivered specifically to antigen-presenting cells (Figure 4.7 (a)). Unspecific delivery of  $\alpha$ GC results in undesired immunomodulation effect, rendering the RNA expression level of cytokines less controllable.

SlpB-functionalisation has not only improved therapeutic effect of drugs, but also achieve intravenous injection-like effect through oral administration, via APCs targeting. This advantage toward therapeutic effect of drug is contributed by the synergy effect of (1) enhanced stability of liposome, (2) enhanced transcytosis by M cells, (3) targeted delivery to liposome to APCs, (4) enhanced endocytosis by APCs, (5) adjuvant effect of SlpB.

Further evaluations are required to evaluate the disadvantages of SlpB-coated carriers. SlpB could form crystalline array on the surface of liposome, which could block the access of receptors to drugs conjugated on the surface of liposome. Therefore, liposome loaded with these types of drugs are unsuitable for SlpB-coating. Furthermore, lysis in lysosome might be required for SlpB-LP due to its highly anionic property, which render it difficult to fuse with cell membrane. Therefore, evaluation on the stability of drugs against lysozyme, particularly nucleic acid-based drugs, might be required prior administration.

Despite there is no regulatory requirement to test preclinical toxicity of drug carriers, it is important to study the potential adverse effect induced by endocytosis of high dose of drug carriers<sup>[127,128]</sup>. Some lipids, e.g., dioleoyl-3-trimethylammonium propane could induce oxidative



stress and exhibit gene silencing effect<sup>[129]</sup>, which could alter the original state of cells if administered overdose. Furthermore, overdose of immunomodulating drugs will result in inflammation or weakening of immune system, where careful investigations are required in dosimetry. On the other hand, previous study has reported that oral administration of drugs might be a safer route for drug administration compared to intravenous injection as oral administration will only induce negligible toxicity. For instances, in spite 1 - 4 ng LPS kg<sup>-1</sup> body mass is the maximum tolerated dose of LPS in human body through intravenous injection, 2 mg LPS kg<sup>-1</sup> body mass administrated orally did not show production of free cytokines, nor induced any adverse effect, even bioavailability of LPS in blood (2 - 4 µg) has already exceed lethal dose by 1000-fold<sup>[130]</sup>. Thus, it suggested that the potential adverse effect of endocytosis of SlpB-coated carriers by intestinal APCs might be lower than anticipation. In addition, with knowledge on bioavailability of SlpB-coated carriers, it is possible to control the dose administered and reduce the odd of inducing adverse effects.

## 4.4 Summary

In this chapter, I have demonstrated that SlpB-functionalisation can enhance transcytosis of liposome through M cells into SED of Peyer's patches and induce active endocytosis by APCs.

SlpB has improved the stability of LP in gut, and induced absorption specifically into Peyer's patches, but not intestine. Active absorption of SlpB-LP into Peyer's patches was facilitated by active transcytosis of SlpB-LP by M cells. In Peyer's patches, active endocytosis of SlpB-LP by APCs, i.e., MΦ and DC will activate translocation and antigen presentation by APCs. APCs have transported SlpB-LP into blood vessels, which have elevated bioavailability of fluorophore. Notably, absorption into Peyer's patches is correlated to bioavailability.

Furthermore, synergy effect of (1) enhanced stability of liposome, (2) enhanced transcytosis by M cells, (3) targeted delivery to liposome to APCs, (4) enhanced endocytosis by APCs, (5) adjuvant effect of SlpB has improved therapeutic effect of <sup>αG</sup>C<sub>LP</sub> by SlpB-functionalisation. Increase in production of T<sub>H</sub>1 cytokines suggested that SlpB-functionalisation has improved therapeutic effect of drug. Moreover, effect resembling intravenous injection through oral administration was obtained, suggesting that oral delivery of SlpB-functionalised carriers can potentially replace drug administration via intravenous injection.

## Chapter 5

### Mechanism of SlpB-DC Binding

In Chapter 3, I have shown that DC-SIGN and Mincle are receptors for SlpB. The results obtained were in aligned with prior studies<sup>[29,33]</sup>. However, how SlpB interact with these receptors remained unknown.

The properties of SlpB receptors might provide hints to the mechanism of binding. Both DC-SIGN and Mincle are C-type lectins, which bind to sugar moieties (Figure 5.1), but not amino acids. Therefore, it is possible that SlpB is a glycoprotein, and C-types lectins interact with sugar moiety in SlpB.

However, previous study have shown that SlpB from *Lv. brevis* is not glycosylated<sup>[29]</sup>, which contradict to the property of C-type lectins acting as receptors to SlpB. Since glycosylation was detected in Slp from *Lt. kefir*<sup>[131]</sup>, which is Slp in Group B Slp, SlpB from *Lv. brevis* might also be glycosylated.

In this chapter, I investigate the presence of sugar moiety in SlpB, and the mechanism of binding of SlpB to C-type lectins.

#### 5.1 Methods

##### 5.1.1 Identification of Sugar in SlpB

Presence of sugar in SlpB (2.5 µg) was analysed with phenol-sulphuric acid method<sup>[132]</sup>.

Then, SlpB was co-incubated with PNGase F for 24 h according to manufacturer's instructions to remove N-glycan and analysed with SDS-PAGE and stained with silver.

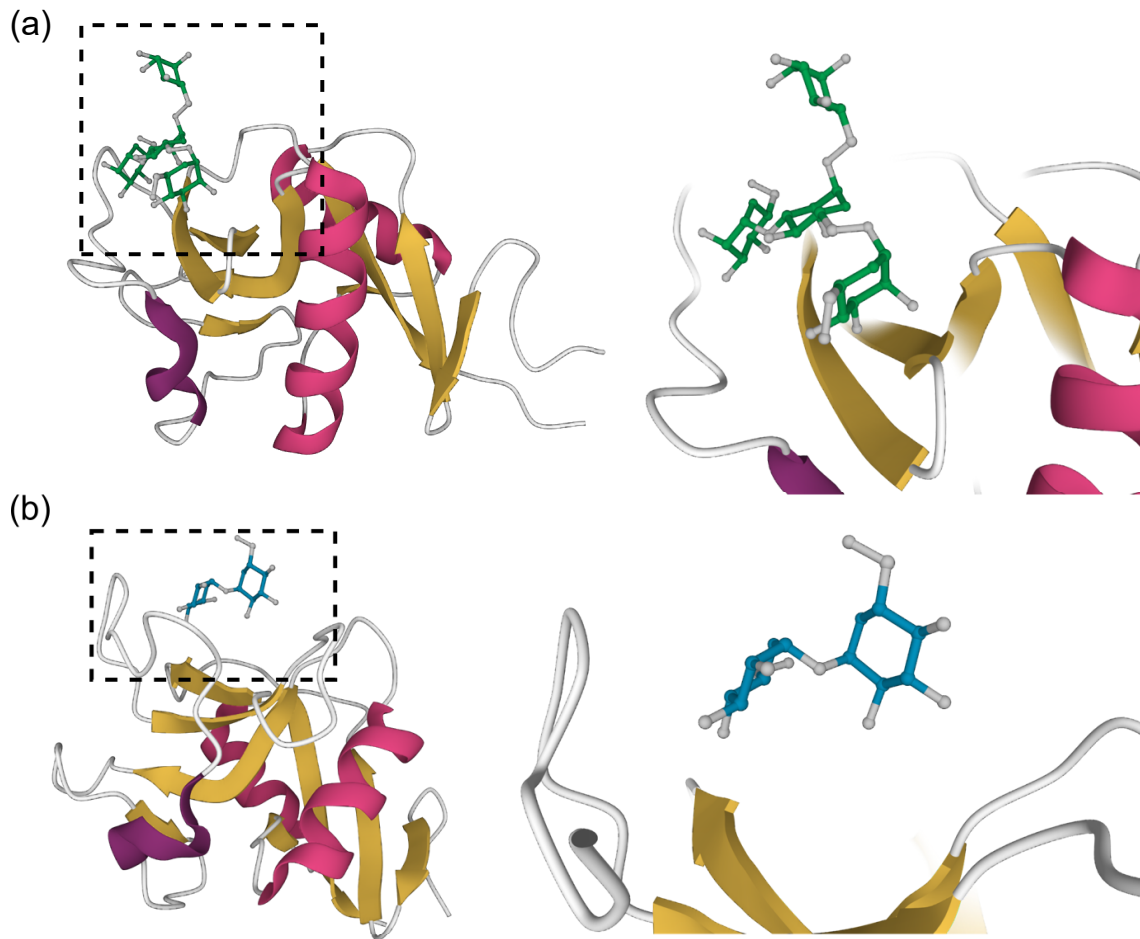


**Figure 5.1** Sugar binding domain on SlpB receptors. (a) Interaction of tetramannose to carbohydrate recognition domain (CRD) of DC-SIGN (PDB: 1SL4). (b) Interaction of trehalose to Mincle (PDB: 4KZV).

### 5.1.2 Competitive Binding Assay for SlpB with Sugars

DC were fixed with 5% formalin solution and co-incubated with 100  $\mu\text{g ml}^{-1}$  D-glucose, D-galactose, D-mannose or 10 mM EDTA for 60 min. Then, 10  $\mu\text{g ml}^{-1}$   $^{125}\text{I}$ -SlpB (molar ratio of sugars to SlpB  $\approx$  2,000:1) was supplemented\* to DC and incubated for another 60 min. The cells were washed thrice after incubation and the fluorescence intensity was measured.

### 5.1.3 *In silico* Analysis of Sugar-SlpB Interaction

As no crystal structure of Slp from lactobacilli has been solved, AlphaFold<sup>[133]</sup> was used to predict the structure of N-terminal of SlpB. Then, geometry-based cavity detection algorithm was used to detect pockets in N-terminal of SlpB, which the procedure includes  $\alpha$ -sphere detection, clustering and pocket characterisation were performed to identify the pockets available in N-terminal of SlpB. Based on the result obtained from pocket identification, molecular dynamics analysis was also conducted with grid-based method to identify the pocket formed generated by molecular dynamics analysis.

Docking analysis was also performed to identify the potential region for mannose binding in N-terminal of SlpB, which indicates the region in SlpB which contains sugars.

### 5.1.4 Trypsinisation of SlpB

Trypsin was supplemented to SlpB at mass ratio of 1 in 10 mM tris-HCl (pH 8.2) and incubated in 37°C for 21 h. Then, the reaction was stopped by adding 0.1% trifluoroacetic acid and freeze at -30°C.

### 5.1.5 Binding of SlpB Fragments to DC

Trypsinised SlpB was tuned to pH 7.0 and supplemented to DC. Trypsinised SlpB, DC supplemented with trypsin, and DC supplemented with trypsinised SlpB were incubated in 37.0°C incubator for 60 min. After incubation, the supernatants were collected. To reduce noise generated by remaining of SlpB fragments in culture plate, DC was washed thrice and all the fluids were collected.

Then, the samples were analysed by high performance liquid chromatography (HPLC) using the following conditions: 100% solvent A for 2 min, increasing to 20% solvent B in solvent A over 15 min, increasing to 45% solvent B in solvent A over 25 min, increasing to 100% solvent

---

\* Sugars were not removed from the solution

B over 5 min, 100% solvent B for 2 min, and decreasing to 0% solvent B (100% solvent A) in 1 min (solvent A: 0.1% trifluoroacetic acid in deionised water; solvent B: 0.1% trifluoroacetic acid in acetonitrile). Signal intensity was measured with absorbance at 220 nm. All peaks were manually collected when necessary.

The fragments which bind to DC were collected, and lyophilised. Then, these fragments were stained with Cy5, and desalted with ZipTip C18.

The Cy5 labelled fragments were co-incubated with DC at 37.0°C for 60 min, washed and the fluorescence intensity was measured.

## 5.2 Results

### 5.2.1 Glycosylation of SlpB and Its Function in DC Interaction

To understand the mechanism of SlpB-C-type lectins interaction, it is important to confirm whether sugar moiety exist in SlpB.

Concentration of sugar in glycoprotein can be quantified with phenol-sulphuric acid method<sup>[132]</sup>. Therefore, by comparing the signal generated by SlpB to water in phenol-sulphuric acid assay, we can verify the existence of sugar in SlpB.

By evaluating SlpB with phenol-sulphuric acid method, significant increase in absorbance at 490 nm was observed in SlpB compared to control (Figure 5.2 (a)). This result indicates that SlpB contains polysaccharide chain, which support my assumption that SlpB contains sugar moiety.

Furthermore, the presence of N-glycan in SlpB was confirmed with enzymatic reaction. After PNGase F treatment, a band with apparent molecular mass of 48 kDa was observed. The molecular mass of the band is similar to the molecular mass of SlpB computed based on amino acid sequence, which suggested that the band was deglycosylated SlpB. The result confirmed that SlpB is a glycoprotein which contain N-glycan.

To further investigate whether the sugar chains in SlpB involve in interaction with host cells, competitive binding assay of SlpB with various types of monosaccharides was performed (Figure 5.3). D-mannose exhibited the strongest inhibitory activity, which has reduced the binding of SlpB to DC by 2.6-fold, while D-galactose and D-glucose reduced binding by 2.3- and 2.0-fold respectively. The inhibitory activity of D-glucose was similar to EDTA (2.0-fold), which is an inhibitor for DC-SIGN binding activity.

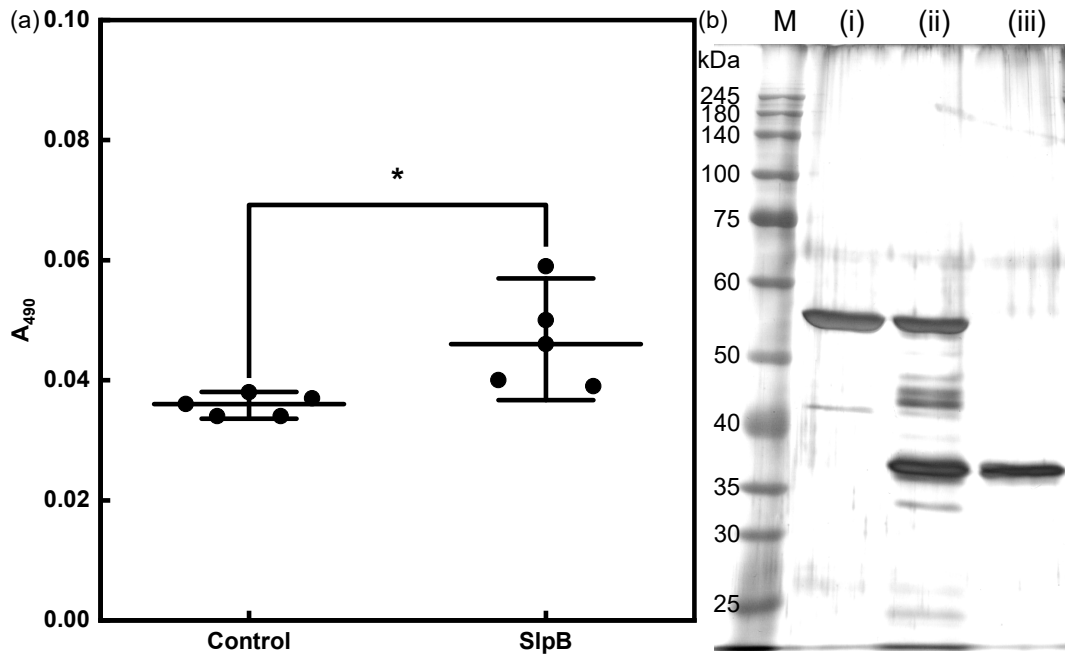


**Figure 5.2** Identification of sugars in SlpB. (a) Phenol-sulphuric acid method. The plots represent data obtained from quintuplicate sample in independent test and the error bars represent 95% confidence interval for mean. Statistical significance was evaluated with Student's t-test. \*  $p < 0.05$ . (b) SDS-PAGE of (i) SlpB, (ii) PNGase F treated SlpB and (iii) PNGase F.

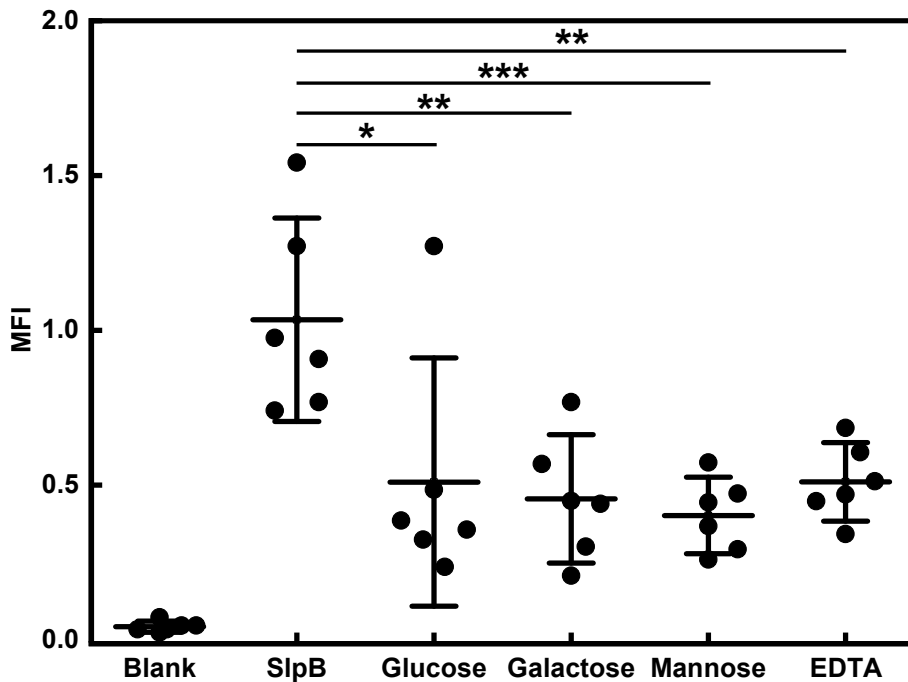


**Figure 5.3** Monosaccharides inhibit binding of SlpB to DC. The plots represent data obtained from sextuplicate sample in independent test and the error bars represent 95% confidence interval for mean. Statistical significance was evaluated with Student's t-test. \*  $p < 0.05$ , \*\*  $p < 0.01$ , \*\*\*  $p < 0.001$ .

Sequence alignment of SlpB to carbohydrates binding domain (Figure 3.7) suggests that these motifs are located in N-terminal of SlpB. Furthermore, computation of isoelectric point of each terminal of SlpB shows that the isoelectric point of N-terminal of SlpB was high. These results suggest that N-terminal of SlpB is responsible for binding to both host receptors and bacterial cell wall, while C-terminal is responsible for formation of crystalline array.

Based on the result obtained in sequence alignment analysis (Figure 3.7), I have conducted *in silico* analysis on structural relationship of mannose and N-terminal of SlpB. N-terminal was used to reduce computation cost as I have already shown that N-terminal is the domain interacts with and contains sugar (Figure 3.7).

As no crystal structure of Slp from lactobacilli has been solved, AlphaFold<sup>[133]</sup> was used to predict the structure of N-terminal of SlpB, and the drug pockets were identified based on the predicted model. 22 pockets were found in N-terminal. Among them, 5 pockets bind to mannose, which is a ligand to DC-SIGN (Figure 5.4 (a - b)).

Mannose binds predominantly carbohydrates binding motifs as described in Figure 3.7. Analysing small molecule binding capability of N-terminal of SlpB with grid-based method suggested that the locations where mannose binds to, exhibits high small molecule binding capability (Figure 5.4 (c - d)). As there are more than 1 binding sites at different locations in N-terminal of SlpB, particularly, there are some mannose binding sites which are located opposite to each other, i.e., regions indicate by (c) and (d) in Figure 5.4 (b), it is possible that part of these small molecules binding sites bind to cell wall, while others bind to DC-SIGN through formation of sugar complex. This result might explain the observation in previous study that the same terminal of SlpBs binds to both cell wall and host. Furthermore, binding sites as shown in Figure 5.4 (d) is in align with the model proposed in previous study that multiple attachment points exist for binding of Slp from *Lv. brevis* on cell wall and adsorb on liposome<sup>[65]</sup>.

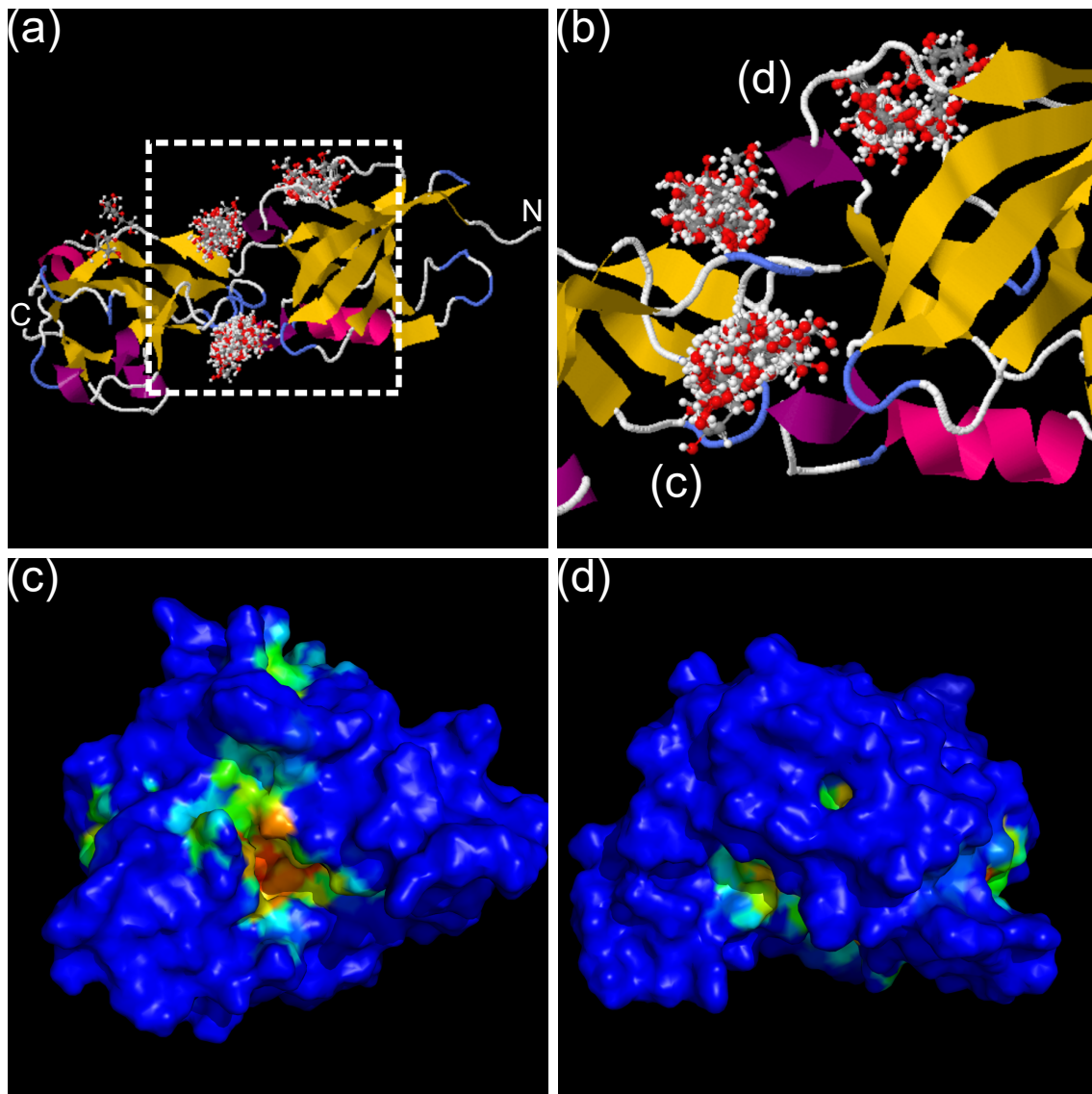


**Figure 5.4** Predicted structure of N-terminal of SlpB and its sugar binding sites. (a) Predicted structure of N-terminal of SlpB and mannose docking. N indicates N-terminal of protein, while C indicates C-terminal of N-terminal of SlpB. (b) Enlarged image of gated region in (a) which shows the locations which bind to high concentration of mannose. (c - d) Analysis of small molecule binding capability of the region labelled in (b). Blue indicates low binding capability while red indicated high binding capability.



### 5.2.2 Prediction of DC-Binding Fragments in SlpB

To verify the model proposed in previous section, trypsinised SlpB was co-incubated with DC for 60 min, and the supernatant was retrieved and analysed with HPLC. The chromatogram obtained was compared with control (Figure 5.5).

The peaks in region i has disappeared in chromatogram after co-incubating with DC, and the intensity of peak 6 decreased by 2.0-fold, peak 7 decreased by 1.5-fold, peak 8 decreased by 3.4-fold, peak 9 decreased by 1.5-fold, peak 10 by 2.1-fold, suggested that fragments of SlpB contained in these fractions binds to DC.

On the other hand, no peak appeared in Figure 5.5 (c), which suggested that the activity of trypsin was completely inhibited, thus proteins on DC were not hydrolysed.

To confirm whether the fragments which bind to DC contain sugar moiety, all peaks in Figure 5.5 (a) were collected for further analysis. Fragment 1 - 5 (Figure 5.5 (a)) were stained with Cy5 and incubated with DC for 60 min to confirmed the result in chromatogram (Figure 5.6). MFI of DC co-incubated with Fragment 1 - 4 increased significantly, while no change was observed for DC co-incubated with Fragment 5, which indicates that Fragment 1 - 4 of SlpB bind to DC.

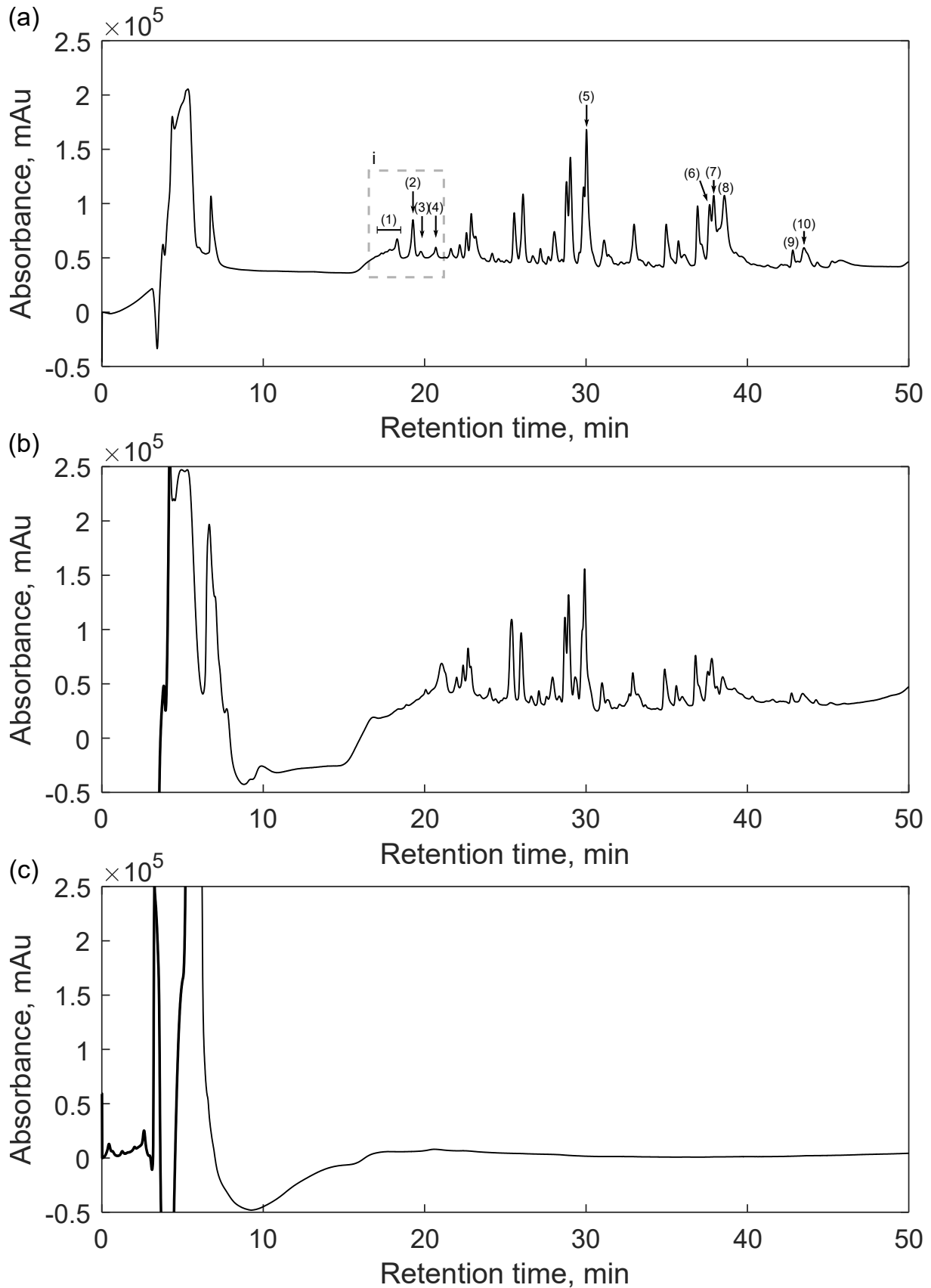


**Figure 5.5** Chromatograms which indicate fragments of SlpB binds to DC. Chromatogram of (a) trypsinised SlpB, (b) trypsinised SlpB after co-incubation with DC, (c) DC co-incubated with trypsin. Peaks 1 - 5 indicates fragments of SlpB used in cell binding assay. Region i (enclosed in grey dashed line) and peaks 6 - 10 shows the fragments of SlpB which bind to DC.

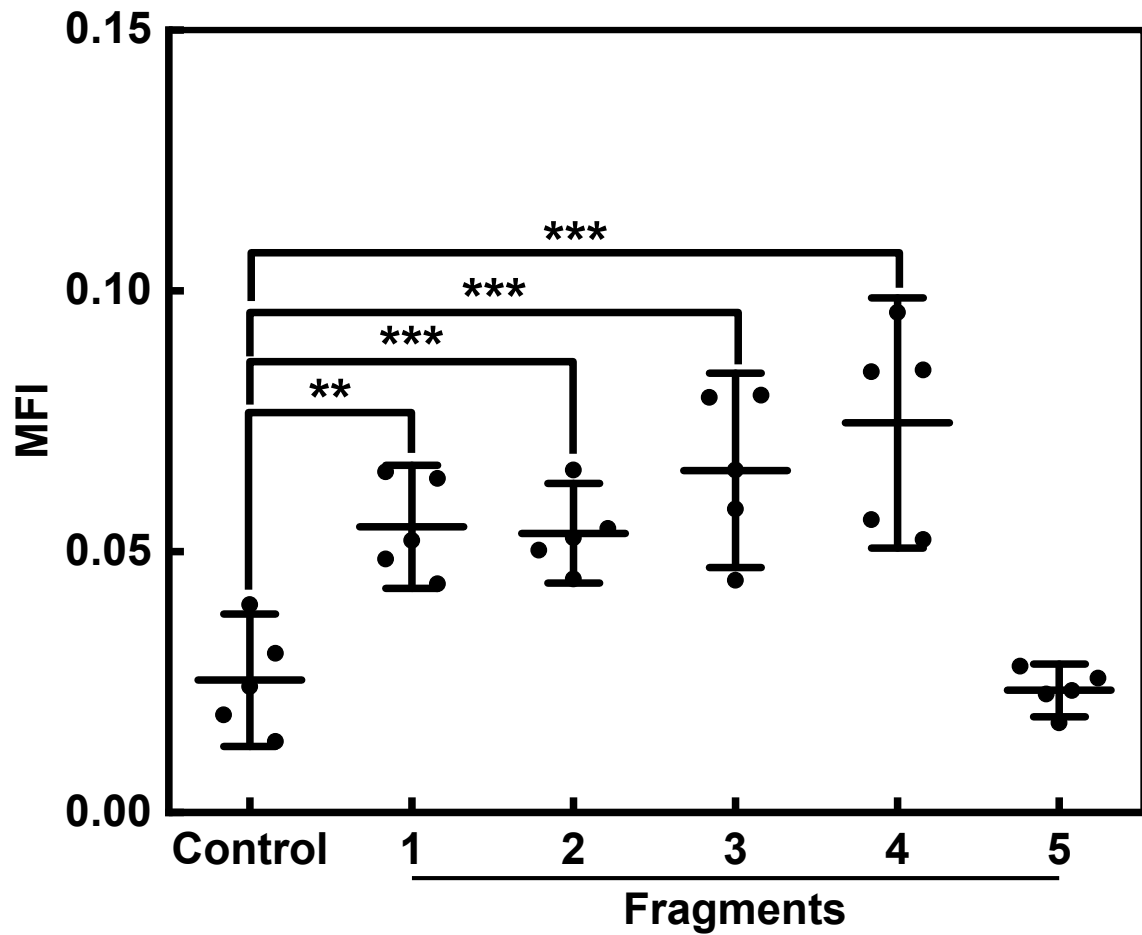


**Figure 5.6** Binding assay of fragments of SlpB to DC. The plots represent data obtained from quintuplicate sample in independent test and the error bars represent 95% confidence interval for mean. Statistical significance was evaluated with Student's t-test. \*\*  $p < 0.01$ , \*\*\*  $p < 0.001$ .

### 5.3 Discussion

Generally, there are 2 potential binding mechanisms of Slp to host receptors or extracellular matrices, either through a single protein unit, or through crystalline array. For instances, although it has been demonstrated that formation of crystalline array of CbsA from *Lactobacillus crispatus* is important in collagen binding<sup>[30]</sup>, a single unit of SlpA from *L. acidophilus* without formation of crystalline array is enough for DC-SIGN binding<sup>[24]</sup>.

In Chapter 3, I have shown that SlpB can bind to DC-SIGN and Mincle without formation of crystalline array. Thus, it suggests that formation of crystalline array is not necessary to mediate SlpB interaction with host receptors. The hypothesis that SlpB is a glycoprotein was tested, and sugar was identified in SlpB by phenol-sulphuric acid assay (Figure 5.2). Interaction of SlpB to DC was interfered by monosaccharides (Figure 5.3). Furthermore, prior studies have shown that DC-SIGN binds to sugar moiety, but not other components<sup>[134-137]</sup>. Therefore, it is necessary for SlpB to bind to DC-SIGN via sugar moiety. Meanwhile, SlpB forms crystalline array with lattice constant of  $\alpha = 8.4$  nm,  $\beta = 5.0$  nm,  $\gamma = 80^\circ$ , covering N-terminal which contains cell wall binding domain. Consider the size of DC-SIGN as tetramer, with diameter of 200 nm<sup>[138]</sup>, DC-SIGN cannot penetrate the crystal lattice formed by SlpB. On the other hand, N-glycan chain was found in SlpB, which is shown by deglycosylation of SlpB by PNGase F. Based on both the knowledge in previous study and results obtained in this study, I have arrived at the model that SlpB interact with DC-SIGN via formation of SlpB-polysaccharide-DC-SIGN complex (Figure 5.7).

As discussed in Section 1.2, conserved N-terminal of SlpB is hydrophilic, particularly, the sugar binding motifs as shown in Figure 3.7 are the fragments with highest hydrophilicity in SlpB. The affinities of these fragments to C18 resin are the weakest, thus the retention time of these fragments are the shortest. These properties of sugar binding domains of SlpB suggests that peaks 1 - 4 might be sugar binding domains of SlpB, and these domains are the domains which binds to DC (Figure 5.6). Besides, sugar binding motifs were also identified in N-terminal of SlpB through *in silico* analyses (Figure 3.7, 5.7). The distribution of sugar binding domains on N-terminal of SlpB suggests that it is possible for N-terminal of SlpB is responsible for both cell wall binding and interaction with host receptors.

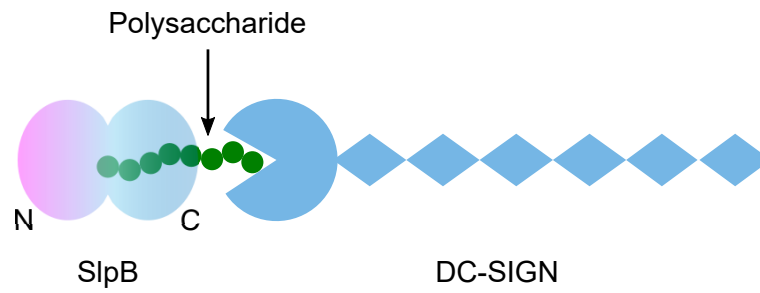


**Figure 5.7** Predicted model of SlpB/DC-SIGN interaction. DC-SIGN binds to the polysaccharide chain which binds to the N-terminal of SlpB.

**Table 5.1** Receptors on M cells and their ligands.

Receptors	Ligands	Ref
PrP <sup>C</sup>	<i>N</i> -acetyl- $\beta$ - <i>D</i> -glucosamin	139
Umod	diacetylchitobiose Man[ $\alpha$ <sub>1-6</sub> ](Man[ $\alpha$ <sub>1-3</sub> ]-Man-O-ethyl	140
Aif1	actin calcium	120
GP2	FimH	118,141

Characteristics of SlpB as glycoprotein also explain enhanced transcytosis of SlpB-LP through M cells (Figure 4.6). Table 5.1 summarises the ligands to receptors on M cells. Among these receptors, Umod is a lectin which could bind to diacetylchitobiose and  $\text{Man}[\alpha_{1-6}](\text{Man}[\alpha_{1-3}]\text{-Man-O-ethyl})$ . Like DC-SIGN and Mincle, Umod potentially interact with SlpB through mannose, and facilitated transcytosis of liposome into Peyer's patches. This is supported by prior study which have shown that SlpA from *L. acidophilus* could bind to Umod and facilitate transcytosis of *L. acidophilus*<sup>[23]</sup>.

## 5.4 Summary

In this chapter, I have investigated the mechanism of SlpB-DC interaction. Sugar moiety was discovered in SlpB by phenol-sulphuric method. Treatment of SlpB with PNGase F revealed that the sugar on SlpB was N-glycan. As sugar is the only ligand discovered for DC-SIGN to date, N-glycan attached on SlpB supposed to involve in SlpB-DC interaction. Moreover, I have also shown that sugar will inhibit binding of SlpB to DC, which is in align with our understanding about the function of DC-SIGN and suggested that sugar is important in mediating SlpB-binding to DC. 4 fragments of SlpB were identified to exhibit binding activity to DC, and these fragments are potentially sugar binding domains in SlpB based on their high hydrophilicity.

## Chapter 6

### Conclusion and Future Prospect

#### 6.1 Summary and Discussion

In this dissertation, I have investigated the potential of SlpB-LP to target intestinal APCs.

In Chapter 2, I have characterised the property of SlpB-coated liposomes. SlpB from *Lv. brevis* JCM 1059 can be coated on the surface of liposomes and form a single layer on the outer surface of liposomes regardless of size and polydispersity. SlpB-coating reduced  $\zeta$  potential of anionic liposomes, thus, increased colloid stability of liposomes. Moreover, I have also demonstrated that SlpB can be coated on various commonly used drug carriers, e.g., microbeads and bacteria, which could expand the repertoire of SlpB-coated carriers for intestinal APCs-targeting. Stability of liposomes is a major concern which have limited the application of liposome as carrier for oral delivery. It is important for liposome to protect and to retain its content to achieve specific delivery at correct dose. This is particularly difficult for liposomes in gut where constant and rapid changes of pH, mechanical stress and enzymatic degradation take place. I have demonstrated that SlpB could improve stability of liposomes against various gut mimicking environments. The effect of SlpB to improve stability of liposomes is particularly distinctive in high pH, gall solution and SIF.

In Chapter 3, the targeting effect of SlpB to enhance endocytosis of drug carriers by APCs was discussed. SlpB binds to C-type lectins, e.g., DC-SIGN and Mincle. Ligand-receptor interaction induced by SlpB has enhanced endocytosis of liposomes, microbeads, Gram-positive and Gram-negative bacteria by both M $\Phi$  and DC. The enhancing effect on endocytosis by APCs was similar to SlpAs. However, as SlpAs could bind to mucosal layer in gut, rendering them unsuitable for APCs targeting, SlpB is a more promising ligand compared to SlpA. The potential mechanism of SlpB-induced endocytosis was also investigated in DC. SlpB could activate DC, and induce rapid internalisation of particles, which potentially resulted in increased endocytic capacity of particles by DC. Besides improving stability and enhanced endocytosis of liposomes, I have shown that

SlpB possess adjuvant effect which could improve the therapeutic effect of drugs. With a  $T_H1$  polariser,  $\alpha$ GC as model drug, I have shown that SlpB could improve therapeutic effect of drugs measured by ELISA and RT-qPCR. Both production and expression of anti-tumour cytokines were increased.

Chapter 4 discussed the capability of SlpB to improve stability of liposome and its capability to target intestinal APCs *in vivo*. SlpB-coating has improved the stability of liposome by 5.4- and 6.1-fold at 1 h and 3 h administration, respectively. Unlike SlpAs, SlpB did not result in retention of liposomes in mucosal layer. SlpB-functionalisation has induced specific uptake into APCs in Peyer's patches by transcytosis through M cells and ligand-mediated endocytosis by APCs. Besides, SlpB-functionalisation has also promoted antigen presentation by APCs in Peyer's patches. Through this route of administration, bioavailability defined as availability of drugs in blood has been improved from 0.02% to 7.3%, which is 427.6-fold higher by SlpB-coating. Furthermore, the retention of drugs in blood has also been lengthen. 1.7% of fluorophore can still be detected in blood at 3 h after administration, while it was undetectable in mice administered with LP. Then, the effect of SlpB on therapeutic effect of drug-loaded liposome was discussed. In *in vivo* study, orally administered SlpB-functionalised liposome could induce therapeutic effect similar to intravenous injection, which suggest that oral delivery of drugs loaded in SlpB-LP could potentially replace intravenous injection or dripping.

In Chapter 5, I have investigated mechanisms underlie SlpB-DC interaction. I have discovered that SlpB is a glycoprotein, in contrast of previous studies. By comparing chromatogram of trypsinised SlpB before and after co-incubation with DC, I have identified the DC-binding fragments in SlpB. Further verification suggests that these fragments are the specific fragments which are responsible in DC interaction, and they are potentially sugar binding domains in SlpB.

Assembling the data obtained from all chapters in this dissertation reveal the mechanism of SlpB-lipid and SlpB-DC interaction, and SlpB-enhanced endocytosis (Figure 6.1). As SlpB can be extracted by chaotropic agent, i.e., 5 M LiCl solution, the binding of SlpB should be mediated by electrostatic charge and van der Waals force of attraction. Analysing the isoelectric point of N-terminal and C-terminal of SlpB has shown that isoelectric point of N-terminal of SlpB was 9.87, while C-terminal was 5.42 (Section 2.3.1), which suggested that binding via electrostatic force is mediated through N-terminal of SlpB and anionic substrate on liposome. As calcium ion exists in the mannose binding pocket of DC-SIGN<sup>[142]</sup>, and it involves in DC-SIGN-mannose binding, which is demonstrated in Figure 5.3 that chelating calcium ion with EDTA could inhibit SlpB-



binding, mannose binding pocket of DC-SIGN must be positively-charged. Positively-charged pocket of carbohydrate binding domain (CRD) of DC-SIGN attract negatively-charged SlpB-LP (Figure 2.2), followed by formation of bond between hydroxy group on mannose of N-glycan of SlpB to CRD of DC-SIGN possibly via calcium ion<sup>[143]</sup>. SlpB-DC-SIGN binding results in ligand mediated endocytosis, and the phagosome and pinosome which contain SlpB-LP will develop into lysosome to lyse SlpB-LP and release the drugs encapsulated in it.

Throughout this study, I have delivered hydrophobic and hydrophilic molecules, small molecules and macromolecules to APCs with SlpB-LP. SlpB has protected these molecules against harsh gut environments, without which these molecules will be degraded before arriving at target site. Furthermore, targeted delivery has also been achieved. Synergy effect of these properties and adjuvant effect provided by SlpB has improved therapeutic effects of drugs. These results have shown that SlpB is a promising ligand to target intestinal APCs compared to other ligands.

## 6.2 Future Prospects and Applications

In this study, I have demonstrated that SlpB-functionlisation could improved stability of liposomes, facilitated transcytosis through M cells, induced and enhanced specific endocytosis into APCs, followed by increased bioavailability in blood. Furthermore, when SlpB-functionalised drug-loaded liposome was delivered, *in situ* mRNA expression of cytokines-related genes were upregulated in Peyer's patches. These results suggested that SlpB is a useful ligand for intestinal APCs targeting via oral delivery.

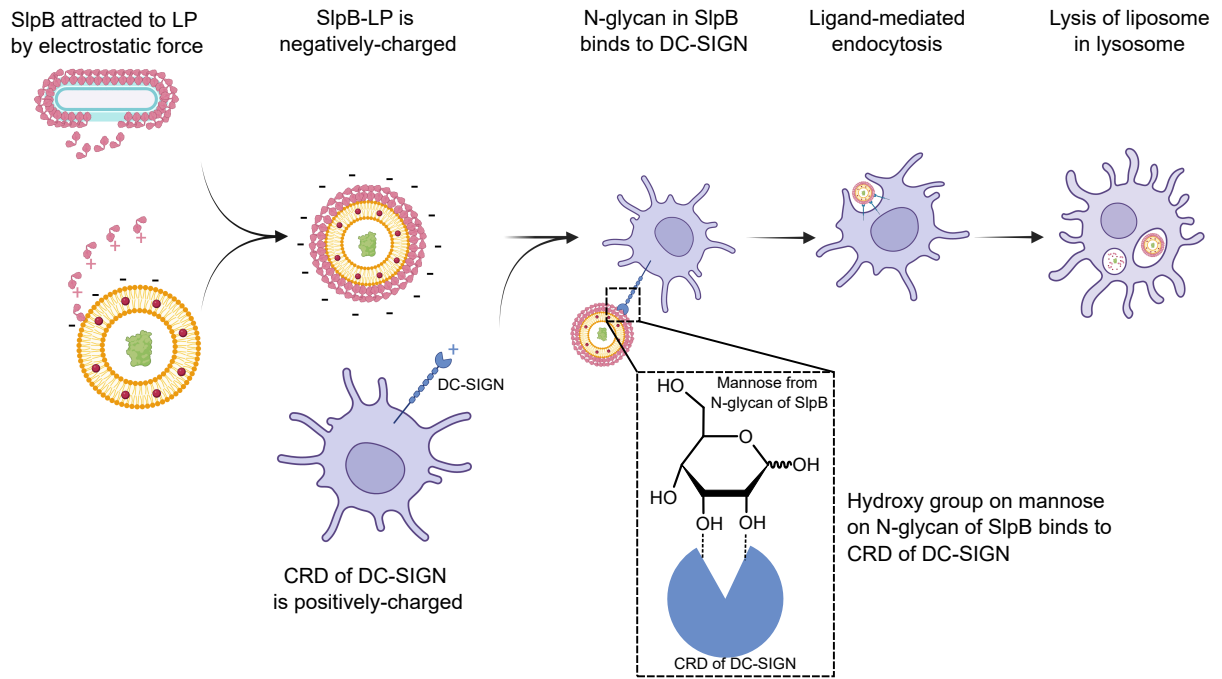


**Figure 6.1** Function of charge in SlpB-lipid interaction and SlpB-DC interaction, and mechanism of endocytosis.

However, several questions remained to be answered in this study to better understand the process of delivery. First, the interaction of M cells with SlpB have to be investigated to understand how SlpB could boost transcytosis of particles through M cells. Previous study has shown that M cells interact with bacterial surface components via GP2, PrP<sup>C</sup> (binds to *N*-acetyl- $\beta$ -*D*-glucosamin<sup>[139]</sup>), Umod (binds to diacetylchitobiose and Man[ $\alpha$ <sub>1-6</sub>](Man[ $\alpha$ <sub>1-3</sub>]-Man-O-ethyl<sup>[140]</sup>) or Aif1 (binds to actin and calcium). Previous study have shown that SlpA from *L. acidophilus* could bind to Umod and facilitate transcytosis of *L. acidophilus*<sup>[23]</sup>, while bare particles, e.g., microbeads and *Lactocaseibacillus rhomnosus* bind to secretory IgA, followed by IgA receptors on M cells<sup>[10,144]</sup>. In Chapter 4, I have shown that SlpB did not bind to GP2 of M cells as the signal intensity originated from GP2 was conserved. Based on the properties of other receptors found on the surface of M cells, Umod is a candidate which involve in transcytosis of SlpB-functionalised particles. Previous study has shown that diacetylchitobiose and Man[ $\alpha$ <sub>1-6</sub>](Man[ $\alpha$ <sub>1-3</sub>]-Man-O-ethyl but not other saccharides could inhibit binding of TNF to Umod<sup>[140]</sup>, suggesting that Umod interacts via sugar moiety. This property hints that SlpB potentially binds to Umod via mannose.

Another question to be clarified is the crystalline array formed on the surface of liposome. The crystalline array of SlpB formed on native *Lv. brevis* surface has lattice constant of  $\alpha = 8.4$  nm,  $\beta = 5.0$  nm,  $\gamma = 80^\circ$ . However, the lattice structure of SlpB crystalline array formed on the surface of anionic liposome remained unclear. Based on the physicochemical property measured, e.g.,  $\zeta$  potential and thickness, I have deduced that a single layer of SlpB with lattice constant similar to the structure on native bacterial surface has formed on liposome. Yet, a direct evidence measured by atomic force microscope or small angle X-ray scattering is required to determine the exact lattice constant of SlpB crystalline array formed on the surface of anionic liposome.

Furthermore, detailed analysis of the sequence and property of polysaccharide chain in SlpB N-terminal has to be performed to understand the function of polysaccharide chain in biological function of SlpB, i.e., understanding the origin of adjuvant effect of SlpB and how SlpB has facilitated uptake of particles.

On the other hand, the adverse effect of SlpB-LP has not been investigated. To deploy SlpB-LP into clinical trial, it is important to investigate the potential adverse effect of SlpB-LP in drug delivery, e.g., overstimulation of intestinal APCs with drug-loaded SlpB-LP.

As M cells and APCs exist in other tissue, e.g., eye<sup>[145]</sup>, thus, with further evaluation of the mechanism of delivery of SlpB-LP, this system could be employed to target ocular APCs.

Despite of the unanswered question, I have demonstrated that SlpB-functionalisation could improved delivery of carriers which have encapsulated hydrophobic, hydrophilic, small and macromolecule to APCs in Peyer's patches. Targeting of APCs with drugs-loaded SlpB-LP has enhanced therapeutic effect of drugs, and induced effect similar to intravenous injection. Bioavailability and retention were also boosted by SlpB-functionalisation, which has provided a useful tools for oral delivery of vaccines, immunomodulatory drugs for various purposes, pharmaceuticals, e.g., insulin and nutraceutical products.

---

# Appendices

# Appendix A

## Materials and Apparatus

### A.1 Materials

Materials	Manufacturer	Origin	Grade or Cat #
RPMI 1640 medium	Nacalai Tesque	Kyoto, Japan	30264-56
Fetal bovine serum	BioWest	Spain	
Fetal bovine serum	BioWest	EU	S1400-500
Dulbecco's phosphate buffered saline (-)	Nacalai Tesque	Kyoto, Japan	14249-95
Phorbol 12-myristate 13-acetate	AdipoGen	Liestal, Switzerland	AG-CN2-0010
Recombinant human IL-4	PeproTech	California, USA	AF-200-04
Recombinant human IFN- $\gamma$	Peprotech	California, USA	AF-300-02
Cytochalasin D	Cayman	Michigan, USA	11330
0.5% trypan blue solution	Nacalai Tesque	Kyoto, Japan	29853-34
2.5 g l <sup>-1</sup> trypsin with 1 mM EDTA	Nacalai Tesque	Kyoto, Japan	32777-15
Dimethyl sulphoxide	Nacalai Tesque	Kyoto, Japan	08904-85
Difco™ MRS broth powder	Becton Dickinson	Maryland, USA	288130
Liposomal KRN7000	Regimmune	California, USA	RGI-2001-P
Anionic liposome	Nippon Oil & Fats	Japan	EL-01-A
Anionic liposome	Nippon Fine Chemical	Japan	PPG-1
Human IL-6 ELISA kit	Biologend	California, USA	430504
Human IL-10 ELISA kit	Biologend	California, USA	430604
Human IL-17A ELISA kit	Biologend	California, USA	433914
Human IL-12/IL-23 (p40) ELISA kit	R&D Systems	Minnesota, USA	DY1240
Substrate solution	R&D Systems	Minnesota, USA	DY999
Sulphuric acid	Nacalai Tesque	Kyoto, Japan	32519-95
Normal goat serum	Jackson ImmunoResearch	Pennsylvania, USA	005-000-001
LAL Endotoxin Assay Kit	GenScript	New Jersey, USA	L00350C
Propidium iodide	MP Biomedicals	Illkirch, France	195458
Fluorescein isothiocyanate	ICN Biomedicals	Ohio, USA	100276
4',6-diamidino-2-phenylindole	Wako	Osaka, Japan	049-18801
Cy™3 monofunctional reactive dye	GE Healthcare	Buckinghamshire, UK	Q13108
Cy™5 monofunctional reactive dye	GE Healthcare	Buckinghamshire, UK	Q15108
Carboxyfluorescein diacetate	Anaspec	California, USA	AS-89000
Bovine serum albumin	Nacalai Tesque	Kyoto, Japan	01862-87
Ovalbumin	Fujifilm Wako	Osaka, Japan	018-09882
FITC-conjugated ovalbumin	Invitrogen	Oregon, USA	O23020
Protein assay CBB solution	Nacalai Tesque	Kyoto, Japan	29449-15
DNase I	Nippon Gene	Toyama, Japan	314-08071
Buffer RLT	Qiagen	Hilden, Germany	79216
Buffer RW1	Qiagen	Hilden, Germany	1053394
Buffer RPE	Qiagen	Hilden, Germany	1018013
70% ethanol	Wako	Osaka, Japan	059-07895
5x RT master mix	Toyobo	Osaka, Japan	FSQ-201
THUNDERBIRD® SYBR® qPCR mix	Toyobo	Osaka, Japan	QPS-201
RNase quiet	Nacalai Tesque	Kyoto, Japan	09147-14
O.C.T. compound	SakuraTek	California, USA	4583

## Appendix A. Materials and Apparatus

Materials	Manufacturer	Origin	Grade or Cat #
Protein marker (Broad)	Takara	Shiga, Japan	3452
Protein marker (Tri-colour)	Nacalai Tesque	Kyoto, Japan	19593-25
Ammonium persulphate	Wako	Osaka, Japan	016-08021
Coomassie brilliant blue R-250	Nacalai Tesque	Kyoto, Japan	S09408-52
CBB R-250 destaining solution	Bio-Rad	USA	1610438
30% acrylamide/bis mixed solution	Nacalai Tesque	Kyoto, Japan	06141-35
N,N,N',N'-tetramethylethylenediamine	Nacalai Tesque	Kyoto, Japan	33401-72
Trisaminomethane	Nacalai Tesque	Kyoto, Japan	35434-21
Sodium dodecyl sulphate	Nacalai Tesque	Kyoto, Japan	31607-65
$\beta$ -mercaptoethanol	Nacalai Tesque	Kyoto, Japan	21438-82
Sucrose	Wako	Osaka, Japan	196-00015
Bromophenol blue	Kanto Chemical	Tokyo, Japan	04319-30
Glycine	Nacalai Tesque	Kyoto, Japan	17109-35
Methanol	Nacalai Tesque	Kyoto, Japan	21914-03
Acetic acid	Nacalai Tesque	Kyoto, Japan	00211-95
Glycerol	Nacalai Tesque	Kyoto, Japan	17018-25
Gelatin	Kanto Chemical	Tokyo, Japan	17009-01
Ethylenediaminetetraacetic acid	Nacalai Tesque	Kyoto, Japan	15130-95
Hydrochloric acid	Fujifilm Wako	Osaka, Japan	080-01066
Boric acid	Wako	Osaka, Japan	021-02195
Trifluoroacetic acid	Nacalai Tesque	Kyoto, Japan	34831-12
Acetonitrile	Nacalai Tesque	Kyoto, Japan	00430-83
Silver stain kit	Kanto Chemical	Tokyo, Japan	N/A
Sodium chloride	Fujifilm Wako	Osaka, Japan	191-01665
Monopotassium phosphate	Nacalai Tesque	Kyoto, Japan	28721-55
Disodium phosphate	Nacalai Tesque	Kyoto, Japan	31738-55
Potassium chloride	Wako	Osaka, Japan	28513-85
Sodium bicarbonate	Wako	Osaka, Japan	191-01305
Sodium carbonate	Wako	Osaka, Japan	199-01585
Sodium hydroxide	Wako	Osaka, Japan	198-13765
D-glucose	Wako	Osaka, Japan	041-00595
D-mannose	Nacalai Tesque	Kyoto, Japan	21306-02
D-galactose	Nacalai Tesque	Kyoto, Japan	16511-75
Gall powder	Wako	Osaka, Japan	073-00092
Lithium chloride	Nacalai Tesque	Kyoto, Japan	20623-85
Silver nitrate	Nacalai Tesque	Kyoto, Japan	31019-17
Sodium thiosulphate pentahydrate	Kanto Chemical	Tokyo, Japan	37295-00
Sodium azide	Wako	Osaka, Japan	195-11092
Formaldehyde	Nacalai Tesque	Kyoto, Japan	16222-65
Polyethylene glycol mono- <i>p</i> -isooctylphenyl ether	Nacalai Tesque	Kyoto, Japan	12967-32
Polyoxyethylene sorbitan monolaurate	Nacalai Tesque	Kyoto, Japan	35624-15
Buffer solution standard (pH 4.01)	Wako	Osaka, Japan	028-03185
Buffer solution standard (pH 6.86)	Wako	Osaka, Japan	025-03195
Buffer solution standard (pH 9.18)	Wako	Osaka, Japan	028-03205
Lipopolysaccharide	Fujifilm Wako	Osaka, Japan	120-05131
Mouse mAb against hDC-SIGN	Santa Cruz	California, USA	sc-23926
Rabbit pAb against hDC-SIGN	Novus	Colorado, USA	NBP2-27408
Mouse mAb against hMincl	NKMax	Gyeonggi-do, Korea	ATGA0175
Goat pAb against mIgG-FITC	Sigma	Mexico	F0257
Cy3-conjugated goat pAb against rIgG	Novus	Colorado, USA	NB120-6939
DyLight405-conjugated goat pAb against rIgG	Rockland	Pennsylvania, USA	611-146-002
Rabbit mAb against mCD23	Novus	Colorado, USA	NBP2-90682
Rabbit pAb against mGP2	EpiGenetek	New York, USA	A67678
TPCK-treated trypsin	Worthington	New Jersey, USA	LS003740

<sup>a</sup> The full name of Wako is Wako Pure Chemical.

## Appendix A. Materials and Apparatus

---

Materials	Manufacturer	Origin	Cat #
100 mm tissue culture dish	Thermo Scientific	Korea	130182
24 well tissue culture plate	TPP	Switzerland	92024
96 well tissue culture plate	True Line	USA	TR5003
96 well Nunc-Immuno™ plate	Thermo Scientific	Denmark	430341
96 well plate	As-One	China	2-8085-02
0.025 µm nitrocellulose membrane filter	Merck Millipore	Cork, Ireland	VSWP02500
0.22 µm PVDF syringe filter	Merck Millipore	Cork, Ireland	SLGV033RB
10K centrifugal filter	Merck Millipore	Cork, Ireland	UFC501024
Parafilm® M	Bemis Company	Wisconsin, USA	P7668
Dialysis tube	As-One	Japan	2-316-02
Filter column	Favorgen	Japan	FAFTC-C50
Total RNA extraction column	Favorgen	Japan	FARBC-C50
C <sub>18</sub> column (5 µm)	Waters	Ireland	186003116
ZipTip C <sub>18</sub>	Millipore	Cork, Ireland	ZTC18S096



## A.2 Apparatus

Apparatus	Manufacturer	Model	Origin
Electronic balance	Shimadzu	UW1020H	Kyoto, Japan
Analytical balance	AND	GR-202	Japan
Copper alloy CO <sub>2</sub> incubator	Sanyo	MCO-20AIC	Japan
NanoDrop spectrophotometer	ThermoFisher Scientific	NanoDrop 2000	Shanghai, P. R. China
UV/Vis microplate reader	Thermo Scientific	Varioskan™ LUX	Vantaa, Finland
Microplate reader	BioRad	iMark	Japan
Flow cytometer	Sony	EC800	Tokyo, Japan
Fluorescent microscope	Bio-Rad	ZOE	Singapore
Fluorescent microscope	Carl Zeiss	Axio Observer	Germany
Laser scanning microscope	Carl Zeiss	LSM 780	Germany
Microplate mixer	As-One	NS-P	Japan
Table-top centrifuge	Kubota	3520	Tokyo, Japan
Angular rotor	Kubota	MA-2024	Tokyo, Japan
Centrifuge	Kubota	3740	Tokyo, Japan
Angular rotor	Kubota	AF5004CH	Tokyo, Japan
Centrifugal vaporiser	EYELA	CVE-100	Tokyo, Japan
Fluorescent image analyser	GE Healthcare	Typhoon FLA 9500	Uppsala, Sweden
Vertical gel tank	ATTO	AE-6500	Tokyo, Japan
Electrophoresis power unit	ATTO	WSE-3100	Tokyo, Japan
Incubator	As-One	IC-300A	Japan
Bio-photorecorder	Advantec	TVS062CA	Japan
Bürker-Türk haemocytometer	Hirschmann EM Technicolor	8100102	Eberstadt, Germany
pH meter	Horiba Scientific	Laqua F-71	Kyoto, Japan
Mini-rotator	As-One	ACR-100	Japan
Scanner	Epson	EW-M630TB	P. R. China
Low temperature incubator	Mitsubishi Electric	SLC-A	Japan
Low speed centrifuge	Tomy	LC-122	Japan
Swinging bucket rotor	Tomy	7115-08 in TS-7	Japan
Cryostat	Leica	CM3050	Germany
Real Time PCR system	Applied Biosystems	StepOne™	Singapore
Nanoparticle analyser	Horiba	SZ-100V2	Japan
Transmission electron microscope	Hitachi	H-8100	Japan

### A.3 Primers for RT-qPCR

All the primers used in this study were obtained from Integrated DNA Technologies.

	Target	Sequence
<i>Homo sapiens</i>		
IFN- $\gamma$	Sense	GGA CCC ATA TGT AAA AGA AGC AGA
	Anti-sense	TCT CAC TCT CCT CTT TCC AAT TCT
IL-2	Sense	ATG TAC AGG ATG CAA CTC CTG TCT T
	Anti-sense	GTT AGT GTT GAG ATG ATG CTT TGA C
IL-4	Sense	AGC CTC ACA GAG CAG AAG ACT CTG
	Anti-sense	CAG CCC TGC AGA AGG TTT CCT TCT C
IL-5	Sense	GCT TCT GCA TTT GAG TTT GCT AGC T
	Anti-sense	TGG CCG TCA ATG TAT TTC TTT ATT AAG
IL-6	Sense	ACT CAC CTC TTC AGA ACG AAT TG
	Anti-sense	CCA TCT TTG GAA GGT TCA GGT TG
IL-10	Sense	CTT CGA GAT CTC CGA GAT GCC TTC
	Anti-sense	GGA TCA TCT CAG ACA AGG CTT GGC
IL-12	Sense	CCT GCT GGT GGC TGA CGA CAA T
	Anti-sense	CTT CAG CTG CAA GTT CTT GGG T
IL-17	Sense	CTC CAG AAG GCC CTC AGA CTA C
	Anti-sense	GGG TCT TCA TTG CGG TGG
TNF- $\alpha$	Sense	CCT CTC TCT AAT CAG CCC TCT G
	Anti-sense	GAG GAC CTG GGA GTA GAT GAG
$\beta$ -actin	Sense	TGG CAC CCA GCA CAA TGA A
	Anti-sense	CTA AGT CAT AGT CCG CCT AGA AGC A
<i>Mus musculus</i>		
GAPDH	Sense	CAT CAC TGC CAC CCA GAA GAC TG
	Anti-sense	ATG CCA GTG AGC TTC CCG TTC AG
IFN- $\gamma$	Sense	CAG CAA CAG CAA GGC GAA AAA GG
	Anti-sense	TTT CCG CTT CCT GAG GCT GGA T
IL-4	Sense	ATC ATC GGC ATT TTG AAC GAG GTC
	Anti-sense	ACC TTG GAA GCC CTA CAG ACG A
IL-5	Sense	GAT GAG GCT TCC TGT CCC TAC T
	Anti-sense	TGA CAG GTT TTG GAA TAG CAT TTC C
IL-6	Sense	TAC CAC TTC ACA AGT CGG AGG C
	Anti-sense	CTG CAA GTG CAT CAT CGT TGT TC
IL-10	Sense	CGG GAA GAC AAT AAC TGC ACC C
	Anti-sense	CGG TTA GCA GTA TGT TGT CCA GC
IL-12	Sense	GGA AGC ACG GCA GCA GAA TAA
	Anti-sense	CTT GAG GGA GAA GTA GGA ATG
IL-17A	Sense	CAG ACT ACC TCA ACC GTT CCA C
	Anti-sense	TCC AGC TTT CCC TCC GCA TTG A
TNF- $\alpha$	Sense	GGT GCC TAT GTC TCA GCC TCT T
	Anti-sense	GCC ATA GAA CTG ATG AGA GGG AG

## Appendix B

### Gradient Extraction from *Lv. brevis* JCM 1059

Gradient extraction from *Lv. brevis* JCM 1059 was performed with 1 M to 5 M LiCl solution and the product of each extract was confirmed with SDS-PAGE (Figure B.1). Although impurities can be found when extraction was performed with 2 - 4 M LiCl solution, thick bands at 52 kDa were also observed (Figure B.1 (b - d)). Furthermore, increase in band intensity at 52 kDa with increasing concentration of LiCl shows that higher concentration of LiCl increase extraction efficiency of SlpB. To reduce the loss of SlpB while removing impurities, in this dissertation, impurities were removed by washing *Lv. brevis* JCM 1059 twice with 1 M LiCl solution, and SlpB was extracted with *Lv. brevis* JCM 1059 with 5 M LiCl solution.

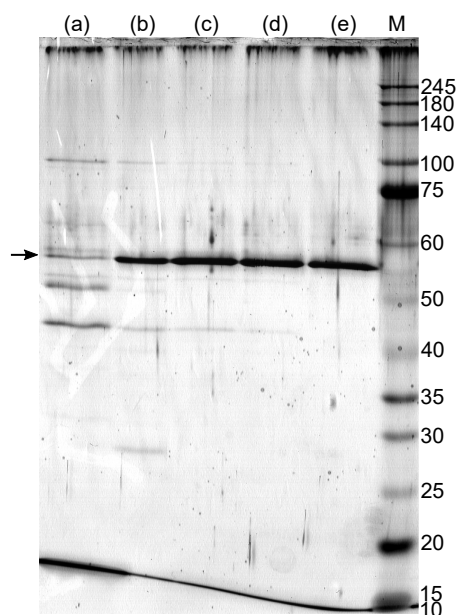


**Figure B.1** SDS-PAGE of product extracted with 1 M to 5 M LiCl solution and stained with silver. Product extracted with (a) 1 M LiCl solution, (b) 2 M LiCl solution, (c) 3 M LiCl solution, (d) 4 M LiCl solution, (e) 5 M LiCl solution. M indicates protein molecular weight marker and arrow points at 52 kDa.

## Appendix C

### Standard Curve for Protein Quantification

This chapter discusses methods used to quantify concentration of Slp. Generally, Bradford assay is a robust and convenient method to evaluate the concentration of protein. However, absorbance at UV/Vis spectrum is generally used to evaluate the concentration and dye:protein ratio of labelled proteins. Therefore, it is important to understand the relationship between UV method and Bradford method.

All reagents and samples used in this chapter were diluted from a vial of stock solution, and same pipettes and analytical balance were used to ensure consistency of data. For BSA standard used in this chapter, a vial of 2.00 mg ml<sup>-1</sup> BSA solution was prepared as stock solution. BSA used in each experiment was prepared by further diluting BSA stock solution.

#### C.1 Bradford Method

Bradford method quantifies protein by dyeing with Coomassie brilliant blue (CBB)<sup>[146]</sup>. CBB is a protein stain which binds to amine groups in protein through ionic interaction via sulphonic acid group in dye, as well as through Van der Waals attraction. This method is simple and relatively robust, and it is one of the standard protocols used in protein quantification. Prior studies of Slp, e.g., Ref. 147, 148 and 55, have used Bradford method for quantification.

In this section, I discuss Slp quantification by standard microplate protocol of Bradford method. To quantify concentration of SlpB, a standard curve was plotted with BSA as standard. 40 µl 1× CBB solution was added to 160 µl BSA of various concentration and SlpB in 96-well plate. Then, the plate was shaken on 52.35 rad s<sup>-1</sup> orbital shaker for 10 min, and let sit for 10 min. Absorbance at 595 nm was measured and the concentration of SlpB was determined based on standard curve (Figure C.1).

The concentration of SlpB extracted was 114.4 µg ml<sup>-1</sup>

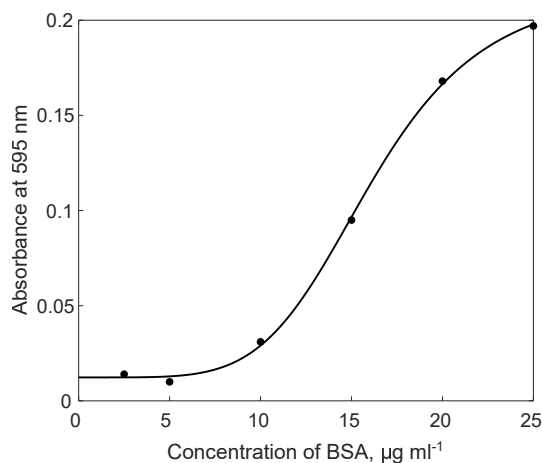


**Figure C.1** Standard curve of Bradford method measured by BSA. Error bars indicate standard deviation. Standard deviations includes 4% error resulted by impurity in BSA and error of pipette.

## C.2 UV Method

Amino acids are building block of proteins. Some amino acids consist of aromatic rings which can absorb energy at ultraviolet (UV) range, e.g., phenylalanine absorbs energy at 260 nm; while tryptophan, tyrosine and cysteine absorb energy at 280 nm. This property can be used to quantify proteins which are rich in aromatic rings, e.g., BSA and SlpB.

To verify whether the concentration of SlpB can be quantified with UV method, absorbance at 280 nm of SlpB was measured, and calculated with extinction coefficient  $\epsilon_{280(\text{SlpB})}$  as  $65,780 \text{ M}^{-1} \text{ cm}^{-1}$ , mass as 50,924 Da. The concentration of SlpB was  $104 \mu\text{g ml}^{-1}$ .

Approximately  $10 \mu\text{g ml}^{-1}$  difference in concentration measured by Bradford method and UV method was observed, due to the difference in ratio of arginine consist in BSA and SlpB, which bind to CBB.

## Appendix D

### Fluorescent Labelling of SlpB

Cy5 labelling of SlpB was confirmed with fluorescent SDS-PAGE. Electrophoresis of  $\text{Cy}^5\text{SlpB}$  was performed and detected with fluorescent image scanner (Figure D.1). Single band of fluorescent protein observed in gel indicates that Cy5 was successfully conjugated on SlpB.

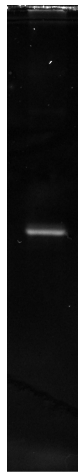


**Figure D.1** SDS-PAGE of Cy5-labelled SlpB.

## Appendix E

### Zeta Potential of Important Materials Used

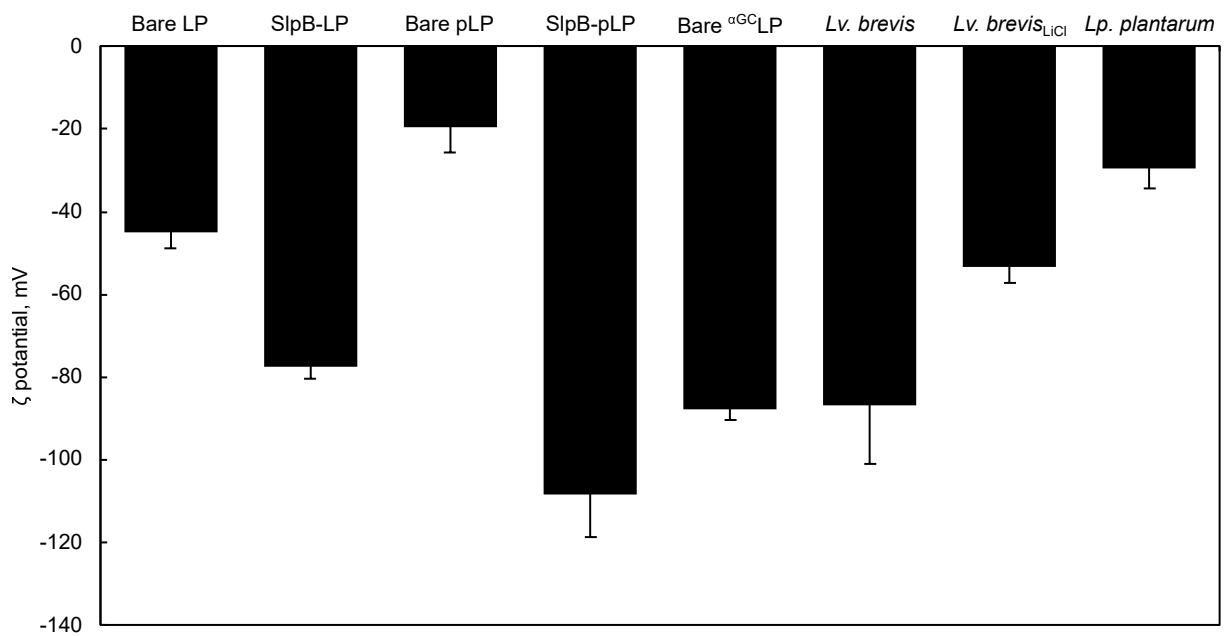


Figure E.1 ζ potential of materials used in this study.

## Appendix F

# Optimisation of Protocols for Differentiation and Polarisation of THP-1 Monocyte

Human leukemic monocytic cell line, THP-1<sup>[83]</sup>, is widely used as a model of monocytes due to its high stability and homogeneity compared to primary peripheral blood mononuclear cells<sup>[149,150]</sup>. Studies have shown that THP-1 monocytes can be differentiated into macrophage-like cell, and polarised into various phenotypes of macrophages and dendritic cells with appropriate stimulant. Nevertheless, various differentiation protocols were reported, and depends on protocol, functional changes, e.g., protein expression might vary significantly<sup>[149,151,152]</sup>. Some protocols have reported that only a small fraction of cells, ranges from 10 - 60% express DC-SIGN<sup>[153,154]</sup>, which are unfavourable to study the function and interaction with specific phenotypes of cells. Therefore, to obtain correctly expressed cell, e.g., > 90% of DC-SIGN<sup>+</sup> cells after IL-4 polarisation<sup>[155]</sup>, optimisation of protocol is necessary.

First, I confirm whether THP-1 can be stimulated and induced into DC. THP-1 monocytes are incubated with sRPMI supplemented with 50 nM PMA for 48 h, followed by 20 ng ml<sup>-1</sup> rhIL-4 for 48 h. Then, the cells were detached by incubating cells in medium containing 5 mM EDTA at 37°C for 15 min. The cells were collected into tubes, and well plate was inspected with microscope to ensure that all cells were detached and collected to prevent bias (Figure F.1).

Then, the cells were fixed with 3.7% formaldehyde and 0.8% methanol, blocked with 3% BSA, followed by incubation with mouse Ab against hDC-SIGN and FITC-conjugated goat Ab against mouse IgG. Then, 5,000 cells were analysed with flow cytometry. Cells without rhIL-4 treatment were used as control (Figure F.2). 93.57% of cells were found to express DC-SIGN, which suggest that the protocol is valid and the cells were in good conditions. Low fraction of DC-SIGN positive cells in prior study was properly resulted from weakening of cells occurred in the process of maintenance and differentiation of THP-1 cells.



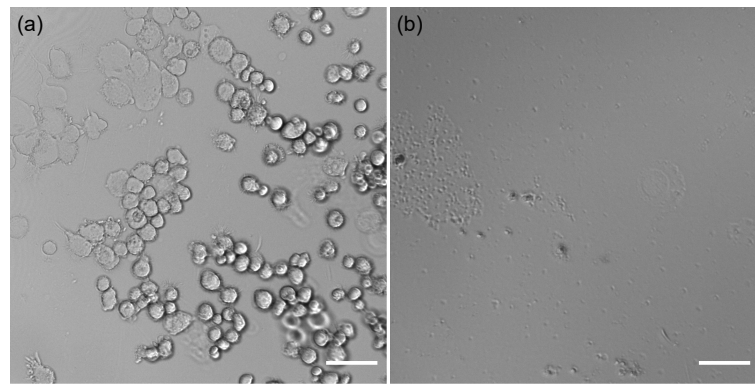


**Figure F.1** Microscopic inspection of well plate after cell detachment. (a) Case which some cells remained attached on plate after EDTA-treatment. This case produces bias on cell analysis. (b) Case which all cells were detached from plate. The scale bars are 50  $\mu\text{m}$ .

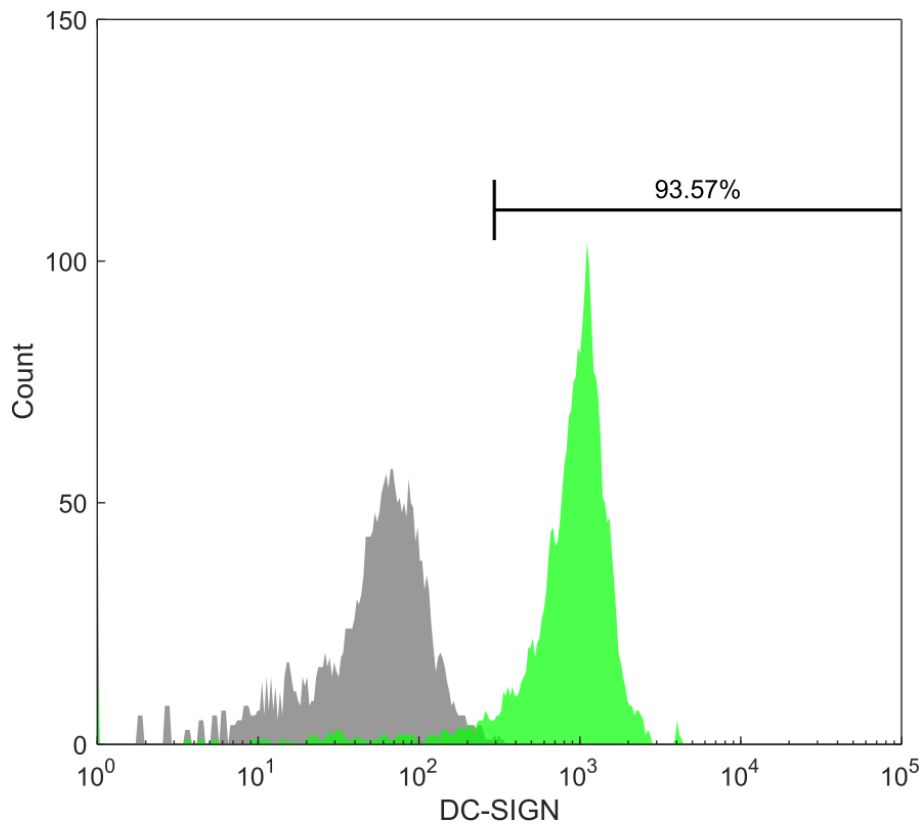


**Figure F.2** Expression of DC-SIGN induced by 50 nM PMA stimulation followed by 20 ng ml<sup>-1</sup> rIL-4, each for 48 h incubation in 37°C, 5.0% CO<sub>2</sub> humidified incubator. 5,000 cells were analysed for each sample. Grey areas indicate control. The numbers indicate percentage of cells in gated region.

## F.1 Optimisation of Concentration of PMA

In this section, I optimise differentiation protocol for THP-1 monocyte to obtain stable phenotypes for *in vitro* studies. As the signature receptor found on DC, DC-SIGN was used as marker to determine degree of polarisation. Furthermore, the conditions of cells after polarisation were also compared. As optimal concentration of IL-4 required for THP-1 macrophage polarisation is known, this section focuses on optimisation of concentration of PMA required to differentiate THP-1 monocytes into imM $\Phi$ .

THP-1 monocyte was suspended in sRPMI supplemented with various concentration of PMA and seeded into 48-well plate at density of  $2.0 \times 10^3$  cells  $\text{mm}^{-1}$ . The cells were incubated in 37.0°C, 5.0% CO<sub>2</sub> humidified incubator for 48 h. Then, the cells were rested in fresh sRPMI for 72 h with medium replacement at every 48 h, followed by polarisation in sRPMI supplemented with 20 ng  $\text{ml}^{-1}$  rhIL-4.

The morphology of cells was observed with fluorescent cell imager at 2 h, 48 h, 120 h and 168 h (Figure F.3). Based on microscopy analysis, I found that THP-1 monocytes began to adhere and flatten at 2 h. After 48 h incubation in sRPMI supplemented with PMA, stellate morphology can be observed. Furthermore, colour changes of culture medium were observed for cells incubated in sRPMI supplemented with  $\geq 30$  nM PMA, indicates metabolic changes, probably due to up-regulation of undesirable gene expression stimulated by PMA\* (Figure F.4).

After polarisation in sRPMI supplemented with 20 ng  $\text{ml}^{-1}$  rhIL-4, cells were detached and collected. Suspended cells were fixed with 3.7% formaldehyde and 0.8% methanol, blocked with 3% BSA, followed by incubation with mouse Ab against hDC-SIGN and FITC-conjugated goat Ab against mouse IgG. For each sample, 10,000 cells were analysed with flow cytometer. DC-SIGN expression level and percentage of DC-SIGN<sup>+</sup> cells were used to determine the optimal concentration of PMA (Figure F.5). Cells without PMA and rhIL-4 treatment were used as control. As shown in Figure F.6, rhIL-4 alone stimulated expression of DC-SIGN by THP-1 monocyte. Both the density of DC-SIGN and percentage of positive cell increase as the concentration of PMA increases. Percentage of DC-SIGN<sup>+</sup> cells (Fig F.5 (b)) were the highest when stimulated with 40 nM PMA, and the ratio of positive cells begins to drop when THP-1 monocyte was stimulated with 50 nM PMA, which might be due to the masking effect of over-priming<sup>[157]</sup>.

---

\* Refer e.g. reference 156

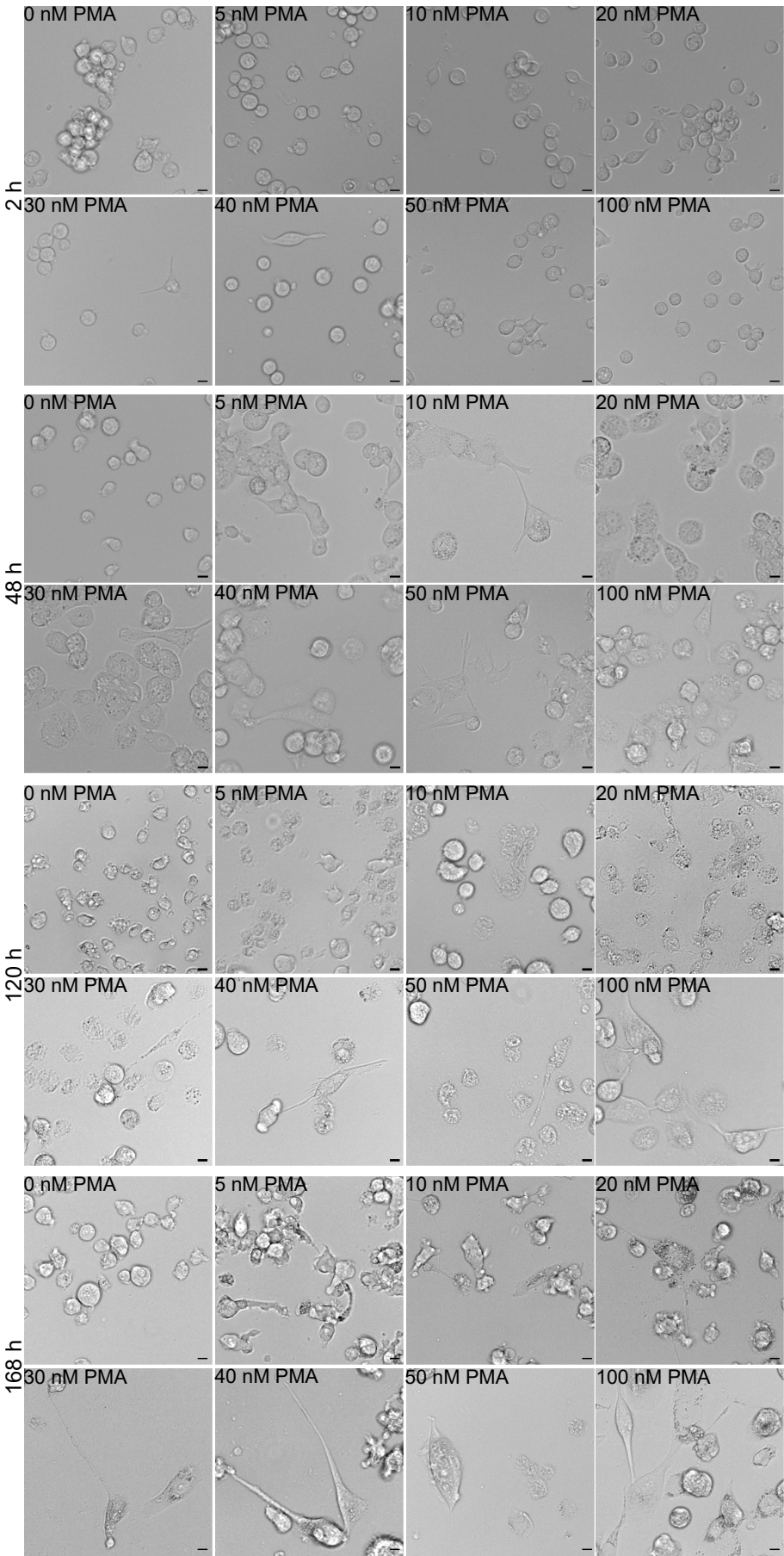


**Figure F.3** Morphology of THP-1 monocytes after stimulation with various concentration of PMA for various length of time. The scale bars are 10  $\mu$ m.

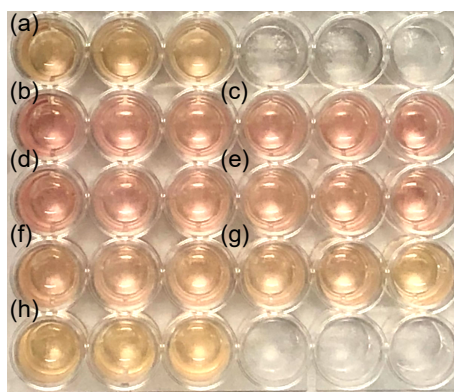


**Figure F.4** Colour of culture medium after 48 h recovery. THP-1 monocytes stimulated with (a) 0 nM, (b), 5 nM, (c) 10 nM, (d) 20 nM, (e) 30 nM, (f) 40 nM, (g) 50 nM, (h) 100 nM PMA. Changes in colour of medium can be observed when THP-1 monocyte was treated with  $\geq 30$  nM PMA.

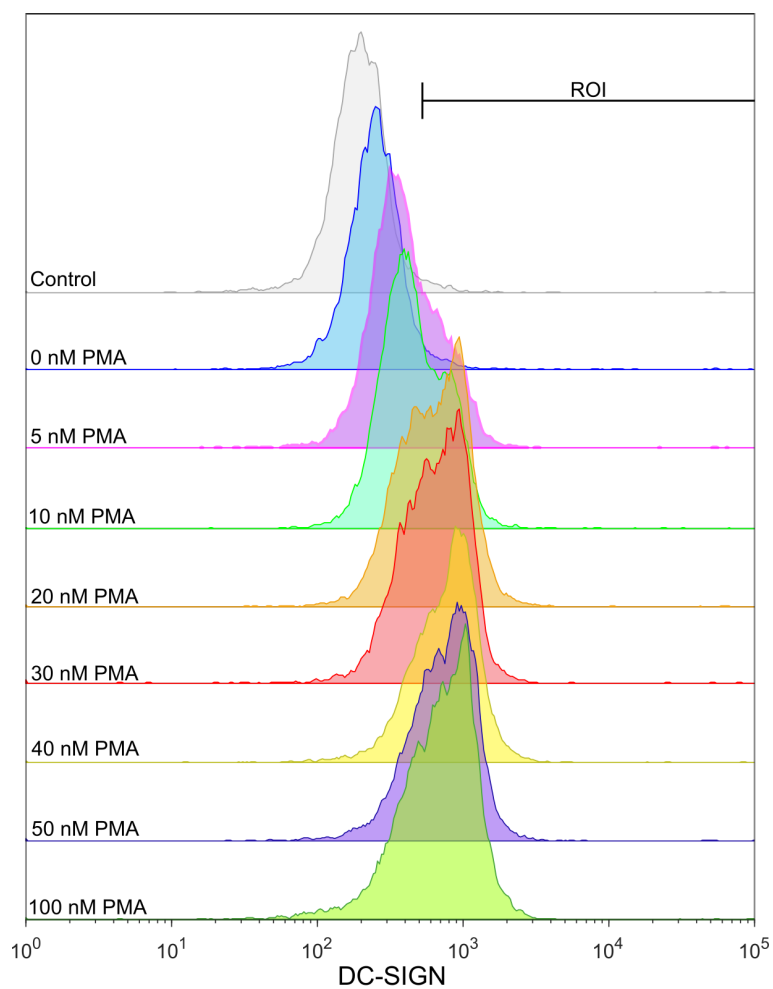


**Figure F.5** Flow cytometry analysis of DC-SIGN expression of DC stimulated with various concentration of PMA. 10,000 cells were analysed for each sample. Grey areas indicate control.

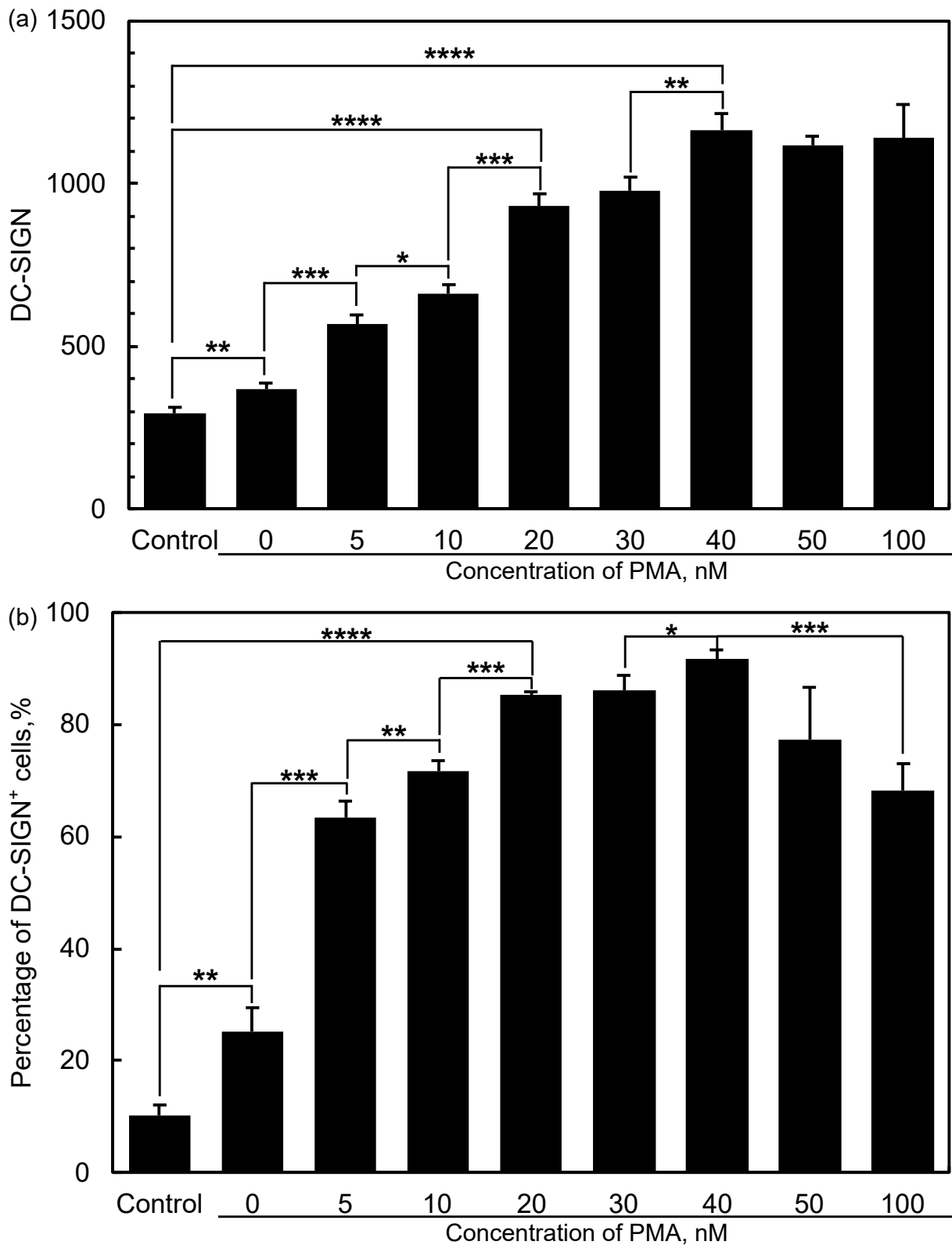


**Figure F.6** Relative density of DC-SIGN expressed in DC stimulated with various concentration of PMA. (a) Signal intensity of DC-SIGN, (b) percentage of DC-SIGN<sup>+</sup> cells. The plot represent data obtained from triplicate sample in independent test and the error bars represent standard deviation of mean. Statistical significance was evaluated with Student's t-test. \*  $p < 0.05$ , \*\*  $p < 0.01$ , \*\*\*  $p < 0.001$ , \*\*\*\*  $p < 0.0001$ .

On the other hand, analysis of cell morphology shows that the minimum concentration of PMA required to induce morphological transformation of THP-1 monocyte was 20 nM PMA (Figure F.7).

Based on these data obtained, in this dissertation, 20 nM PMA was used to differentiate THP-1 monocyte to reduce undesired effect of PMA stimulation on cells.

## **F.2 Optimal Concentration of LPS for DC Maturation**

To identify optimal concentration of LPS required for DC maturation, titration of LPS was performed.

DC was incubated in sRPMI supplemented with various concentration of LPS in 37°C, 5.0% CO<sub>2</sub> humidified incubator for 24 h. Then, the supernatants were collected, and concentration of IL-6 were evaluated with ELISA; viability of cells were evaluated with 3-(4,5-dimethylthiazol-2-yl)-2,5-diphenyltetrazolium bromide assay with DC without LPS treatment as control. Then, curve of IL-6 production and cell viability was plotted against concentration of LPS (Figure F.8). Production of extracellular IL-6, which is a signature cytokine of mature DC, increases linearly with concentration of LPS, suggesting that higher concentration of IL-6 is capable to stimulate higher degree of DC maturation. On the other hand, cell viability decrease when 1 µg ml<sup>-1</sup> was supplemented. To reduce noise generated as a result of cell weakening and pyroptosis, 100 ng ml<sup>-1</sup> LPS was used in both MΦ induction and DC maturation in this study.

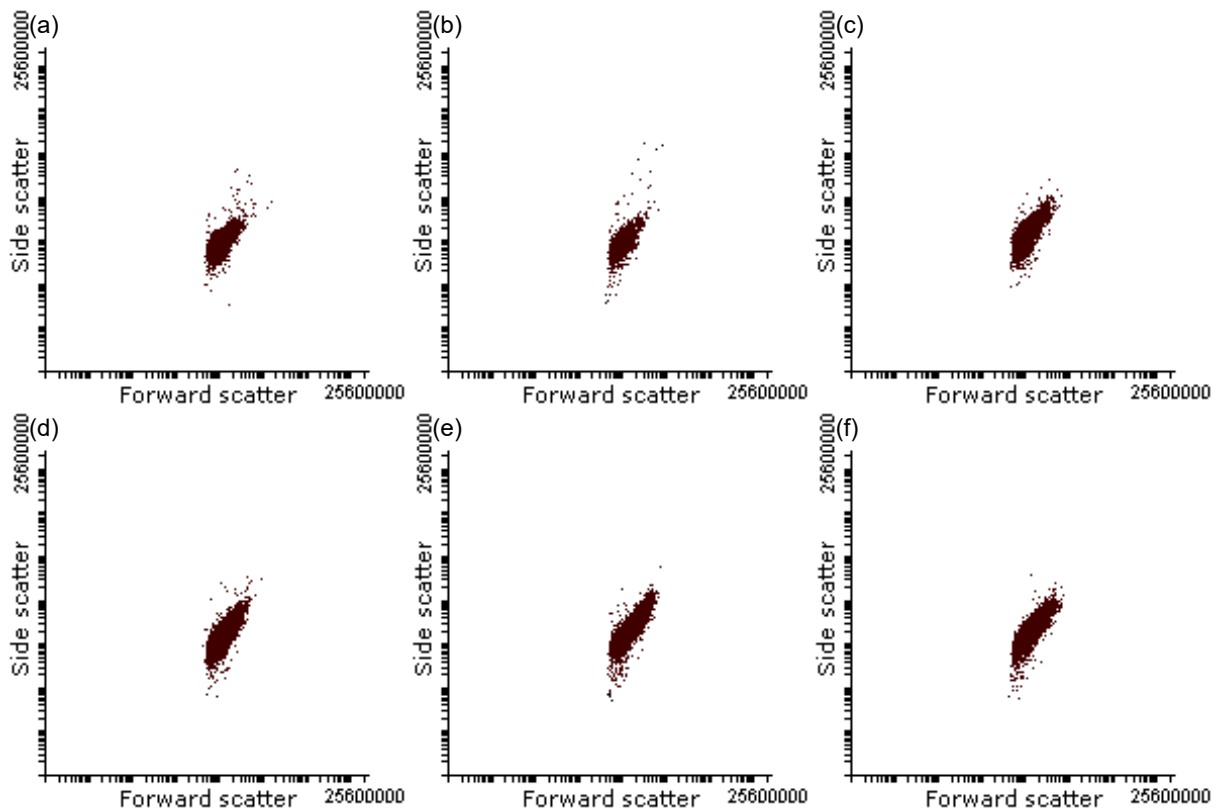


**Figure F.7** Difference in cell morphology based on scattering signal. (a) control, cell treated with (b) 0 nM, (c) 5 nM, (d) 10 nM (e) 20 nM, (f) 30 nM PMA and 20 ng ml<sup>-1</sup> rhIL-4.

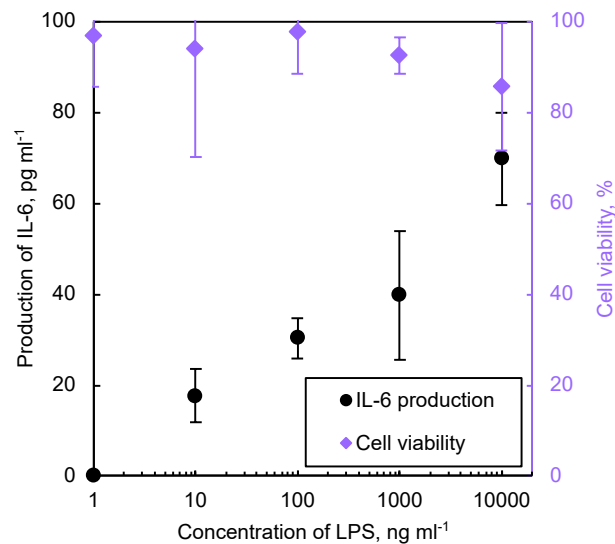
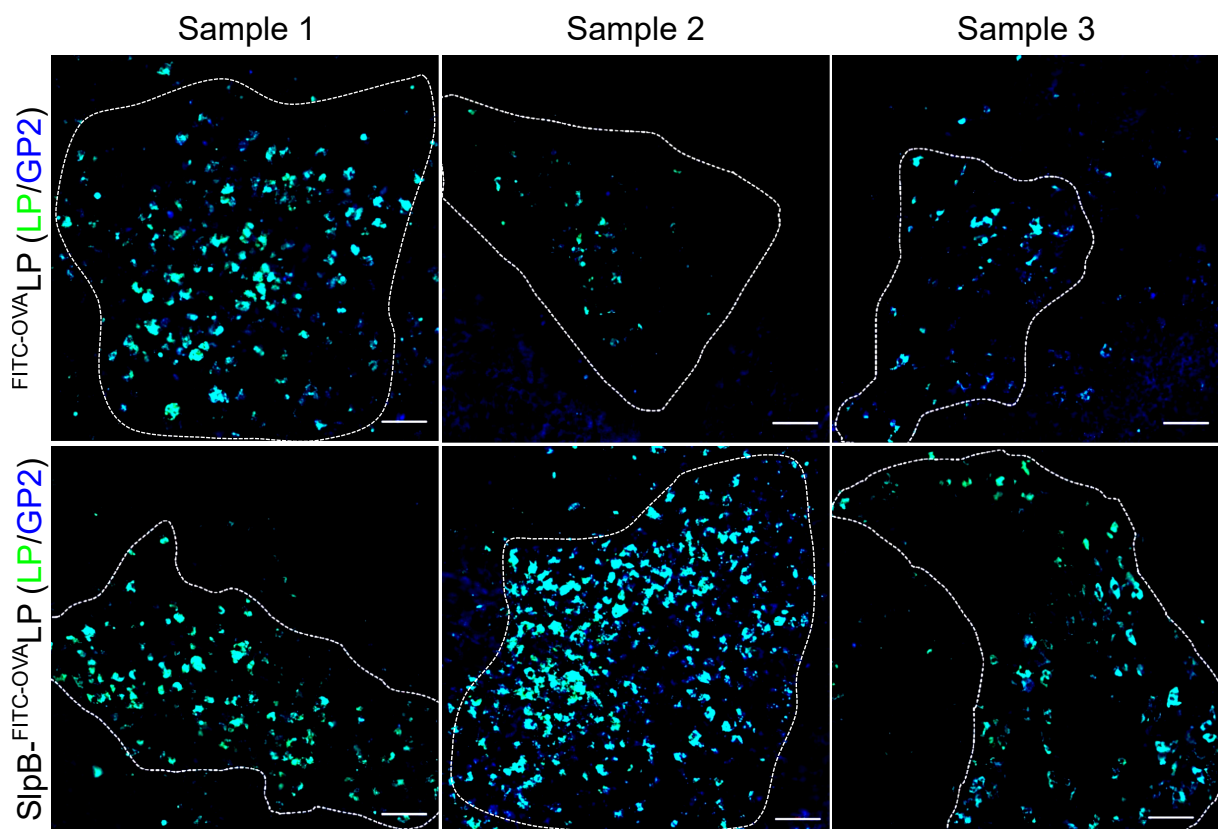


**Figure F.8** Relationship between IL-6 production and cell viability against concentration of LPS. The plot represent data obtained from triplicate sample in independent test and the error bars represent standard deviation of mean.

## Appendix G

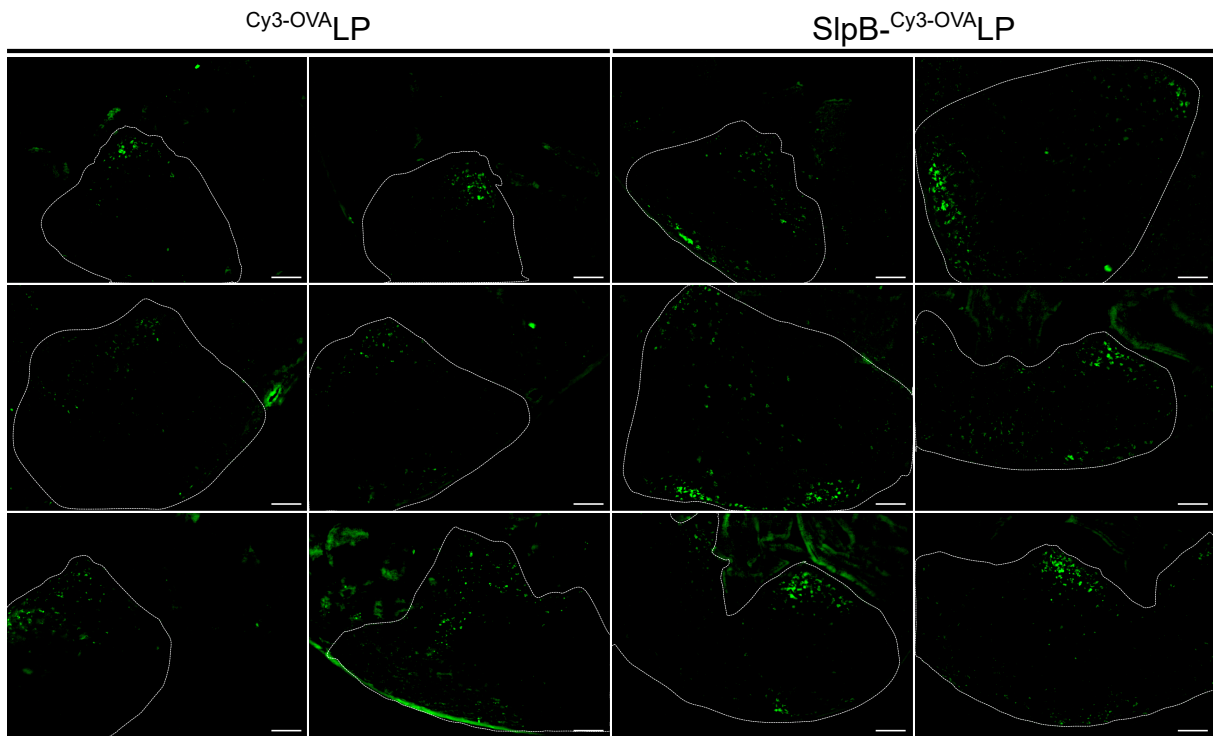
### Supplementary Figures

#### G.1 Micrographs used in statistical analysis in Figure 4.5 (n)



**Figure G.1** Micrographs used in statistical analysis in Figure 4.5 (n). Region of interest used in statistical analysis are gated with white line. The scale bars are 50  $\mu$ m



**G.2 Micrographs used in statistical analysis in Figure 4.7 (h)**

**Figure G.2** Micrographs used in statistical analysis in Figure 4.7 (h). Region of interest used in statistical analysis are gated with white line. The scale bars are 50  $\mu\text{m}$

## Appendix H

### Growth Curves of *Lv. brevis* and THP-1 Cells

#### H.1 Growth of *Lv. brevis* JCM1059

Growth of *Lv. brevis* JCM1059 at 30.0°C was evaluated to determine time required to achieve each growth phase. 1 µl cyro-preserved *Lv. brevis* JCM1059 was inoculated in 5 ml MRS broth in screw-capped test tube (Φ16 mm). The test tube was tightly capped, sealed with Parafilm<sup>®</sup>, and incubated statically in 30.0°C incubator for 48 h.

Then, 5 µl bacteria suspension was inoculated in 5 ml fresh MRS broth in screw-capped test tubes. The test tubes were tightly capped, sealed with Parafilm<sup>®</sup>, and incubated statically in 30.0°C bio-photorecorder. Optical density at 660 nm of each test tubes were measured every 30 min (Figure H.1). The growth curve shows that initial stationary phase of *Lv. brevis* JCM1059 is achieved at 40 h. At initial stationary phase, the maximum mass of *L. brevis* is achieved while the rate of protein degradation is not as high as late stationary phase. Therefore, 40 - 48 h is optimum to yield SIp from *Lv. brevis* JCM1059.

Based on the growth curve, SIp was yielded from *Lv. brevis* JCM1059 at 40 - 48 h.

#### H.2 Growth of THP-1 Monocytes

For each lot of FBS, the growth curve of THP-1 monocytes is plotted to determined the optimal duration of cultivation for cell maintenance. Approximately  $1 \times 10^5$  cells ml<sup>-1</sup> THP-1 monocytes were seeded in 10 ml sRPMI medium in 3 tissue culture flasks. The flasks were incubated in 37.0°C, 5.0% CO<sub>2</sub> humidified incubator, and the medium were replaced with fresh medium every 48 h. 10 µl of sample from each flasks were extracted, mixed with 10 µl 0.5% trypan blue staining solution, and the number of live and death cells were counted with haemocytometer, and a growth curve was plotted (Figure H.2). As the fraction of death cells increased significantly when the number of cell exceed  $9 \times 10^5$  cells ml<sup>-1</sup>. Therefore, the THP-1 monocyte is maintained at  $2 - 9 \times 10^5$  cells ml<sup>-1</sup> throughout this dissertation.

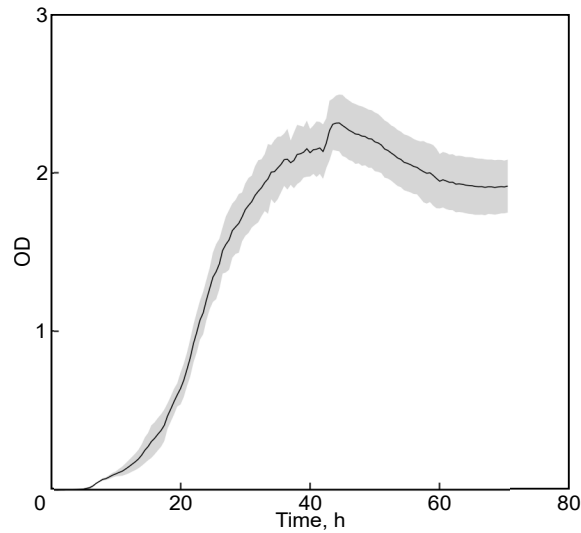


**Figure H.1** Growth curve of *Lv. brevis* JCM1059 when incubated statically at 30°C. The plot represents data obtained from triplicate sample in independent test and the error bars represent standard deviation of mean.

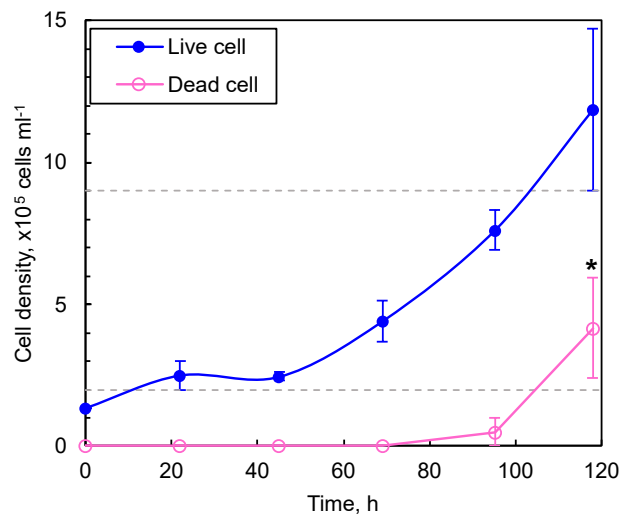


**Figure H.2** Example of growth curve of THP-1 monocytes when cultured in tissue culture flasks and incubated statically in 37°C, 5.0% CO<sub>2</sub> humidified incubator. The plot represent data obtained from triplicate sample in independent test and the error bars represent standard deviation of mean. Statistical significance was evaluated with Student's t-test. \*:  $p < 0.05$ .

## Reference

- [1] Paracelsus T. *Septem Defensiones 1538*, vol. 2, chap. Die dritte Defension wegen des Schreibens der neuen Recepte. Darmstadt, Germany: Wissenschaftliche Buchgesellschaft, 1965. 510.
- [2] Pond S M & Tozer T N. *Clin Pharmacokinet*, 1984. **9**(1): 1.
- [3] Wickramasinghe S N. *Clin Lab Haematol*, 1987. **9**(3): 271.
- [4] Wylon K, Dölle S & Worm M. *Allergy Asthma Clin Immunol*, 2016. **12**(1).
- [5] Ahn H & Park J H. *Biomater Res*, 2016. **20**(1).
- [6] Vishwakarma N, Jain A, Sharma R et al. *AAPS PharmSciTech*, 2019. **20**(2).
- [7] Darwis Y, Khan A A, Mudassir J et al. *Int J Nanomed*, 2013: 2733.
- [8] Sosnik A & Augustine R. *Adv Drug Deliver Rev*, 2016. **103**: 105.
- [9] Peyer J C. *Exercitatio anatomico-medica de glandulis intestinorum, earumque usu & affectionibus*. Amsterdam, Netherlands: Henrik Wetstein, 1681.
- [10] Rios D, Wood M B, Li J et al. *Mucosal Immunol*, 2016. **9**(4): 907.
- [11] Childers N K, Denys F R, McGee N F et al. *Reg Immunol*, 1990. **3**: 8.
- [12] Chen Y, Wu J, Wang J et al. *Diabetologia*, 2018. **61**(6): 1384.
- [13] Song J G, Lee S H & Han H K. *J Nanobiotechnol*, 2021. **19**(1).
- [14] Tenchov R, Bird R, Curtze A E et al. *ACS Nano*, 2021. **15**(11): 16982.
- [15] Jensen V B, Harty J T & Jones B D. *Infect Immun*, 1998. **66**(8): 3758.
- [16] Suzuki S, Yokota K, Igimi S et al. *Microbiology*, 2020. **165**(2): 188.
- [17] Sahay B, Ge Y, Colliou N et al. *Gut Microbes*, 2015. **6**(6): 392.

- [18] Cai Z, Xu P, Wu Z et al. *J Funct Foods*, 2018. **51**: 16.
- [19] Chinthamani S, Settem R P, Honma K et al. *PLoS One*, 2017. **12**(3): e0173394.
- [20] Buck B L, Altermann E, Svingerud T et al. *Appl Environ Microbiol*, 2005. **71**(12): 8344.
- [21] Åvall Jääskeläinen S, Lindholm A & Palva A. *Appl Environ Microbiol*, 2003. **69**(4): 2230.
- [22] Antikainen J, Anton L, Silanpää J et al. *Mol Microbiol*, 2002. **46**(2): 381.
- [23] Yanagihara S, Kanaya T, Fukuda S et al. *Int Immunol*, 2017. **29**(8): 357.
- [24] Konstantinov S R, Smidt H, de Vos W M et al. *Proc Natl Acad Sci U S A*, 2008. **105**(49): 19474.
- [25] Fagan R P & Fairweather N F. *Nat Rev Microbiol*, 2014. **12**: 211.
- [26] Salminen S, von Wright A, Morelli L et al. *Int J Food Microbiol*, 1998. **44**(1): 93.
- [27] Kapczynski D R, Meinersmann R J & Lee M D. *Curr Microbiol*, 2000. **41**: 136.
- [28] Zhang J, Gao J, Guo Y et al. *Curr Microbiol*, 2017. **74**: 1123.
- [29] Acosta M P, Ruzal S M & Cordo S M. *Int J Biol Macromol*, 2016. **92**: 998 .
- [30] Sillanpää J, Martínez B, Antikainen J et al. *J Bacteriol*, 2000. **182**(22): 6440 .
- [31] Toba T, Virkola R, Westerlund B et al. *Appl Environ Microbiol*, 1995. **61**(7): 2467.
- [32] Taverniti V, Stuknyte M, Minuzzo M et al. *Appl Environ Microbiol*, 2013. **79**(4): 1221.
- [33] Acosta M P, Goyette-Desjardins G, Scheffel J et al. *Front Immunol*, 2021. **12**: 602067.
- [34] Wang R, Jiang L, Zhang M et al. *Sci Rep*, 2017. **7**: 44029.
- [35] Garrote G L, Delfederico L, Bibiloni R et al. *J Dairy Res*, 2004. **71**(2): 222.
- [36] Golowczyc M A, Mobili P, Garrote G L et al. *J Dairy Res*, 2009. **76**(1): 111.
- [37] Bradshaw W J, Kirby J M, Roberts A K et al. *FEBS J*, 2017. **284**(17): 2886.
- [38] Ryan A, Lynch M, Smith S M et al. *PLOS Pathog*, 2011. **7**(6): 1.
- [39] Doig P, Emödy L & Trust T J. *J Biol Chem*, 1992. **267**(1): 43.
- [40] Wang Y, Wei Y, Yuan S et al. *BMC Microbiol*, 2016. **16**: 183.

- [41] Banerjee A, Tsai C L, Chaudhury P et al. *Structure*, 2015. **23**(5): 863.
- [42] Martin J F, Palomino M M, Cutine A M et al. *Appl Microbiol Biotechnol*, 2019. **103**(12): 4839.
- [43] Åvall Jääskeläinen S, Hynönen U, Ilk N et al. *BMC Microbiol*, 2008. **8**: 165.
- [44] Masuda K & Kawata T. *Microbiol Immunol*, 1980. **24**(4): 299.
- [45] Sára M & Sleytr U B. *J Bacteriol*, 2000. **182**(4): 859.
- [46] Sleytr U B, Schuster B, Egelseer et al. *FEMS Microbiol Rev*, 2014. **38**: 823.
- [47] Lanzoni-Mangutchi P, Banerji O, Willson J et al. *Nat Commun*, 2022. **13**: 970.
- [48] Herrmann J, Jabbarpour F, Bargar P G et al. *Biophys J*, 2017. **112**(9): 1841.
- [49] Chung S, Shin S H, Bertozzi C R et al. *Proc Natl Acad Sci U S A*, 2010. **107**(38): 16536.
- [50] Küpcü S, Sára M & Sleytr U B. *Biochim Biophys Acta*, 1995. **1235**(2): 263.
- [51] Mader C, Küpcü S, Sára M et al. *Biochim Biophys Acta*, 1999. **1418**(1): 106.
- [52] Mader C, Küpcü S, Sleytr U B et al. *Biochim Biophys Acta*, 2000. **1463**(1): 142.
- [53] Toca-Herrera J L, Krastev R, Bosio V et al. *Small*, 2005. **1**(3): 339.
- [54] Martín-Monila A, Moreno-Flores S, Perez E et al. *Biophys J*, 2006. **90**(5): 1821.
- [55] Hollmann A, Delfederico L, Glikmann G et al. *Biochim Biophys Acta*, 2007. **1768**: 393.
- [56] Delcea M, Karstev R, Gutberlet T et al. *Soft Matter*, 2008. **4**(7): 1414.
- [57] Meng J, Wang Y Y, Hao Y P et al. *Int J Biol Macromol*, 2021. **183**: 457.
- [58] Wang W, Shao A, Feng S et al. *Int J Pharm*, 2017. **529**(1-2): 227.
- [59] Guan J, Shen Q, Zhang Z et al. *Nat Commun*, 2018. **9**: 2982.
- [60] Shannahan J H, Podila R, Aldossari A A et al. *Toxicol Sci*, 2015. **143**(1): 136.
- [61] Jiang X, Pan D, Tao M et al. *J Agric Food Chem*, 2021. **69**(27): 7593.
- [62] Shao A. *The Study on Surface Layer Protein Coating Liposomes as Oral Vaccine Vector*. Master's thesis, Zhejiang University of Technology, 2017.

- [63] Schneitz C, Nuotio L & Lounatma K. *J Appl Microbiol*, 1993. **74**(3): 290.
- [64] Jones D T, Taylor W R & Thornton J M. *Bioinformatics*, 1992. **8**(3): 275.
- [65] Hollmann A, Delfederico L, De Antoni G et al. *Colloids Surf , B*, 2010. **79**(1): 191 . Slp coating on liposome - mechanism, brevis.
- [66] Filion M C & Phillips N C. *Biochim Biophys Acta*, 1997. **1329**(2): 345.
- [67] Romøren K, Thu B J, Bols N C et al. *Biochim Biophys Acta*, 2004. **1663**(1-2): 127.
- [68] Jakava-Viljanen M, Ávall Jääskeläinen S, Messner P et al. *J Bacteriol*, 2002. **184**(24): 6786.
- [69] Nguyen S, Alund S J, Hirorth M et al. *Colloids Surf , B*, 2011. **88**(2): 664.
- [70] Nishimura Y. *Hepatitis B derived carriers to effectively express pharmaceutical activity in target cancer cells*. Ph.D. thesis, Kobe University, 2013.
- [71] Lengyel M, Kállai-Szabó N, Antal V et al. *Sci Pharm*, 2019. **87**(3): 20.
- [72] Shirakawa T & Kitagawa K. *Hum Vaccin Immunother*, 2018. **14**(1): 159.
- [73] Leschner S & Weiss S. *J Mol Med*, 2010. **88**: 763.
- [74] Stritzker J, Weibel S, Hill P J et al. *Int J Med Microbiol*, 2007. **297**(3): 151.
- [75] Choudhary A, Renganathan T & Pushpavanam S. *J Fluid Mech*, 2019. **874**: 856.
- [76] Ishida M, Namai F, Shigemori S et al. *Appl Environ Microbiol*, 2020. **86**(20).
- [77] Kristoffersen S M, Ravnum S, Tourasse N J et al. *J Bacteriol*, 2007. **189**(14): 5302.
- [78] Piacentini E, Mazzei R & Giorno L. *Membranes*, 2021. **11**(2): 137.
- [79] Saad N, Urdaci M, Vignoles C et al. *J Microbiol Biotechnol*, 2009. **19**(12): 1635.
- [80] Wu M, Liu X, Bai H et al. *ACS Appl Mater Interfaces*, 2019. **11**(10): 9850.
- [81] Moore G E, Gerner R E & Franklin H A. *JAMA*, 1967. **199**(8): 519.
- [82] Casella J F, Flanagan M D & Lin S. *Nature*, 1981. **293**(5830): 302.
- [83] Tsuchiya S, Yamabe M, Yamaguchi Y et al. *Int J Cancer*, 1980. **26**(2): 171.

- [84] von Eichel-Streiber C, Sauerborn M & Kuramitsu H K. *J Bacteriol*, 1992. **174**(20): 6707.
- [85] Sun Q, Smith G M, Zahradka C et al. *Infect Immun*, 1997. **65**(2): 537.
- [86] Cicchetti G, Maurer P, Wagener P et al. *J Biol Chem*, 1999. **274**(47): 33616.
- [87] Zhou D, Mooseker M S & Galán J E. *Science*, mar 1999. **283**(5410): 2092.
- [88] Bowman G D, Nodelman I M, Hong Y et al. *Proteins*, 2000. **41**(3): 374.
- [89] Andar A U, Hood R R, Vreeland W N et al. *Pharm Res*, 2013. **31**(2): 401.
- [90] Mitchell M J, Billingsley M M, Haley R M et al. *Nat Rev Drug Discov*, 2021. **20**: 101.
- [91] Nussinovitch A. *Polymer Macro- and Micro-Gel Beads: Fundamentals and Applications*, chap. Beads as Drug Carriers. 1st edn. New York, USA: Springer. ISBN 978-1-4419-6617-9, 2010. 191 – 230.
- [92] Villaverde A, García-Fruitós E, Rinas U et al. *Microb Cell Fact*, 2012. **11**: 76.
- [93] Daniel C, Roussel Y, Kleerebezem M et al. *Trends Biotechnol*, 2011. **29**(10): 499.
- [94] Claesen J & Fischbach M A. *ACS Synth Biol*, 2015. **4**(4): 358.
- [95] Liu P, Weinreb V, Ridilla M et al. *Sci Adv*, 2017. **3**(11).
- [96] Kobayashi E, Motoki K, Uchida T et al. *Oncol Res*, 1995. **7**(10-11): 529 .
- [97] Varin A, Mukhopadhyay S, Herbein G et al. *Blood*, 2010. **115**(2): 353 362.
- [98] Rennick J J, Johnston A P R & Parton R G. *Nat Nanotechnol*, 2021. **16**(3): 266.
- [99] Porta J C, Han B, Gulsevin A et al. *Sci Adv*, 2022. **8**: eabn7232.
- [100] Buttaro C & Fruehauf J. *Curr Gene Ther*, 2010. **10**(1): 27.
- [101] Zariri A & van der Ley P. *Expert Rev Vaccines*, 2015. **14**(6): 861.
- [102] Peiser L, Gough P J, Kodama T et al. *Infect Immun*, 2000. **68**(4): 1953.
- [103] Kléna J, Zhang P, Schwartz O et al. *J Bacteriol*, 2005. **187**(5): 1710.
- [104] Morita M, Motoki K, Akimoto K et al. *J Med Chem*, 1995. **38**(12): 2176.
- [105] Chang D H, Osman K, Connolly J et al. *J Exp Med*, 2005. **201**(9): 1503.



- [106] Ishikawa A, Motohashi S, Ishikawa E et al. *Clin Cancer Res*, 2005. **11**(5): 1910.
- [107] Nieda M, Okai M, Tazbirkova A et al. *Blood*, 2004. **103**(2): 383.
- [108] Giaccone G, Punt C J A, Ando Y et al. *Clin Cancer Res*, 2002. **8**(12): 3702.
- [109] Parekh V V, Wilson M T, Olivares-Villagómez D et al. *J Clin Invest*, 2005. **115**(9): 2572.
- [110] Gonzalez-Aseguinolaza G, de Oliveira C, Tomaska M et al. *Proc Natl Acad Sci USA*, 2000. **97**(15): 8461.
- [111] Wang X F, Zhang M J, He N et al. *J Med Chem*, 2021. **64**(15): 11554.
- [112] Hynönen U, Westerlund-Wikström B, Palva A et al. *J Bacteriol*, 2002. **184**(12): 3360.
- [113] Jung C, Hugot J P & Barreau F. *Int J Inflam*, 2010. **2010**: 1.
- [114] Corr S C, Gahan C C & Hill C. *FEMS Immunol Med Microbiol*, 2008. **52**(1): 2.
- [115] Smith M W & Peacock M A. *Am J Anat*, 1980. **159**(2): 167.
- [116] Nakamura Y, Kimura S & Hase K. *Inflamm Regener*, 2018. **38**(1).
- [117] Rosner A J & Keren D F. *J Leukocyte Biol*, 1984. **35**(4): 397.
- [118] Hase K, Kawano K, Nochi T et al. *Nature*, 2009. **462**(7270): 226.
- [119] Nakato G, Hase K, Suzuki M et al. *J Immunol*, 2012. **189**(4): 1540.
- [120] Kishikawa S, Sato S, Kaneto S et al. *Nat Commun*, 2017. **8**(1).
- [121] Clark M A, Hirst B H & Jepson M A. *Infect Immun*, 1998. **66**(3): 1237.
- [122] Iyoda T, Ushida M & Inaba K. *Cytometry Research*, 2012. **22**(1): 25.
- [123] Kaneko K, McDowell A, Ishii Y et al. *J Pharm Pharmacol*, 2017. **69**(12): 1724.
- [124] Carnaud C, Lee D, Donnars O et al. *J Immunol*, 1999. **163**: 4647.
- [125] Heller F, Fuss I J, Nieuwenhuis E E et al. *Immunity*, 2002. **17**(5): 629.
- [126] Park H, Li Z, Yang X O et al. *Nat Immunol*, 2005. **6**(11): 1133.
- [127] Patel P, Vyas N & Raval M. Safety and Toxicity issues of Polymeric Nanoparticles, oct 2021.

- [128] Ojer P, Iglesias T, Azqueta A et al. *Eur J Pharm Biopharm*, nov 2015. **97**: 206.
- [129] Umakoshi H, Tanabe T, Suga K et al. *Int J Biol Sci*, 2011. **7**(3): 253.
- [130] Inagawa H, Kohchi C & Soma G I. *Anticancer Res*, Jul 2011. **31**: 2431.
- [131] Cavallero G J, Malamud M, Casabuono A C et al. *J Proteomics*, 2017. **162**: 20.
- [132] DuBois M, Gilles K A, Hamilton J K et al. *Anal Chem*, 1956. **28**(3): 350.
- [133] Jumper J, Evans R, Pritzel A et al. *Nature*, 2021. **596**(7873): 583.
- [134] Valverde P, Delgado S, Matínez J D et al. *ACS Chem Biol*, 2019. **14**(7): 1660.
- [135] Menon S, Rosenberg K, Graham S A et al. *Proc Natl Acad Sci U S A*, 2009. **106**(28): 11524.
- [136] Geijtenbeek T B H, van Duijnhoven G C F, van Vliet S J et al. *J Biol Chem*, 2002. **277**(13): 11314.
- [137] Mitchell D A, Fadden A J & Drickamer K. *J Biol Chem*, 2001. **276**(31): 28939.
- [138] Cambi A, de Lange F, van Maarseveen N M et al. *J Cell Biol*, 2004. **164**(1): 145.
- [139] Rybner C, Finel-Szermanski S, Felin M et al. *J Cell Biochem*, 2002. **84**(2): 408.
- [140] Sherblom A P, Decker J M & Muchmore A V. *J Biol Chem*, 1988. **263**(11): 5418.
- [141] Terahara K, Yoshida M, Igarashi O et al. *J Immunol*, 2008. **180**(12): 7840.
- [142] Porkolab V, Chabrol E, Varga N et al. *ACS Chem Biol*, 2018. **13**(3): 600.
- [143] Vasta G, Ahmed H, Nita-Lazar M et al. *Front Immunol*, 2012. **3**: 199.
- [144] Mantis N J, Cheung M C, Chintalacheruvu K R et al. *J Immunol*, 2002. **169**: 1844.
- [145] Oya Y, Kimura S, Nakamura Y et al. *Front Immunol*, 2021. **12**. URL <https://www.frontiersin.org/articles/10.3389/fimmu.2021.779709>.
- [146] Bradford M M. *Anal Biochem*, 1976. **72**(1-2): 248.
- [147] Hynönen U, Kant R, Lähteinen T et al. *BMC Microbiol*, 2014. **14**(1): 199.
- [148] Wong W S & Yung P T. *2014 36th Annual International Conference of the IEEE Engineering in Medicine and Biology Society*, 2014.

- [149] Auwerx J. *Experientia*, 1991. **47**(1): 22.
- [150] Chanput W, Mes J J & Wichers H J. *Int Immunopharmacol*, 2014. **23**(1): 37.
- [151] Park E K, Jung H S, Yang H I et al. *Inflamm Res*, 2007. **56**(1): 45.
- [152] Aldo P B, Craveiro V, Guller S et al. *Am J Reprod Immunol*, 2013. **70**(1): 80.
- [153] Zhang X. *Cell surface somponents required for lactic acid bacteria uptake into THP-1*.  
Master's thesis, Tokyo Institute of Technology, 2021.
- [154] Jin C, Wu L, Li J et al. *J Biomed Biotechnol*, 2012. **2012**: 1.
- [155] Puig-Kröger A, Serrano-Gómez D, Caparrós E et al. *J Biol Chem*, 2004. **279**(24): 25680.
- [156] Chou S F, Chen H L & Lu S C. *Biochem Biophys Res Commun*, 2002. **296**(1): 48.
- [157] Feng Y H, Zhu Y N, Liu J et al. *Int Immunopharmacol*, 2004. **4**(6): 713.